Control Strategies For A Subsea Multiphase Electric Pump System

by

Tian Xiang MEI

B.Sc., M.Eng. and M.Sc.

A Doctoral Thesis
Submitted In Partial Fulfilment of The Requirements
For The Award of Doctor of Philosophy of
The Loughborough University of Technology

June, 1994

Supervisor: Professor Roger M. Goodall
Department of Electronic and Electrical Engineering

To My Great Nation:

--- CHINA

Declaration

This is to certify that I am responsible for the work submitted in this thesis and that the original work is my own, except where due reference to previous work has been acknowledged.

I also certify that neither this thesis nor the original work contained therein has been submitted to this or any other institution for a higher degree.

T.X. Mei.

Acknowledgements

The author wishes to express his gratitude and appreciation to his supervisor Professor Roger M. Goodall for his encouragement, helpful advice and friendship throughout the research work.

Thanks are due to Mr. T. M. Lodge and Mr. A. R. Creswick of Linear Motors Ltd. for arranging financial support and research facilities, which made the research possible.

The author would also like to thank many friends and colleagues for their support during his research studies; particularly those who have been working on the MEPS project.

Finally and above all the author dedicates his love to his family, whom he owes so much. Without their love and moral support, the author would not have been able to complete this work.

Contents

Abstract

This thesis presents the design, simulation and real time implementation of control strategies of a subsea multiphase electric pump system, which consists of a pair of piston type pumps, a permanent magnet linear synchronous motor (PLSM), a voltage source inverter and a control unit. The pump is required to operate efficiently and effectively for pure oil, pure gas, and for a mixture of the two.

The thesis starts with modelling for the system simulation, which is partitioned into two parts. The first part covers the mechanics of the motor slider and pistons, and the dynamics of the fluids to be pumped. The mechanics of the slider and pistons are represented by a second order model. A non linear model obtained from the gas laws is used for simulation of gas, and a distributed parameter model is developed to simulate the oil case. Based on the simulation of the models which were developed, a linear but time variant simplified model with parameter uncertainty is set up to enable design of controllers for the system, where the parameter uncertainty is bounded by two extreme load conditions.

The second part is the modelling of the motor. Three phase and d-q axis models are obtained for simulation of the motor and design of inner current loop respectively. By using closed loop current control and vector control of the synchronous motor, a linear simplified model is obtained to represent the electrical dynamics of the motor, again for design of the system controllers.

Based on the simplified models, three control approaches are studied and compared on the basis of robustness and performance against parameter variations and system uncertainty. The three controllers are cascade control plus feedforward terms, internal model control and optimal tracking control. Full simulations are then carried out to verify the design. Finally a scaled down system using a double sided PLSM is developed to implement the real time digital control, where one side of the motor is used to drive the motor and the other side to produce opposing forces for simulation of the load conditions. Dedicated hardware and software are developed for the two sides respectively.

Both the simulation and the real time implementation have proved that the developed control system is satisfactory for all possible load conditions and that the design meets the required performance.

Nomenclature

A_P	state matrix
A, A_1	cross sectional area
a	wave speed or speed of pressure pulse, acceleration
a_F	acceleration of fluids in pipes
a_{ref}	acceleration of fluids in pipes
B_P	input matrix
B, B_1, B_2	Allievi constant or pipeline constant
C_P	output matrix
C	pipeline capacitance
C_M, C_P	known constants in characteristic equations
C^+, C^-	names used in characteristic equations
$CS(n)$	control signal to inner current loop
$CS_{af}(n)$	control signal from acceleration feedforward term
$CS_{vf}(n)$	control signal from velocity feedforward term
$CS_p(n)$	control signal from position feedback loop
$CS_v(n)$	control signal from velocity feedback loop
c	specific heat ratio
c_P	constant pressure specific heat
c_v	constant volume specific heat
$\cos(\phi)$	power factor
D	inner diameter of a pipe
E_g	induced EMF, induced EMF vector
E_R	modulus of rigidity of pipe material
$E(s)$	function of control error in s domain
$e(\infty)$	steady state error
F	force
F_L	load force
F_R, F_Y, F_B	forces of phase locking.
F_{ref}	demanded force
F_1, F_2, F_3	motor force components
$FL1$	load force at the side of cylinder 1
$FL2$	load force at the side of cylinder 2

f	low pass filter of IMC
	Darcy-Weibach friction factor
f_D	Darcy-Weibach friction coefficient
f_H	Hagen-Peiseuille friction coefficient
f_{max}	maximum frequency
f_s	sample frequency
G_{PI_vec}	feedback term of current control loop
G_{fa}	acceleration feedforward gain
G_{fv}	velocity feedforward gain
G_{ff}	feedforward term of optimal tracking controller
G_p	proportional gain of optimal tracking controller
G_P	proportional gain of position loop in cascade control
G_{Pv}	proportional gain of velocity loop in cascade control
G_{PX}	proportional gain of optimal tracking in discrete time
G_I	integration gain of optimal tracking controller
G_{IX}	integration gain of optimal tracking in discrete time
G_i	integration gain of position loop in cascade control
G_v	velocity gain of optimal tracking controller
G_{vb}	velocity gain of optimal tracking controller in discrete time
G_{vf}	feedforward gain of optimal tracking in discrete time
g	gravity
H	piezemetric head
H_A, H_C, H_R, H_P	piezemetric heads at computational points in xt plane
$H_{1,NS}$, $H_{2,1}$, $H_{P2,1}$	piezemetric heads at a junction
$H(s)$	transfer function
$H_e(s)$	transfer function of electrical part
$H_p(s)$	system transfer function
I_f	assumed current of equivalent circuit of magnet
I_m	current magnitude
i_d, i_q	d-q axis currents
i_{d_ref}, i_{q_ref}	demanded d-q axis currents
i_R, i_Y, i_B	phase currents
i_α ,i_β	$\alpha-\beta$ axis currents
K_{g1}	stiffness due to gas in cylinder 1
K_{g2}	stiffness due to gas in cylinder 2
K_{P_vec}	proportional gain of current control loop
K_{I_vec}	integration gain of current control loop
k_b	bulk modulus

k_g	bulk modulus of gas
k_{liq}	bulk modulus of liquid
k_v	viscous friction coefficient
k_{fs}	viscous friction coefficient of motor
k_{fF}	viscous friction coefficient of fluids in pipes
k_0	overall stiffness
L	pipe length
L_R, L_Y, L_B	self inductances of three phases
L_s, L_{s1}	values of self inductance
l_1	initial effective length of cylinder 1
l_2	initial effective length of cylinder 2
M_{fR}, M_{fY}, M_{fB}	mutual inductances between motor phase and equivalent circuit of magnet
M_{fM}	magnitude of mutual inductance
M_{RY}, M_{YB}, M_{BR}	mutual inductances between three phases
M_s, M_{s1}	values of mutual inductance
m, m_0	mass
m_s	mass of motor slider plus fluids in cylinders
m_F	mass of fluids in pipes
m_g	mass of gas
m_{liq}	mass of liquid
P, P_1	pressure
P	pole pitch of linear motor
P_0	initial pressure
p_1	ideal plant of IMC
Q	flow rate
Q_A, Q_C, Q_R, Q_P	flow rates at computational points
$Q_{1,NS}$, $Q_{2,1}$, $Q_{P2,1}$	flow rates at a junction
q, q_1	regulators of IMC
R	weighting factor of optimal tracking controller
r	input
T_{on_R}, T_{off_R}	on and off time periods of upper GTO in red phase
T_{on_Y}, T_{off_Y}	on and off time periods of upper GTO in yellow phase
T_{on_B}, T_{off_B}	on and off time periods of upper GTO in blue phase
T_s	sample period of position/velocity loops
t	time
t_P, t_R, t_S	time at computational points
t_s	sample period of current loop

u_d	input signal
V	volume
V, v_F	average velocity of fluid over a cross sectional area
V_{DC}	d.c. link voltage
V_g	volume of gas
V_{g0}	initial volume of gas
V_{liq}	volume of liquid
V_m	voltage magnitude
V_R, V_R'	voltage vectors
V_1, V_2	voltage vectors
V_1', V_2'	voltage vectors
v	velocity
$v(n)$	derived outer loop velocity
$v_1(n)$	derived inner loop velocity
v_d, v_q	d-q axis voltages
v_{d_ff}, v_{q_ff}	d-q voltages demanded by feedforward terms of current loop
v_{d_PI}, v_{q_PI}	d-q voltages demanded by feedback terms of current loop
v_R, v_Y, v_B	phase voltages
v_{ref}	reference velocity
v_{TOP}	top velocity
$\boldsymbol{X}$	state vector
x	position,
	distance along pipe
$x(n)$	position in discrete time
x_A, x_C, x_R, x_P	distances at computational points along a pipe
x_{ref}	reference position
Y	output vector
Z	elevation of a pipe
Z_f	impedance of equivalent circuit of magnet
ΔF_0	net force applied on slider
ΔP	pressure difference
Δt	time step
ΔV	volume difference
Δx	distance step
α	angle of a pipe from horizontal level
ϕ	phase angle
γ	electrical angle between stator and slider coordinates
	or electrical angle of motor slider

γ_1	electrical angle between stator and slider coordinates,
	angle of injected current in auto positioning
γ_2, γ_3	compensating angles for calculation of phase voltages
λ	multiplier in characteristic method
μ	viscosity
	Poisson' ratio of pipe material
θ	characteristic grid mesh ratio,
	load angle, current angle
θ_1	angle of phase voltage
ρ	frequency ratio
	mass density
ρ_g	density of gas
ρ_{liq}	density of liquid
τ_e	electrical time constant
ζ	interpolation constant in characteristics method

CHAPTER 1.

INTRODUCTION

1973 -- The Oil Crisis.

This crisis had a strong impact on industries and scientific researches and forced human beings to reconsider and change attitude of using resources granted by the nature. On one hand, producing oil and gas more effectively and using existing fields efficiently become more important issues in the oil industry. On the other hand, development of new technologies and new devices has been speeded up to provide system designs and applications with higher efficiency, lower costs and better reliability.

Development of a.c. motor drives in the last two decades is a typical example. There has been a surge of interest in the subject of variable speed a.c. drives since the crisis, for their ability to deliver energy and maintenance cost reductions and space savings by proving an adjustable speed capability, in accordance with motor load variation, and by eliminating mechanical or coupling gears. Great advancements in four major fields have made the development possible.

First of all, new power electronic devices, starting with the thyristor, then the power transistor and the power MOSFET, and more recently the Gate Turn Off thyristor (GTO) have enabled the switching of high power levels at high frequencies. Faster, smaller and cheaper switching devices are being produced as a result of the continuous work in solid state technology. Secondly, the vector control theory and the Pulse Width Modulation (PWM) technique are so well developed that a.c. motors can be controlled as easily as d.c. motors. The a.c. drives nowadays can compete in terms of performance and functions with d.c. drives in addition to many other advantages. Thirdly, constant development of control theory has enabled design of different controllers to tackle various problems and provide high performance. Modern control concepts such as the robust control, optimal control and adaptive control have been advanced and many applications have emerged. Finally, rapid progress of very large scale integrated circuits (VLSI) has resulted in the availability of powerful and inexpensive microprocessors with much reduced sizes. In power electronics equipment, microprocessors can be utilised not only to trigger power switching devices with complex switching patterns, but also to implement sophisticated digital control algorithms.

1.1. Motivation.

The oil crisis stimulated development in many areas and the oil industry now benefits from it as a consequence. This thesis presents a control design and real time control of a subsea oil - gas pump system using an a.c. motor drive, developed for offshore oil fields.

Currently, the number of new major oil and gas fields is reducing. The trend in the future of the oil industry will be the development of marginal fields. A key issue regarding marginal field development is transportation of hydrocarbons either to existing infrastructure or to land. A pump is needed to increase transportation capacity by increasing transportation velocity and increasing pressure and therefore compressing gas. This also improves reservoir recovery as the pressure of the well head is reduced and reduces the risk of hydrate formation.

Based on this assumption, Mobil Oil Corporation started a programme in 1989 to develop an electrical multiphase pump system primarily for subsea application.

1.2. System Description.

The pump system contains two pumps which are 90 degrees out of phase as shown in Figure 1.1. Constant flow rate can be obtained at input and output by combined movements of two pumps, hence pressures in the transportation pipes can be kept constant. The piston type pump is required to handle three phase fluids consisting of Oil, Gas and Sea water in unknown and varying ratios and the pump is to be designed to operate subsea to depths of 750 m and at distances of up to 200 km from surface point of supply.

Each pump consists of a single stage double acting reciprocating pump, the fluid circuits (the cylinders and the pipes), two parallel connected double sided permanent magnet linear synchronous motors (refer to subsequently as DPLSM), a power supply unit and control unit.

The motor converts electrical into mechanical power to drive the motor slider, which is directly coupled to two pistons heads. Non return valves located outside the cylinders work in accordance with the direction of the slider motion such that the cylinder at one side discharges fluids while the other sucks fluids. Maximum production capacity is 40,000 barrels per day, which is about 265 m^3 / *hour*.

1.3. Thesis Objectives

This thesis describes simulation, control design and real time controller implementation of the pump system. The direct aim of the control is quite straightforward, to drive the motor slider and the piston to follow defined position / velocity trajectories. However the work embraces a wide range of diverse disciplines and therefore yields many difficulties to be overcome, which are described as follows.

- <u>Electrical machines:</u> The machine employed in the system works as a motor, to convert electrical power to mechanical power and therefore to drive the pump. Since the DPLSM exhibits non linear, highly interacting multivariable characteristics, vector control is necessary to ensure that the a.c. motor behaves in a similar way to a d.c. motor. Modelling of the motor and the vector control are two basic tasks to be performed.

- <u>Power electronics:</u> The power electronics converts electrical power from fixed frequency and fixed amplitude a.c. to variable frequency and voltage a.c. to meet the requirement from the motor.

- <u>Fluid dynamics:</u> The dynamics of fluids in the pump and the pipes are of non linear and time varying nature. Gas is governed by the gas law, and liquids have the characteristics of distributed parameter system governed by two partial differential equations. Modelling of the fluid dynamics for the computer simulation, simplification of the model and bound of parameter uncertainty are key requirements for the control design.

- <u>Control Theory:</u> Control strategies are to be developed to ensure the stability, accuracy and overall performance of the system. One of the major difficulties in controlling such a pump is the rapid change and non linearity of the load conditions, which results in uncertainty of system dynamics and parameters and in the difficulty of identification. The controllers to be designed must be able to handle various loads and to maintain desired performance and stability.

- Microprocessors and Signal Processing: Microprocessors bridge the gap between the control action and the power electronics. The signal processing processes feedback signals, performs control algorithms and converts the control output into switching signals for the power electronics.

The control is of vital importance as a good performance of the pump system is demanded, and simulation provides the effective means of evaluating the control design. In the thesis, a mathematical model is established to simulate the overall system and a simplified model is developed to enable design of controllers for the system. The concept of system uncertainty is used in the control design. Different control approaches are investigated to ensure desirable control design. The proposed controllers are initially proved by full computer simulation. The last section of the thesis describes the design of the hardware and software for real time control. Implementation of the system design is realised on a scaled down DPLSM, and the proposed controllers are used to prove the control design.

1.4. Structure of The Thesis.

This thesis is organised as follows.

Chapter 2 presents the background of the project and relevant research work concerned with the permanent magnet linear synchronous machine (referred as PLSM), a. c. motor drives, novel power electronics and control theory. A literature review is included in the chapter as well.

In chapter 3, a general perspective of the project and the project requirement are presented. Motivations for adoption of the DPLSM, the piston type pump and the voltage source inverter are described. The operation of the pump system is described and the system parameters are also given in the chapter. Control strategy and design methodology are covered at the end of the chapter.

In chapter 4, a mathematical model is developed for the computer simulation of the pump. The model includes two parts: the dynamics of the moving slider connected with two piston heads and the fluid dynamics. A simplified model is then derived from the simulation results for the control design purpose. The parameter uncertainty of the simplified model is also studied.

Chapter 5 is allocated to the modelling of the motor. Results of the parameter test of the linear motor are presented at the beginning of the chapter. Two electrical models are established to simulate the motor based on the test parameters. One is a three phase model and the other is a d - q axis model. The parameter variations are considered in the modelling.

In chapter 6, an inner current control loop is designed to implement the vector control. A practical approach is investigated to identify the transfer function of the inner closed loop, to be used for the outer loop control design. A load angle control method is discussed to improve the inverter capacity and the power factor of the motor drive.

The design requirement is firstly specified in chapter 7 and designs of outer position controllers are explained in details. Those designed controllers are studied and evaluated in terms of performance, stability and robustness against system uncertainty. Digital control is also discussed in the chapter, which is necessary for implementation of the real time digital control and the computer simulation

In chapter 8, the full computer simulation of the overall system is carried out to assess the performance of the proposed control algorithms. Different load conditions are involved in the simulation. The load angle control is simulated as well.

Chapter 9 presents the hardware design of the real time control for the system. It includes system structure, selection and design of the microprocessors, position transducer and its interface, current transducer and its interface, power converter interface and communications.

Chapter 10 presents the software design of the real time control. Overall software structure, different modules with different functions, computing time, and software protection are explained in the chapter.

In chapter 11, the implementation of the entire real time control system using proposed controllers is carried out on a test rig, a scaled down DPLSM. A motor / generator (braking) operation is developed, where two sides of the machine are powered from two independent inverters which are controlled by two dedicated microcontrollers. The motor side is to perform the designed control system and the generator side is to simulate the load characteristics.

Chapter 12 covers conclusions arising from this work and possible further work.

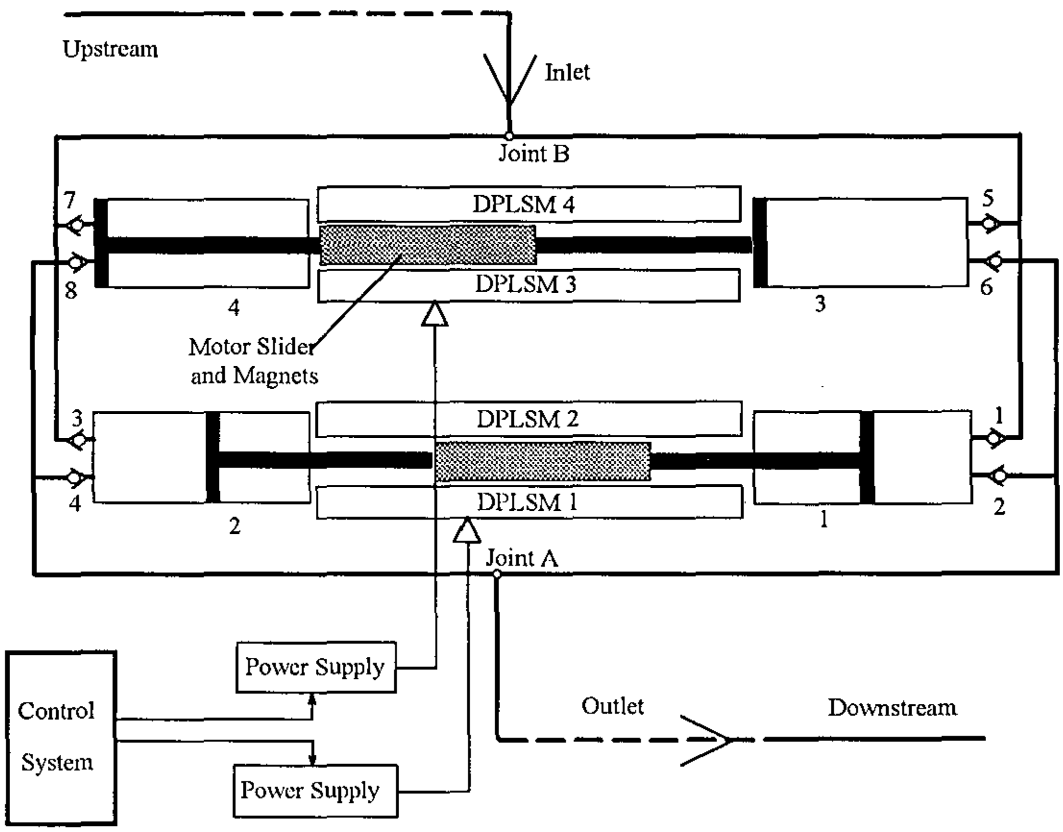

Figure 1.1. Configuration of The Pump System.

CHAPTER 2.

BACKGROUND

This chapter describes the background to the project and information relating to relevant research work. It is concerned with a.c. linear motor drive and control theory, development in both of which have been influenced by the revolutionary progress of microelectronics.

The background of the project is firstly presented in section 2.1. A review of the evolution of a.c. drive and linear motors is given in section 2.2. Relationship between the development of the microprocessors, power electronics and application of control theory is briefly described in the section 2.2 as well. Evolution of the control theory is reviewed in section 2.3. The literature review is covered in the last section.

2.1. Background of The Project

Initial attempts in offshore hydrocarbon exploitation occurred as early as 1896 off the coast of California, and were originally confined to fixed platforms. Until 1946 about nine wells were also drilled from rigid structures in the shallow coastal waters of the Gulf of Mexico off the Louisiana coast. The modern era in offshore oil activities started in 1947 when a mobile platform was used to drill a well 12 miles from the Louisiana shore. In the years since the advent of mobile platforms, there has been a corresponding increase in the demand for oil and gas and the scope of offshore exploration and development. There have been many novel technologies developed and applied in current offshore fields. Mobile rigs are mainly used for exploratory drilling due to their highly flexibility, and these can also be used in the production stages. However this approach is considered to be an inefficient use of equipment, especially in shallow waters, and as a result fixed structures or platforms have played a major role in the production process stage [1]. On the other hand, there have been some problems unsolved in the production process of offshore fields.

- In the current oil industry, the pressure of the reservoir drives the well stream (i.e. the pumped fluids) directly to the process module. At lower pressures, production capability is reduced, and injection of water is currently used to increase the well pressure. However the injected water is then mixed up with the oil such that production efficiency is reduced.

- Too many platforms are required. Each well head covers only a limited area of resource and many platforms are often required to cover a field. However, the platforms are very costly and it is not economically possible to cover the entire area of a field.

- Due to the reducing numbers of new major oil and gas fields and daily increasing demands, the trend future is the development of marginal fields. Those marginal fields include reservoirs of limited size and in areas of existing major fields which are not covered by platforms, and which are economically impossible to be developed by using platforms.

So, there has existed a need for a pump to increase transportation pressure and thereby to increase transportation capacity as velocity is increased and gas is compressed, to improve reservoir recovery as the pressure of the well head is reduced, to reduce numbers of platforms required as a flexible pump can replace some sub platforms and to reduce the risk of hydrate formation. Based on these factors, the project to develop a highly efficient and flexible electrical multiphase pumping system was initiated, primarily for subsea application.

The concept shows a variety of possible applications such as in surface installations either on a platform or on land, in marginal satellite fields, or in satellite fields with decreasing production pressure tied in to existing platforms with process facilities. The extreme approach would be to pump large amounts of unprocessed fluid directly to shore from remote well heads.

In addition to the need from oil industry, recent progress of necessary technologies has made it feasible to develop such a system, which is described in next two sections.

Since the project was started, a lot of progress has been made, including the design and manufacture of a prototype motor, a piston type pump and a scaled down motor. The prototype motor and the piston pump are utilised in a land based development system. The scaled down motor together with its dedicated equipment are used to simulate subsea operation.

An attempt to develop control algorithms for the system was performed where the concept of optimal control was used to design the position control loop and trial and error was used to select control gains for the current loop [20]. In the design of the position loop the motor dynamics and load characteristics were ignored and a linear time invariant second order model was used, in which only the mechanical time constant of the slider was involved. The design was evaluated by the scaled down motor with no load applied and by computer simulation based on the assumption that the load force is constant and does not affect the system dynamics. It seemed that performance was reasonable except for the size of the steady errors. However the controller is unlikely to work properly on the real system mainly because:

- The linear time invariant model is too simple to represent the real system as the actual system consists of not only the slider and pistons but also the fluids and electrical components such as the motor winding and the power inverter.

- The model dynamics vary with the ratio of oil - gas mixture in the system, while the optimal control requires sound knowledge of the system. The ratio of the mixture at any particular time instant is unknown and may change rapidly, i.e. there are great uncertainties in the system. Therefore uncertainties must be involved in control designs.

- The design of the current loop is of critical importance in order to achieve desirable overall performance of the system. More work could be done to study performance of the loop and the design is not isolated but related to the position control loop to ensure a proper design.

Therefore it is necessary to study the characteristics of the entire system, to establish proper models for the system and to design suitable controllers for both current loop and position loop. The control system to be designed should be stable and robust against variations of the system, should provide high overall performance in all load conditions, and should be able to eliminate steady error so as to achieve the best possible volumetric efficiency.

2.2. Evolution of Motor Drive and Linear Motor

Motor drive technology is mainly concerned with two disciplines - the electric motor and the power electronics. The invention of the motor was far earlier than that of the latter. The first primitive electric motor was built following Oersted's discovery of the magnet effect of an electric current in 1820. By 1890 the main types of rotating machine had been invented and next forty years was the golden age of machine development while electronics was in its infancy [2, 3].

The concept of linear machines is not new neither. The earliest linear electric motor can be traced back as early as 1838, only seven years after Faraday's discovery of the laws of induction. However no substantial use was made of the linear machine until Professor E. R. Laithwaite began work on linear induction motors in Manchester in the 1950. Surveys of recent progress in linear motors show that the major use of linear machines is for industrial purposes and so far the linear induction machine has played a dominant role and is now being challenged by linear synchronous motors [5, 6]. This challenge has only become economically possible with the reduction in price of high power semiconductor switching devices. The machines are produced mainly for low speed applications and are used in the mechanical handling, crane transportation and metal handling fields. Higher speed applications using linear motors are well known MAGLEV systems [5].

It is likely that forms of linear machines other than in induction will come into industrial use, and linear synchronous machines with permanent magnet excitation are being preferred for some applications. The technology enabling its development has become available over the last few years. Reliable inverter equipment can be designed, rare earth magnets including those using the relatively new neodymium-iron-boron material are marketed. It is no doubt that permanent magnet machines are more expensive than induction machines, but they can offer much improved performance and efficiency.

Until a decade ago, it was extremely difficult to drive an a. c. motor with adjustable speed. Unlike the control of a d.c. motor with clear, linear relationships between the state variables, there is not a clear separation of functions of an a.c. motor. With the progress of power electronics and microelectronics and the associated application hardware and software offering high reliability in a relatively compact form, various kinds of adjustable frequency and sine wave inverters have become available [7 - 9]. Especially, switching devices such as power transistors and gate turn-off thyristors have permitted a wide application of pulse width modulated voltage source inverters (VSI's). At the same time vector control theories have presented an opportunity to demonstrate high performance with a. c. motors.

In 1971 two important papers on the control of induction motor were published by Blashke and Shubenko, Shreiner and Gildebrand [6, 16, 17]. These proposed a method of control analogous to that of a d. c. machine and variously known as field oriented control, vector control, transvector control or transvektor control. The concept as originally put forward was difficult for the original engineers to grasp and the technology was not sufficiently well developed for easy implementation. However in 20 years since the original idea, much progress has been made [3, 4, 16, 17] and it appears likely that this will be the dominant technique in the future. Compared to the induction motor a synchronous motor is easier to control since its field orientation is known at all times .

As mentioned above, the role which the microprocessor technology has played in the development of the a.c. motor drive is apparent. With microprocessors, implementation of complex switching patterns of power electronics and of algorithms for the field oriented control can be all digitally realised with high flexibility and low cost. Also the microprocessors can be used to execute sophisticated control algorithms to improve the accuracy, stability and performance of the electric drives, where the control algorithms may be derived from either conventional approaches or modern control techniques.

2.3. Evolution of Control Theory

Feedback control mechanisms have been used for millennia. The first applications of the feedback principle can be traced back to ancient Greece: the water clock of Ktesibios (300 B.C.) employed a float regulator.

There have been several landmarks in development of the control theory. The first mathematical analysis of a feedback system via differential equations was presented by Maxwell (1868) and a mathematical theory of regulators was formulated by Vyshnegradskii (1877). The invention of the negative feedback amplifier at Bell Laboratories by Black prior to World War II marks another milestone in the use of feedback. The stability problems were explained through the frequency domain analysis techniques by Bode and Nyquist. The frequency domain techniques display a general robustness to parameter changes, which probably accounts for its popularity in the drive industry [4].

Modern control theory, mainly based on state space analysis, started to emerge in the late 1950's. The concept of optimal control was introduced where if the control objectives are formulated in terms of the integral square error (ISE) the optimal feedback controller can be found "analytically" without trial and error [39]. Meanwhile adaptive control has been well under development, which includes different approaches such as auto-tuning, model reference and self-tuning regulators [43]. Identification techniques, in addition to their other uses, have been progressed to support development of adaptive control theory [44].

A lot of attention has been paid to the issue of control system robustness since the late 1970's. Robust control addresses many issues of practical importance like model uncertainty and model error. Many control schemes have been developed concerning with the robustness of controllers. Various modelling methods [50, 51], syntheses for linear and non linear systems [52, 53], analyses in time domain and frequency domain [56, 57], and some applications have been presented [61, 62]. However robust control is still being under development and there has been no unique solution for various applications.

2.4. Literature Review

A fair amount of research has been done on drives of permanent magnet rotating motors. Most work has been concentrated on study of performance of the permanent magnet synchronous motor vector control [21 - 25] and some published papers have introduced position or speed control loops for their particular applications.

A servo drive system employing a permanent magnet rotary motor has been published by P. Pillay et al. [26], where a speed control loop and a current control loop are involved. The current control loop aims at controlling the three phase currents to follow the reference phase currents derived from d - q axis currents and the rotor position. A simple model using only the mechanical time constant of the motor has been used for the speed control loop and a pseudo-derivative feedback controller has been developed.

T. Liu et al developed a multiprocessor based fully digital control architecture for permanent magnet synchronous rotary motor [27]. Three control loops have been developed, which are the current loop, the speed loop and the position loop To obtain high sampling rate, two 32 bit MC68020 microprocessors are employed for executing three controllers in parallel. Modern control concepts such as H_2 and H_∞ were engaged in the design of the speed control loop, while proportional control is employed for the position loop.

D Naunin et al [28] and others [29, 30] have also presented some similar work. Most these studies are carried out for servo drives and at relatively low power level. The simplified linear models using mechanical time constant only have been often involved in the designs, and load conditions have hardly been considered.

On linear motor applications, recent surveys have been carried out by J.F. Eastham and G.W. McLean. Those surveys show that the PLSM is becoming an active area for study and is beginning to be preferred for some applications. However industrial applications are limited and little work has been published so far.

A microprocessor based controller for a PLSM has been presented by Glausen and Leonhard [31] used as a positioning drive. The motor employed in the application is at a much lower rating compared with the present application. An optimal control approach together with a speed loop has been developed, where the model of the motor and converter combination was assumed to be a double integrator model. The load dynamics and the friction effects were neglected, an assumption which is not valid for the subsea pump application.

A novel control scheme using a tri-state switching controller for a 400 W reciprocating linear motor has been investigated by R. Maresca [32]. It was a non linear control system which made use of phase locked loop techniques and the load characteristics were analysed. However controllers of this kind cannot achieve high dynamic performance and the load characteristic is different from the present application.

Force control of the PLSM has been presented by L. F. Goldberg, which was employed to test free-piston Stirling engines [33]. The PLSM was used as a load for the engine. The secondary of the motor, where the permanent magnets are mounted, was fixed, and the primary of the motor was the moving part. Control of the motor force was developed to follow demanded load characteristics and a number of different sensors such as force and acceleration sensors were employed.

One of the key features of the system described in this thesis, compared with the work just described, is that the present application can only have a position transducer and phase current sensors as feedback signals. Force and other sensors are not available for practical reasons. Moreover, the fundamental requirement for the subsea pump application is a position / velocity control scheme rather than the force control described in that paper.

CHAPTER 3.

DESCRIPTION OF THE PUMP SYSTEM.

This chapter describes the pump system and presents related information required for the thesis. The project requirement is firstly described in section 3.1, which sets out the final aim for the design of all elements employed in the system. Section 3.2 describes the motivations for adopting the piston type pump, the DPLSM and the VSI. Operational description of the pump system is covered in section 3.3. Control strategy and design methodology are discussed in sections 3.4 and 3.5 respectively. Mechanical and electrical parameters of the pump system are presented in section 3.6.

It should be noted that the author is not involved in the design of the motor and the pumps, and it is not therefore the author's intention to discuss these issues in any detail. Only basic concepts and design results related to this thesis are introduced.

3.1. Project Requirement

A requirement of the project was specified by Mobil Oil Corporation, which set up standards and guidelines for selection and design of the entire system. A list of the requirement is given as follows.

- Handle any gas/oil ratio
- Sustain rapid changes of ratio
- Increase the pressure by 35 bar
- Capacity > 40,000 barrels / day (265 m^3 / *hour*)
- Pump should be for operation in water depths down to 750 meters
- Minimum maintenance
- Life time 20 years.

The requirement was specified based on many factors, but especially well conditions. For example, a typical well will produce oil, gas, water and even sand particles. The nature of the well stream may vary considerably, and so it is required that the pump system should be multiphase and should function efficiently for all mixtures of water, oil and gases. The system will work in a deep sea environment, therefore it requires high reliability and must be substantially maintenance free.

3.2. Piston Type Pump, DPLSM and VSI Inverter.

The entire pump system includes four main units, these being the motor, the power inverter, the control and the pump. The control is the main work to be carried out in this thesis. The reason for adopting of the piston type pump, the DPLSM and the VSI are described in this section.

3.2.1. Piston Type Pump

As stated in the project requirement, the pump must be able to handle any ratio of oil gas mixture and maintain high pressure. This is first priority to be considered in the design of a pump, otherwise the whole project would be pointless. There are two groups of pumps: dynamic pumps and positive displacement pumps. The dynamic pumps work well with oil and water but pressure is dramatically reduced as gas concentration increases. Positive displacement pumps can be either screw pumps or piston pumps. Like dynamic pump, screw pumps work well with oil and water, but are also unable to maintain working pressure in high percentage gas mixture. However, piston pumps can deal with all conditions and pressure is almost constant for any gas oil ratio. Therefore this type of pump was chosen for this application.

3.2.2. DPLSM

The d.c. motor was the first practical device to convert electrical power into mechanical power. Inherently straightforward operating characteristics, flexible performance and high efficiency encouraged wide use of d.c. motors in many types of industrial drive application. However the d.c. motor drive has also many drawbacks when compared to a.c. motor drives. These include lack of robustness and overload capability, lower torque and speed bandwidths and the need for regular brush and commutator maintenance. The high maintenance requirement was the main reason that the d.c. motor was the first candidate excluded from consideration.

A.c. motors are widely used in industrial drive applications, mainly because of the low rotor inertia, lack of maintenance, long life and low cost. Although the a.c. motor exhibits a non linear, highly interacting multivariable control structure and hence a complex scheme is needed to obtain high performance variable speed control, these obstructions can be overcome by the introduction of microprocessors and novel power electronics.

The final choice is therefore between a linear motor or a rotary motor. If a rotary motor was selected, additional mechanical parts would have to be introduced to translate the rotational motion to a linear one such that it can drive the piston type pump. Such mechanical parts are not desirable in the system as they would introduce additional maintenance, especially since the inertia of the piston together with the variable load would place a high strain on the big-end bearings of the crank shaft.

The choice of a linear motor to meet the required specification results in a simplification of the mechanical drive train. It suffers from a lower efficiency, but this is not a dominant factor in the system specification. The complete concept offers the following advantages.

- Simple and rugged mechanical design. Only one moving part is needed. The power is magnetically coupled to the pump avoiding troublesome mechanical transmission elements.

- Minimum bearing forces occur. The only bearings needed are the guiding elements used to keep the slider in position relative to the stator.

- Cavitation damage in rotary pumps due to multi-phase pumping of oil and gas can be eliminated.

The main disadvantages are that the kinetic energy of the moving parts must be reversed every stroke and the surface speed of the secondary cannot be increased by using a gear-box. These drawbacks tend to increase difficulty of the control.

There are mainly two kinds of linear motor, the linear induction motor and the linear synchronous motor. To achieve a workable design, a permanent magnet synchronous motor using high performance magnet material was chosen despite the fact that the linear induction motor (referred as LIM) is likely to be less expensive. Main considerations for adopting this kind of the motor are given as follows.

- The PLSM exhibits attractive power density and efficiency characteristics, whereas the linear induction motor suffers from low efficiency and poor power factor.

- The end effect of a linear synchronous motor produces a considerably smaller reduction in performance than a linear induction motor.

- The PLSM has a large torque to inertia ratio. This allows an improved dynamic performance.

- With regard to the rating of the inverter, the PLSM has an advantage as long as field weakening is avoided. This is mainly due to the rotor losses in the LIM.

- Position control of the PLSM is simpler compared with the LIM.

A double sided short secondary construction was designed to reduce large normal reaction forces on the slider bearings. The slider contains the permanent magnet poles which are chevron shaped to reduce cogging forces. The motor has been designed and built: Figures 3.1 shows a picture of the slider with two piston heads connected at its end; Figure 3.2 is a picture of the motor stator in a container.

3.2.3. Inverter

Having decided to use a DPLSM for driving the pump, an inverter has to be selected. Inverters can be broadly divided into two classes, current source and voltage source. In a current source inverter, the current from the d.c. source is maintained at an effectively constant level, irrespective of load or inverter conditions. This is achieved by inserting a large inductor in series with the d.c. supply to enable changes of inverter voltage to be accommodated at low values of di/dt. The inductor must have an inductance of ten to twenty times the motor leakage inductance to smooth the rectifier ripples and to maintain current flow during commutation. The current source inverter is robust and provides very good performance. However for the highest performance requirements, the fastest possible response, the widest possible speed bandwidth, it leaves something to be desired. The speed of response is a big problem since the d.c. link inductor introduces significant lags into the control system [2].

A voltage source inverter operates from a constant d.c. link voltage, which is achieved by connecting a big capacitor in parallel with d.c. link. The voltage source inverter does not suffer from the sluggish dynamic performance as there is no inductor existing in the d.c. link, hence faster response is expected especially where the PWM strategy is used to control the inverter.

The voltage source inverter and the current source inverter have their own advantages and disadvantages. The voltage source inverter is preferred for the application mainly because the system requires fast responses to rapid load changes caused by the fluid dynamics.

3.3. Pump System.

The pump system consists of two horizontally opposed piston pairs. Each pair is driven by two parallel connected DPLSM. The complete configuration has been shown in Figure 1.1 in chapter 1 and Figure 3.3 gives the simplified diagram which shows the pumps and the fluid pipes only. Two piston pairs operate 90 degrees out of phase such that the combined input and output flow rate is constant. The reason behind the idea of constant flow is that the pressures at Joint A and Joint B can be assumed to be constant if the pressures upstream (i.e. the well) and downstream (i.e. the surface) of the transportation pipes are constant. The assumption is approximately true since pressures at the surface and well heads do not change rapidly and can remain stable for a relatively long period.

To ensure constant output flow consider the diagram in Figure 3.3. In the diagram, piston (1) is at the beginning of its suction stroke and hence piston (2), opposite to piston (1), is at the beginning of its pumping stroke. Piston (3), 90 degrees out of phase, is at the mid-point of its suction stroke and piston (4) is at the mid-point of its pumping stroke. The required velocity of each piston to achieve constant flow is shown in Figure 3.4. In order to meet the production requirement, a peak velocity of 4.2 m/s has to be achieved. The stroke length of each piston is 1.5 m and the period for a complete cycle which reaches the top speed is 1.429 s. In order to achieve the peak velocity in such a time, the required acceleration is 11.76 m/s^2. The profiles for a single piston are shown in Figure 3.5. Hence it can be seen that each DPLSM must follow a constant acceleration / deceleration profile over every cycle. The effect of running the two piston pairs 90 degrees out of phase and having each piston pair on both halves of the cycle is to produce a constant output of oil/gas equivalent to the velocity of 4.2 m/s, which gives the flow rate 267.2 m^3/hr and therefore the production 40,310 barrels/day to meet the requirement.

The motive force produced by the DPLSM is used to accelerate the piston and the oil/gas mixture in the cylinder, in the pipe between the cylinders and Joint A (referred as the outlet pipe) and in the pipe between the cylinders and Joint B (referred as the inlet pipe) as well as to overcome a pressure due to static column of oil in the transportation pipes between the upstream end and Joint A.

As mentioned above, there are non return valves at the junctions between the cylinders and pipes. When the slider moves from one end to the other end, say from left to right, there are three different stages in terms of the valves' on and off states regardless of the nature of the fluids.

- Stage 1: All valves are closed, pressure is increased in the cylinder 1 and decreased in the cylinder 2 when the slider starts moving towards the right end. High stiffness exists in both cylinders because of the compressibility of fluids.

- Stage 2: When the pressure in the cylinder 2 is lower than that in the inlet pipe, valve 3 opens. High stiffness still exists in the cylinder 1 but the dynamics of fluid in the inlet pipe and the cylinder 2 affect the characteristics of the load on the left side.

- Stage 3: When the slider moves further to the right, the pressure in the cylinder 1 will be higher than that in the outlet pipe and valve 2 opens. The characteristics of the load are determined by the fluid dynamics of both inlet and outlet pipes.

When direction of the movement is reversed, the pressure drops in the cylinder 1 and rises in the cylinder 2 such that valves 2 and 3 are closed. Then the pump repeats the same stages in the opposite direction with valves 1 and 4 in action.

The pump goes through three stages in every stroke. The time of every stage depends on the ratio of oil - gas mixture. The higher the percentage of oil the higher the stiffness, and hence the quicker the pressure builds up in the cylinder, This shortens the stage 1 and stage 2 times and extends stage 3. The reverse occurs for a high percentage of gas.

It should be noted that absolute steady flow cannot be achieved due to the effect of fluid compressibility, even if the demanded velocity profiles were followed ideally.

3.4. Control Strategy.

As described above, the two pumps in the system work in 90 degrees out of phase and hence require two dedicated power supplies with relatively independent controllers, although an overall supervisory control is needed to create and monitor the two reference profiles. On the other hand, the same control algorithms can be employed by both controllers since the same system configuration and parameters, and therefore the same dynamics, are applied to the two pumps. This means that the system can be analysed and the control algorithms developed based on one pump only, and this is the general approach used hereafter in this thesis. Under this assumption, the dynamics of the fluids involved in the system are restricted to that in the inlet and outlet pipes. Neither pipe has been given a fixed length at this stage because the length will be related to the actual conditions surrounding a particular subsea well head. A range of the lengths has been defined to allow for these conditions, and the controller will be designed to be able to handle the various lengths of the inlet and outlet pipes.

As well as achieving the desired velocity profiles, the control system must ensure that the motor slider and hence the piston remain within the limit of the cylinders to avoid any damage of the pump. On the other hand, either of the piston heads must be as close to the relative cylinder end as possible at every end of stroke to achieve the best volumetric efficiency. A target of the accuracy at stroke end is set to be 5 *mm*. Those restrictions on the position mean that the best control scheme to employ is position control rather than direct velocity control. The demanded velocity profiles will be ensured if the position control is achieved. Also an inner current loop is needed for implementing the vector control so that linear characteristics of the a. c. motor can be obtained.

Figure 3.6 gives a schematic of the drive system, which contains the fluid circuit, the motor slider and the piston, the PWM controlled voltage source inverter, the interface circuits between the microprocessor and the other hardware, the current loop with the vector control, the outer position control loop, the feedback current sensors and the position transducer. The complete system is to be controlled by an Intel 80C196 microcontroller via the use of relevant algorithms implemented in the software, as shown in the dashed block of Figure 3.6. The entire control can be partitioned into five main sections described as follows.

- PWM module. This module converts the three phase voltage command signals from the current control loop into the pulses for firing the inverter power devices. The voltage of each phase is compared with a triangular carrier and the points of intersection of two waves define inverter switching instants. The inverter output is then a rectangular wave, the width of which is proportional to the required voltage so as to create a fundamental component at the signal frequency. The frequency of the carrier signal is much higher than that of fundamental component so that the harmonics in the motor current are small.

- Inner Current Control Loop. A prerequisite for high performance position control in an adjustable speed a.c. drive is fast control of motor force. The purpose of this inner current control is to produce a force on the slider which follows the force demanded by the outer position control loop. This is achieved by the use of the vector control. It calls for transformation of the stator current vector into a moving frame of reference given by the slider permanent pole centre. By splitting the transformed stator current vector into direct and quadrature components, inputs for decoupled control of the necessary flux and force are obtained much as occurs in a separately excited d.c. motor. For this application the direct component is not necessary as the permanent magnet produces the flux, which is in fixed relation to the slider position. The phase currents and the slider position must be fed back to close the control loop as shown in Figure 3.6. In the design of the controller, the inner loop bandwidth should be made significantly higher than that of outer loop position control in order to ensure the accurate responses and the robustness of the complete control system.

- Outer Position Control Loop. The position loop controls the slider to follow the reference position demanded by the trajectory generator. Fluid in the cylinders and the pipes is accelerated and decelerated as the slider and hence the piston moves. The actual position is fed back from the position transducer and compared with the reference position. Any error between the actual position and reference position will be used in the control compensator to produce a demand for a correcting force from the inner current loop. In addition, feedforward terms may be used in a variety of ways to improve the tracking performance.

- Reference Generator. The reference generator calculates the demanded position, velocity and acceleration signals according to a demanded pump flow rate. Constant acceleration of the piston is required up to midpoint of each stroke and constant deceleration is required for the rest of the stroke such that the velocity follows a triangular profile and the position follows a quadratic waveform.

- Supervisory Control. As well as managing the phase difference between the two pumps, the supervisory control will perform many other functions, which can be performed by software only and hence no extra cost is needed as a microcontroller is to be employed. Those additional functions are:

  Interfacing - Reading and validating commands via interface card.

  Monitoring - Recording of relevant control parameters during the operation so that the performance can be analysed and the control errors of the current and position loops can be checked against the reference to ensure correct operation.

  Protection - If one of the control error becomes dangerously high, power failure occurs or overload conditions happen, appropriate actions will be triggered to avoid any damages. The action will include emergency shutdown, slow down, or a warning signal.

  Ramp up and ramp down - To avoid rapid change of the flow rate, the demanded profiles have to be increased or decreased smoothly.

  Initial Position Searching - It will also search for the initial absolute position of the slider after the system is powered up since an incremental position transducer is used to measure the position.

3.5. Methodology of Control Design.

Modelling, Design, Evaluation and Implementation is the procedure commonly used in control system designs. The modelling is the first step, which sets up the dynamic characteristics of a system to be controlled. The model could be formulated either in transfer function form or state space form or both, depending on what design approaches are to be used. The next step is to decide the structure and parameters of the controllers to be used. Many approaches are available after nearly a hundred years development of the control theory. However there is no systematic method for all applications and different methods may be preferred for various problems. Evaluation is a very important step towards a desirable design. It verifies designs in terms of accuracy, stability, robustness and overall performance. The evaluation can be carried out with some design software packages and computer simulation to achieve high efficiency and effective analysis. Implementation is the final step and also the target of the control system design, since proper design must ultimately be proved on the real system. The implementation normally comes through the design of hardware and real time software.

This thesis is basically following a similar procedure to design the controller for the pump system. A highlight of the main work in each step is described as follows:

- Modelling. The pump system must be able to handle any oil - gas mixture. Since the characteristics of oil are completely different from that of gas, different models are necessary for gas and oil respectively. The gas law is used to represent the dynamics when there is pure gas or predominantly gas, whereas two partial differential equations for the fluid dynamics, the equation of momentum and the equation of continuity are used to model the oil or oil dominant case. All equations are non linear and the latter two have the characteristics of a distributed parameter system. Compared with fluid dynamics, the model of the electrical model is simpler although it is also non linear. Moreover there are two kinds of variation in terms of the system dynamics and parameters. One is the variation due to the change of oil - gas mixture rate, which could be rapid. The other is the variation caused by different pumping stages. Various conditions and parameters have to be used in different pumping stages as different sections of the fluid circuit and valves are to be involved in each stage. The pumping stage changes from one to another in short time period and the time period of the each stage varies depending upon the actual mixture.

- Control Approaches. There are two kinds of approach available to deal with variations: adaptive control and robust control. Adaptive control sets up a dynamic controller which varies as the system alters in order to achieve the desired performance. Its best performance is achieved on linear system with fixed dynamic structure and slow parameter variations. However the system under consideration is a distributed parameter system with high non linearity and rapid variation in both its dynamics and its parameters. Moreover a model for the oil - gas mixture is not obtainable due to complexity and varying formats of the mixture. Thus it is extremely difficult to introduce adaptive algorithms for the system control. The only possibility left is to design a control with fixed structure and fixed parameters, which has best robustness against system variations i.e. works well in all conditions. Although the dynamics of oil - gas in any mixture is too difficult and too complicated to model, they are between the pure oil and pure gas cases, from which a bound of the variations can be worked out. Based on this concept, a simplified model with uncertainty bound needs to be derived to enable the control design.

- Simplified Model. It is desirable to develop a linear model to represent the system with defined uncertainties for the purpose of designing the controllers. That means that simplification and linearisation of the system are needed. On the other hand, the linear model must have the major properties of the real system so that controllers to be designed based on the model are valid. In this thesis, both analysis of the system characteristics and computer simulation are involved to develop such a model. Full computer simulation is carried out to validate the simplification. The model will be partitioned into two parts, one for the electrical motor and the other for the slider, piston and fluid dynamics.

- Control Design. Having decided to employ a control with high robustness for the system, there are many approaches to choose from. It is neither practical nor meaningful to go through all methods and thus three selected methods are to be designed and evaluated, which internal model control, cascade control and optimal tracking. A control design software package SIMBOL is used during the design and initial evaluation. Accuracy, stability, robustness, disturbance rejection and overall performance of every controller are analysed and compared. Feedforward terms are introduced to improve the tracking performance. For full computer simulation and real system control, the developed controllers are to be converted into digital format. Consideration for the conversion is part of the design task.

- Full Evaluation. Although the model developed in the first stage is too complicated to serve the design purpose, it more accurately represents the characteristics of the pump system and provides more effective means of assessing the design. Thus simulation software using the model and the digital controller is used for the full evaluation. Simulations for the different pipes length and load conditions are carried out for proving the design.

- Implementation. Implementation is the final confirmation of the control design. It requires design of necessary hardware and real time control software. Since the full scale system has not been available yet, it has been carried out on a scaled down DPLSM. The two stators of the double sided machine are powered and controlled separately to act as a motor and a generator respectively. The motor side is to simulate the control system. It includes a hardware interface, the microcontroller and real time software which computes control algorithms for all the control loops. The generator side, equipped with a dedicated hardware interface, microcontroller and software for the load force control, controls the machine to follow defined opposing force patterns so as to simulate the load characteristics.

3.6. System Parameters.

The motor and the piston pump has been designed and built. Electrical and mechanical parameters of the pump system are given as follows.

Stroke length	1500 mm
Minimum time per cycle	1.429 s
Maximum velocity	4.20 m/s
Average velocity	2.10 m/s
Acceleration	11.76 m/s^2
Discharge rate	267.2 m^3/hr
Diameter of piston	150 mm
Length of piston	3700 mm
Distance between two cylinder ends	5220 mm

Diameter of inlet pipe	100 - 150 mm
Diameter of outlet pipe	100 - 150 mm
Length of inlet pipe	10 - 40 m
Length of outlet pipe	10 - 40 m
Inlet pressure	35 bar
Outlet pressure	70 bar
Total mass of moving part	1400 kg
Viscous friction coefficient	60 - 120 $N \cdot s/m$
Length of slider	2700 mm
Number of the magnet poles	18
Pole pitch	150 mm
Slot width	13 mm
Tooth width	12 mm
Slot depth	40 mm
Air gap	3.0 mm
Winding:	3 phase
	2 slots per pole per phase
	5/6 chorded
Armature resistance per phase	0.07585 Ω
Self inductance per phase	3.227 ± mH
Mutual inductance per phase	-1.112 ± mH
Assumed equivalent current in slider	1.0 A
Peak mutual inductance between stator coil and equivalent circuit	4.983 H
Main power supply (line)	660 V, 50 Hz
Frequency	0 - 14.0 Hz

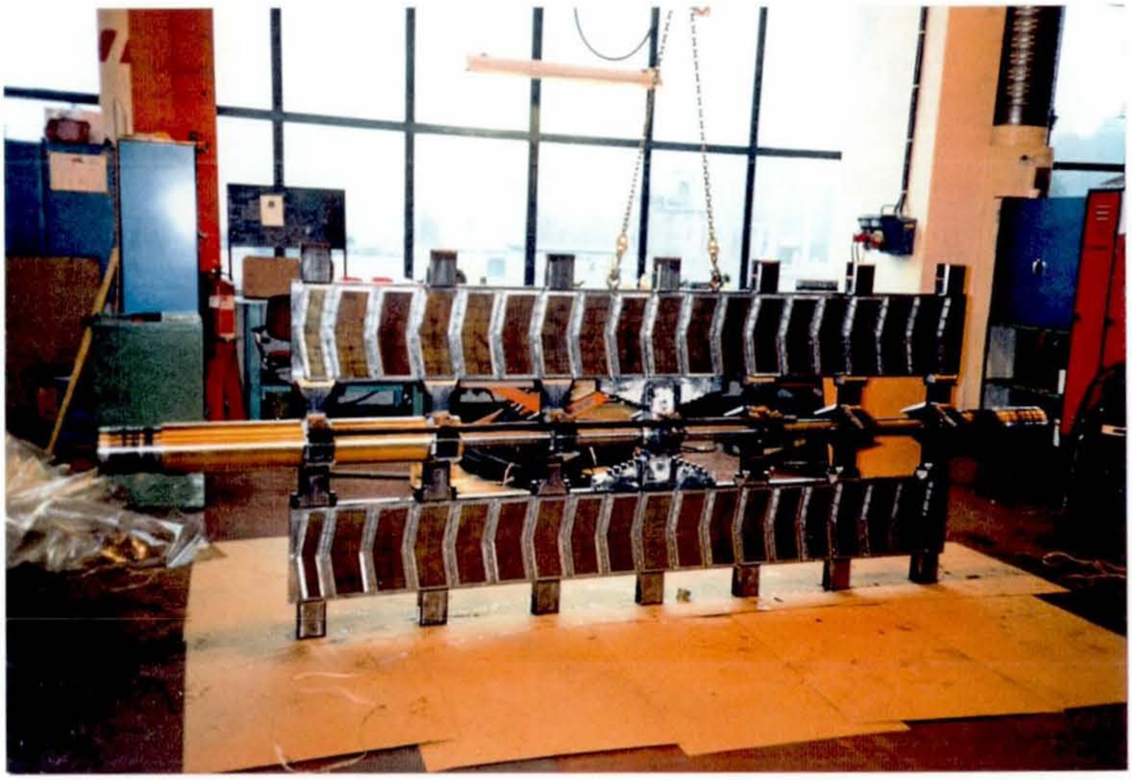

Figure 3.1. Picture of the motor slider with the piston

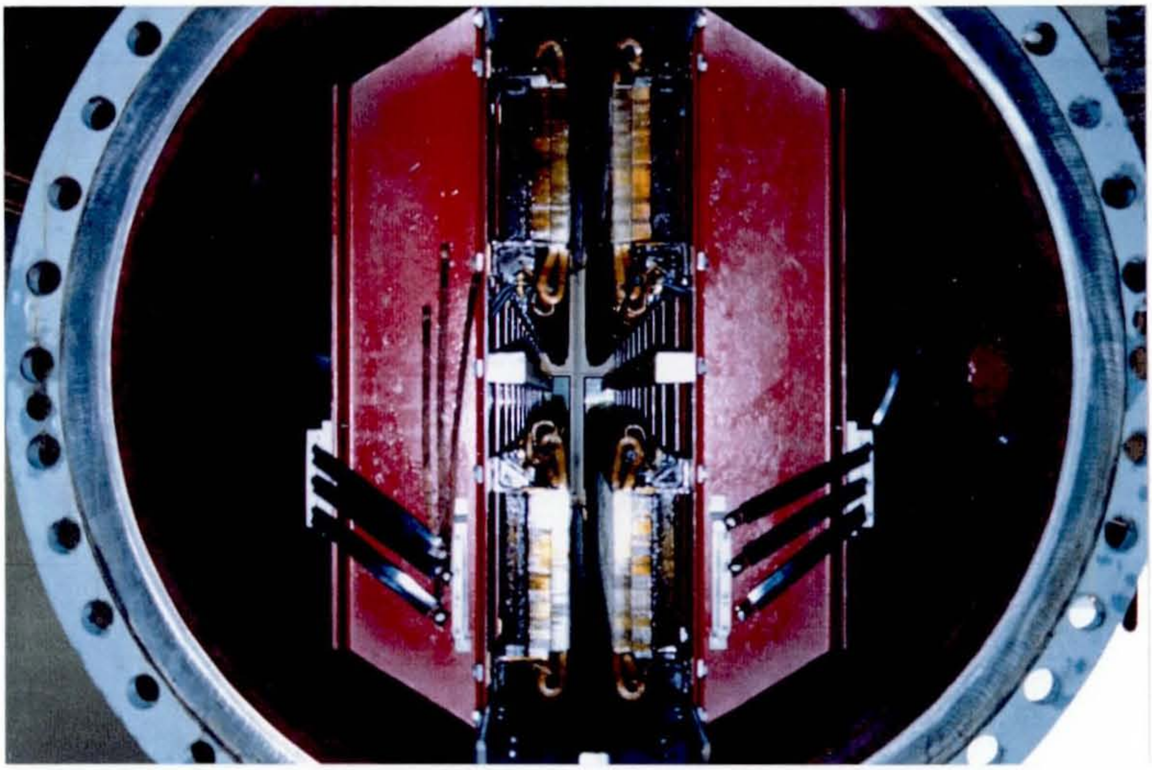

Figure 3.2. Picture of the motor stator in the motor container

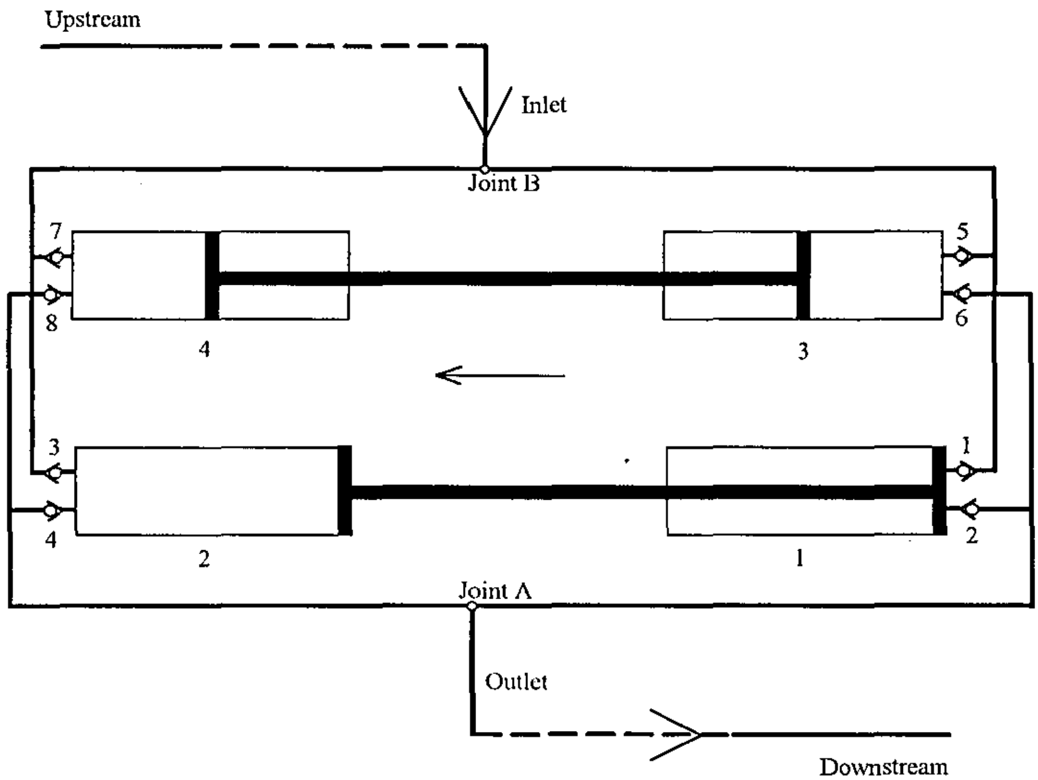

Figure 3.3. Oil / Gas Flow Into and Out of the Pump

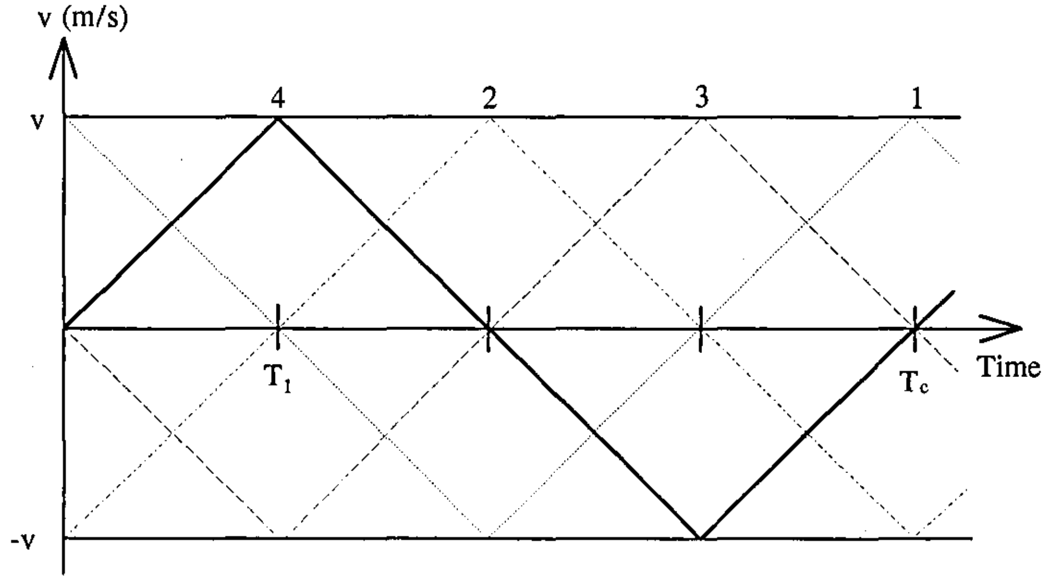

T_c = cycle time, T_1 = time of pump status shown in Fig. 3.3
v = total pump flow rate

Figure 3.4. Velocity Profiles for Each Piston

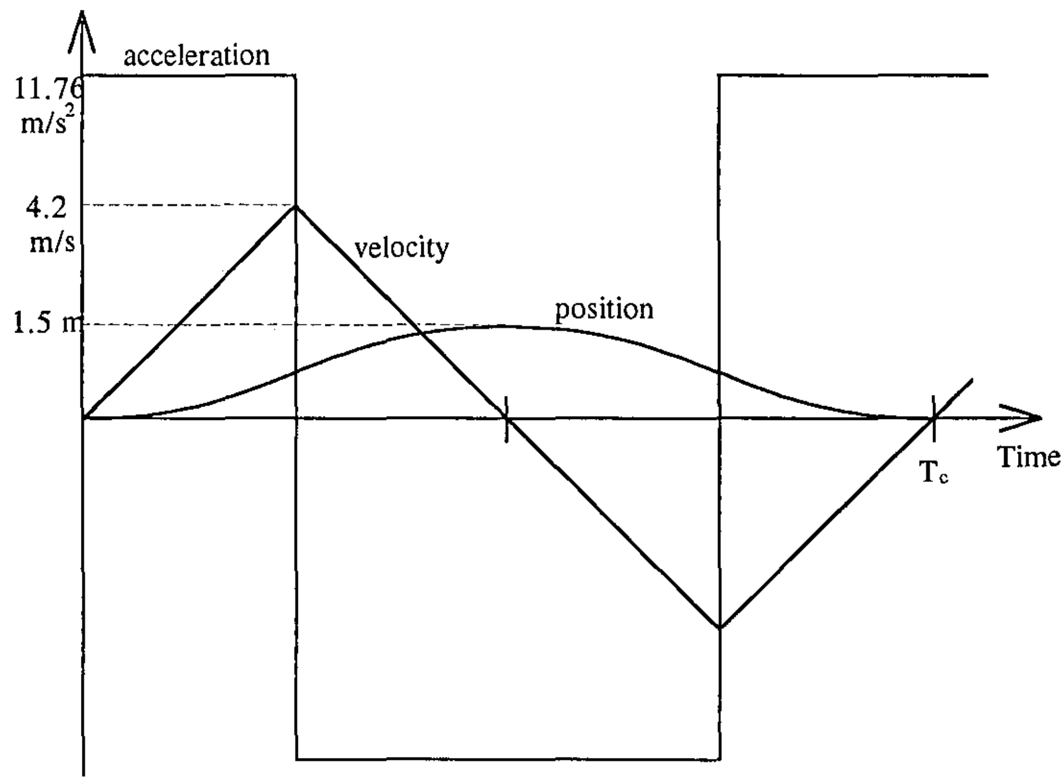

Figure 3.5. Reference Profiles for a Single Piston

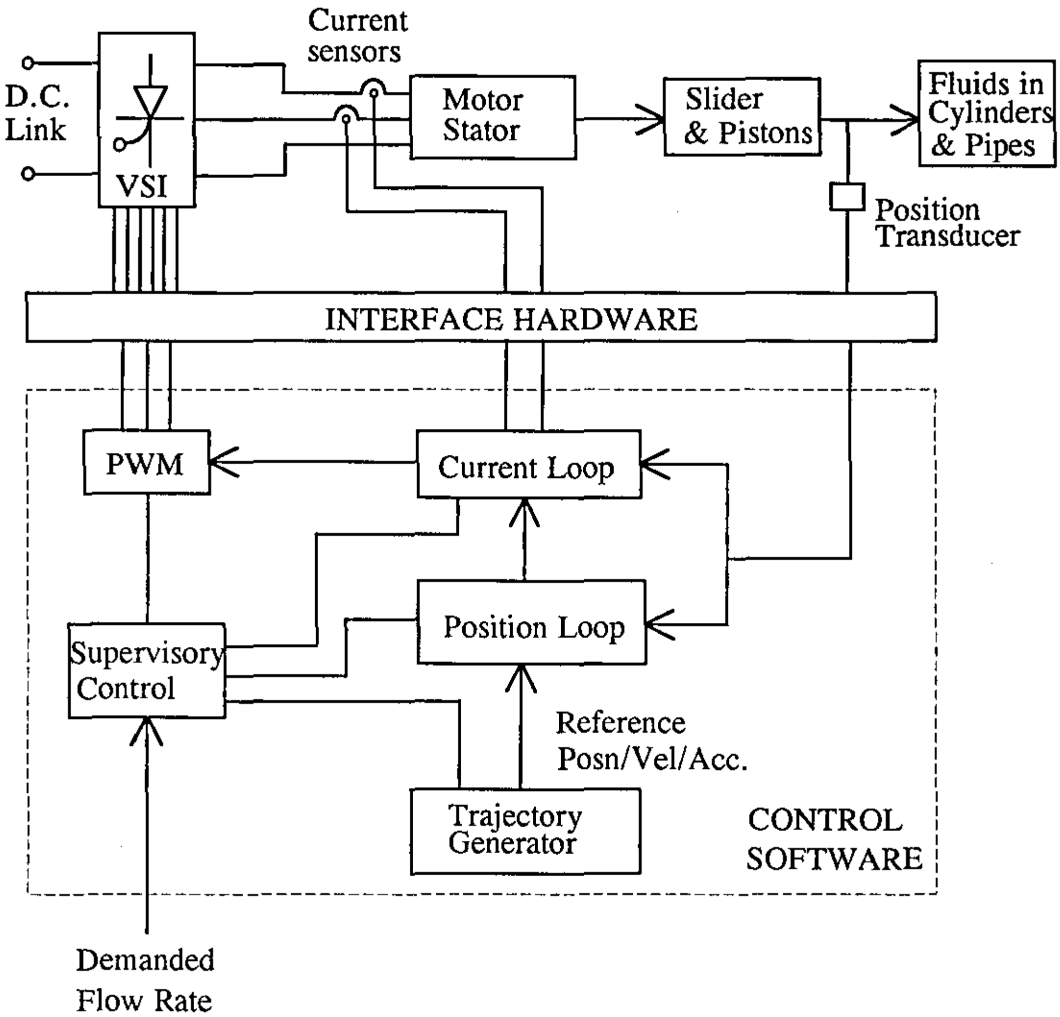

Figure 3.6. Schematic of Drive System.

CHAPTER 4.

MODELLING OF THE PUMP AND FLUIDS

Modelling of the pump system can be partitioned into two parts: the electrical model of the motor and the mechanical model of the motor slider, pistons and fluids. This chapter presents the modelling of the mechanical part.

Accuracy and simplicity are two important issues which must be addressed when a model is developed. Very often the two issues are in conflict with each other. From the simulation point of view, it is desirable to have a precise model and in many cases a reasonably complex model is acceptable if a powerful computer is to be used to perform the task, although some simplifications have to be made and it also means probably a lot more programming work. However a perfect representation of a real system is not possible, and compromises between the two objectives always have to be made when a model is established. On the other hand, a complex model tends to increase the difficulty in control designs since a real system tends to be high order and to some extent non linear, and also may be time varying as in this case. In this chapter two different models of the system are developed for the simulation and the control design respectively. A full model is firstly developed for the computer simulation where the principles of the fluid mechanics are utilised. Secondly a simplified model for the purposes of control design is derived from the complex model via the analysis and the simulation. The control design will be valid so long as the simplification does not neglect any major properties of the system.

The fluids to be pumped can be further divided into two groups, liquids and gases. Liquids and gases have fundamentally different characteristics, principally because they differ in their behaviour when compressed. When a liquid is compressed, it changes volume only slightly compared with the volume change a gas would undergo when exposed to the same pressure. At higher pressures, the relative change in air volume is smaller, but the difference between air and liquid compressibility will always be several orders of magnitude. Fundamental models to simulate fluids have to be related to the nature of the fluids, and the mechanics of real fluids are almost always based upon a continuum model which asserts that a fluid does not consist of discrete particles but is rather a continuum within which the variation of properties from one point to another occurs continuously and not by discrete steps [64].

In this chapter, simulation models for the slider mechanics, dynamics of pure oil and characteristics of pure gas are introduced in sections 4.1, 4.2 and 4.3 respectively. In section 4.4, an open loop simulation is carried out to investigate system characteristics via the step responses. The simulation results are also presented and analysed in section 4.4. Then a simplified model for control design purpose is derived in section 4.5. Uncertainty bounds of the simplified model are derived from extreme load conditions, which is also given in section 4.5.

4.1. Simulation Model of Motor Slider and Pistons.

The control strategy aims to control the position of the motor slider and therefore the desired output of the model is the position. The total force applied on the slider will be the driving force produced by the motor minus the resistive load force from pumped fluids. To obtain the model having the position x and therefore velocity v as its output, Newton's Law must be introduced concerning the total mass of the moving part and viscous friction.

$$m \cdot \frac{d^2 x}{dt^2} + k_v \cdot \frac{dx}{dt} = F - F_L \qquad (4\text{-}1)$$

In order for a computer to implement the model, it is preferable to have it in state space form. A second order model requires two variables, the most straight forward two being position and velocity. Hence the state space model can be written down directly as:

$$\frac{d}{dt}\begin{bmatrix} x \\ v \end{bmatrix} = \begin{bmatrix} 0 & 1 \\ 0 & -k_v/m \end{bmatrix} \cdot \begin{bmatrix} x \\ v \end{bmatrix} + \begin{bmatrix} 0 \\ 1/m \end{bmatrix} \cdot [F - F_L] \qquad (4\text{-}2)$$

Equation 4-2 gives a mathematical model in the form which can be implemented in the computer simulation.

Equation 4-1 (or 4-2) gives the dynamics of the slider and pistons, which would be a linear, time invariant second order system if the load force is irrelevant to the system dynamics. However the dynamics of the system are greatly affected by the load force F_L. It will in fact be dominant in the equation since it represents the output of the pumping action. If it were not dominant, it would mean that the pump is somewhat inefficient. It also represents the largest uncertainty because of the variability of the fluids being pumped. Therefore equation 4.1 or 4.2 is insufficient for either the simulation or the control design. To complete the modelling, the characteristics of fluids must be included to replace the load force F_L in the above equations.

4.2. Simulation Model of Pure Oil.

The flow processes of any liquids are governed by two differential equations, the momentum equation and the continuity equation. These two equations are very complicated and difficult to analyse. They are normally simplified in many cases by assuming that flows are steady.

The aim of the model being developed in this section is to simulate an unsteady flow of oil in two pipe sections, the inlet and the outlet pipes, and to study the effect of fluid transients on the system.

4.2.1. Momentum Equation

The momentum equation for a compressive liquid flow through a cylindrical tube in the longitudinal direction (x) is utilised. The equation is in terms of centreline pressure $P(x,t)$ and average velocity $V(x,t)$ over the cross area. It is then converted into a form using the hydraulic grade line $H(x,t)$ sometimes called piezometric head, or in short, the head, which essentially gives the pressure changes with the effect caused by variations in the height Z.

$$\frac{1}{\rho}\cdot\frac{\partial P}{\partial x}+V\cdot\frac{\partial V}{\partial x}+\frac{\partial V}{\partial t}+g\cdot\frac{\partial Z}{\partial x}+f_D\cdot V\cdot|V|+f_H\cdot V=0 \qquad (4\text{-}3)$$

where Z is elevation of a pipe, g is gravity, ρ is density, D is diameter of the pipe, $f_H=32\cdot\mu\cdot L/(\rho\cdot g\cdot D^2)$ is Hagen-Poiseuille friction coefficient where μ is viscosity of fluid, $f_D=f\cdot L/(2\cdot g\cdot D)$ where f is Darcy-Weibach friction factor.

The head $H(x,t)$ may replace $P(x,t)$ using the equation

$$P=\rho\cdot g\cdot(H-Z) \qquad (4\text{-}4)$$

$$\frac{\partial P}{\partial x} = \rho \cdot g \cdot (\frac{\partial H}{\partial x} - \frac{\partial Z}{\partial x}) \tag{4-5}$$

This partial differentiation assumes the density ρ to be substantially constant in comparison with H or Z. Equation 4-3 can then be replaced by: [64 - 67]

$$g \cdot \frac{\partial H}{\partial x} + V \cdot \frac{\partial V}{\partial x} + \frac{\partial V}{\partial t} + f_D \cdot V \cdot |V| + f_H \cdot V = 0 \tag{4-6}$$

4.2.2. Continuity Equation

The continuity equation is developed from the general principle of conservation of mass.

$$\frac{\partial(\rho \cdot A)}{\partial t} + \frac{\partial(\rho \cdot A \cdot V)}{\partial x} = 0 \tag{4-7}$$

by derivation, [64 - 67]

$$V \frac{\partial H}{\partial x} + \frac{\partial H}{\partial t} - V \cdot \sin\alpha + \frac{a^2}{g} \cdot \frac{\partial V}{\partial x} = 0 \tag{4-8}$$

where:

$$a^2 = \frac{k_b / \rho}{1 + (2k / E_R)(1+\mu)} \approx k_b / \rho \tag{4-9}$$

a is wave speed, k_b is bulk modulus of elasticity of fluid, E_R and μ represent the modulus of rigidity and Poisson's ratio of the pipe material respectively.

4.2.3. Solution By Characteristics Method

The equations which describe fluid flows are non linear partial differential equations with various boundary conditions. No general solution of these equations has been found so far and there is therefore no general theoretical treatment of the fluid motion. However, the general equations do serve to define the scope of any problem involving fluids. In many instances certain approximations can be made which reduce the complexity of these equations and permit solutions accurate enough for most purposes [66, 67]. In this section, the method of characteristics is used to transform the partial differential equations into particular normal differential equations. These latter equations may then be integrated to yield finite difference equations which are conveniently handled numerically in the computer simulation.

The continuity and momentum equations 4-6 and 4-8 form a pair of quasi-linear hyperbolic partial differential equations in terms of two dependent variables, velocity and hydraulic-grade-line elevation, and two independent variables, distance along the pipe and time. The equations are transformed into four ordinary differential equations by the characteristics method [66, 67].

The two equations of motion and continuity are identified as E_1 and E_2

$$E_1 = g \cdot \frac{\partial H}{\partial x} + V \cdot \frac{\partial V}{\partial x} + \frac{\partial V}{\partial t} + f_D \cdot V \cdot |V| + f_H \cdot V = 0 \tag{4-10}$$

$$E_2 = V \cdot \frac{\partial H}{\partial x} + \frac{\partial H}{\partial t} - V \cdot \sin\alpha + \frac{a^2}{g} \cdot \frac{\partial V}{\partial x} = 0 \tag{4-11}$$

The equations are combined linearly using an unknown multiplier λ, which is a standard mathematical procedure and dimension of λ is s^{-1}.

$$E = E_1 + \lambda \cdot E_2 = 0$$

Therefore:

$$\lambda\left[\frac{\partial H}{\partial x}\left(V + \frac{g}{\lambda}\right) + \frac{\partial H}{\partial t}\right] + \left[\frac{\partial V}{\partial x}\left(V + \frac{a^2}{g}\lambda\right) + \frac{\partial V}{\partial t}\right] - \lambda V \sin\alpha + f_D \cdot V|V| + f_H \cdot V = 0$$

(4-12)

Any two real, distinct values of λ will again yield two equations in terms of the two dependent variable H and V which in every way are equivalent to equations 4-10 and 4-11. Appropriate selection of two particular values of λ leads to simplification of equation 4-12. In general both H and V are functions of x and t. For each small section of the fluid, position x is function of time t and

$$\frac{dx}{dt} = V + \frac{g}{\lambda} = V + \frac{a^2}{g} \cdot \lambda \tag{4-13}$$

Equation 4-12 becomes the ordinary equation:

$$\lambda \cdot \frac{dH}{dt} + \frac{dV}{dt} - \lambda \cdot V \cdot \sin\alpha + f_D \cdot V \cdot |V| + f_H \cdot V = 0 \tag{4-14}$$

In this case, λ takes values

$$\lambda = \pm\frac{g}{a} \tag{4-15}$$

$$\frac{dx}{dt} = V \pm a \tag{4-16}$$

Substituting equation 4-15 into 4-12 and combining with 4-16 lead to two pairs of equations which are grouped and identified as C^+ (4-17 & 4-18) and C^- (4-19 & 4-20) equations.

$$\frac{g}{a} \cdot \frac{dH}{dt} + \frac{dV}{dt} - \frac{g}{a} \cdot V \cdot \sin\alpha + f_D \cdot V \cdot |V| + f_H \cdot V = 0 \tag{4-17}$$

$$\frac{dx}{dt} = V + a \tag{4-18}$$

$$-\frac{g}{a} \cdot \frac{dH}{dt} + \frac{dV}{dt} + \frac{g}{a} \cdot V \cdot \sin\alpha + f_D \cdot V \cdot |V| + f_H \cdot V = 0 \tag{4-19}$$

$$\frac{dx}{dt} = V - a \tag{4-20}$$

Thus two real values of λ have been used to convert the original two partial differential equations to two total differential equations, equations 4-17 and 4-19, each with the restriction that it is valid only when the respective equations 4-18 and 4-20 are valid.

It is convenient to visualise the solution as it develops on the independent variable plane, i.e. the *xt* plane. Equation 4-18 plots as a straight line on the *xt* plane; and similarly equation 4-20 plots as a straight line given in Figure 4.1. These lines on the *xt* plane are the "characteristic" line along which equations 4-17 and 4-19 are valid. The latter equations are referred to as compatibility equations, each one being valid only on the appropriate characteristic line.

Multiplying each of equations 4-17, 4-18, 4-19 and 4-20 by dt and using a first order approximation, the finite difference form of the equations can be obtained:

$$H_P - H_R + \frac{a}{gA}(Q_P - Q_R) - \frac{Q_R \Delta t}{A}\sin\alpha + \frac{a \cdot f_D}{gA^2} Q_R \cdot |Q_R| \Delta t + \frac{a \cdot f_H}{gA} Q_R \cdot \Delta t = 0 \tag{4-21}$$

$$x_P - x_R = (V_R + a)(t_P - t_R) \tag{4-22}$$

$$H_P - H_s - \frac{a}{gA}(Q_P - Q_s) - \frac{Q_s \Delta t}{A}\sin\alpha - \frac{a \cdot f_D}{gA^2} Q_s \cdot |Q_s| \Delta t - \frac{a \cdot f_H}{gA} Q_s \cdot \Delta t = 0 \tag{4-23}$$

$$x_P - x_S = (V_S - a)(t_P - t_S) \tag{4-24}$$

In the method of specified time interval, with conditions known at A, B and C, a linear interpolation can be used to find Q, H at points R and S.

$$\frac{x_C - x_R}{x_C - x_A} = \frac{Q_C - Q_R}{Q_C - Q_A} \tag{4-25}$$

By use of equation 4-24, recognising that $x_P = x_C$, $x_C - x_A = \Delta x$.

$$Q_R = \frac{Q_C - \zeta(Q_C - Q_A)}{1 + \frac{\theta}{A}(Q_C - Q_A)} \tag{4-26}$$

Similarly,

$$Q_S = \frac{Q_C - \zeta(Q_C - Q_B)}{1 - \frac{\theta}{A}(Q_C - Q_B)} \tag{4-27}$$

$$H_R = H_C - (\frac{Q_R \theta}{A} + \zeta)(H_C - H_A) \tag{4-28}$$

$$H_S = H_C + (\frac{Q_S \theta}{A} - \zeta)(H_C - H_B) \tag{4-29}$$

where $\theta = \frac{\Delta t}{\Delta x}$ $\zeta = \theta \cdot a$

Let:

$$C_P = H_R + Q_R(B + \frac{\Delta t}{A}\sin\alpha - \frac{a \cdot f_D \cdot \Delta t}{g \cdot A^2}|Q_R| - \frac{f_H \cdot a}{g \cdot A}\Delta t) \quad (4\text{-}30)$$

$$C_M = H_S - Q_S(B - \frac{\Delta t}{A}\sin\alpha - \frac{a \cdot f_D \cdot \Delta t}{g \cdot A^2}|Q_S| - \frac{f_H \cdot a}{g \cdot A}\Delta t) \quad (4\text{-}31)$$

where $B = a/(g \cdot A)$

From 4-21 and 4-23, one can obtain:

$$H_P = (C_P + C_M)/2 \quad (4\text{-}32)$$

$$Q_P = (C_P - C_M)/(2 \cdot B) \quad (4\text{-}33)$$

In this method, a pipe is partitioned into a number of sections (referred as grid) along pipeline. In using the defined grid with interpolations, it is necessary to solve six equations in turn to find Q and H for any interior section in a pipeline. They are equations 4-26 to 4-29 and equations 4-32 and 4-33. The model can be used for all three stages of pumping oil. The differences between those stages are different pipe sections and thus boundary conditions involved in solving the equations. In stage 1, all valves are closed and only fluids in the two cylinders are involved. The boundary conditions will be the flow rate downstream of the suction cylinder (determined by the velocity of the slider), and the flow rate at each cylinder end (zero in each case). In stage 2, the conditions in the discharge cylinder are the same as those in stage 1. The suction valve opens, thus the inlet pipe is involved and the pressure head at the upstream end of the inlet pipe (Joint B) is constant. Finally in stage 3, both inlet and outlet pipes are involved since all relevant valves are opened. The pressures at both Joint A and Joint B are constant.

An important limitation must be recognised in the selection of the grid mesh ratio. To be assured of stability, the Courant condition must always be satisfied [66].

$$\Delta t \cdot (V + a) \le \Delta x \quad (4\text{-}34)$$

Thus the characteristic through P, C^+ and C^-, must not fall outside the line segment AB in Figure 4.1.

4.2.4. Oil Mixed with a Small Percentage of Gas

Although pure oil is assumed in establishing the model, 'real pure oil' can hardly be achieved in practice, because liquids are almost always mixed with small amounts of gases. When mixed with a small percentage of gas, the oil will still dominate the characteristics of the fluid and the model developed above is still valid. However its effective bulk modulus will be reduced substantially and hence the propagation velocity of a pressure wave in a pipeline containing a liquid can be greatly reduced. For ease of analysis, it is assumed that a pipeline contains a fluid which consists of a liquid with gas bubbles uniformly distributed throughout. The total volume V can be expressed as the sum of the liquid volume V_{liq} and the gas volume V_g. The gross bulk modulus of elasticity is defined as:

$$k = -\frac{\Delta P}{\Delta V / V} \tag{4-35}$$

and the bulk moduli of the individual components can be expressed by

$$k_{liq} = -\frac{\Delta P}{\Delta V_{liq} / V_{liq}} \tag{4-36}$$

$$k_g = -\frac{\Delta P}{\Delta V_g / V_g} \tag{4-37}$$

Combining these three expressions yields

$$k = \frac{k_{liq}}{1 + (V_g / V) \cdot (k_{liq} / k_g - 1)} \tag{4-38}$$

The mixture density in terms of the liquid and gas densities can be expressed as:

$$\rho = \frac{m_{liq} + m_g}{V} \tag{4-39}$$

or

$$\rho = \rho_{liq} \cdot \frac{V_{liq}}{V} + \rho_g \cdot \frac{V_g}{V} \tag{4-40}$$

It is natural that the gas content in liquids tends to reduce the speed of the pressure pulses. For example, gas bubbles in oil could be visualised as springs loaded with the oil. A pressure pulse compresses the spring, which accelerates the oil mass, which in turn, compresses another spring. Thus the wave would travel through the liquid at a lower velocity than in a homogeneous liquid, in which the wave is transmitted directly from one particle to the next. V_g and k_g in equations 4-38 and 4-40 can be derived from the gas law, which are given as follows.

$$V_g = V_{g0} \cdot (\frac{P_0}{P})^{\frac{1}{c}} \tag{4-41}$$

$$k_g = \frac{P - P_0}{1 - (P_0/P)^{\frac{1}{c}}} \tag{4-42}$$

In addition to the effect of gas bubbles mixed in the oil, the effective overall bulk modulus can be considerably lowered by mechanical compliance, depending on the thickness of the cylinders and pipes and the actual working pressures. After modification of the density and the bulk modulus according to equations 4-38 to 4-40, the same method developed for pure oil simulation can be used for both the oil dominant mixture case and the flexible container case.

4.3. Simulation Model of Pure Gas.

Gases show a very strong relationship between pressure, temperature and density. The most familiar equation (of state) relating three properties is the ideal gas law. If the constant pressure specific heat C_p and the constant volume specific heat C_v are introduced, the relationship between pressure and volume can be expressed as [65].

$$P \cdot V^c = K_{g0} \tag{4-43}$$

where $C = {C_p}/{C_v}$ is a constant called specific heat ratio.

Since the cross section is fixed, the effective volume of the cylinder (volume 1 and volume 2 shown in Figures 4.2 and 4.3) can be decided at any time by the effective length of the cylinder related to the position of the slider. When the discharge valve or the suction valve is closed, the pressure can be calculated from equation 4-43 due to initial conditions. The pressures in the inlet and outlet pipes are both constant so that the load force at either side of the slider is constant after the relevant valve is opened, since the highly compressible gas tends to absorb any transient disturbances caused in the transportation pipes [66]. The net force applied on the slider is the sum of two load forces due to the pressures produced in the two cylinders.

$$
\begin{aligned}
F_L &= K_{g1} * (l_1 - x)^{-c} - K_{g2} * (l_2 + x)^{-c} && 0 \le x \le 0.128 \\
F_L &= K_{g1} * (l_1 - x)^{-c} - 62.67 \times 10^3 && 0.128 < x \le 0.665 \qquad (4\text{-}44) \\
F_L &= 62.67 \times 10^3 && x \ge 0.665
\end{aligned}
$$

where $K_{g1} = 1.317 \times 10^5$ and $K_{g2} = 1.317 \times 10^4$.

When the gas is mixed with a small percentage of oil, the gas remains the dominant factor of the fluid. The oil can be regarded as incompressible compared to the gas. Space occupied by the oil causes reduction of the initial volume of the gas such that the overall compressibility is decreased and the stiffness is increased, but this is a very marginal effect.

4.4. Simulation.

As shown in equation 4-44, the model of the gas is non linear but has a rather simple format. The model can be easily linearised and the characteristics of the system can be mathematically analysed. However the model for the oil case is too complex to analyse directly from these equations. To investigate its properties and dynamics, the computer simulation of the open loop system is carried out where the model for the motor slider and pistons and the algorithms developed for modelling the liquids by the characteristics method are included.

4.4.1. Boundary Conditions

Boundary conditions are necessary when the model is simulated, which are related to the slider position, the velocity and the pressures at joints A and B. Figures 4.2

and 4.3 show two different work modes of the pump system. In Figure 4.2, the cylinder at right side works in the discharge mode and the other at left side works in the suction mode. The reverse direction of the slider movement is shown in Figure 4.3.

At the either end of a single pipe, only one of the compatibility equations is available. For the upstream end, equation 4-23 holds along C^- characteristic, and for the downstream boundary, equation 4-21 holds along C^+ characteristic. These are linear equations in H_p and Q_P; each conveys to their respective boundaries the complete behaviour and response of the fluid in the pipeline during the transient. An auxiliary equation is needed in each case that specifies H_P and Q_P, or some relation between them. That is, the auxiliary equation must convey information on the behaviour of the boundary to the pipeline. Each boundary condition is solved independently of the other boundary, and independently of the interior point calculations. Relevant boundary conditions in this system are considered as follows.

- <u>Discharge As A Specified Function Of Time At Upstream End.</u> When one of cylinders is working in the discharge case, the flow delivered from the cylinder equals the multiplication of the velocity of the piston head and cross sectional area of the cylinder. The head can be easily derived from the flow rate. (at point *km1* in Figure 4.2 and point *km2* in Figure 4.3)

$$\begin{aligned} Q_P &= V_m \cdot A \\ H_P &= B \cdot Q_P + C_M \end{aligned} \tag{4-45}$$

- <u>Suction As A Specified Function Of Time At Downstream End.</u> When one of the cylinders is working in suction, the flow at the downstream end is also related to the piston velocity and cross area of the cylinder. Thus the head can be derived from the flow rate as well (at point *km2* in Figure 4.2 and point *km1* in Figure 4.3).

$$\begin{aligned} Q_P &= V_m \cdot A \\ H_P &= C_P - B \cdot Q_P \end{aligned} \tag{4-46}$$

- <u>Constant Head At Joint A (discharge valve opens).</u> As stated earlier, the pressures at Joint A can be assumed to be constant, i.e. the pressure at the downstream end of the outlet pipe is constant after the discharge valve is open (at point *1* of the pipe 3 in Figure 4.2 and point *1* of the pipe 4 in Figure 4.3). The flow rate can be derived from the constant head.

$$H_P = \frac{1}{\rho \cdot g} \cdot P_{ref}$$
$$Q_P = \frac{1}{B}(C_P - H_P) \qquad (4\text{-}47)$$

- Constant Head At Joint B (suction valve opens) Similarly, the pressure at Joint B is assumed to be constant. This means that the pressure at the upstream end of the inlet pipe is constant after suction valve is open (at point *1* of the pipe 4 in Figure 4.2 and point *1* of the pipe 3 in Figure 4.3).

$$H_P = \frac{1}{\rho \cdot g} P_0$$
$$Q_P = \frac{1}{B}(H_P - C_M) \qquad (4\text{-}48)$$

- Dead End At Downstream End (discharge valve closes). When a cylinder is in the suction mode, the relevant discharge valve keeps closed until the pressure in the cylinder is higher than that in the pipe. In this case, the flow delivered at the downstream end (pump end) is 0 (at point *1* of the cylinder 1 in Figure 4.2 and point *1* of the cylinder 2 in Figure 4.3).

$$Q_P = 0$$
$$H_P = C_P \qquad (4\text{-}49)$$

- Dead End At Upstream End (suction valve closes). Similarly, the suction valve keeps closed until the pressure in the suction cylinder is lower than that in the inlet pipe. In this case the flow rate at the upstream end equals 0. (at point *1* of the cylinder 2 in Figure 4.2 and point *1* of the cylinder 1 in Figure 4.3).

$$Q_P = 0$$
$$H_P = C_M \qquad (4\text{-}50)$$

4.4.2. Series Connections

The cylinders and the pipes are connected in series, with non return valves in between. Various sizes of the pipes will have different effects on the system dynamics. However, this type of junction as shown in Figure 4.4, although a diameter changes, applies equally well to a single-diameter pipe with a change in roughness, thickness, or constraint condition, or any combination of these possible variations [66].

At the junction:

$$Q_{1,NS} = Q_{2,1} \qquad\qquad H_{1,NS} = H_{2,1}$$

so:

$$Q_{p2,1} = \frac{C_{P1} - C_{M2}}{B_1 + B_2} \qquad H_{P2,1} = \frac{B_2 \cdot C_{P1} + B_1 \cdot C_{M2}}{B_1 + B_2} \tag{4-51}$$

4.4.3. Software and Assumptions

In the pure gas case, a program is written to solve equations 4-2 and 4-44. Equation 4-44 consists of three expressions, which are used in different stages of the pumping operation.

In the pure oil case, a simulation software is written to solve the equation 4-2 and implement equations 4-26 to 4-29, 4-32 and 4-33 with all given boundary conditions for the slider and the oil respectively. Although only part of the boundary conditions are needed in the open loop simulation, all operation stages and related boundary conditions are considered in the software such that the same program can be used in the full simulation of the overall system. Details of the software will be described as a part of full simulation in chapter 8. Like all other simulations some assumptions in which minor factors are ignored are made to simplify the simulation and to reduce computing time.

- Pressures at joint A and joint B are constant.
- Friction losses in the pump cylinders are ignored because the surface finishing of the cylinder is much smoother and the length is relatively short compared to the pipes.
- The fluid in the pipes is stable before the related valves open, i.e. it has steady initial conditions.
- Ideal non return valves are simulated, and loss in the valves is included in the total loss.

- Losses due to bends and roughness of the pipes are included in the total loss.

4.4.4. Open Loop Simulation

As step responses of systems can explicitly demonstrate the system characteristics and are easier to implement, a step signal of the driving force is used in the computer simulation as an input for the model. The slider and the two pistons are driven from one end of the motor towards the other end and therefore pumping the fluids in the cylinders. The variables of interest in the simulation are the slider position, the slider velocity and the resistive forces (or pressures) produced on the motor slider.

Figure 4.5 gives the responses of the slider position and velocity, and Figure 4.6 gives the load force, both for the pure gas. Figures 4.7 and 4.8 show the step responses of the position and the velocity in the pure oil case where the diameter of the inlet and outlet pipes is 150 *mm* and different lengths of pipes are examined (outlet + inlet). Figures 4.9 and 4.10 show the responses of the two load forces (FL1 and FL2) applied on two sides of the slider where the pipe lengths are 10+10*m* and 20+10 *m* respectively, and Figures 4.11 and 4.12 show the spectra of the load forces where the pipe lengths are 20+10 *m* and 40+20 *m* respectively. The constant components of the load forces are excluded from the spectra. Figure 4.13 shows the step responses of the slider position where the diameter of the pipes is reduced to 100 *mm*.

From the simulation results and the properties of the fluids, some conclusions related to the system dynamics can be drawn as follows.

- Pure Gas. The gas exhibits two important properties. Firstly it is highly compressible and thus the system dynamics demonstrate the lower stiffness in stage 1 of the pumping operation, compared to that of the pure oil case. As shown in the simulation results, the pressure in the cylinder rises slowly as the piston compresses the gas when the slider moves. Secondly as the pure gas has very low density compared to the liquids and the slider, the mass of the gas can be neglected.

- Pure Oil. The oil behaves very differently from the pure gas case. High stiffness occurs at stages 1 and 2 as the compressibility of the oil is low.

When the oil in the pipes is involved, its mass is comparable to the mass of the slider. The force produced by the motor will have to accelerate not only the slider but the mass of the oil. The longer the pipe is, the greater the mass will be, and the simulation results clearly show that the movement of the slider is slower when the total length of the pipes is increased, provided the same driving force is applied on the system. Therefore the mass of the oil must be taken into account in the system dynamics.

- Pulsating Forces. The pulsating forces superimposed on the steady loads are caused by travelling waves in transient flows. At the beginning of every pumping stroke, the slider always gains some speed before the valves open because of the compressibility of the fluid inside the cylinder. When one valve opens, the slider and hence the oil in the cylinder with an initial speed create an impact on the oil in the pipes. Consequently a force is applied to the mass of the oil, the force is propagated through the oil by wave action. This takes finite time and so the entire mass involved does not experience the force at the same time due to the fluid elasticity. Consequently the fluid state in the relevant pipe is changed from rest to a transient period. The cycle period of the oscillations is determined by the total length of the pipes, the bulk modulus of the oil and density of the fluid given as $4 \cdot L / a$ [66, 67], where L is the pipe length and a is the speed of the travelling wave. From simulation the oscillations can approximately be represented by damped sinusoidal signals. The damping factor is related to the fluid friction and the imperfect elasticity of the fluid and the pipe wall. The amplitude of the signal is determined by the initial condition when the valve is opened.

  Figure 4.14 shows the frequency spectra of the two signals obtained from the system with the same pipe length but different diameters. The two frequencies are slightly different, which is due to the fact that the slider travels more slowly with the smaller diameter pipes, hence the average effective length (pipe length + cylinder length) is longer and the travelling wave takes slightly a longer time.

  Since the distance which the slider travels is only a small portion of the total length which the wave travels, the pulsating forces are approximately independent of the slider movement and thus the system dynamics. Therefore the oscillations can be regarded as external disturbances as far as the control system is concerned. This means that the controller must be designed to be robust to all possible disturbances.

- Diameters Of The Pipes. When the cross sectional area of the pipes is reduced, the liquid is pumped slower than that in the pipes with larger diameter, as indicated in Figures 4.7 and 4.13. This is because the acceleration of the oil in the thinner pipes is increased and the force available to pump the oil is therefore decreased (assuming the same force is applied to the slider).

  Also, the amplitude of the pulsating pressure in the smaller diameter case is higher. This is because that the initial velocity of the flow in the smaller pipes is higher, which causes higher disturbances.

4.5. Simplified Model and Uncertainty.

The models developed above are described either by the non linear equations for the gas or the partial differential equations for the oil. In addition, both the parameters and the structure of the overall dynamics of the system are time varying. Firstly, the system always goes through three stages in every pumping stroke and the dynamics vary from one stage to another. Secondly, the ratio of oil and gas mixture is to be varied from time to time. The flow format of the fluid mixture is unpredictable and therefore models of the mixed fluids are extremely complicated and sometimes almost impossible to establish [64, 65]. However the characteristics of the fluid mixture are between the pure oil and the pure gas. It is reasonable to set up an operational bound for the system in all conditions using the models of two extreme cases and then to design a controller which works well within the defined bound. While the bound is set up, linearisation of the non linear models and simplification of the distributed parameter models need to be carried out as the linear models are still desirable from the control design point of view. The simulations have shown that this should be possible.

4.5.1. No Load Case

The no load case is the simplest situation in the system, where the motor is not loaded, or the pump is pumping gas in stage 3. In this case, only the dynamics of the motor slider need to be involved and the load force will not greatly affect the system characteristics.

$$F - F_L = m \cdot a + k_f \cdot v \qquad (4\text{-}52)$$

Where F_L is the constant load. We have the transfer function

$$H_m(s) = \frac{1}{m \cdot s^2 + k_f \cdot s} \qquad (4\text{-}53)$$

where $m = 1400\ kg$ is the mass of the slider and the pistons and $60 < k_f < 120$ $N \cdot s \cdot m^{-1}$ is the viscous friction coefficient due to the oil for cooling and lubricating in the motor.

4.5.2. Valves Closed, Pure Gas Case

Equation 4-44 gives the total load force produced in the cylinders due to the compressibility of the gas when the non return valves are closed. This is a function of the slider position, which can be linearised over a number of representative operating points and thus equation 4-52 becomes

$$F = m \cdot a + k_f \cdot v + k_0 \cdot x \qquad (4\text{-}54)$$

The values of k_0 in various operating points can be obtained by differentiating the load force in equation 4-44.

$$\frac{d}{dt}(F_L) = c \cdot K_{g1} * (l_1 - x)^{-c-1} + c \cdot K_{g2} * (l_2 + x)^{-c-1} \qquad (4\text{-}55)$$

The second term exists only in stage 1. Because pure gas is the case where the lowest bound exists, the most interesting value is the minimum k_0. By differentiating equation 4-55, it can be easily obtained that the minimum value occurs at the moment when the pumping stages change from stage 1 to stage 2 and the slider position is at $x = 0.128\ m$. In stage 1, $k_0 = 3.299 \times 10^5\ N \cdot m^{-1}$ at the slider position $x = 0.128\ m$. In stage 2 of the pumping operation, the first term in equation 4-55 decides the values of k_0 and the minimum value is $k_0 = 6.226 \times 10^4$. Therefore the following transfer function is obtained for stages 1 and 2 in the pure gas case.

$$H_m(s) = \frac{1}{m \cdot s^2 + k_f \cdot s + k_0} \tag{4-56}$$

where $k_0 \geq 3.299 \times 10^5$ in stage 1 and $k_0 \geq 6.226 \times 10^4$ in stage 2.

4.5.3. Valves Closed, Pure Oil Case

Pure oil is the other extreme case where the highest bound exists. When all non return valves are closed in the stage 1, the quantity of the oil in the cylinders is negligible compared to the total mass of the slider, and the stiffness of the oil dominates the dynamics of the system. From the definition of the bulk modulus,

$$\Delta P = -k_b \cdot \frac{\Delta V}{V_0} \tag{4-57}$$

where $k_b = 2.0685 \times 10^9$ Pa for the crude oil. So the total load force is the sum of forces developed in the two cylinders, given as follows.

$$F_L = A \cdot k_b \cdot \frac{1}{l_1} \cdot x + A \cdot k_b \cdot \frac{1}{l_2} \cdot x + \Delta F_0 \tag{4-58}$$

Where ΔF_0 is the initial net force on the slider. Substituting relevant parameters into the equation shows that the pumping operation is in stage 1 when the position is between 0 and 0.307 *mm*, stage 2 when the position is between 0.307 and 2.91 *mm* and stage 3 when the position is greater than 2.91 *mm*. In stage 1 the maximum value of k_0 is derived and the transfer function of the system is the same as that given in 4-56 with $k_0 = 2.043 \times 10^8$ $N \cdot m^{-1}$. In stage 2, k_0 is equal to 2.15×10^7 $N \cdot m^{-1}$ which is less than that in stage 1 as the second term in equation 4-58 disappears.

4.5.4. Valves Open, Pure Oil Case

When both suction and discharge valves are opened in the stage 3, the stiffness k_0 no longer exists and the force is that required to accelerate the slider and fluids and to overcome the pressure difference between the inlet and outlet pipes. As shown in the simulation results, the dominant factor affecting the system characteristics is the total mass of the moving parts in the system. The total mass is the sum of the mass of the slider and pistons, and the mass of the fluid in the inlet and outlet pipes. The mass of the slider has a fixed value, while the mass of the liquid being pumped is decided by the nature of the fluid and the pipe diameters and lengths, where the pure oil case with the maximum pipe length determines the upper bound. To allow design flexibility of the pump system, a range of the pipe lengths and diameters has been defined, and the controller to be designed should be able to handle the worst case.

The equivalent mass of the fluid in the pipes is also affected by the diameter of the pipes. When the cross sectional area of the pipes equals that of the cylinders, the actual mass of the oil plus the mass of the slider is the total mass to be driven because the oil will be pumped at the same speed as the motor slider. When the cross sectional area of the pipes is different from the cylinders, an equivalent mass can be derived from the ratio of the diameters of the cylinders and the pipes. Suppose that m_s is the mass of the slider plus the oil in the cylinders, m_F is the mass of the oil in the pipes, k_{fs}, k_{fF} are the viscous friction coefficients of the slider and of the oil in the pipes respectively, F is the force supplied on the slider, P_1 is the pressure at the connection point between the cylinder and the pipes, P_0 is the constant pressure at the end of the pipes. v, a is the velocity and acceleration of the slider, v_F, a_F is the velocity and acceleration of the oil in the pipes, A is the inner cross area of the cylinders and A_1 is that of the pipes. Two dynamic equations can be established for the slider and the oil in the pipes, given as follows.

$$F - P_1 \cdot A = m_s \cdot a + k_{fs} \cdot v \tag{4-59}$$

$$P_1 \cdot A_1 - P_0 \cdot A_1 = m_F \cdot a_F + k_{fF} \cdot v_F \tag{4-60}$$

Because the flow rate of any liquids at any cross areas must be continuous,

$$v \cdot A = v_F \cdot A_1$$

Therefore,

$$v_F = \frac{A}{A_1} \cdot v \tag{4-61}$$

$$a_F = \frac{A}{A_1} \cdot a \tag{4-62}$$

Substituting equations 4-60, 4-61 and 4-62 into equation 4-59 gives,

$$F - P_0 \cdot A = \left(m_s + \frac{A^2}{A_1^{\ 2}} \cdot m_F \right) \cdot a + \left(k_{fs} + \frac{A^2}{A_1^{\ 2}} \cdot k_{fF} \right) \cdot v \tag{4-63}$$

Equation 4-63 indicates that the mass of the oil can be converted into an equivalent one such that a single variable can be used in the system dynamics. The equivalent mass of the oil in the pipes is inversely proportional to the square of the cross sectional area. Figures 4.15 and 4.16 compare the simulated step responses of the position and velocity against that of an ideal second order linear model with the stiffness k_0 being 0. The two sets of curves are virtually indistinguishable, which indicates that the system dynamics in stage 3 can also be represented by the second order linear system. The equivalent mass and the viscous friction are increased 2.25 times when the diameter of the pipes is reduced from 150 *mm* to 100 *mm*. The viscous friction is determined by the roughness of the pipes, the actual value of which will be decided by the actual pipes to be used in the system - only an estimated value is given here.

So the transfer function given in equation 4-53 has the values of $m \le 4135\ kg$ and $k_f \le 1000\ N \cdot s \cdot m^{-1}$.

4.6. Summary.

Two models for the mechanics of the slider and the fluids have been developed in this chapter. The first is the full model for the computer simulation, where the fundamental equations of gases and liquids are used. The characteristics method is used to solve the partial differential equations of the oil model.

From simulation studies of the first model, a simplified model has been derived for use in the control design. To form an unique representation of the simplified model in the all stages and the pumping conditions, equations 4-53 and 4-56 can be combined together with their uncertainty bounds given as follows.

Model:

$$H(s) = \frac{1}{m \cdot s^2 + k_f \cdot s + k_0} \tag{4-64}$$

Uncertainty Bounds In The Stage 1:

$$
\begin{aligned}
m &= 1400 \\
k_f &= [60, 120] \\
k_0 &= [3.299 \times 10^5, 2.043 \times 10^8]
\end{aligned}
\tag{4-65}
$$

Uncertainty Bounds In The Stage 2:

$$
\begin{aligned}
m &= [1400, 2768] \\
k_f &= [60, 500] \\
k_0 &= [6.226 \times 10^4, 2.15 \times 10^7]
\end{aligned}
\tag{4-66}
$$

Uncertainty Bounds In The Stage 3:

$$
\begin{aligned}
m &= [1400, 4135] \\
k_f &= [60, 1000] \\
k_0 &= 0.0
\end{aligned}
\tag{4-67}
$$

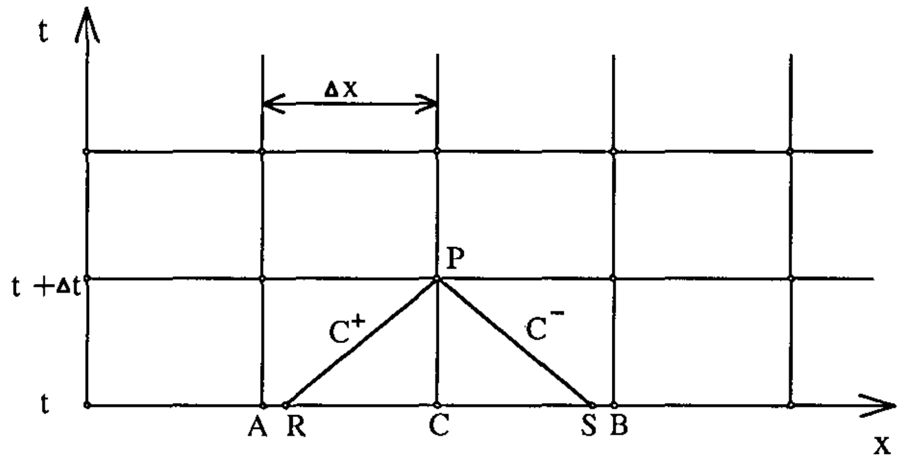

Figure 4.1. Characteristic lines in the xt plane

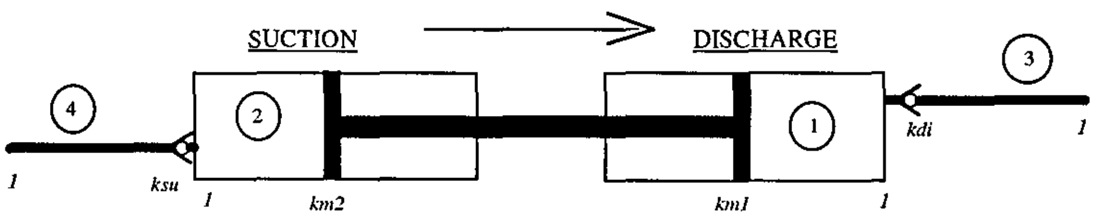

Figure 4.2. Pump Action 1

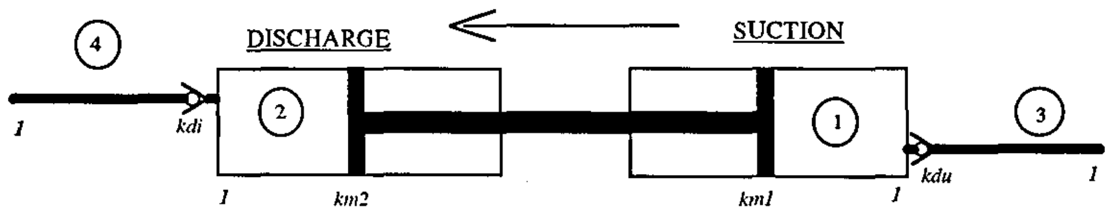

Figure 4.3. Pump Action 2

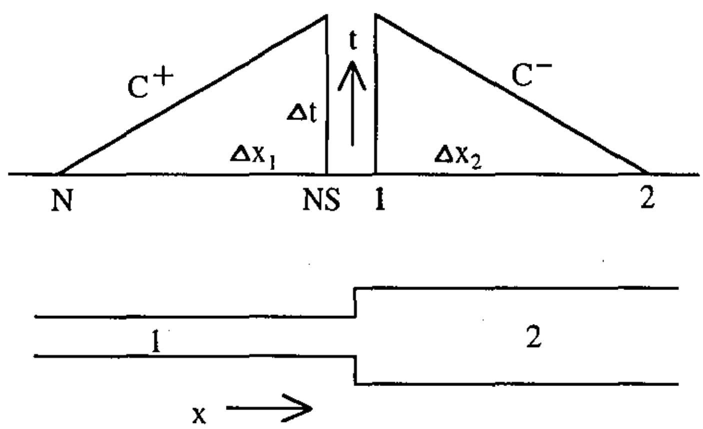

Figure 4.4. Series junction

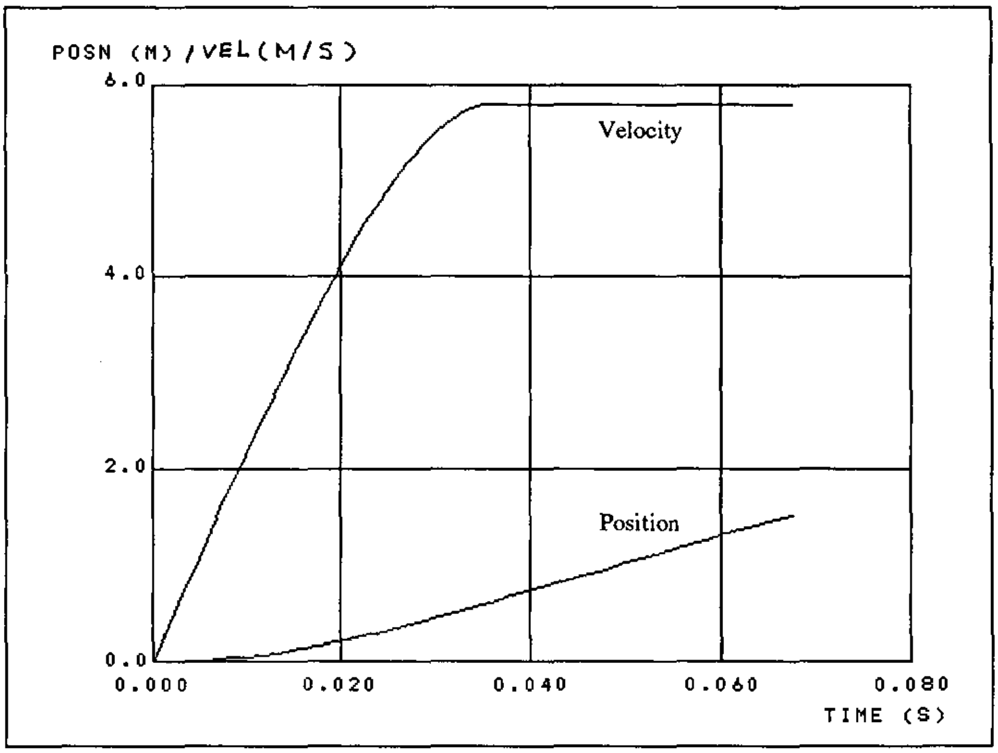

Figure 4.5. Step Responses of Pure Gas Case

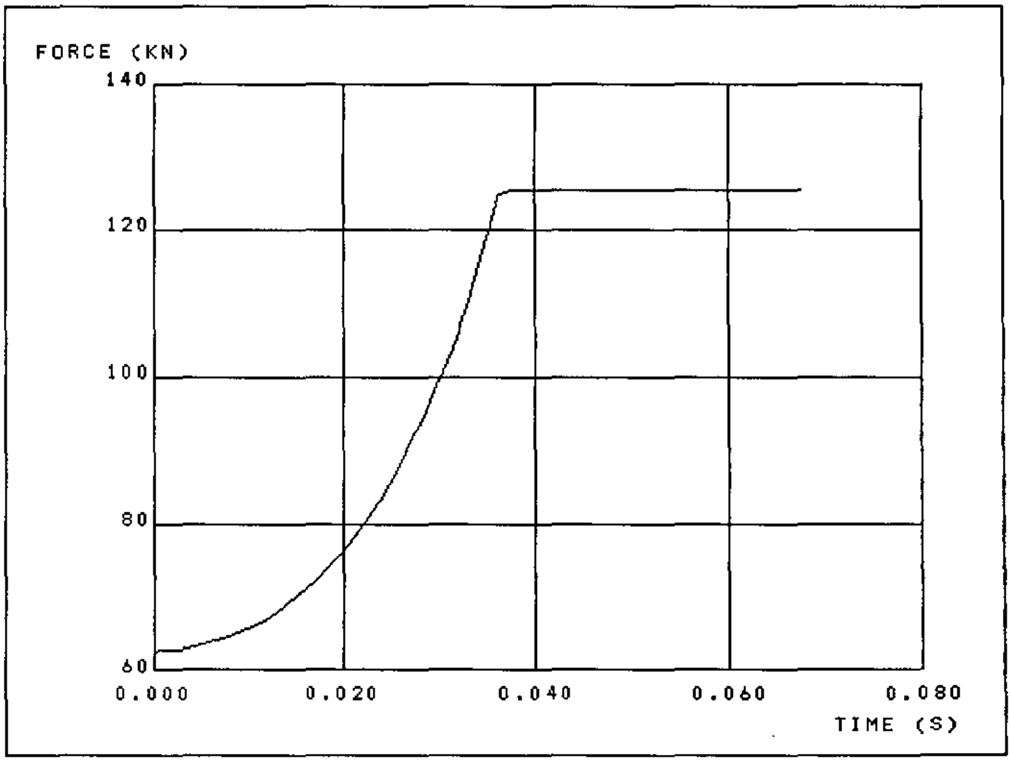

Figure 4.6. Load Force of Open Loop In Pure Gas Case

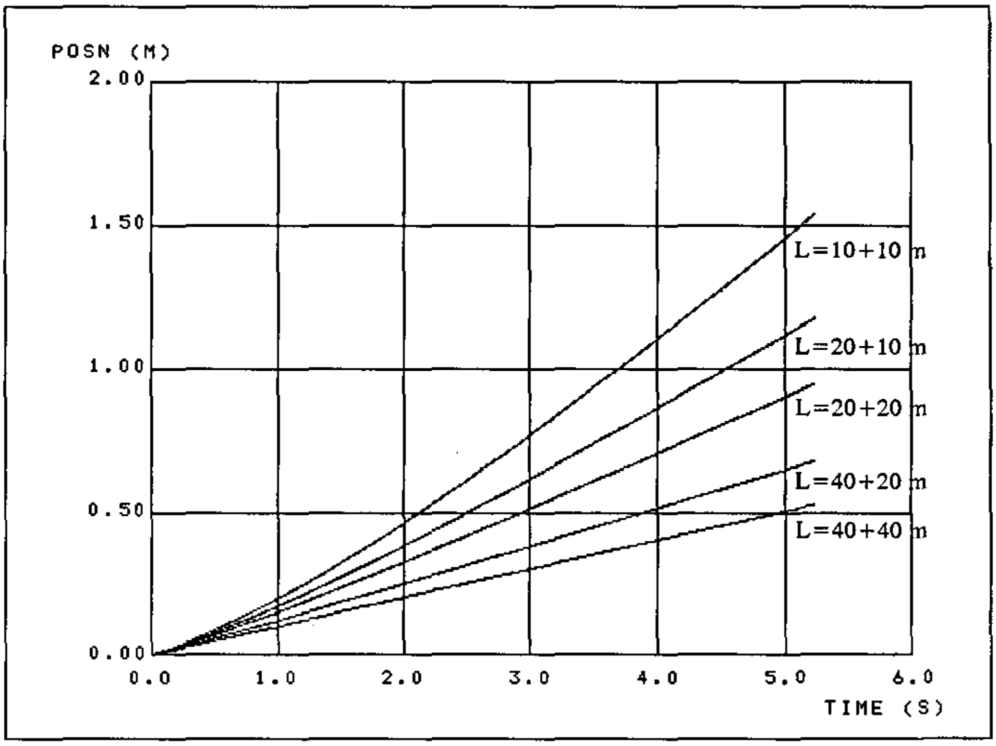

Figure 4.7. Position Responses of Step Force Input

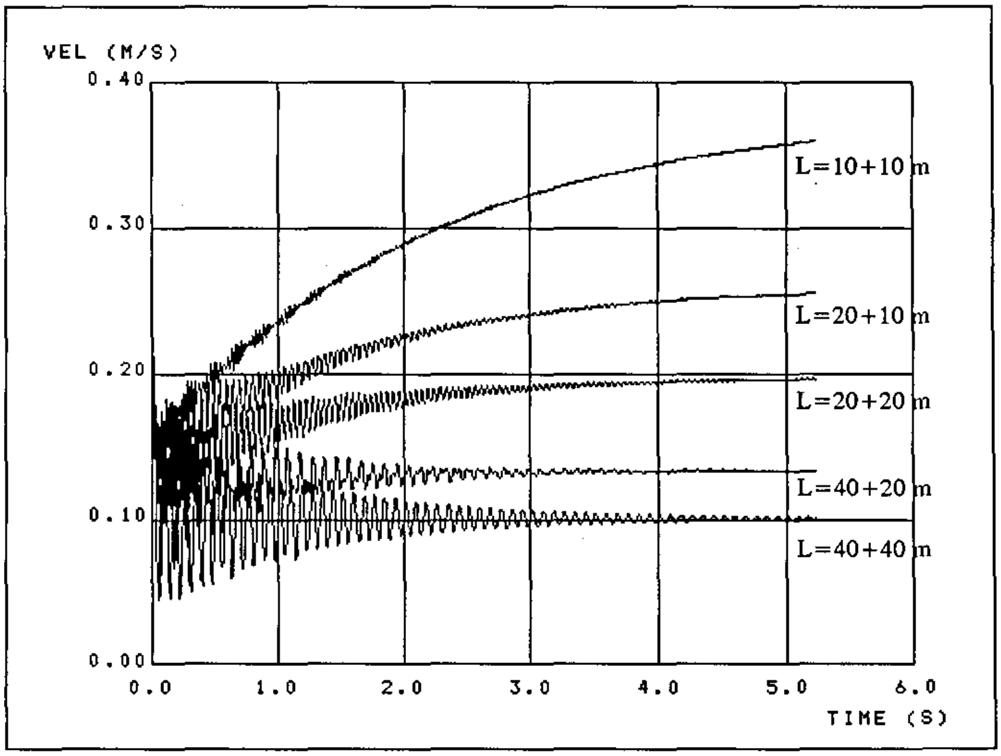

Figure 4.8. Velocity Responses of Step Force Input

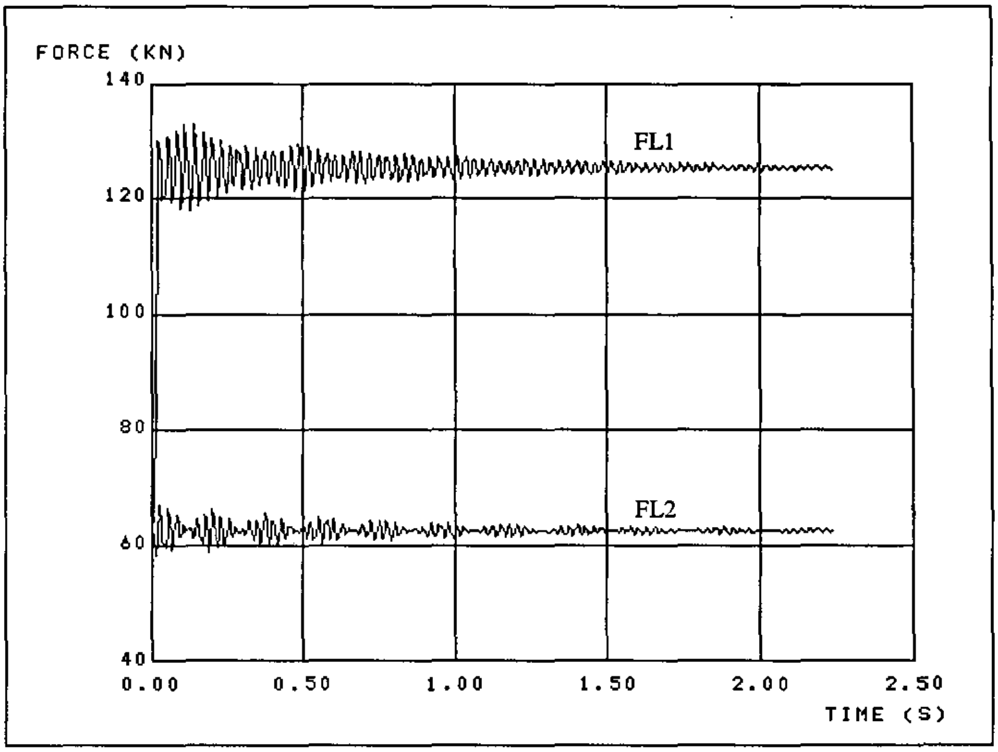

Figure 4.9. Responses of Load Forces (Pipe Length = 10 +10 m)

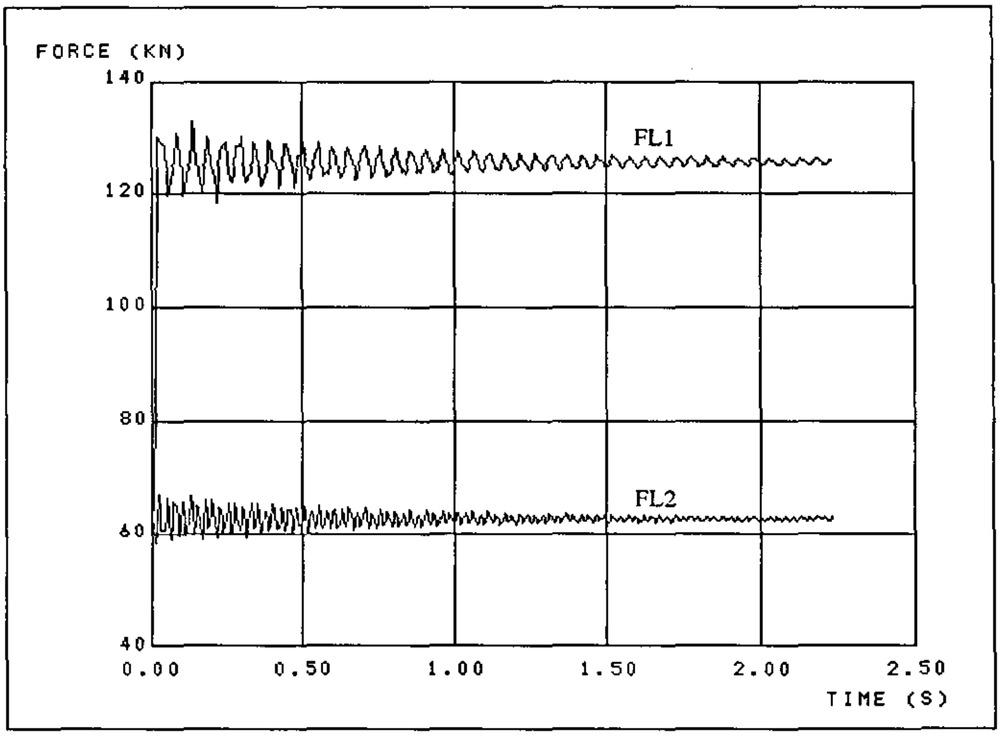

Figure 4.10. Responses of Load Forces (Pipe Length = 20+10 m)

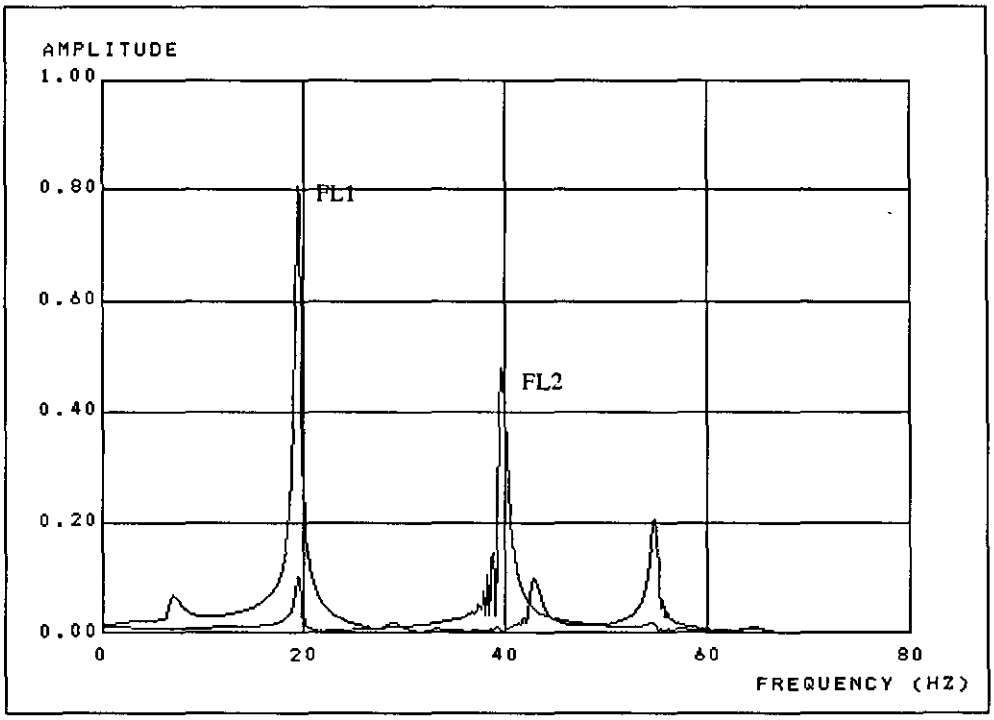

Figure 4.11. Frequency Spectra of Load Forces
(Pipe Length = 20+10 m)

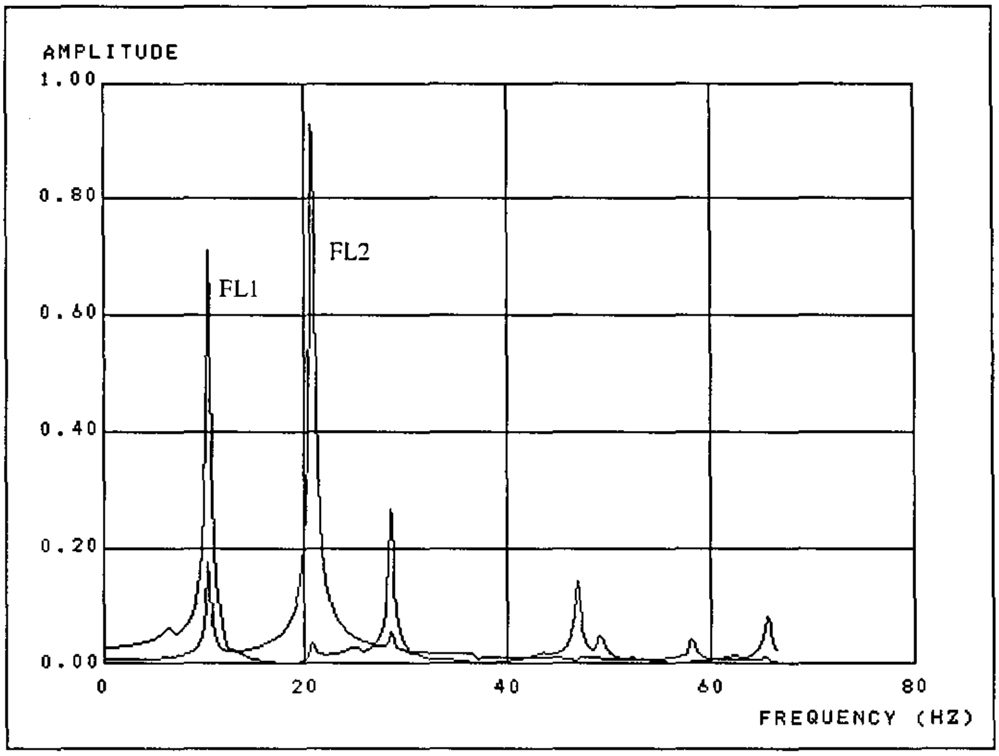

Figure 4.12. Frequency Spectra of Load Forces
(Pipe Length = 40+20 m)

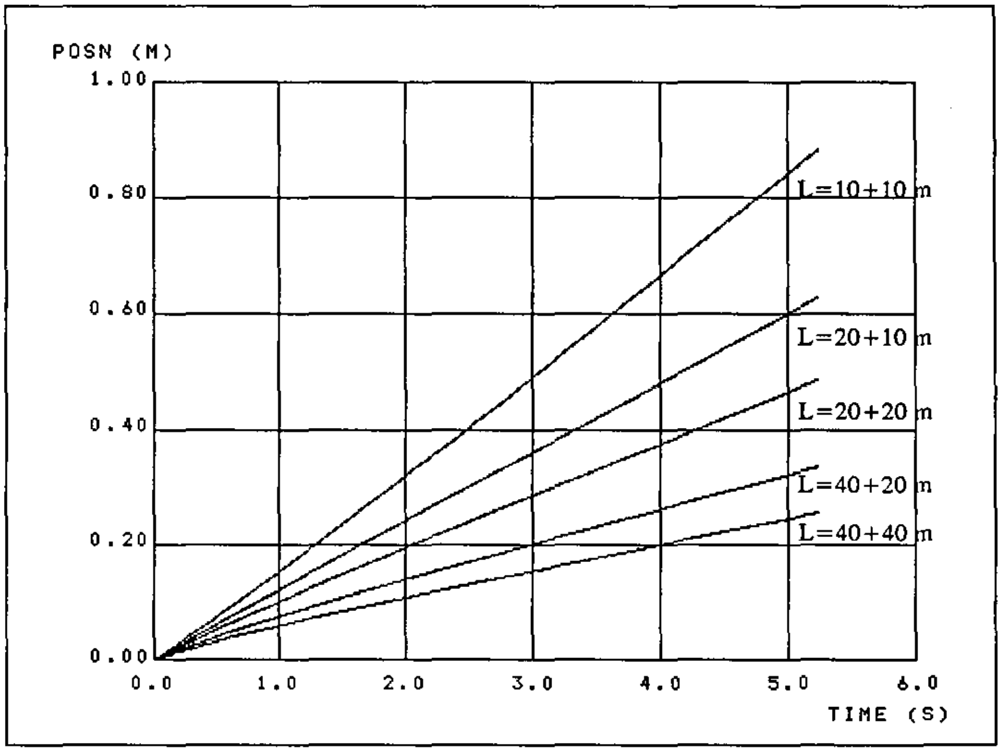

Figure 4.13. Position Responses (Diameter of Pipes = 100 mm)

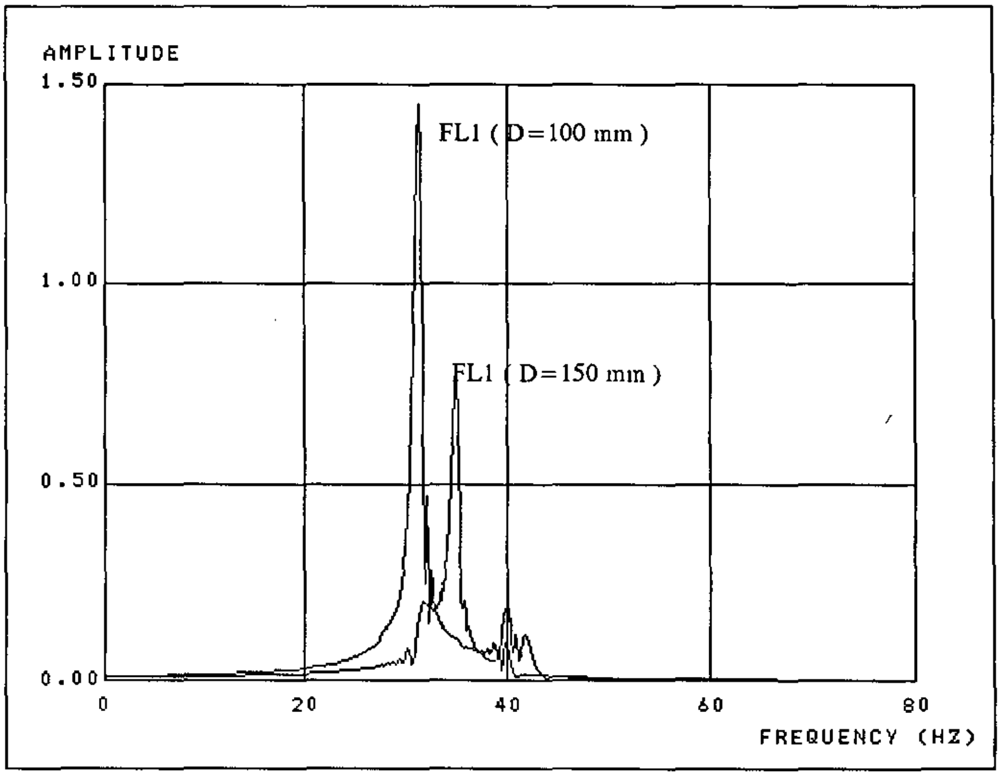

Figure 4.14. Load Force Spectra (L = 10+10 m)

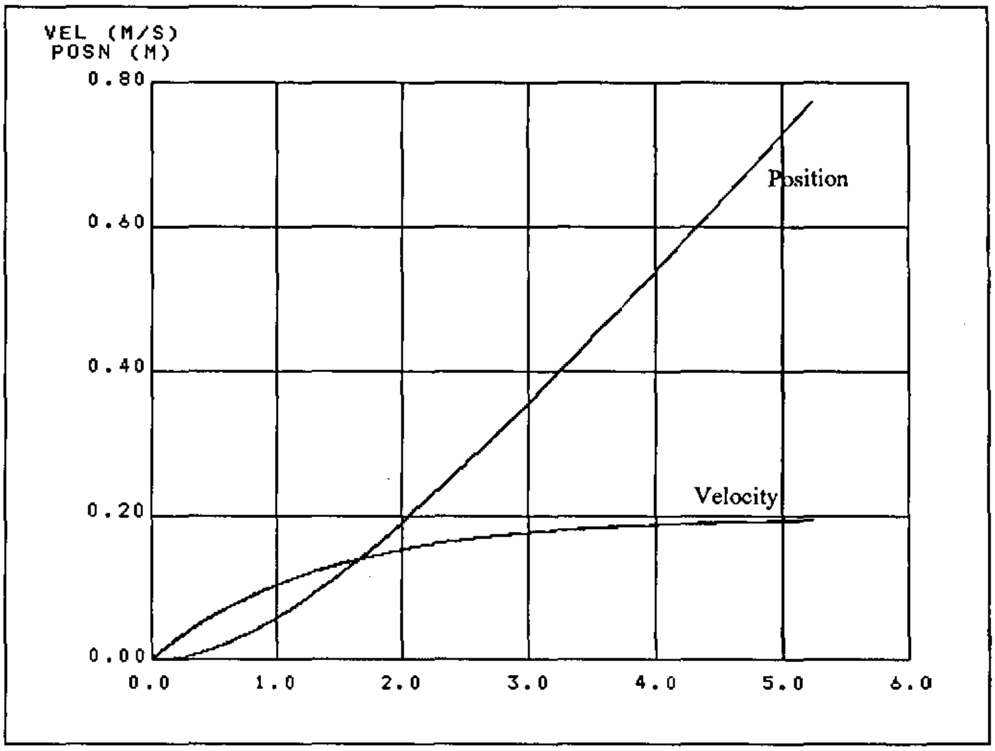

Figure 4.15. Step Responses in Stage 3 (L=20+20 m, D=150 mm)

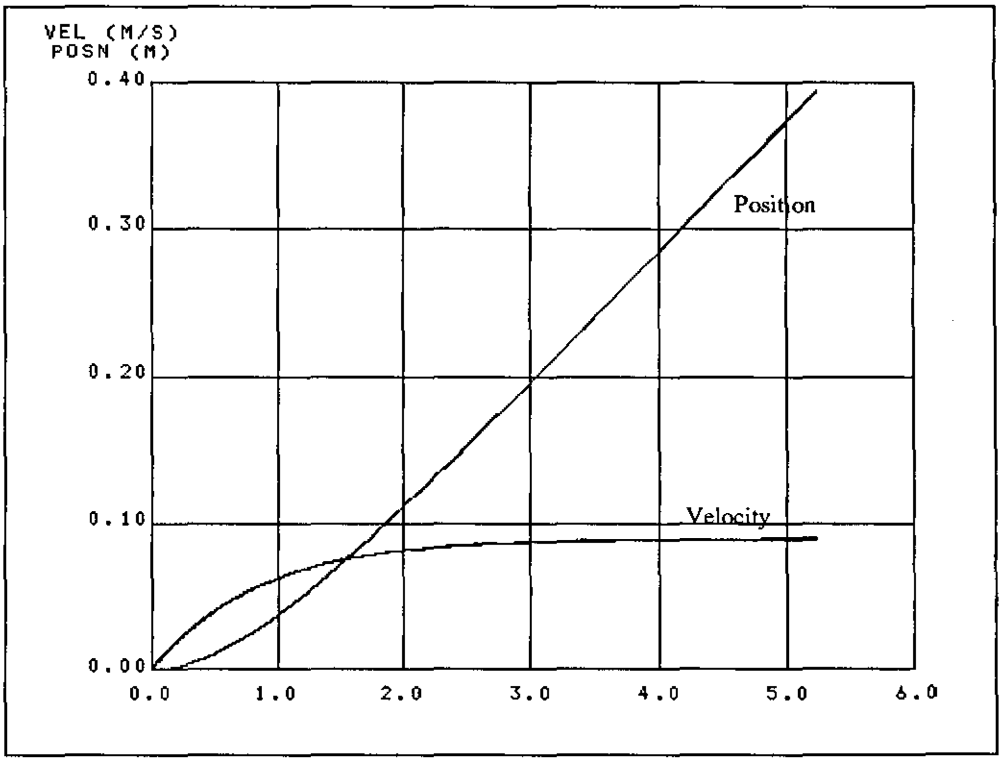

Figure 4.16. Step Responses in Stage 3 (L=20+20 m, D=100 mm)

CHAPTER 5.

MODELLING OF THE MOTOR

Modelling of a synchronous motor is to develop a group of mathematical equations representing the interaction between voltage, current and magnetic field in the motor. Naturally a proper equivalent circuit with correct parameters of the motor is essential in order to establish an effective simulation model. The motor parameters are best obtained from tests of the motor, which need to be undertaken before the modelling is performed. Based on a commonly used equivalent circuit, and using motor parameters obtained from the test results, a simulation model is developed in this chapter which demonstrates the relationships between the three phase voltages, the three phase currents and the permanent magnets. The model can represent the motor in a way directly related to the physical machine, and this can be used for the computer simulation. On the other hand this model is not the best one to expose the features of the motor and it is difficult to use for the design of the current control loop. To resolve this shortcoming, the Park transform is used to establish a second model for the motor in the d - q axis format.

As mentioned earlier, the modelling accuracy is very often in conflict with simplicity. The higher the accuracy, the more complex a model tends to be. In fact all models are idealised in some way, and in this case some minor effects of the motor are ignored in the modelling, as follows.

- Saturation. The saturation of the motor is neglected since the machine has been designed and built to avoid working in saturation mode [19]. In addition, the controller to be used for the system will set up a limit level for the load condition so that high saturation will be unlikely.

- End effect. Distortion of the gap flux density due to the end effect was investigated and calculated using the finite element method in the motor design procedure. It showed that the effect is quite small and can be neglected [19].

- Induced EMF. The ideal sinusoidal form of the induced EMF is used in the modelling and analysis, which is supported by the motor test described in the next section.

In this chapter, the test results of the motor are presented and the mathematical representations of the motor parameters are derived in section 5.1. Two simulation models, the ordinary three phase model and the d - q axis model, are set up in sections 5.2 and 5.3 respectively.

5.1. Parameter Test of The DPLSM.

Figure 5.1 shows a commonly used equivalent circuit for permanent magnet motors [19, 20, 38], which makes the model simple and reasonably accurate. The circuit forms a link between the internal electromagnetic processes and the external performance characteristics. Each phase consists of a voltage source, a resistance and an inductance and three phases are connected in 'star' form. The permanent magnets are modelled by a coupled current-forced circuit on the moving slider as shown. There are mutual inductances between phases and between each phase and the permanent magnets. The motor test has been carried out to provide necessary parameters for the modelling.

Resistances of three phases are basically identical and constant. Although the resistance of the winding is a function of the temperature, the motor will work in a stable environment such that the temperature will be relatively constant.

The EMF induced by the permanent magnets was measured from the outputs of the three phases of the stator while the slider is driven by hydraulic actuators. A constant slider speed was maintained during the measurement. The result is shown in Figure 5.2. The EMFs induced in the three phase windings follow the ideal sinusoidal waveforms and thus can be represented by the ideal mutual inductances between the three phases of the stator and the slider equivalent circuit, given as follows.

$$M_{fR} = M_{fM} \cdot \cos(\frac{\pi}{p}x) = M_{fM} \cdot \cos(\gamma) \qquad (5\text{-}1)$$

$$M_{fY} = M_{fM} \cdot \cos(\frac{\pi}{p}x - \frac{2\pi}{3}) = M_{fM} \cdot \cos(\gamma - 120) \qquad (5\text{-}2)$$

$$M_{fB} = M_{fM} \cdot \cos(\frac{\pi}{P}x + \frac{2\pi}{3}) = M_{fM} \cdot \cos(\gamma + 120) \qquad (5\text{-}3)$$

where x is the slider position, P is the pole pitch of the motor, γ is the relative electrical angle of the slider and $M_{fM} = 4.983\ H$.

Self inductances and mutual inductances of the motor stator vary with the position of the slider as shown in Figures 5.3 and 5.4 respectively. The variations of these inductances are caused by the physical arrangement of the permanent magnets, which affects the flux path in the air gap when the slider is at different positions. The diagrams of the slider magnets and the winding of the stator are shown in Figure 5.5 and 5.6 respectively. When the magnet poles are at the centre position between the red phase coils they have the least effect on the red phase, thus the self inductance of the red phase has the minimum value at this position. When the magnet poles are under the red phase coils, they have the most effect on the phase and thus the inductance has the maximum value. This effect is repeated every half pole pitch and thus there is a periodical component in addition to the constant inductance. The wavelength of the component is half of the pole pitch. Since the coils of three phases are physically apart from each other by 1/3 pole pitch, the periodical components of self inductances of three phases have a same frequency but 120 degree phase difference from each other. The magnets have the similar effect on the mutual inductances between phases. When the magnet poles are located between the red and yellow phase coils, the relevant inter phase mutual inductance between those two phases has the maximum value. When they are under the blue phase, the inductance has minimum value.

Two kinds of mathematical representations have been used in modelling the variations, which are the basic sinusoidal waveform and absolute value of sinusoidal waveform [38]. Results in reference 38 indicated that the sinusoidal waveform may be sufficient to represent the variations, although the latter one is a better representation. The two waveforms are compared with the test result as shown in Figure 5.7. The basic sinusoidal waveform is preferred in this case because it is easier to deal with mathematically. The actual expressions to be used in the modelling are given as follows.

$$L_R = L_s - L_{s1} \cdot \cos(\frac{2\pi}{P}x) = L_s - L_{s1} \cdot \cos(2\gamma) \qquad (5\text{-}4)$$

$$L_Y = L_s - L_{s1} \cdot \cos(\frac{2\pi}{P}x + \frac{2\pi}{3}) = L_s - L_{s1} \cdot \cos(2\gamma + 120) \tag{5-5}$$

$$L_B = L_s - L_{s1} \cdot \cos(\frac{2\pi}{P}x - \frac{2\pi}{3}) = L_s - L_{s1} \cdot \cos(2\gamma - 120) \tag{5-6}$$

$$M_{RY} = -M_s - M_{s1} \cdot \cos(\frac{2\pi}{P}x - \frac{2\pi}{3}) = -M_s - M_{s1} \cdot \cos(2\gamma - 120) \tag{5-7}$$

$$M_{YB} = -M_s - M_{s1} \cdot \cos(\frac{2\pi}{P}x) = -M_s - M_{s1} \cdot \cos(2\gamma) \tag{5-8}$$

$$M_{BR} = -M_s - M_{s1} \cdot \cos(\frac{2\pi}{P}x + \frac{2\pi}{3}) = -M_s - M_{s1} \cdot \cos(2\gamma + 120) \tag{5-9}$$

where $L_s = 3.227\ mH$, $L_{s1} = 0.0328\ mH$, $M_s = 1.112\ mH$ and $M_{s1} = 0.069\ mH$. The sinusoidal component of the self inductance is about 1% of the constant component and the sinusoidal component of the mutual inductance is 6.2%.

The amplitude of the sinusoidal component in those inductances is far less than the constant component. However this does not automatically mean that it will not affect the performance of the motor. In the next sections the component is considered in the modelling to study the influence of the variations. Moreover the variations could be comparable to the constant component for some machines[38], mainly depending on the construction of the machines. From this point of view, it is also worthwhile to include the variations of this kind in the derivation of the model to maintain the generality of the modelling.

5.2. Mathematical Model of The Equivalent Circuit

The dynamic equation of the equivalent circuit can be found from the application of simple circuit laws. From the diagram shown in Figure 5.1, the three phase currents produces,

$$\begin{bmatrix} v_R \\ v_Y \\ v_B \end{bmatrix} = \begin{bmatrix} R_s + sL_R & sM_{RY} & sM_{BR} & sM_{fR} \\ sM_{RY} & R_s + sL_Y & sM_{YB} & sM_{fY} \\ sM_{BR} & sM_{YB} & R_s + sL_B & sM_{fB} \end{bmatrix} \cdot \begin{bmatrix} i_R \\ i_Y \\ i_B \\ I_f \end{bmatrix} \tag{5-10}$$

To establish the model for the computer simulation, consider the 'loop' containing v_R and v_Y in the equivalent circuit of the motor.

$$v_R - v_Y - R_s i_R - \frac{d}{dt}(L_R i_R) - \frac{d}{dt}(M_{RY} i_Y) - \frac{d}{dt}(M_{RB} i_B) - \frac{d}{dt}(M_{fR} i_f)$$
$$+ R_s i_Y + \frac{d}{dt}(L_Y i_Y) + \frac{d}{dt}(M_{RY} i_R) + \frac{d}{dt}(M_{YB} i_B) + \frac{d}{dt}(M_{fY} I_f) = 0 \quad (5\text{-}11)$$

and the 'loop' containing v_Y and v_B.

$$v_Y - v_B - R_s i_Y - \frac{d}{dt}(L_Y i_Y) - \frac{d}{dt}(M_{RY} i_R) - \frac{d}{dt}(M_{YB} i_B) - \frac{d}{dt}(M_{fY} I_f)$$
$$+ R_s i_B + \frac{d}{dt}(L_B i_B) + \frac{d}{dt}(M_{YB} i_Y) + \frac{d}{dt}(M_{RB} i_R) + \frac{d}{dt}(M_{fB} I_f) = 0 \quad (5\text{-}12)$$

In addition, because of the star connection,

$$i_R + i_Y + i_B = 0 \quad (5\text{-}13)$$

The blue phase current can be substituted from equation 5-13 into equations 5-11 and 5-12 and combined with equations 5-4 to 5-9 into matrix form to give

$$\begin{bmatrix} D_{11} & D_{12} \\ D_{21} & D_{22} \end{bmatrix} \frac{d}{dt} \begin{bmatrix} i_R \\ i_Y \end{bmatrix} = \begin{bmatrix} C_{11} & C_{12} \\ C_{21} & C_{22} \end{bmatrix} \begin{bmatrix} i_R \\ i_Y \end{bmatrix} + \begin{bmatrix} v_R - v_Y \\ v_Y - v_B \end{bmatrix} + v \cdot I_f \frac{\partial}{\partial x} \begin{bmatrix} M_{fY} - M_{fR} \\ M_{fB} - M_{fY} \end{bmatrix} \quad (5\text{-}14)$$

where,

$$C_{11} = -R_s - \frac{2\pi}{P} v (L_{s1} + 2M_{s1}) \sin(2\gamma)$$
$$= -0.07585 - 0.00715 \cdot v \cdot \sin(2\gamma) \quad (5\text{-}15)$$

$$C_{12} = R_s + \frac{2\pi}{P} v (L_{s1} + 2M_{s1}) \sin(2\gamma + 120)$$
$$= 0.07585 + 0.00715 \cdot v \cdot \sin(2\gamma + 120) \quad (5\text{-}16)$$

$$C_{21} = -R_s - \frac{2\pi}{P} v (L_{s1} + 2M_{s1}) \sin(2\gamma - 120)$$
$$= -0.07585 - 0.00715 \cdot v \cdot \sin(2\gamma - 120) \quad (5\text{-}17)$$

$$C_{22} = -2R_s + \frac{2\pi}{P} v (L_{s1} + 2M_{s1}) \sin(2\gamma)$$

$$= -0.1517 + 0.00715 \cdot v \cdot \sin(2\gamma) \quad (5\text{-}18)$$

$$\begin{aligned} D_{11} &= (L_s + M_s) - (L_{s1} + 2M_{s1})\cos(2\gamma) \\ &= 4.339 \times 10^{-3} - 0.1708 \times 10^{-3} \cos(2\gamma) \end{aligned} \quad (5\text{-}19)$$

$$\begin{aligned} D_{12} &= -(L_s + M_s) + (L_{s1} + 2M_{s1})\cos(2\gamma + 120) \\ &= -4.339 \times 10^{-3} + 0.1708 \times 10^{-3} \cos(2\gamma + 120) \end{aligned} \quad (5\text{-}20)$$

$$\begin{aligned} D_{21} &= (L_s + M_s) - (L_{s1} + 2M_{s1})\cos(2\gamma - 120) \\ &= 4.339 \times 10^{-3} - 0.1708 \times 10^{-3} \cos(2\gamma - 120) \end{aligned} \quad (5\text{-}21)$$

$$\begin{aligned} D_{22} &= 2(L_s + M_s) + (L_{s1} + 2M_{s1})\cos(2\gamma) \\ &= 8.678 \times 10^{-3} + 0.1708 \times 10^{-3} \cos(2\gamma) \end{aligned} \quad (5\text{-}22)$$

In equation 5-14, the time derivative of the mutual inductances between the permanent magnet equivalent circuit and each of the phases has been replaced by a partial derivative with respect to the slider position with the consequent multiplication by the time derivative of position i.e. velocity.

Further analysis of equations 5-15 to 5-22 shows that the effect of those sinusoidal components in the inductances on D_{11} to D_{22} can indeed be neglected compared to the constant component but the resistive terms C_{11} to C_{22} can be affected when the motor speed is not very low. The values could be varying with the slider position by 40% when the slider reaches the peak velocity 4.2 *m/s*. Apparently, C_{11} to C_{22} should not be neglected without further analysis and these terms will be included in the computer simulation to study the effect of the variations on the motor. For comparison, a simplified model can be derived from equation 5-14 when the constant phase inductances and inter phase mutual inductances are used,

$$\begin{bmatrix} L_s + M_s & -L_s - M_s \\ L_s + M_s & 2(L_s + M_s) \end{bmatrix} \frac{d}{dt} \begin{bmatrix} i_R \\ i_Y \end{bmatrix} = \begin{bmatrix} -R_s & R_s \\ -R_s & -2R_s \end{bmatrix} \begin{bmatrix} i_R \\ i_Y \end{bmatrix} + \begin{bmatrix} v_R - v_Y \\ v_Y - v_B \end{bmatrix} + \frac{\partial}{\partial x} \begin{bmatrix} M_{fR} - M_{fY} \\ M_{fY} - M_{fB} \end{bmatrix} vI_f \quad (5\text{-}23)$$

Equation 5-14 (or 5-23) establishes a model of the permanent magnet linear synchronous motor. Given the phase voltages, the model can be easily solved in the computer simulation to give the phase currents. The currents are converted into mechanical force in the motor to drive the slider and therefore to pump the fluids.

Force developed in a PLSM is related to three phase currents, self and mutual inductances of the stator, mutual inductances between the slider equivalent circuit and the three phases. Their relations can be mathematically described as shown in equation 5-24 [19].

$$F=\frac{1}{2}\begin{bmatrix} i_R & i_Y & i_B & I_f \end{bmatrix}\cdot\begin{bmatrix} pL_R & pM_{RY} & pM_{RB} & pM_{fR} \\ pM_{YR} & pL_Y & pM_{YB} & pM_{fY} \\ pM_{BR} & pM_{BY} & pL_B & pM_{fB} \\ pM_{fR} & pM_{fY} & pM_{fB} & pL_f \end{bmatrix}\cdot\begin{bmatrix} i_R \\ i_Y \\ i_B \\ I_f \end{bmatrix} \tag{5-24}$$

Where $p=\frac{\partial}{\partial x}$

By multiplying the matrices together and reorganising all terms, the total force produced by the motor can be expressed as follow.

$$F=I_f\cdot\left[i_R\cdot pM_{fR}+i_Y\cdot pM_{fY}+i_B\cdot pM_{fB}\right]+\frac{1}{2}\left[i_R{}^2\cdot pL_R+i_Y{}^2\cdot pL_Y+i_B{}^2\cdot pL_B\right]$$

$$+\left[i_Ri_Y\cdot pM_{RY}+i_Ri_B\cdot pM_{RB}+i_Yi_B\cdot pM_{YB}\right]=F_1+F_2+F_3 \tag{5-25}$$

Equation 5-25 shows that the force produced in the motor is decided by the three phase currents and the motor parameters. The motor parameters are fixed once the motor is designed and built, so the only decisive factor is the current. The total force can be partitioned into three terms. Substituting the inductances given in equations 5-1 to 5-9 into equation 5-25 gives the three terms as follows.

$$F_1=-I_f\frac{2\pi}{P}M_{fM}\left[i_R\sin(\gamma)+i_Y\sin(\gamma-120)+i_B\sin(\gamma+120)\right] \tag{5-26}$$

$$F_2=L_{s1}\frac{2\pi}{P}\left[i_R{}^2\cdot\sin(2\gamma)+i_Y{}^2\cdot\sin(2\gamma+120)+i_B{}^2\cdot\sin(2\gamma-120)\right] \tag{5-27}$$

$$F_3=2M_{s1}\frac{2\pi}{P}\left[i_Ri_Y\sin(2\gamma-120)+i_Yi_B\sin(2\gamma)+i_Bi_R\sin(2\gamma+120)\right] \tag{5-28}$$

To compare the three force components, three phase sinusoidal currents are used

$$\begin{aligned} i_R&=I_m\cos(\gamma+\theta)\\ i_Y&=I_m\cos(\gamma+\theta-120)\\ i_B&=I_m\cos(\gamma+\theta+120)\end{aligned} \tag{5-29}$$

where θ is the load angle. Substituting the three phase currents into equations 5-26 to 5-28 gives,

$$F_1 = \frac{2\pi}{P} \cdot \frac{3}{2} \cdot I_m \cdot M_{fM} \cdot I_f \cdot \sin(\theta) \tag{5-30}$$

$$F_2 = \frac{2\pi}{P} \cdot \frac{3}{2} \cdot I_m \cdot \frac{1}{2} \cdot L_{s1} \cdot I_m \cdot \sin(2\theta) \tag{5-31}$$

$$F_3 = -\frac{2\pi}{P} \cdot \frac{3}{2} \cdot I_m \cdot M_{s1} \cdot I_m \cdot \sin(2\theta) \tag{5-32}$$

Since the load angle is normally controlled close to 90 degrees to obtain high efficiency, which will be discussed in next chapter, and the maximum operation current is less than 1000 A, we have

$$\begin{aligned} M_{fM} \cdot I_f &= 4.983 \\ |\sin(\theta)| &> |\sin(2\theta)| \\ M_{s1} \cdot I_m &\leq 0.069 \\ \frac{1}{2} \cdot L_{s1} \cdot I_m &\leq 0.0164 \end{aligned}$$

Substituting these values into equations 5-30 to 5-32 shows that the second and the third terms of the force are far less than the first term even when the maximum phase current is supplied. Therefore the second and the third terms in equation 5-25 can be neglected.

To summarise, equations 5-14 and 5-25 form the simulation model of the motor electrical part based on the equivalent circuit shown in Figure 5.1. Equations 5-23 and 5-26 give the simplified model where the motor parameters are assumed to be constant.

5.3. D -- Q Axis Model.

The model developed above is non linear and complicated and therefore difficult to analyse for designing the current loop to implement vector control. This disadvantage can be overcome by the use of Park transformation to develop the d-q axis model. This model can be derived by transforming three phase currents and voltages in the model developed in the last section into d-q axis voltages and d-q axis currents, i.e. the three phase components are converted into the magnetic flux generating component and the force generating component. The Park transformation in the slider reference frame is given as [27, 35].

$$\begin{bmatrix} i_\alpha \\ i_\beta \end{bmatrix} = C_1 \cdot \begin{bmatrix} i_R \\ i_Y \\ i_B \end{bmatrix} \tag{5-33}$$

$$\begin{bmatrix} i_d \\ i_q \end{bmatrix} = C_2 \cdot \begin{bmatrix} i_\alpha \\ i_\beta \end{bmatrix} \tag{5-34}$$

where

$$C_1 = \frac{2}{3} \cdot \begin{bmatrix} 1 & \frac{-1}{2} & \frac{-1}{2} \\ 0 & \frac{\sqrt{3}}{2} & \frac{-\sqrt{3}}{2} \end{bmatrix}$$

$$C_2 = \begin{bmatrix} \cos\gamma & \sin\gamma \\ \sin\gamma & -\cos\gamma \end{bmatrix}$$

Equation 5-33 converts the three phase currents to an orthogonal two phase currents with respect to the stator axis. Equation 5-34 transfers the two axis current into d-q axis current, which represents the stator current in the slider coordinates with γ being the current load angle. The vector diagrams of the two transformations are given in Figures 5.9 and 5.10.

Rearranging and combining equations 5-33 and 5-34 together gives

$$\begin{bmatrix} i_R \\ i_Y \\ i_B \end{bmatrix} = \begin{bmatrix} \cos(\gamma) & \sin(\gamma) \\ \cos(\gamma - \frac{2\pi}{3}) & \sin(\gamma - \frac{2\pi}{3}) \\ \cos(\gamma + \frac{2\pi}{3}) & \sin(\gamma + \frac{2\pi}{3}) \end{bmatrix} \cdot \begin{bmatrix} i_d \\ i_q \end{bmatrix} \tag{5-35}$$

Similarly,

$$\begin{bmatrix} v_R \\ v_Y \\ v_B \end{bmatrix} = \begin{bmatrix} \cos(\gamma) & \sin(\gamma) \\ \cos(\gamma - \frac{2\pi}{3}) & \sin(\gamma - \frac{2\pi}{3}) \\ \cos(\gamma + \frac{2\pi}{3}) & \sin(\gamma + \frac{2\pi}{3}) \end{bmatrix} \cdot \begin{bmatrix} v_d \\ v_q \end{bmatrix} \tag{5-36}$$

Including the equivalent current gives

$$\begin{bmatrix} i_R \\ i_Y \\ i_B \\ I_f \end{bmatrix} = \begin{bmatrix} \cos(\gamma) & \sin(\gamma) & 0 \\ \cos(\gamma - 120) & \sin(\gamma - 120) & 0 \\ \cos(\gamma + 120) & \sin(\gamma + 120) & 0 \\ 0 & 0 & 1 \end{bmatrix} \cdot \begin{bmatrix} i_d \\ i_q \\ I_f \end{bmatrix} \tag{5-37}$$

By substituting equations 5-36 and 5-37 into the equation 5-10 and rearranging the equation, the stator three phase equations of the motor can be transformed into stator d-q axis equations as below,

$$\begin{bmatrix} v_d \\ v_q \end{bmatrix} = \begin{bmatrix} L_s + M_s - M_{s1} - \frac{1}{2}L_{s1} & 0 & 0 \\ 0 & L_s + M_s + M_{s1} + \frac{1}{2}L_{s1} & 0 \end{bmatrix} \cdot \begin{bmatrix} i_d' \\ i_q' \\ I_f \end{bmatrix}$$

$$+ \begin{bmatrix} R_s & \frac{\pi}{P}v(L_s + M_s + M_{s1} + \frac{1}{2}L_{s1}) & 0 \\ -\frac{\pi}{P}v(L_s + M_s - M_{s1} - \frac{1}{2}L_{s1}) & R_s & -M_{fM}\frac{\pi}{P}v \end{bmatrix} \cdot \begin{bmatrix} i_d \\ i_q \\ I_f \end{bmatrix}$$

(5-38)

As seen in the last section the amplitude of the variations of the stator inductances are far less than the value of the constant components, hence L_{s1} and M_{s1} can be eliminated from equation 5-38. Then following model is derived,

$$\begin{bmatrix} v_d \\ v_q \end{bmatrix} = \begin{bmatrix} R_s + (L_s + M_s)p & \frac{\pi}{P}v(L_s + M_s) & 0 \\ -\frac{\pi}{P}v(L_s + M_s) & R_s + (L_s + M_s)p & -M_{fM}\frac{\pi}{P}v \end{bmatrix} \cdot \begin{bmatrix} i_d \\ i_q \\ I_f \end{bmatrix} \tag{5-39}$$

The force produced in the motor can also be expressed in d-q axis current components. This is simply achieved by the use of equation 5-35. Substituting equation 5-35 into equation 5-26 gives

$$F_1 = -\frac{3}{2} \cdot I_f \cdot M_{fM} \cdot \frac{\pi}{P} \cdot i_q \tag{5-40}$$

Substituting equations 5-4 to 5-9 and equation 5-35 into equations 3-27 and 3-28 respectively gives,

$$F_2 = \frac{3}{2} \cdot L_{s1} \cdot \frac{\pi}{P} \cdot i_d \cdot i_q \tag{5-41}$$

$$F_3 = 3 \cdot M_{s1} \cdot \frac{\pi}{P} \cdot i_d \cdot i_q \tag{5-42}$$

Therefore the total force produced by the motor is equal to the sum of three force components in the general case as given in equation 5-43.

$$F = -\frac{3}{2} \cdot \frac{\pi}{P} \cdot M_{fM} \cdot I_f \cdot i_q + \frac{3}{2} \cdot \frac{\pi}{P} \cdot (L_{s1} + 2M_{s1}) \cdot i_d \cdot i_q \tag{5-43}$$

In equation 5-43, the first term is determined by the peak value of the mutual inductance between the stator and the equivalent circuit of the slider magnet and the q axis current. Since M_{fM}, I_f and P of the PLSM are fixed values, the term is proportional to the q axis current I_q . The second term of the equation is related to both q axis and d axis currents. It is related to the sinusoidal components (L_{s1} , M_{s1}) of phase inductances and inter phase mutual inductances and not to constant components.

To simplify the model, the second term in equation 5-43 is compared against the first term. The d axis current must be kept reasonably low, and 20% of the q axis current may be the maximum range in order to obtain high efficiency [35]. Substituting all relevant values into the equation shows that the first term is several orders of magnitude greater than the maximum value of the second term, hence the second term can be neglected without harm. Therefore the parameter variations appear to have little effect on the overall dynamic performance of the motor in this case.

5.4. Summary.

In this chapter two mathematical models of the electrical part of the motor have been developed, the three phase model and the stator d-q axis model in the slider reference frame. Both models will be used in the computer simulation and the d-q axis model in the design of the current control loop. Parameter variation of the motor due to the permanent magnets has been observed from the test. This variation will have certain effect on the performance of the motor, depending on the motor velocity as described in the ordinary three phase model. However it appears not to have much impact on the overall dynamics in this case because the variations are quite small compared to the constant values. This will be further studied using the computer simulation in the next chapter.

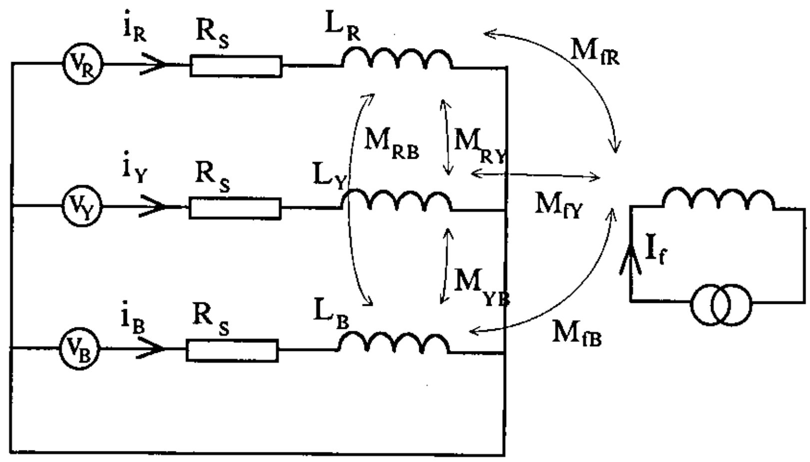

Figure 5.1. Eqivalent Circuit of The Motor

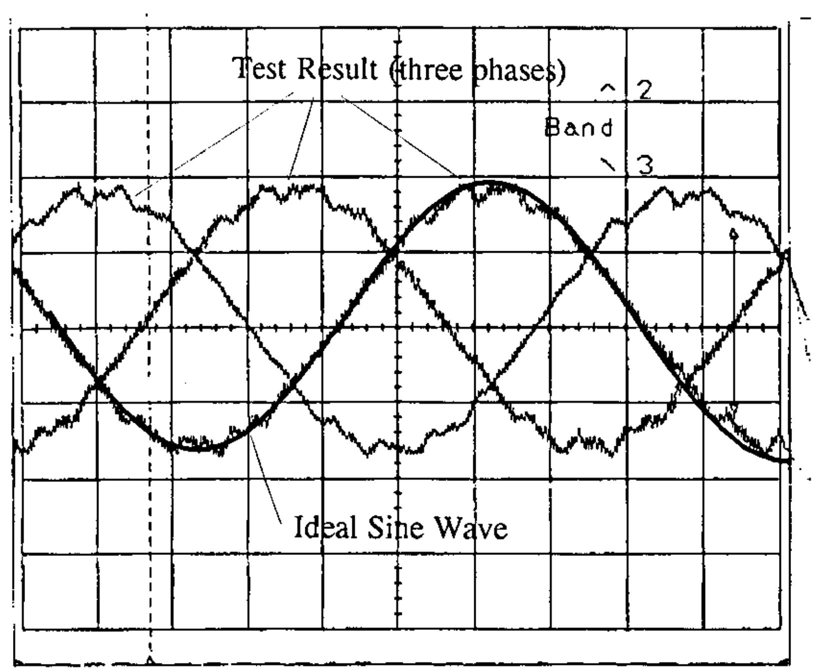

Figure 5.2. E.M.F. at constant speed

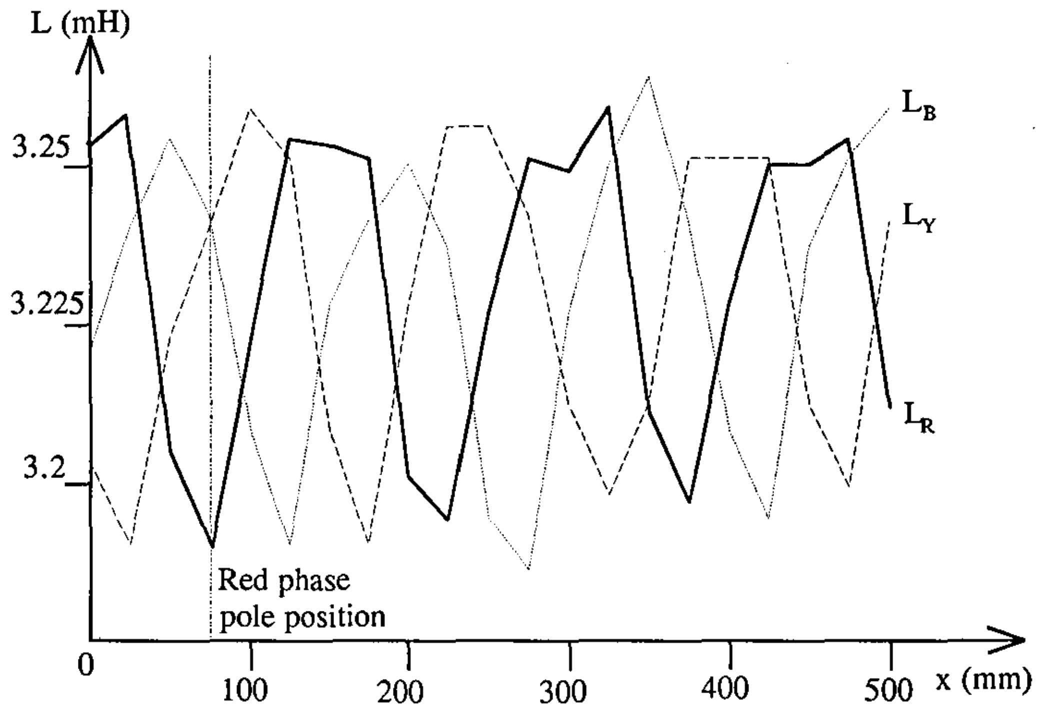

Figure 5.3. Self Inductances of Motor Stator (Test Result)

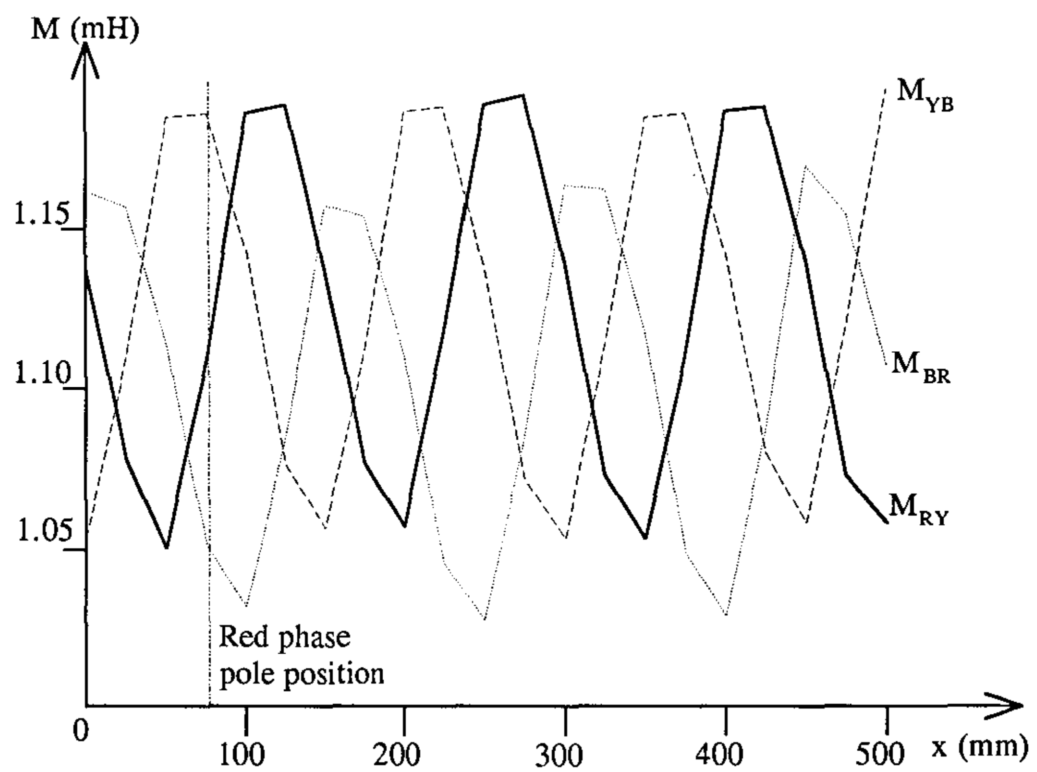

Figure 5.4. Mutual Inductances of Motor Stator (Test Result)

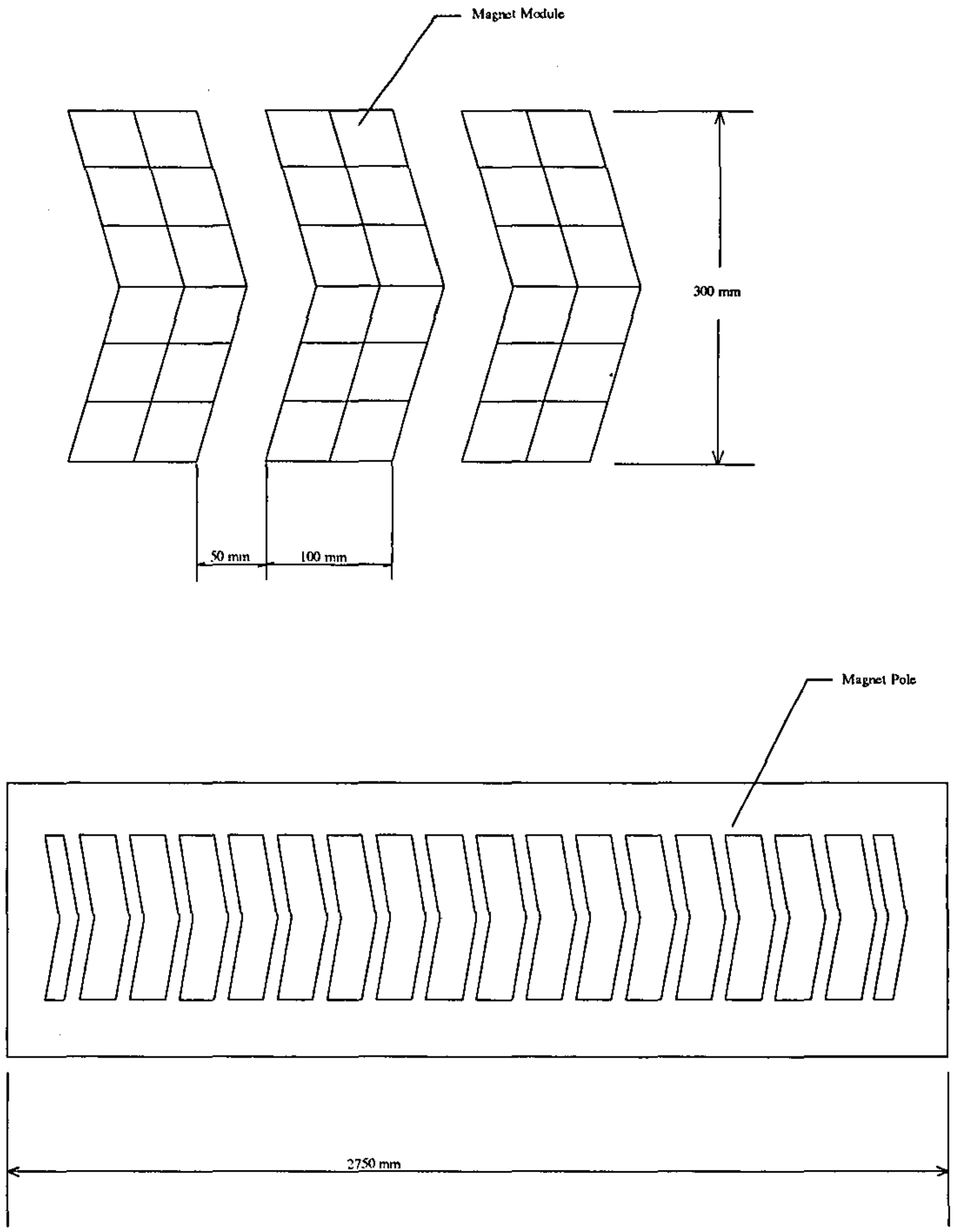

Figure 5.5. Diagram of the Slider Magnets

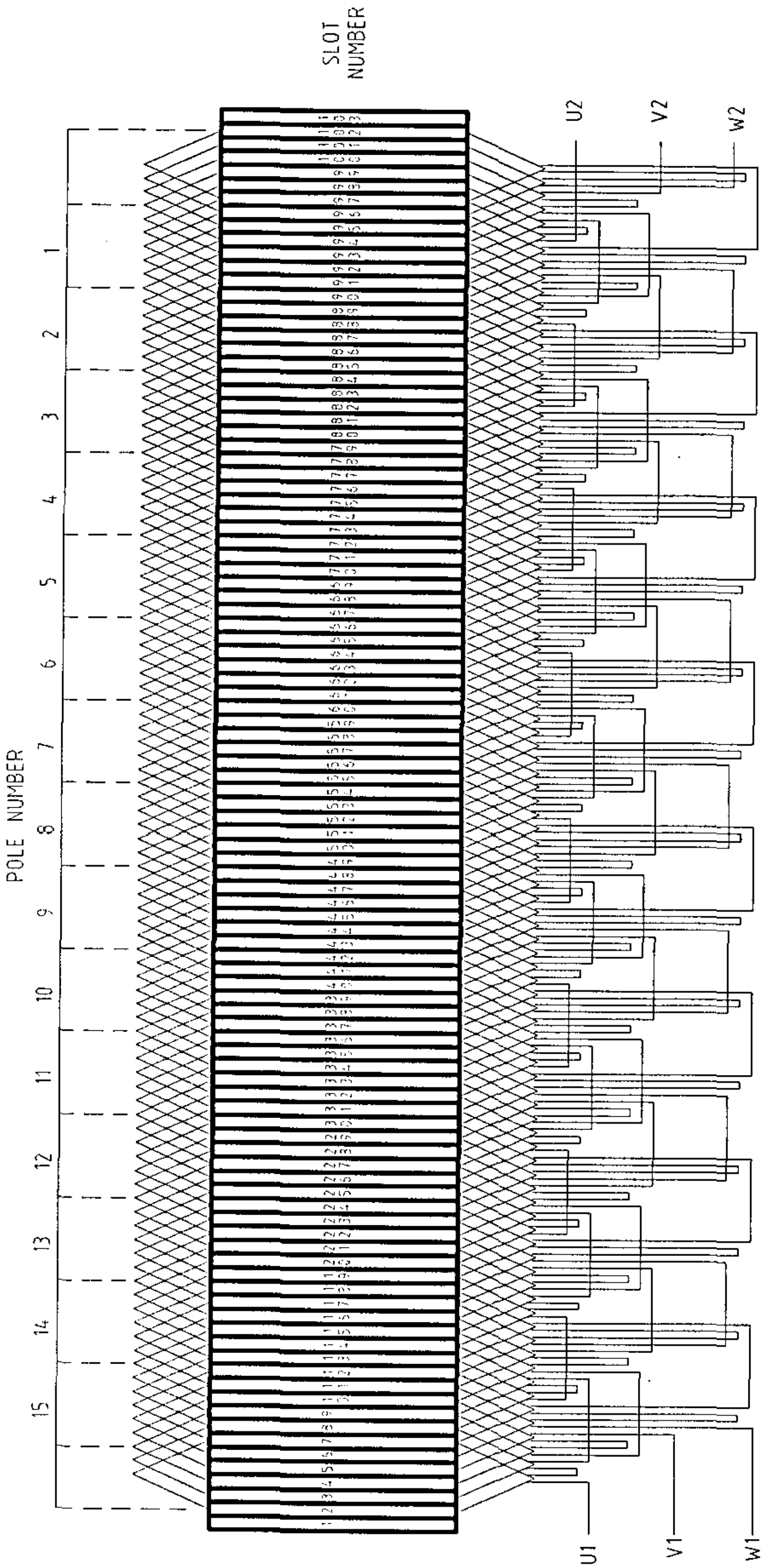

Figure 5.6. Winding Diagram of the Motor Slider

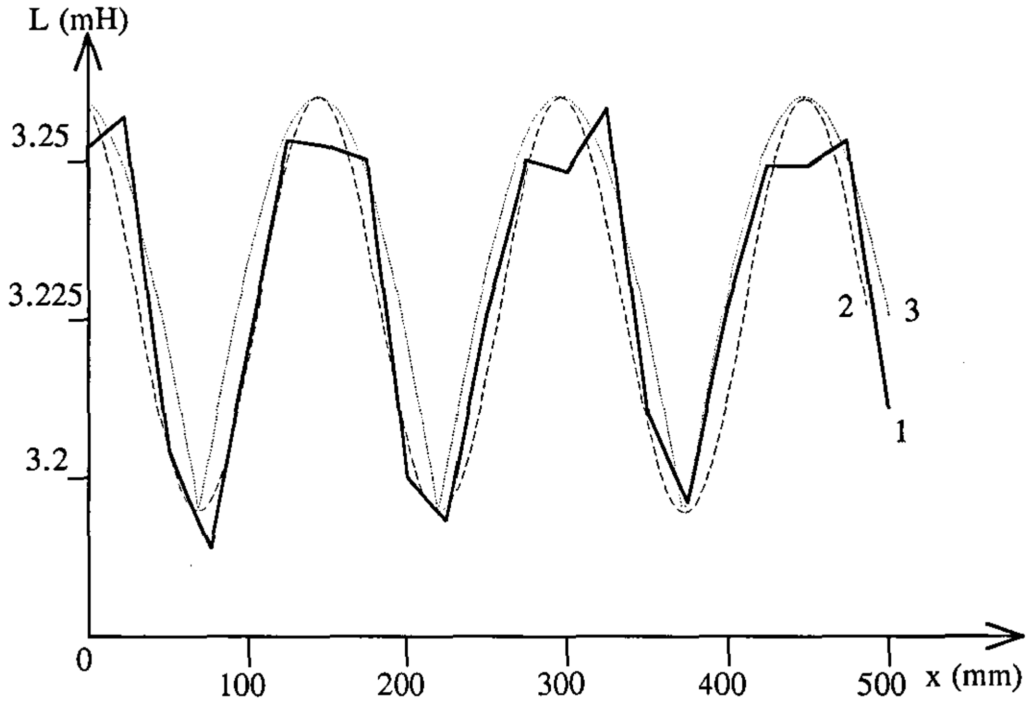

Figure 5.7. Simulated Self Inductance
(1 -- test result, 2 -- sin wave, 3 -- absolute value of sin wave)

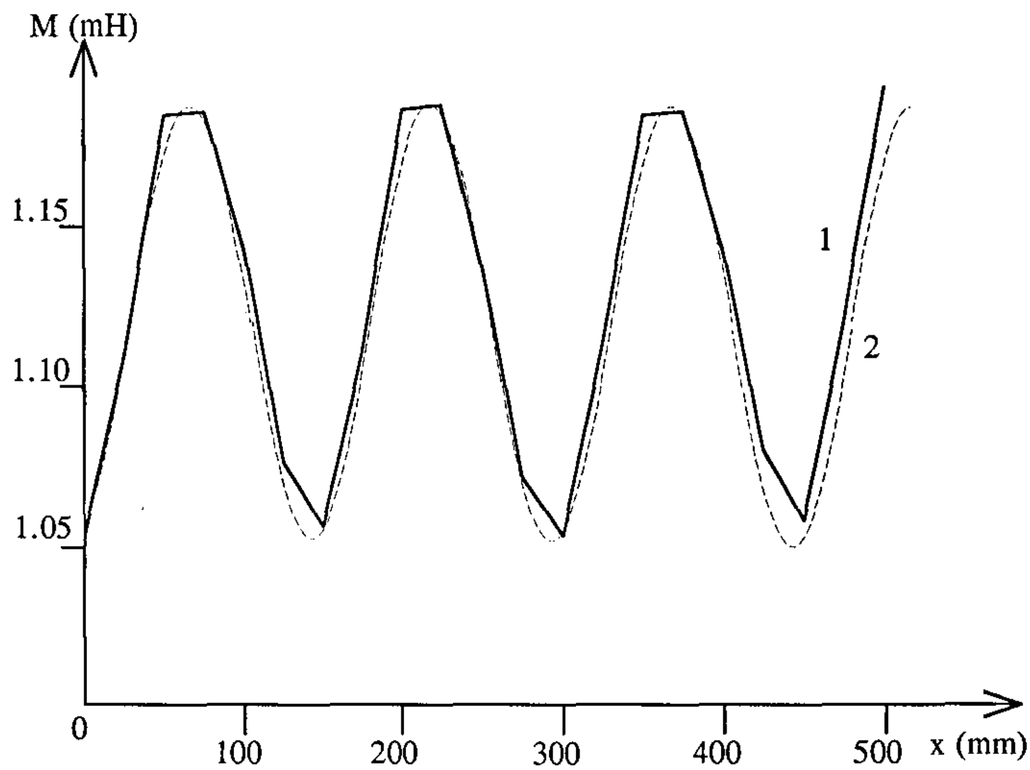

Figure 5.8. Simulated Mutual Inductance
(1 -- test result, 2 -- sin wave)

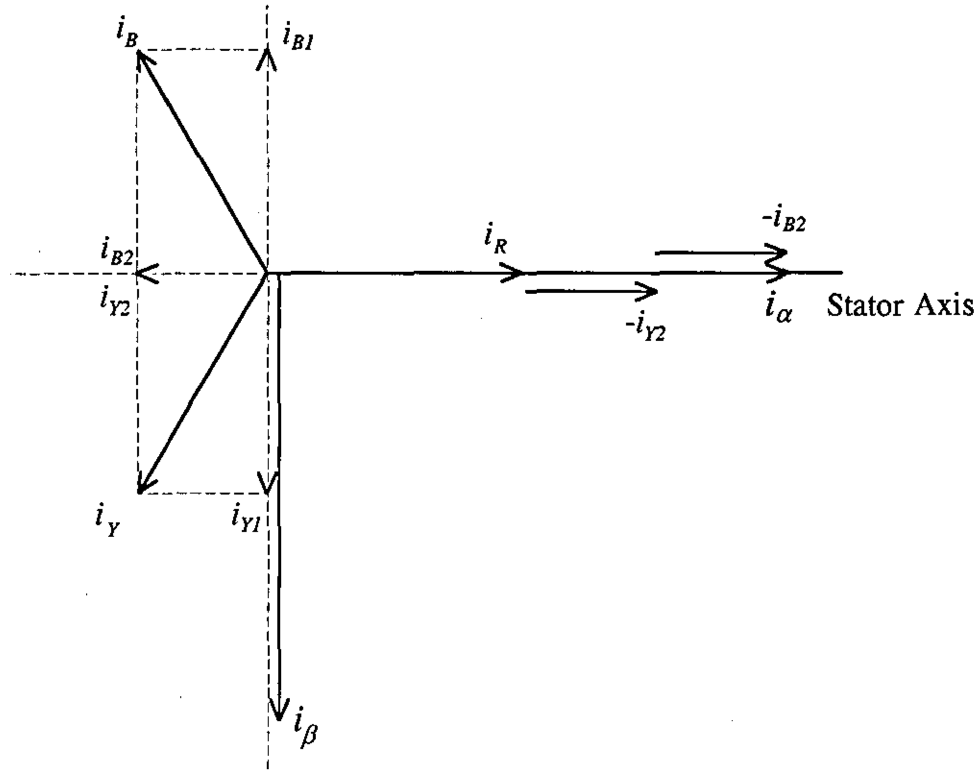

Figure 5.9. Vector Diagram of 3 - 2 Axis Transformation

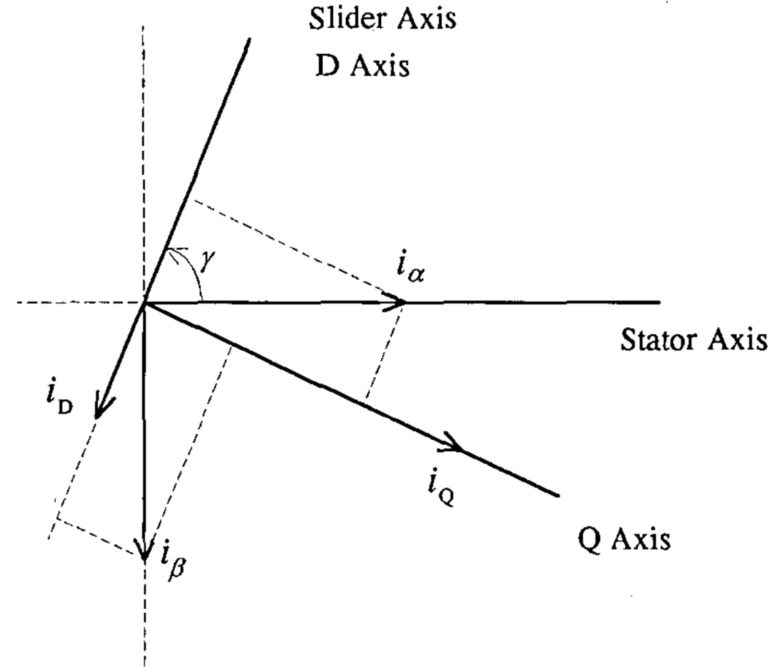

Figure 5.10. Diagram of Vectors with Respect to
The Slider Axis and The Stator Axis

CHAPTER 6.

DESIGN OF CURRENT CONTROL LOOP

The principle of vector control of a.c. machines is very similar to control of a separately excited d.c. machine. In the control of a d.c. motor there is a clear separation of function with clear linear relationships between state variables. The field current produces the required flux and the armature current produces torque (force in the case of linear motors). Armature current control permits direct control of the torque, which is required for good dynamic response in high performance closed loop drives. However this is not the case in a.c. motors. There is no direct relation between motor current, flux and torque. The torque is approximately equal to the input power divided by the synchronous speed. The variables which are readily available for control are the voltage, the frequency, the current, the speed and the load angle in the case of the synchronous motor.

Vector control methods have now presented an opportunity to control a.c. motors in a similar high performance manner to d.c. motors. The overall action is to produce a force on the slider which follows the demanded input signal.

The vector control of a.c. motors is one of the most recent developments in drive technology, and likely to be one of the most significant. It achieves from the standard industrial a.c. motor a dynamic performance at least the equal of an advanced d.c. motor drive system. Speed holding is exact; maximum torque is available at all speeds up to base speed; there is no dead band of torque or speed control. This greatly exceeds the capability of the variable voltage and variable frequency (VVVF) type of drive. An additional advantage is the fast dynamic response of the true vector drive, which ensures the accurate response of the complete control system.

In this chapter, the vector control strategy used in the control system is presented in section 6.1. Section 6.2 describes design of the current controller. Effects of the load angle on the performance of the system are discussed in section 6.3. Simulation results are presented in section 6.4. Based on the vector control principle and current feedback control, the non linear dynamic model of the motor drive can be simplified and linearised. The resultant linear model for the design of the outer loop position control is given in section 6.4. A summary of the chapter is presented in section 6.5.

6.1. Vector Control Scheme

A prerequisite for high performance speed or position control in all adjustable speed a.c. drives is responsive control of force. The relationships between the stator current amplitudes and instantaneous force can be conveniently described with the aid of vector notation. With a stator fed machine, it calls for transformation of the stator current vector into a moving frame of reference given by the slider current vector. By splitting the transformed stator current vector into direct and quadrature components, i_d and i_q, respectively, inputs for decoupled control of flux and force are obtained as in the case of a separately excited d.c. machine, where i_d is analogous to the field current and i_q is analogous to the armature current of the d.c. machine. Equations 5-33 and 5-34 have given the Park transformation to convert the three phase current into the d - q axis current. The vector relationships between the phase current and the vector current have been illustrated in Figures 5.9 and 5.10.

Since, in the PLSM, the magnetic flux generated from the slider is in fixed relation to the slider, the flux angular position is determined by the slider position, which is in alignment with the d axis. The instantaneous position of the slider d axis defined by the slider magnet flux is at the angle γ with respect to the phase A stator axis. At every instant the stator current vector can be decoupled into its two orthogonal components, i_d and i_q , along the slider d and q axes.

Since the incremental permeability of rare earth magnet materials is nearly that of free space, the magnet thickness appears as large series air gaps in the magnetic paths, which cause almost equal d and q axis inductances in the surface mounted permanent magnet machine [15, 21]. Thus the force is directly proportional to the q axis component of the stator current. This is also proved by equation 5-43, where the d axis current related term (second term) is much smaller than the first one and thus can be neglected. Hence, with the application of the vector control, independent control of force and flux producing currents are possible.

Figure 6.1 shows the vector control strategy of the permanent magnet linear synchronous motor. Two of the stator phase currents are obtained from two current sensors and the third current is derived from the other two because of the star connection of the motor. The three phase currents are fed back into the controller and converted to two axis currents with respect to the stator frame. The two axis currents are then transformed into the d - q axis currents with respect to the current position of the motor slider and therefore an equivalent angle, between the slider and stator frames, expressed in electrical degrees.

The currents i_d and i_q are compared with the reference d - q axis currents i_{d_ref} and i_{q_ref} in the current control regulator to give demanded d - q axis voltages v_d and v_q. The reference current i_{q_ref} is in fact proportional to the force demanded by the outer loop position / velocity controller. Once the demanded force F_{ref} is known, i_{q_ref} can be calculated by using equation 5-40. The reference current i_{d_ref} is almost irrelevant to the force produced by the PLSM, however control of the current affects the performance of the drive system [35, 36].

The required input phase voltages needed to produce the phase current, and therefore the commanded i_d and i_q, are calculated from the inverse Park Transformation which is given as follows:

$$\begin{bmatrix} v_R \\ v_Y \\ v_B \end{bmatrix} = C_1^{-1} \cdot C_2^{-1} \cdot \begin{bmatrix} v_d \\ v_q \end{bmatrix} \qquad (6\text{-}1)$$

where

$$C_1^{-1} = \begin{bmatrix} 1 & 0 \\ -\frac{1}{2} & \frac{\sqrt{3}}{2} \\ -\frac{1}{2} & -\frac{\sqrt{3}}{2} \end{bmatrix}$$

$$C_2^{-1} = \begin{bmatrix} \cos(\gamma_1) & \sin(\gamma_1) \\ \sin(\gamma_1) & -\cos(\gamma_1) \end{bmatrix}$$

where $\gamma_1 = \gamma + \gamma_2 + \gamma_3$ is the angle between the slider and stator frames to transform the voltages v_d and v_q back to their equivalent three phase system in the stator coordinates. The three components of the phase angle γ_1 have to be considered.

- The angle γ, which represents the electrical angle of the last sampled position of the motor slider. This is achieved by using a position transducer, which is also required by the outer loop controllers.

- An angle γ_2, which is caused by the new values of v_d and v_q demanded by the current control regulator.

- An angle γ_3, which is used to compensate for the total time delay mainly introduced by the computing time of the software and the switching delay of the inverter. The value of the angle depends on the current velocity of the motor.

The three phase voltages supplied onto the motor are then realised via the Pulse Width Modulation which converts the values of these voltages into relevant logic pulses to switch on and off the GTOs of the inverter.

6.2. Current Controller

6.2.1. Current Regulator

The current regulator controls real d - q axis currents to follow the reference values. Because this is the innermost loop and its performance will certainly affect that of the entire system, it is desirable to have a tight controller which minimises the errors and gives the highest bandwidth such that fast responses and robustness can be firstly achieved in this control loop. The equation used for the control design is 5-39, which is the model of the PLSM. To make the control problem clearer, the equation is rearranged.

$$(L_s + M_s)\frac{di_d}{dt} + R_s \cdot i_d + \frac{\pi}{P} \cdot v \cdot (L_s + M_s) \cdot i_q = v_d \qquad (6\text{-}2)$$

$$(L_s + M_s)\frac{di_q}{dt} + R_s \cdot i_q - \frac{\pi}{P} \cdot v \cdot (L_s + M_s) \cdot i_d - M_{fM} \cdot \frac{\pi}{P} \cdot v \cdot I_f = v_q \qquad (6\text{-}3)$$

Equations 6-2 and 6-3 show that this is a two input two output system. The velocity v is a function of time and its dynamics are much slower that of the currents.

Many publications have presented various structures for the current controllers. One method is to control the VSI directly to produce the required phase currents, where several control strategies are available such as the hysteresis current controller, the ramp comparison controller and the predictive controller [21, 22, 26]. Some other methods have also been developed. Pillay et al have developed a control algorithm that decouples the control of i_d and i_q currents such that the control regulators for i_d and i_q can be obtained independently [23]. To simplify the model, Liu et al have presented a control structure where the reference and real d axis current are both assumed to zero [27]. Furthermore, Naunin et al compared performances of current controllers in rotor and stator reference systems [28].

These proposed controllers are supported either by computer simulations or real tests or both. They are uniquely studied in time domain, mostly using step responses, which is very important in the design procedure and one may achieve the required performance by 'trial and error' when the whole system is not too complicated. However, a high frequency bandwidth of the current loop in the subsea pump system is the basis of ensuring fast responses and robustness of the entire system. In addition, the frequency responses provide a clearer guidance to derive an equivalent transfer function of the inner loop for design of the outer loop controllers. Thus it is desirable to investigate the performance of the current controller both in the time domain and the frequency domain.

A control scheme, consisting of two PI units for controlling d and q axis currents respectively and feedforward terms for improving the control performance, is developed for the system. Figure 6.2 gives the block diagram of the controller, where PLT stands for the process plant representing the electrical part of the motor drive.

6.2.2. Command Feedforward Control

The control scheme is in fact a combination of open and closed loop operations. The feedforward strategy used in the controller is called Command Feedforward Control [41], which is essentially an open loop control. Feedforward control is normally used to anticipate the effects of a command input on the process outputs and to modify manipulations generated by a closed loop controller in such a way that error in the process output is reduced or eliminated. In this particular case, it predicts the steady state values of the output voltages v_d and v_q from the reference inputs i_{d_ref} and i_{q_ref}, where the interactions between d - q axis variables are included. The equations relating v_d and v_q are given in equations 6-2 and 6-3, which define all the feedforward terms and produce the corrective output voltages. The expressions of these feedforward terms are given as follows.

$$v_{d\_ff} = R_s \cdot i_{d\_ref} + \frac{\pi}{P} \cdot v \cdot (L_s + M_s) \cdot i_{q\_ref} \tag{6-4}$$

$$v_{q\_ff} = R_s \cdot i_{q\_ref} - \frac{\pi}{P} \cdot v \cdot (L_s + M_s) \cdot i_{d\_ref} - M_{fM} \cdot \frac{\pi}{P} \cdot v \cdot I_f \tag{6-5}$$

6.2.3. Closed Loop Controller

The accuracy of feedforward control depends on the accuracy of knowledge of the process transfer function. Any inaccuracies in this control are compensated for by a closed loop controller.

Design of the controller is based on such specifications as wide current bandwidth for quick responses, good dynamic and static behaviour and ease of tuning. A conventional PI controller is chosen for the current loop control, which is given in equation 6-6.

$$G_{PI\_vec}(s) = K_{P\_vec} + \frac{K_{I\_vec}}{s} \tag{6-6}$$

The PI controller is a very effective controller and commonly used in the drive industry [26]. The proportional gain determines the bandwidth of the closed loop and the integration gain eliminates steady state errors. The gains are decided and performance of the controller is assessed by computer simulation, both in the time domain and the frequency domain.

6.2.4. Sample Period

The sample period chosen for a computer control system can have a significant impact on its performance. The sample period can affect the stability of the system and how rapidly disturbances and command inputs are responded to. It is usually desirable to make the sample period as short as possible in order to achieve rapid response and minimise the adverse effects of the sample period on stability. However the digital processing required for the vector control of the motor is of considerable complexity; in particular, the various multipliers and function generators are needed for the coordinate transformation. Some other factors such as computer capacity, clock frequency and control accuracy also restrict the selection of the sample period. The choice is mainly made based on following considerations.

- Bandwidth of Control Loop. High bandwidth of the current loop is required to ensure fast responses of the whole system. The higher bandwidth requires a smaller sample period.

- Accuracy of Flux Vector Position. A good accuracy of the flux vector position, which is derived from the feedback position, is needed since this is the basis of coordinate transformation. Thus it requires sufficiently fast sampling frequency, as a large sample period may result in the incorrect reconstruction of stator current and hence flux vector [20].

- Computing Time. The signal processing required for the vector control together with the current control loop is of considerably complexity. The total computing time in each sampling period depends on both the microprocessor to be used and the efficiency of software to be programmed.

- PWM and VSI. In the PWM process, the switching frequency should be much higher than that of the fundamental signals in order to minimise the size of the voltage harmonics order. However, restrictions on the switching frequency are switching losses and pulse widths. The switching losses in the inverter could be dramatically increased with the increase of the carrier frequency, which reduces efficiency and causes heat dissipation problems. The width of switching pulses affects the control accuracy of the inverter. The higher the carrier frequency and the narrower the pulses, the less will be the accuracy of the control. In addition, computing time must be allowed to generate the PWM signals.

Considering all factors listed above, a sample time period (t_s) 1.5 *ms* is initially chosen for the current control loop. By using this sample period, the controller can achieve:

- Sample frequency $f_s = \frac{1}{t_s} = 666.67\ Hz$

- Switching frequency $f_s = \frac{1}{t_s} = 666.67\ Hz$

For the highest fundamental frequency: $f_{max} = \dfrac{peak\,speed}{2.0 \times pole\,pitch} = 14\ Hz$,

Achieved frequency ratio $\rho = \dfrac{f_s}{f_{max}} = 47.6\ times$

- The worst resolution

  of the flux vector in electrical degrees is: $\dfrac{t_s \cdot peak\,speed \cdot 180}{pole\,pitch} = 7.56^0$

- 1.5 *ms* for computing time and pulse width of the switching logic.

6.3. Load Angle Control

The load angle of the motor can be controlled by adjusting the d axis current. The conventional control method is to force $i_d = 0$ so as to produce maximum force for a given stator current [4, 20, 27]. However, control of the current i_d affects the performances of a drive system such as inverter capacity and power factor. Based on the idea of the field weakening, Leonhard suggested operation with $i_d = 0$ up to the voltage which is reached at the base speed; a further increase in speed can then be obtained by shifting the current into the unstable region, i.e. load angle more than 90 degrees, while maintaining constant voltage [4]. Morimoto et al presented unity power factor control and constant flux linkage control methods, which are suited for constant speed drive applications and for interior magnet motors respectively [36]. In this section a different approach is presented for improving both the inverter capacity and the power factor of the drive, where the d axis current is controlled proportional to the q axis current such that the load angle is kept constant [35].

6.3.1. Phase Currents

From equation 5-35, three phase currents can be represented by the d-q axis currents.

$$\begin{bmatrix} i_R \\ i_Y \\ i_B \end{bmatrix} = \sqrt{i_d^{\,2} + i_q^{\,2}} \cdot \begin{bmatrix} \sin(\gamma + \theta) \\ \sin(\gamma - 2\pi/3 + \theta) \\ \sin(\gamma + 2\pi/3 + \theta) \end{bmatrix} \tag{6-7}$$

where $\theta = \tan^{-1}(i_d / i_q) = \tan^{-1}(K_\theta)$ is constant.

If $i_d = 0$, equation 6-7 becomes,

$$\begin{bmatrix} i_R \\ i_Y \\ i_B \end{bmatrix} = i_q \cdot \begin{bmatrix} \sin(\gamma) \\ \sin(\gamma - 2\pi/3) \\ \sin(\gamma + 2\pi/3) \end{bmatrix} \tag{6-8}$$

The phase currents will be increased when i_d is not equal to 0. The fractional increase in current is:

$$\frac{\Delta I}{I} = \frac{\sqrt{i_d^2 + i_q^2} - |i_q|}{|i_q|} = \sqrt{(i_d / i_q)^2 + 1} - 1 \tag{6-9}$$

Table 6.1 gives the increase of the phase currents for the different values of angle θ. From the current point of view, the angle should be limited, otherwise the phase currents will be increased dramatically.

Table 6.1. Percentage Increase of I

θ	10	20	30	40	50	60	70	80
%	1.5	6.4	15.5	30.5	55.6	100	192	575

6.3.2. Phase Voltages

Assuming that it is a three phase balanced situation, the outcome of the analysis of one phase can represent that of other phases. For the red phase, substituting equation 5-35 into 5-10 gives,

$$\begin{aligned} v_R = {} & R_s \cdot \sqrt{i_d^2 + i_q^2} \cdot \sin(\gamma + \theta) + (L_s + M_s + \frac{1}{2} L_{s1} + M_{s1}) \cdot \frac{\pi}{P} \cdot v \cdot \sqrt{i_d^2 + i_q^2} \cdot \cos(\gamma + \theta) \\ & + \frac{3}{2}(L_{s1} - M_{s1}) \cdot \frac{\pi}{P} \cdot v \cdot \sqrt{i_d^2 + i_q^2} \cdot \cos(3\gamma + \theta) - M_{fM} \cdot I_f \cdot \frac{\pi}{P} \cdot v \cdot \sin(\gamma) \\ & + \frac{d\, i_d}{dt} \cdot \left[(L_s + M_s + \frac{1}{2} L_{s1} + M_{s1}) \cdot \cos(\gamma) + \frac{1}{2}(L_{s1} - M_{s1}) \cdot \cos(3\gamma) \right] \\ & + \frac{d\, i_q}{dt} \cdot \left[(L_s + M_s - \frac{1}{2} L_{s1} - M_{s1}) \cdot \sin(\gamma) + \frac{1}{2}(L_{s1} - M_{s1}) \cdot \sin(3\gamma) \right] \end{aligned} \tag{6-10}$$

The operation is such that the motor mainly has to overcome the steady pressure and to drive the total mass of the slider and the fluids in the pipes under constant acceleration or deceleration. Therefore the motor works in steady state for most of time from the motor force and current point of view, i.e. $di_d / dt \approx 0$ and $di_q / dt \approx 0$, for which the last two terms in equation 6-10 are equal to zero. In addition, the third term in the equation can also be neglected because its amplitude is much smaller than the second term, considering the values of the motor parameters. Therefore equation 6-10 can be simplified to:

$$v_R = R_s \cdot \sqrt{i_d^{\,2} + i_q^{\,2}} \cdot \sin(\gamma + \theta) + (L_s + M_s + \frac{1}{2} L_{s1} + M_{s1}) \cdot \frac{\pi}{P} \cdot v \cdot \sqrt{i_d^{\,2} + i_q^{\,2}} \cdot \cos(\gamma + \theta)$$
$$- M_{fM} \cdot I_f \cdot v \cdot \frac{\pi}{P} \cdot \sin(\gamma) \qquad (6\text{-}11)$$

or

$$v_R = R_s \cdot \sqrt{i_d^{\,2} + i_q^{\,2}} \cdot \sin(\gamma + \theta) + (L_s + M_s + \frac{1}{2} L_{s1} + M_{s1}) \cdot \frac{\pi}{P} \cdot v \cdot i_q \cdot \cos(\gamma)$$
$$+ (L_s + M_s + \frac{1}{2} L_{s1} + M_{s1}) \cdot \frac{\pi}{P} \cdot v \cdot i_d \cdot \sin(\gamma) - M_{fM} \cdot I_f \cdot v \cdot \frac{\pi}{P} \cdot \sin(\gamma)$$
$$(6\text{-}11\text{-}a)$$

If $i_d = 0$, equation 6-11 becomes:

$$v_R' = R_s \cdot i_q \cdot \sin(\gamma) + (L_s + M_s + \frac{1}{2} L_{s1} + M_{s1}) \cdot \frac{\pi}{P} \cdot v \cdot i_q \cdot \cos(\gamma)$$
$$- M_{fM} \cdot I_f \cdot v \cdot \frac{\pi}{P} \cdot \sin(\gamma) \qquad (6\text{-}12)$$

Variation of the phase voltage due to the d - q axis currents i_d and i_q can be separated into two cases, where the motor works as a motor and generator respectively. As mentioned earlier, the constant pressure in the system applies an opposing load force on the slider, which means that the machine used in this system almost always works in the motor mode. So only the motor case is discussed here.

Rewriting equations 6-11 and 6-12 into vector format:

$$V_R = V_1 + V_2 - E_g \qquad (6\text{-}13)$$

$$V_R' = V_1' + V_2' - E_g \qquad (6\text{-}14)$$

where V_1 and V_1' represent the resistive terms in equations 6-11 and 6-12 respectively, V_2 represents the $\sqrt{i_d^2 + i_q^2}$ term in equation 6-11 and V_2' represents the i_q term in equation 6-12. The effect of the resistive term is much smaller than that of other terms and therefore can be neglected [35] and a vector diagram is then obtained as shown in Figure 6.3. The diagram clearly shows that the phase voltages are decreased when i_d is increased from zero if the correct direction of rotation is chosen.

The amplitude of the phase voltage can be derived as follow.

$$V_2 = V_2' / \cos(\theta) \tag{6-15}$$

$$V_R' = \sqrt{(E_g)^2 + (V_2')^2} = \nu \cdot \frac{\pi}{P} \cdot \sqrt{M_{fM}{}^2 \cdot I_f{}^2 + (L_s + M_s + \frac{1}{2} L_{s1} + M_{s1})^2 \cdot i_q{}^2} \tag{6-16}$$

$$\begin{aligned} V_R &= \sqrt{V_2^2 + E_g^2 - 2V_2 \cdot E_g \cdot \cos(\pi/2 - \theta)} \\ &= \nu \cdot \frac{\pi}{P} \cdot \left[M_{fM}{}^2 \cdot I_f{}^2 + \frac{(L_s + M_s + L_{s1}/2 + M_{s1})^2 \cdot i_q{}^2}{\cos^2(\theta)} \right. \\ &\quad \left. -2M_{fM} \cdot I_f \cdot (L_s + M_s + \frac{1}{2} L_{s1} + M_{s1}) \cdot i_q \cdot \tan(\theta) \right]^{1/2} \end{aligned} \tag{6-17}$$

The increase of phase voltage is defined to be:

$$\frac{\Delta V}{V} = \frac{V_R - V_R'}{V_R} \tag{6-18}$$

It is not a difficult task to calculate the increase of the phase voltages when the angle θ changes from zero to a certain value. Typical values are given in table 6.2.

6.3.3. VI Rating

The increase of the VI rating depends on which one of the voltage and the current varies more quickly, as the voltage decreases and the current increases.

By definition,

$$\frac{\Delta VI}{VI}=\frac{V\cdot I-V'\cdot I'}{V'\cdot I'}=(1+\frac{\Delta V}{V})(1+\frac{\Delta I}{I})-1 \qquad (6\text{-}19)$$

By substituting equations 6-16 and 6-17 into 6-18 and 6-19, table 6.2 may be prepared.

Table 6.2. Change of Current, Voltage and VI Rating (during acceleration period)

		$m =$ 1400 kg		$m =$ 4135 kg	
θ^0	Current	Voltage	VI rating	Voltage	VI rating
5	+0.38%	-3.21%	-2.84%	-3.88%	-3.51%
10	+1.54%	-6.45%	-5.01%	-7.75%	-6.33%
15	+3.53%	-9.77%	-6.58%	-11.66%	-8.55%
20	+6.42%	-13.21%	-7.64%	-15.67%	-10.25%

6.3.4. Power Factor

By definition, the angle ϕ in power factor $\cos(\phi)$ is the angular difference between the phase voltage and the current. The vector diagram in Figure 6.3 shows that, while i_d is increased, the angle of the phase voltage revolves slower than that of the phase current, and they revolve in the same direction.

Table 6.3 shows how the power factor of the motor varies with the angle θ, where $(180+\theta_1)$ represents the phase voltage angle and $(180+\theta)$ represents the phase current angle.

Table 6.3 Change of The Power Factor (during acceleration period)

	$m =$ 1400 kg			$m =$ 4135 kg		
θ^0	θ_1^0	$\phi=\theta_1-\theta$	$\cos(\phi)$	θ_1^0	$\phi=\theta_1-\theta$	$\cos(\phi)$
0	23.72	23.72	0.9155	30.68	30.68	0.851
5	24.56	19.56	0.9423	33.11	28.11	0.882
10	25.47	15.47	0.9638	34.70	24.70	0.9085
15	26.45	11.45	0.98	36.47	21.47	0.93
20	27.62	7.62	0.9912	38.51	18.51	0.9483
30	30.49	0.49	1.0	43.78	13.78	0.9712
40	34.85	-5.15	0.996	51.99	11.99	0.9782

Whether ϕ is increased or decreased depends on the angle θ: when θ is smaller than the angle of the phase voltage, an increase of θ decreases the angle ϕ and improves the power factor; when θ is greater than the angle of the phase voltage, an increase of θ increases the angle ϕ and worsens the power factor (see Figure 6.3). Therefore as is i_d initially increased from zero, the power factor is improved. Then an optimal value is achieved, $\cos(\phi) \approx 1$, when $\theta \rightarrow \theta_1$. After that, the power factor becomes worse if the angle θ is increased further, i.e. it exhibits a turning point. This is another reason why the θ cannot be too big.

6.4. Simulation and Simplified Model

To examine the controller and to select control gains, computer simulation is used. Two models are programmed for comparison, where equations 5-14 and 5-25 are employed for the machine with sinusoidal components of the inductances; eqs. 5-23 and 5-26 for that without the parameter variations. Because this is a part of the whole system simulation, details of the programme will be discussed in chapter 8.

6.4.1. Frequency Responses

Because only the current control loop is concerned, the frequency response of the q axis current is simulated by disregarding the mechanical parts in the simulation programme and assuming a value for the velocity. The simulation is carried out to examine three sets of the control gains and two velocity values (v = 0, v = 4 m/s) respectively. For each controller, a series of i_{q_ref} with different frequencies is fed into the model as the system input. The amplitudes and phases of the current responses are then obtained from the three controllers having different gains, chosen to give nominal bandwidths of 20, 30 and 40 Hz, which are listed in tables 6.4 to 6.6 respectively. From the results, it can be shown:

- When the value of the velocity changes from 0 to 4 m/s, the frequency responses is only slightly affected, which means that the effect of the velocity on the characteristics of the current control loop can be neglected when an effective closed loop control is applied.

- The right hand column of each table gives responses of an ideal first order system, which are very close to the responses of the control loop. Figure 6.4 presents simulation results of the controller 2 and that of the ideal model. Therefore the dynamic of the closed current loop can approximately be represented by a first order model.

$$H_e(s) = \frac{i_q}{i_{q\_ref}} = \frac{F}{F_{ref}} = \frac{1}{\tau_e \cdot s + 1} \quad (6\text{-}20)$$

where τ_e is the electrical time constant, which are 4.0, 5.0 and 7.5 *ms* for the three controllers respectively. Hence bandwidths of the three are 40, 32 and 21 *Hz* respectively. A further increase of the bandwidth is very difficult for the current system configuration due to number of reasons such as voltage supply and switching frequency of the inverter.

Table 6.4. Frequency Responses of Control Gain One ($G_p = 1.0$, $G_i = 16.7$)

	$v =$ 0		$v =$ 4 *m/s*		first order
f (*Hz*)	Gain (*db*)	Phase (^{o})	Gain (*db*)	Phase (^{o})	(4.0 *ms*)
1	0.0778	0	0.0778	0	0.0 (-1.48^o)
5	0.424	-5.4	0.35	-5.4	-0.07 (-7.36)
10	0.289	-14.4	0.234	-12.6	-0.6 (-14.5)
20	-0.45	-28.8	-0.245	-25.2	-0.98 (-27.3)
40	-2.732	-47.52	-2.472	-49.68	-3.03 (-46.0)
100	-8.742	-66.6	-10.07	-75.6	-8.64 (-68.9)
500	-22.29	-84.6	-25.02	-88.2	-22.0 (-85.6)

Table 6.5. Frequency Responses of Control Gain Two ($G_p = 0.8$, $G_i = 13.3$)

	$v =$ 0		$v =$ 4 *m/s*		first order
f(*Hz*)	Gain (*db*)	Phase (^{o})	Gain (*db*)	Phase (^{o})	(5.0 *ms*)
1	0.099	0.0	0.101	0.0	0.0 (-1.8^o)
5	0.506	-5.4	0.366	-5.4	-0.11 (-8.93)
10	0.265	-18.0	0.214	-14.4	-0.41 (-17.4)
20	-0.837	-32.4	-0.39	-28.8	-1.44 (-32.1)
40	-3.77	-51.84	-3.11	-51.84	-4.12 (-51.5)
100	-10.36	-70.2	-10.9	-75.6	-10.4 (-72.3)
500	-24.08	-84.6	-25.76	-86.4	-23.9 (-86.4)

Table 6.6. Frequency Responses of Control Gain Three ($G_p = 0.5$, $G_i = 6.67$)

	$v =$ 0		$v =$ 4 *m/s*		first order
f (*Hz*)	Gain (*db*)	Phase (^{o})	Gain (*db*)	Phase (^{o})	(7.5 *ms*)
1	0.156	0	0.163	0	0.0 (-2.7^o)
5	0.677	-12.15	0.307	-9.45	-0.24 (-13.3)
10	0.006	-27.9	0.206	-19.8	-0.87 (-25.2)
20	-2.19	-48.6	-0.661	-41.4	-2.76 (-43.3)
40	-6.446	-64.8	-5.049	-69.12	-6.58 (-62.1)
100	-13.82	-75.6	-13.49	-79.2	-13.66 (-78)
500	-27.70	-82.8	-27.702	-86.4	-27.5 (-87.6)

6.4.2. Step Responses

The second simulation is used to examine the step responses of the control loop, where the model of the motor slider is included. The input is a step force required to accelerate the slider. The reference force is reset to zero when the slider reaches the peak velocity and hence the step responses at the maximum velocity can also be examined.

- Figures 6.5 (*) and 6.6 show the step responses where the velocity of the slider is 0 and 4.2 *m/s* respectively. Obviously, controller 1 follows the demanded current well since it has the highest bandwidth. The response of controller 2 is very close to that of controller 1. Controller 3 has the slowest response, specially when the slider is at the peak velocity.

- By nature, the controller with higher bandwidth tends to demand higher input signals for the fast response. Figures 6.7 and 6.8 demonstrate that instantaneous peak voltages are required when the system tries to follow the step input. The higher the bandwidth of the controller, the greater value is required. This may cause problems to the inverter as the voltage of any system is always limited. A compromise between controllers 1 and 3, i.e. controller 2, may be reasonable.

- Figure 6.9 compares controller 2 with and without the integration term. If the I term is removed from the controller, a control error appears and the response of the system varies with the velocity of the slider.

- Accuracy of the position feedback signals also affects the performance of the control loop, especially when the velocity is derived from the position signal. In the system a truncation error 0.25 *mm* is introduced by the digital position sensor. Figure 6.10 shows the results of the controller 2 with and without the truncation errors. Where the truncation error is simulated, the response becomes quite noisy.

- Load angle control does not affect the responses of the current i_q. Figures 6-11 and 6-12 give the simulation results where the current angle is 20^0. For

(*) Scales on Figures 6.5 to 6.13 are not very common, because of the software library used in the plotting program, where +00n means x10^{+00n}.

the control of the i_d, a higher integration value is required in order to eliminate the effect of the slider velocity, as shown in Figure 6-12. However the i_q remains unaffected, as shown in Figure 6-11.

- Figures 6.13 and 6-14 give the step responses of the i_q and the phase current where the sinusoidal components of the inductances of the motor are included. From the simulation, it is shown that the overall force production of the motor is not affected by the parameter variation, as the same current is required to produce the demanded force in both responses. However, the step response of the i_q is slightly slower than that without the parameter variation. This situation has been initially studied in chapter 5 and it can be best explained by the equations 5-15 to 5-18, in which the resistive terms are affected by the parameter variation. This effect means a little adjustment on the electrical time constant of the simplified model and it should not cause any serious problems.

6.5. Summary

This chapter has presented the design of the vector control and current control loop, where command feedforward control and conventional PI control are combined together in order to achieve high performance and simple design at the same time. Simulation is used to support the design and system analysis in both frequency domain and time domain. Load angle control is introduced to improve the inverter capacity and the power factor of the system.

By employing the controller developed in this chapter, the dynamics of the motor can be simply represented by a first order model as described in equation 6-20. This greatly simplifies the model of the motor and the design of the outer position / velocity controller for the whole system.

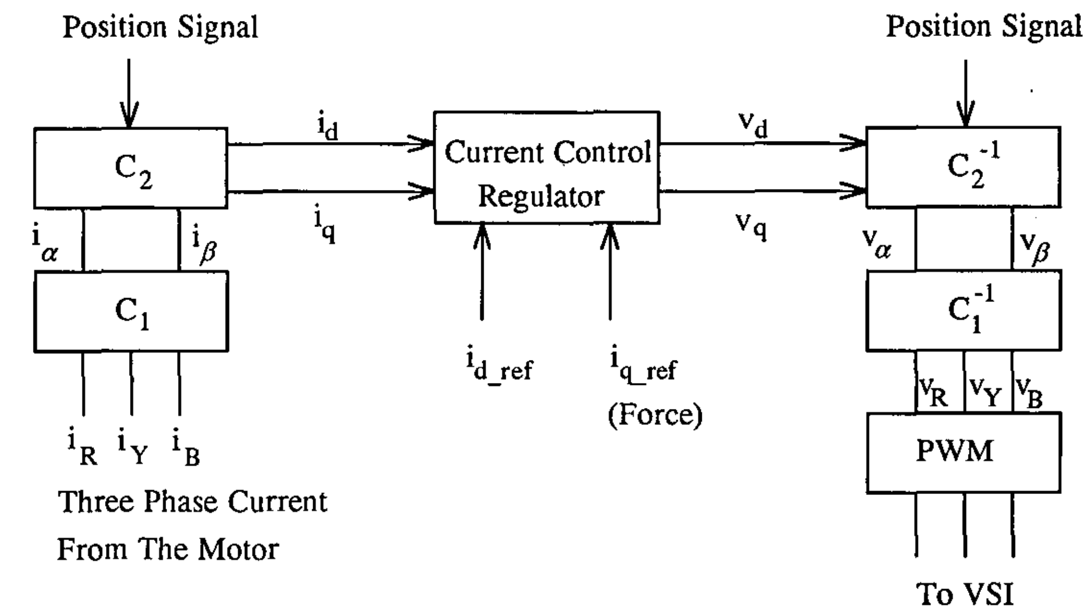

Figure 6.1. Block Diagram of The Vector Control Scheme

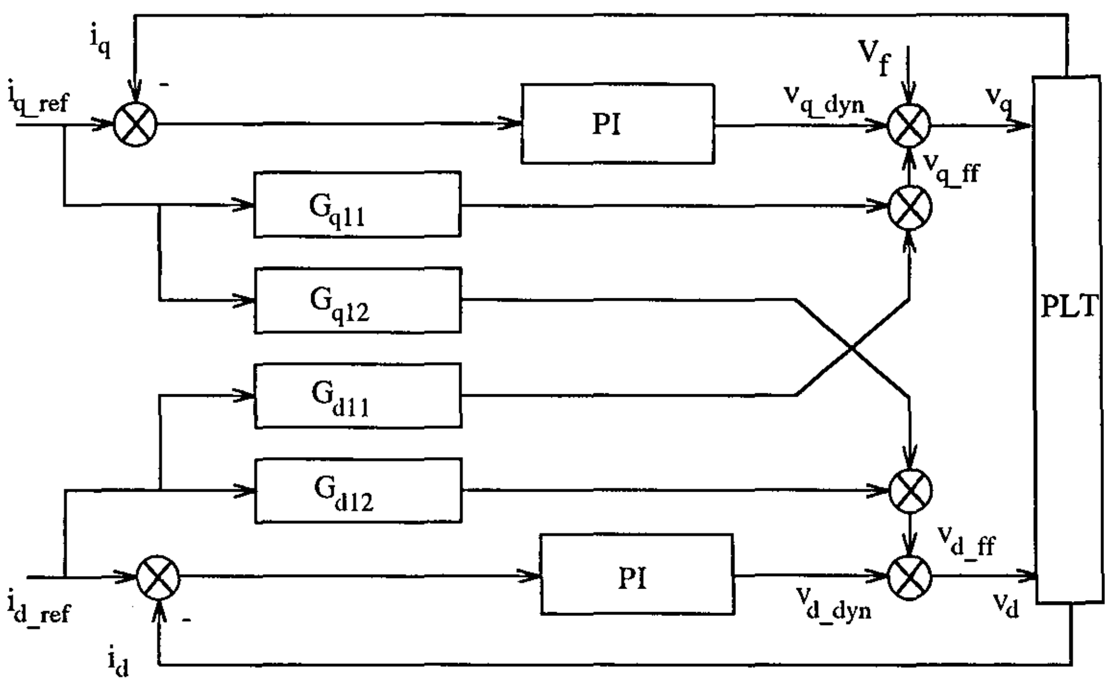

Figure 6.2. Diagram of Current Control Regulator

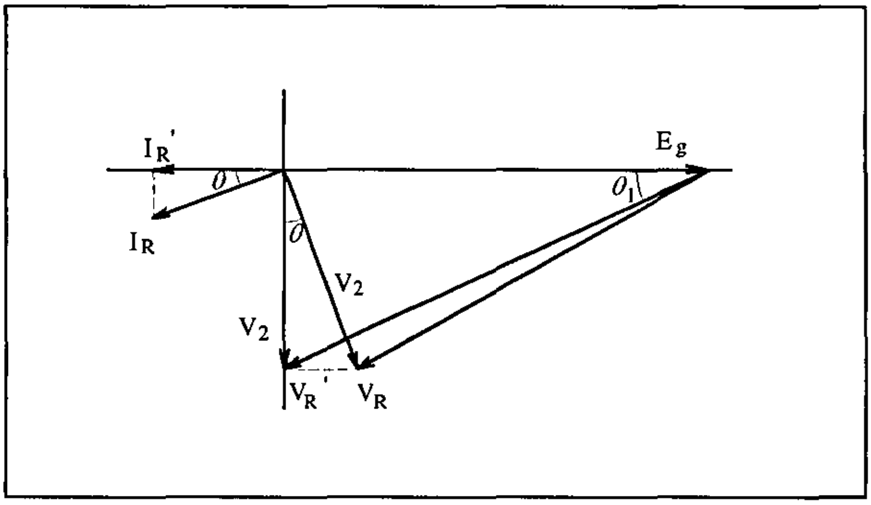

Figure 6.3. Vector Diagram of Steady State Operation

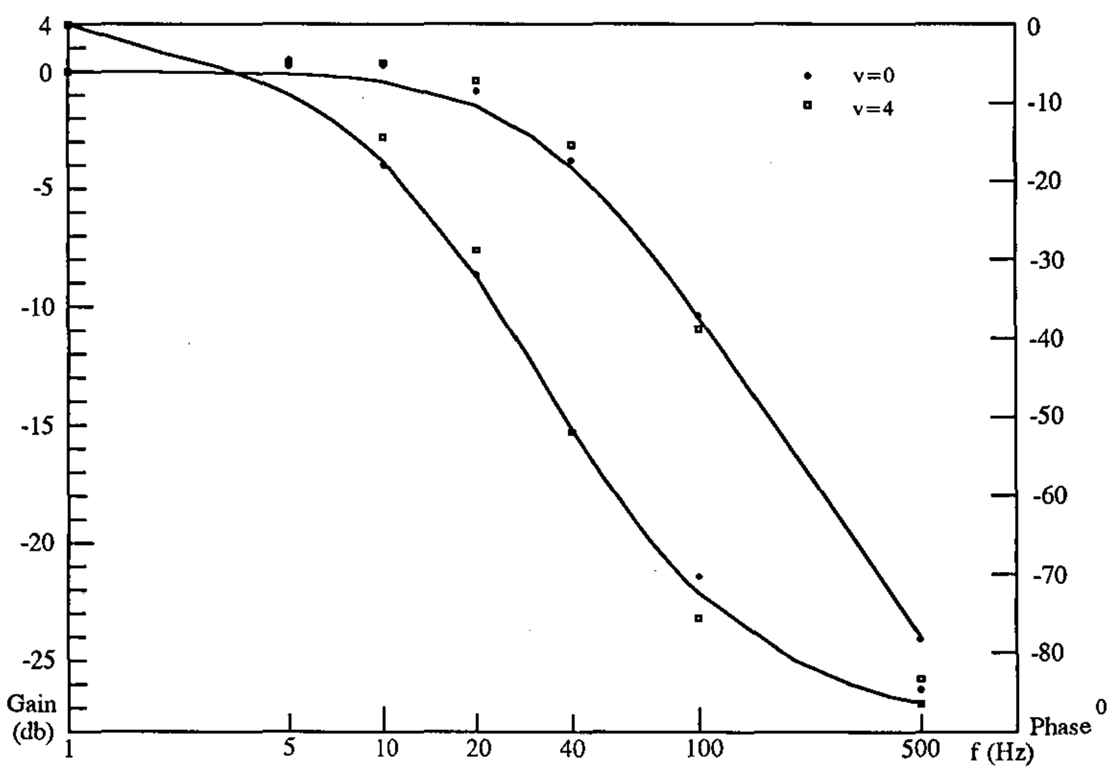

Figure 6.4. Frequency Responses of Control Gain 2

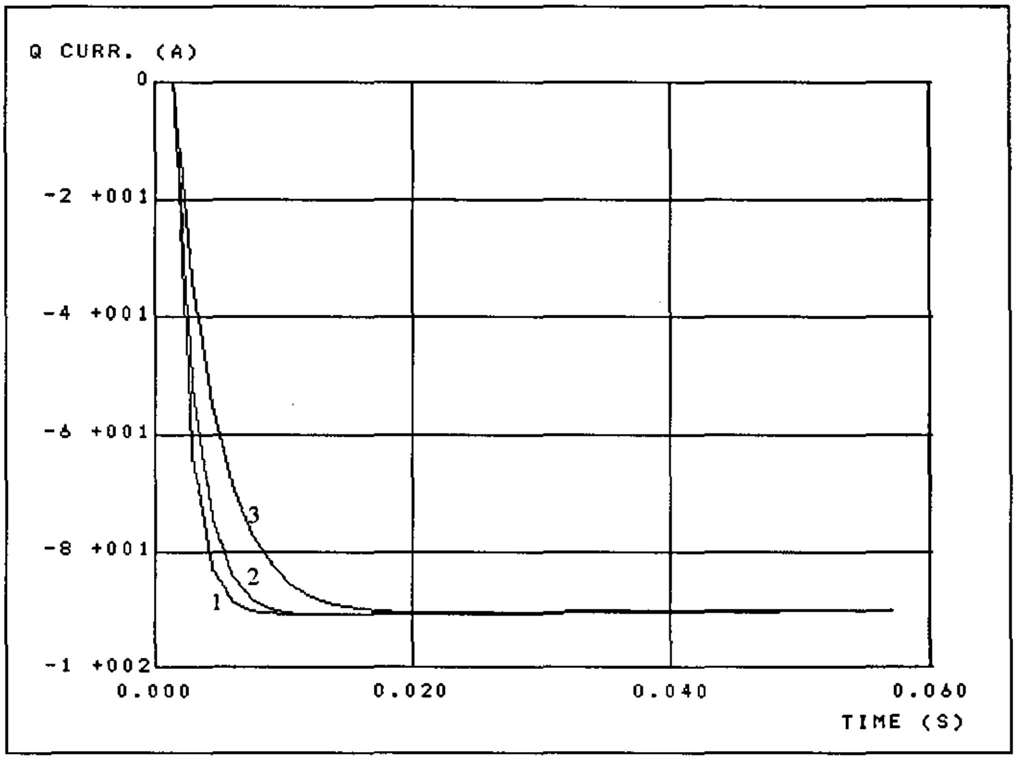

Figure 6.5. Step Responses ($v = 0\ m/s$)

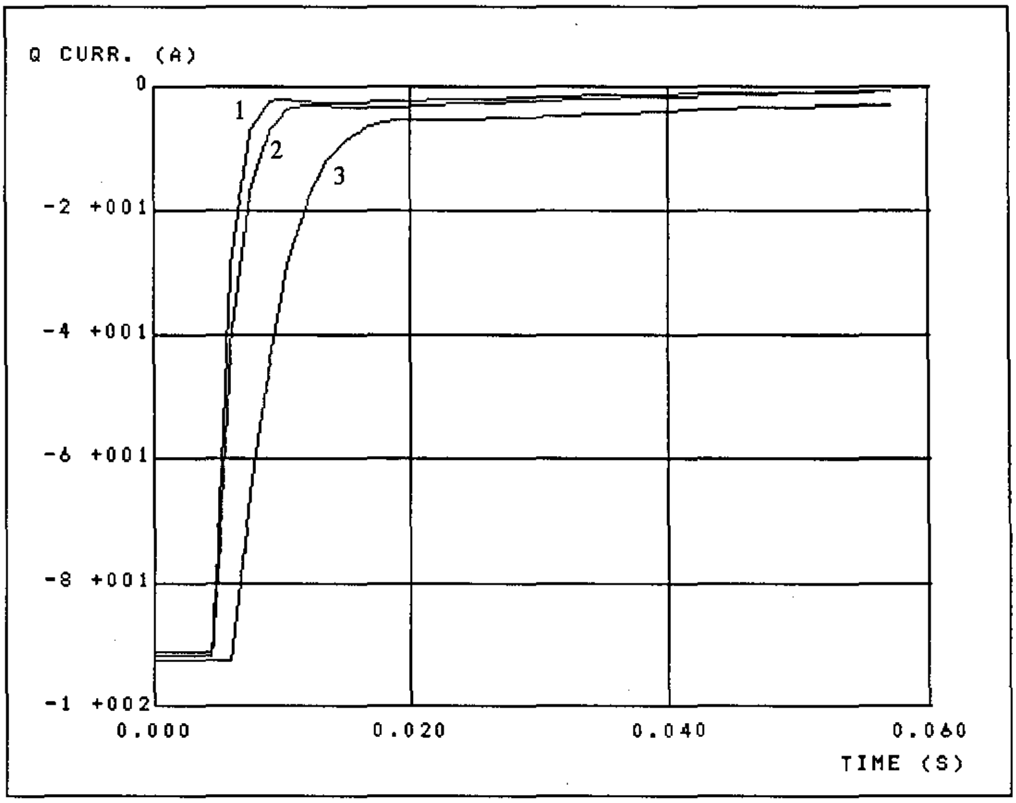

Figure 6.6. Step Responses ($v = 4.2\ m/s$)

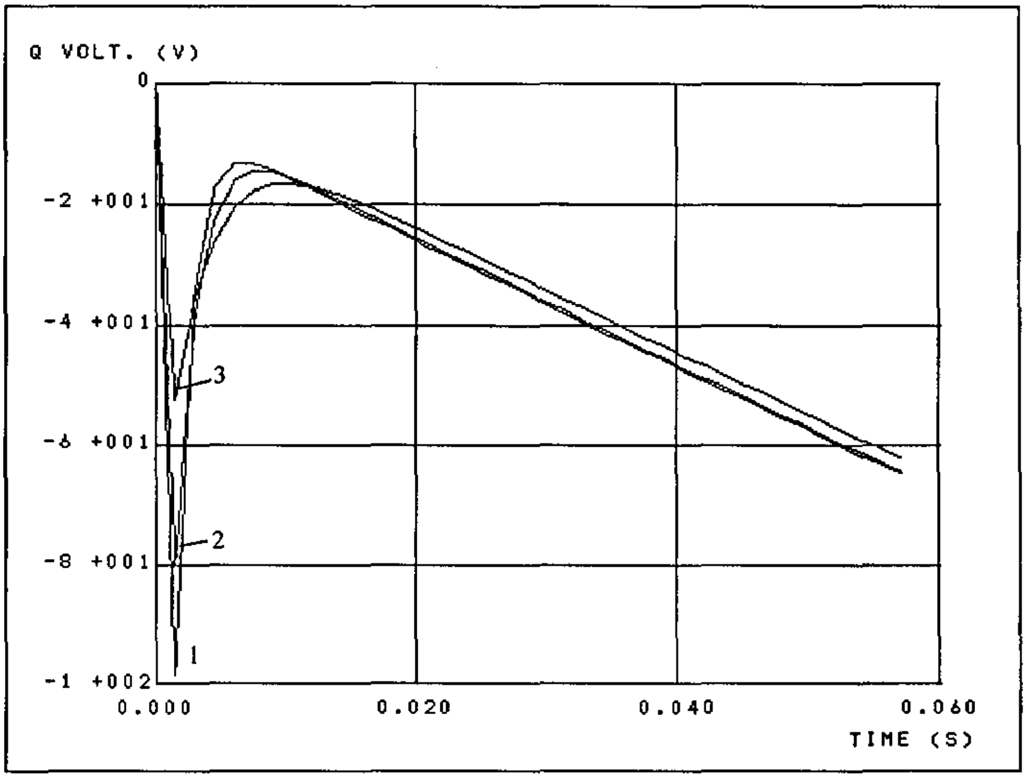

Figure 6.7. Q Axis Voltage ($v = 0\ m/s$)

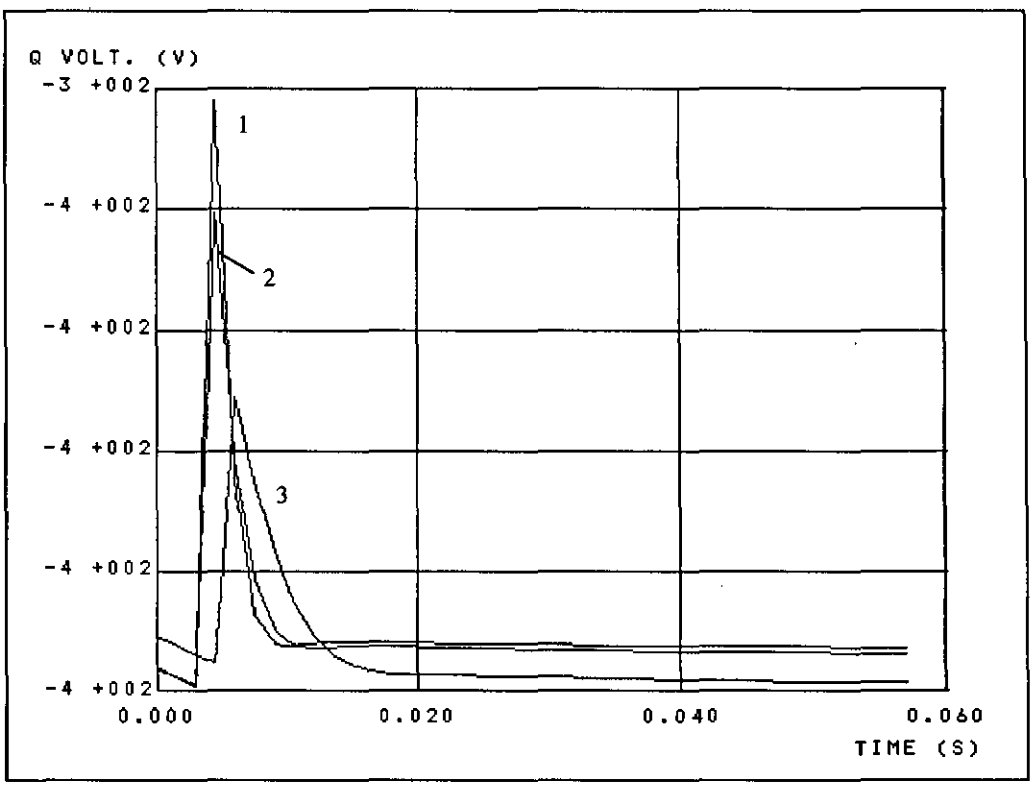

Figure 6.8. Q axis Voltage ($v = 4.2\ m/s$)

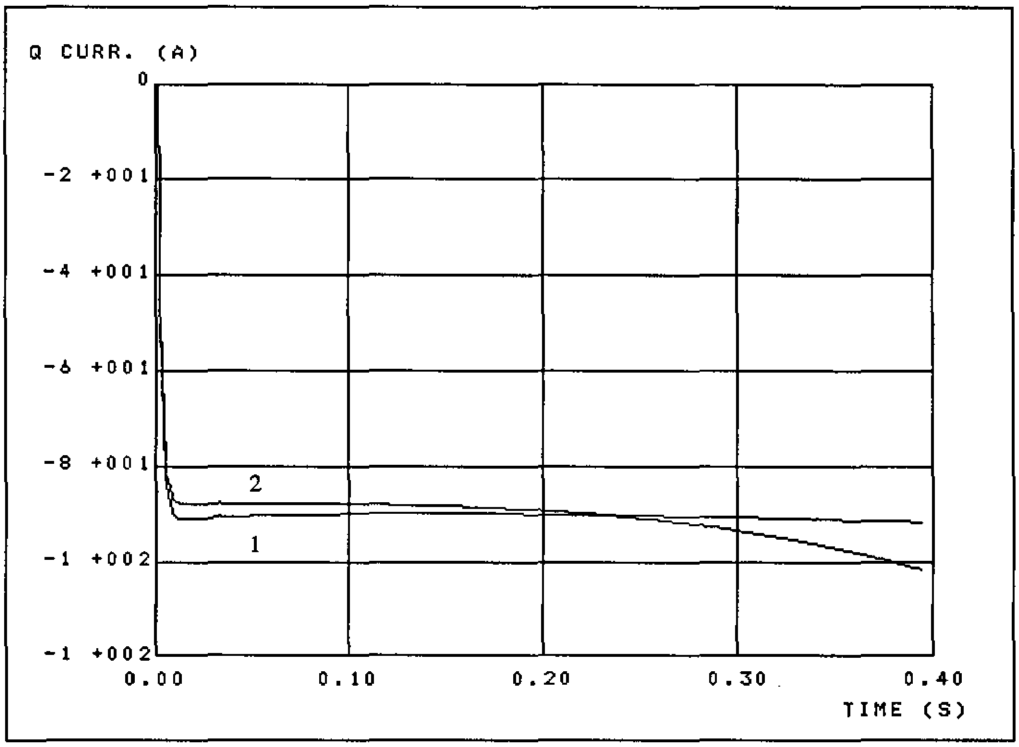

Figure 6.9. Step Responses with I (1) and without I term (2)

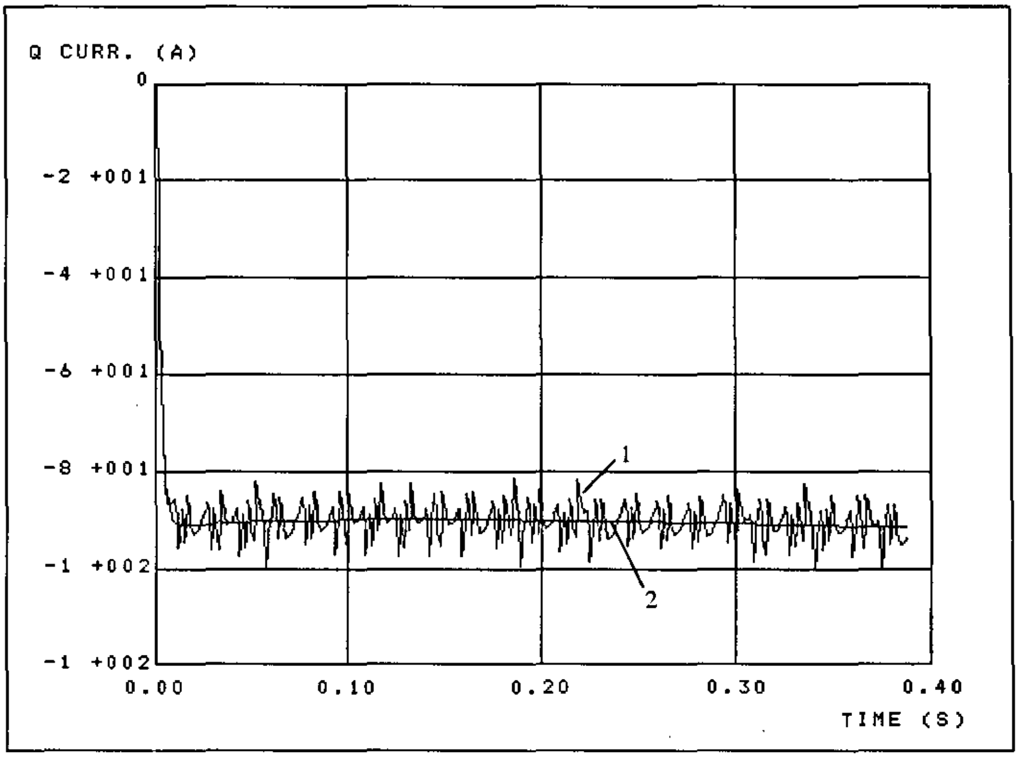

Figure 6.10. Step Responses with (1) and without (2) Position Error

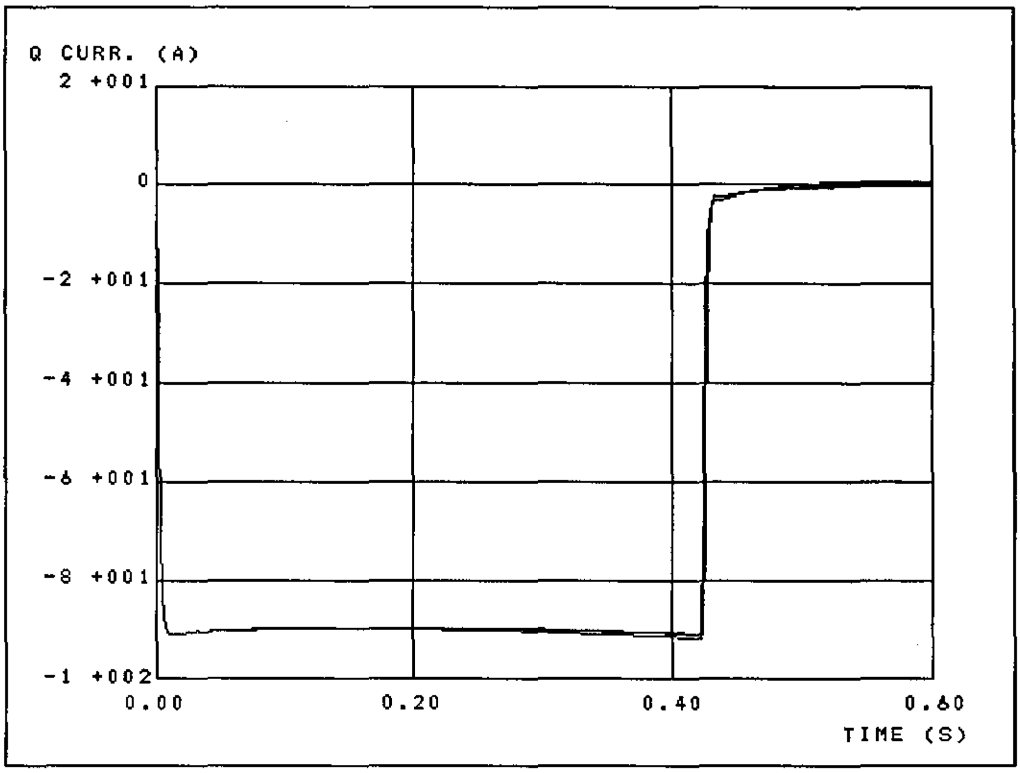

Figure 6.11.Responses of i_q Where Current Angle Is 20°

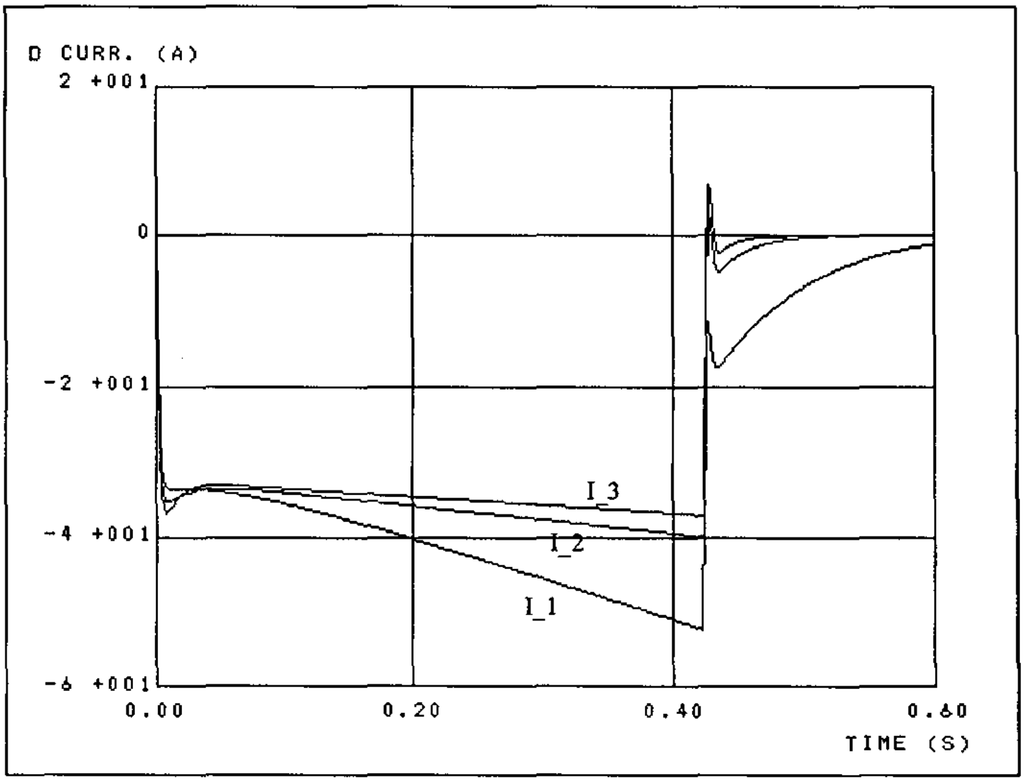

Figure 6.12.Responses of i_d Where Current Angle Is 20°

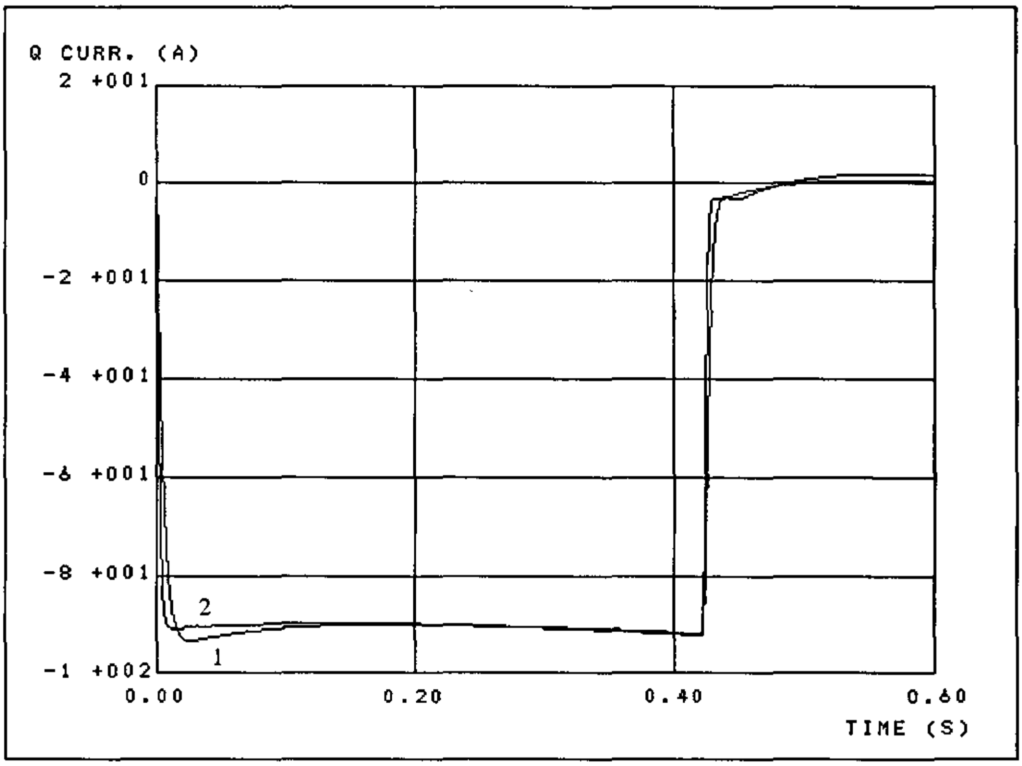

Figure 6.13. Step Responses with (1) and without (2) Parameter Variations

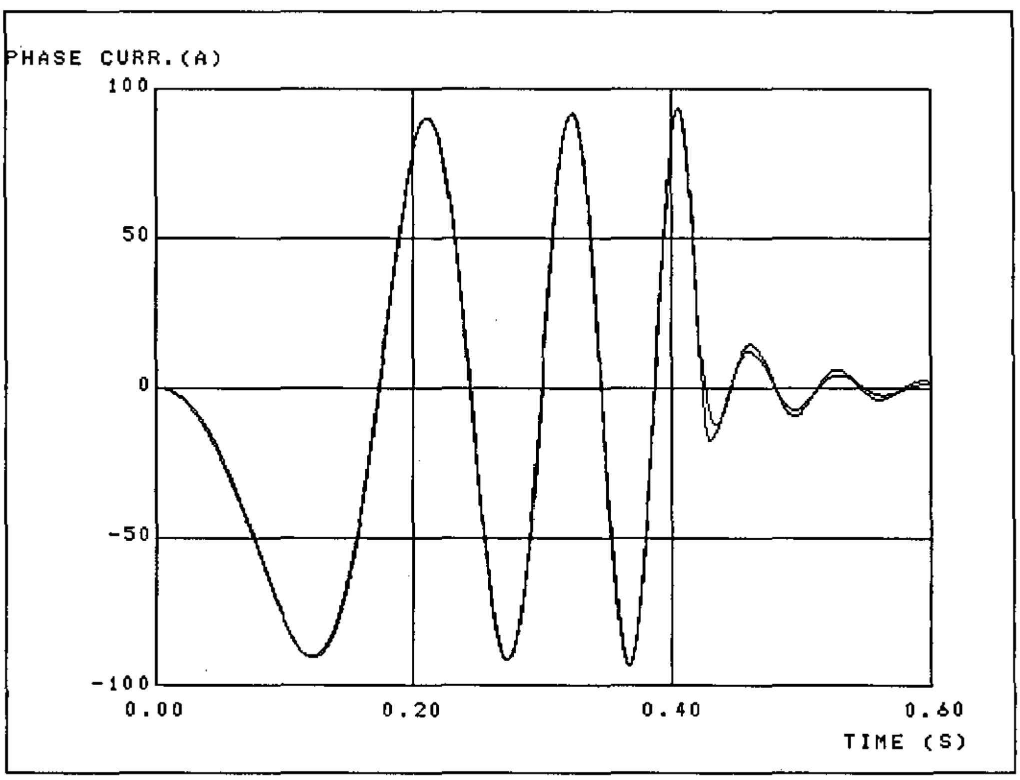

Figure 6.14. Red Phase Current In Two Cases.

CHAPTER 7.

DESIGN OF POSITION / VELOCITY CONTROL

In the previous chapter, the vector control and the current controller design have been discussed in great detail. It has been shown that the dynamics of the force production can be simplified to a first order model by designing the controller carefully. Together with the model of the mechanical part of the system developed in chapter 4, they enable the design of the position / velocity controller.

Because of the complexity of the system being studied, a controller must be designed to be able to follow the demanded trajectory as well as to cope with various load conditions and high uncertainty. Adaptive control may be one of the solutions, but it would lead to a more complicated system. Therefore one of the primary objectives of the study was to establish whether the necessary performance could be achieved for all load cases without using adaptive control, i.e. a controller with good robustness should be developed for the application. Having said that, there are numbers of control methods leading to a robust controller. It is neither practical nor necessary to go through all design approaches and thus three methods are chosen for the system, which are conventional cascade control, internal model control and optimal tracking control.

H^∞ can be very effective for handling uncertainties from known modelling approximations to unknown parameters and disturbance signals [63]. Its popularity stems from two important results. Firstly, a sufficient condition for closed loop stability to be robust against a set of plant perturbations is given by a bound on the H^∞ norm of a stable closed loop transfer function. Secondly, the H^∞ norm of a stable transfer function matrix represents a bound on the maximum energy gain from the input signals to the output. However, formation of the uncertainty bound of the present application in frequency domain is more complex than that in time domain. The design may unnecessarily lead to a more complex solution [63]. This method has not been studied in this thesis as time was not available to carry out the study.

Controllers may be designed using classical frequency domain technique or modern state space methods. The frequency domain techniques display a general robustness to parameters changes. The state space method can have proper placement of the poles given an accurate knowledge of the drive parameters. In this chapter, the cascade controller and the internal model controller are both designed in the frequency domain, where the continuous controller is designed and initially assessed and then the resultant s-domain function is expressed in terms of z for the full computer simulation and the real time implementation. The optimal tracking controller is designed using the state space method.

In this chapter, the simplified model of the whole system is presented and the design requirement is derived in section 7.1. Designs of the cascade control, the internal model control and the optimal tracking control are discussed in sections 7.2, 7.3 and 7.4 respectively. Initial evaluations of the control laws are carried out by using the simplified model in section 7.5. Accuracy, stability, robustness, disturbance rejection and overall performance of each controller are initially analysed and compared. Selection of the sample period for the outer loop is discussed in the next section.

7.1. Design Requirement

In chapters 4 and 6, two simplified models have been developed for the different parts of the pump system, given in equations 4-64 and 6-20 respectively. Combining these two models together, the controlled plant can be represented by a simple third order system.

$$H_p(s) = \frac{1}{(m \cdot s^2 + k_f \cdot s + k_0) \times (\tau_e \cdot s + 1)} \tag{7-1}$$

The uncertainly bounds for different pumping stages are defined in equations 4-65 to 4-67, which are re-presented as follows.

Pump Stage 1:

$$\begin{aligned} m &= 1400 \\ k_f &= [60, 120] \\ k_0 &= [3.299 \times 10^5, 2.043 \times 10^8] \end{aligned} \tag{7-2}$$

Pump Stage 2: $m = [1400, 2768]$

$$k_f = [60, 500] \quad (7\text{-}3)$$
$$k_0 = [6.226 \times 10^4, 2.15 \times 10^7]$$

Pump Stage 3:

$$m = [1400, 4135]$$
$$k_f = [60, 1000] \quad (7\text{-}4)$$
$$k_0 = 0.0$$

Since the simplified model of the process plant and its uncertainty bounds have been obtained, it is necessary to define a requirement for the design of the position controller. The design requirements can be specified from the project requirement as well as the simulation results presented in previous chapters.

- Firstly and most importantly, the controller must be able to maintain reasonable margins of stability of the system in all pumping stages with various load conditions, i.e. gas, oil, or any mixture of gas and oil. The bounds of the system uncertainty are defined in equations 7-2 to 7-4.

- Secondly, the controller must be able to keep the steady state error to less than 5 *mm* under maximum acceleration in order to obtain the maximum pump efficiency. A zero steady state error would be mostly desirable.

- Thirdly, the maximum transient period must be less than 0.35 *s*. This is due to: 1) the reference trajectory acceleration changes sign at the middle of every stroke and the piston takes 0.357 *s* to reach the end after that point; 2) in the pure gas case, it takes a longer time before the discharge valve opens and thus the time period between the opening of the valve and the piston reaching the end of stroke is relatively short (about 0.4 *s*). To guarantee the minimum stroke end error, the system should reach the steady state before the piston reaches the end of stroke.

- A good tracking performance is essential for achieving constant flow rate in the transportation pipes and therefore reducing or eliminating pressure surges caused by fluid dynamics.

- The controller should also be able to handle possible disturbances, as the dynamics of the fluids in the inlet and outlet pipes may produce some disturbances especially in the case of high percentage of oil.

- A time delay caused by the software and inverter should be accommodated. An estimated value of the delay is about 1.5 *ms*.

- The sampling period must not affect the overall performance when the designed controller is converted to a digital controller for the computer implementation.

7.2. Cascade Control

Cascade control refers to the use of multiple feedback loops to control a multistage process. The result of the use of cascade control usually is improved performance, particularly because the effects of disturbances can be minimised by the addition of the inner loops. Cascade control may prove useful whenever a process has intermediate response variables that can be measured. In fact, the idea of cascade control has already been used to design the current loop independently from the outer position / velocity loops.

In addition to the innermost current loop, the control scheme of the system consists of a position controller with an inner velocity loop. A block diagram of the controller is given in Figure 7.1 where the plant represents the model defined by the equation 7-1. Since the sequence force $\rightarrow$ velocity $\rightarrow$ position conforms very well to the structure of the system, cascade control has following advantages [4, 26].

- Design and commissioning can be achieved step by step regarding only one part of the system at one time. Therefore the design procedure is greatly simplified. This is under the assumption that the bandwidth of the control increases towards the inner loops, with the current loop being the fastest and the position loop being the slowest.

- Cascade control is normally robust against system uncertainty because of the high bandwidth of the inner loops.

- Protective functions can be easily implemented by limiting internal variables such as i_q.

7.2.1. Control Compensators

The bandwidths of the control loops can be decided based on the input signals, where the input reference position is a quadratic waveform. At the peak speed 4.2 *m/s* with the stroke length 1.5 *m*, the maximum fundamental frequency of the reference position is 0.7 *Hz*. By using a Fourier analysis to the quadratic waveform, it can be shown that amplitudes of the harmonics in the position signal are:

First	774 *mm*, 0.7 *Hz*;
Third	28.7 *mm*, 2.1 *Hz*;
Fifth	6.20 *mm*, 3.5 *Hz*;
Seventh	2.26 *mm*, 4.9 *Hz*;
Ninth	1.06 *mm*, 6.3 *Hz*;
Eleventh	0.58 *mm*, 7.7 *Hz*.

The other components higher than eleventh are not comparable. Therefore a bandwidth for the position loop is selected to be about 6 - 7 *Hz*. Consequently, the bandwidth for the velocity loop should be that between the position and current loops, around 15 *Hz*.

After the bandwidths for both position and velocity loops have been decided, it is quite straight forward to design the controllers. A proportional control for the velocity loop and a proportional control plus integral action for the position loop are found satisfactory. The design work is carried out based on a system analysis and design package, SIMBOL, running in a PC computer, where analysis in both frequency and time domains is available. The simplified model given in equation 7-1 is used as the plant. The electrical time constant $\tau_e = 10\ ms$ is used to represent the characteristics of the current loop and a 1.5 *ms* time delay is included in the system. By using open loop Nyquist Plot and closed loop Bode Plot, gains for the velocity and then the position loop can be easily obtained, which gives: G_{pv}=150000 is the proportional gain of the velocity loop, G_p=20, G_i=165 are the proportional and integral gains of the position loop respectively. The performance of the controller can be initially assessed.

- The system is stable against the parameter variations. Figure 7.2 gives the open loop Nyquist Plot in one of the extreme cases where m=4135 *kg*, i.e. pure oil in stage 3. The margins in stage 1 are even better as shown in

Figure 7.3. Thus the phase margin of the system is about 35^0 and the gain margin is about 10.45 *db*.

- The system is also robust against the parameter variations, as shown in closed loop Bode Plots for some cases in Figures 7.4 to 7.7. In Figures 7.4 and 7.5, the bandwidth of the position loop only varies from 39 to 41 *rads/s* (6.2 - 6.5 *Hz*) when the total mass changes from $m=1400$ *kg* to $m=4135$ *kg*.

  Even with stiffness $k_0 = 2\times 10^5$, the system still shows a good robustness as shown in Figure 7.6. When the stiffness reaches the maximum value, i.e. pure oil in stage 1, the bandwidth is quite low as indicated in Figure 7.7. However the durations of stages 1 and 2 in the pure oil case are very short before the system enters stage 3 and the control performance in these two stages is therefore less important than the stability.

- The controller shows capability of the disturbance rejection as well. Figures 7.8 and 7.9 give the frequency responses of the controller output to the disturbance forces applied on the pistons, where $m=1400kg$ and $m=4135kg$. The minimum reduction of the disturbances is 5.6×10^{-7} *m/N*.

7.2.2. Steady State Error

The steady state error is of primary importance during pump stage 3. The transfer function of the closed loop system in this stage is given as follows.

$$H(s)=\frac{G_p\cdot G_{pv}\cdot s+G_{pv}\cdot G_i}{m\cdot\tau_e\cdot s^4+(m+k_f\cdot\tau_e)\cdot s^3+(k_f+G_{pv})s^2+G_p\cdot G_{pv}\cdot s+G_{pv}\cdot G_i} \tag{7-5}$$

To analyse the steady state error, the transfer function of the control error is used.

$$E(s)=\frac{e(s)}{x_i(s)}=\frac{m\cdot\tau_e\cdot s^4+(m+k_f\cdot\tau_e)\cdot s^3+(k_f+G_{vp})s^2}{m\cdot\tau_e\cdot s^4+(m+k_f\cdot\tau_e)\cdot s^3+(k_f+G_{vp})s^2+G_p\cdot G_{vp}\cdot s+G_{vp}\cdot G_i} \tag{7-6}$$

From Final Value Theorem and considering the constant acceleration input of a $m\cdot s^{-2}$, the steady error can be derived.

$$e(\infty) = \lim_{s\to 0} s \cdot E(s) \cdot \frac{a}{s^3} = \frac{k_f + G_{vp}}{G_{vp} \cdot G_i} \cdot a \approx \frac{1}{G_i} \cdot a \tag{7-7}$$

That means that the steady error at top speed (for which the acceleration is 11.76 $m \cdot s^{-2}$) could be as high as 71.3 *mm*, which is obviously not acceptable to the system.

7.2.3. Feedforward Terms

To improve the performance as well as to maintain the robustness of the cascade control, a feedforward term G_{fv} is introduced as show in Figure 7.10. Because the feedforward control is basically open loop, it will not affect the stability of the system. Then the transfer function of the system becomes,

$$H(s) = \frac{G_{fv} \cdot G_{pv} \cdot s^2 + G_p \cdot G_{pv} \cdot s + G_{pv} \cdot G_i}{m \cdot \tau_e \cdot s^4 + (m + k_f \cdot \tau_e) \cdot s^3 + (k_f + G_{pv}) s^2 + G_p \cdot G_{pv} \cdot s + G_{pv} \cdot G_i} \tag{7-8}$$

and the transfer function of the control error is,

$$E(s) = \frac{m \cdot \tau_e \cdot s^4 + (m + k_f \cdot \tau_e) \cdot s^3 + (k_f + G_{pv} - G_{fv} \cdot G_{pv}) s^2}{m \cdot \tau_e \cdot s^4 + (m + k_f \cdot \tau_e) \cdot s^3 + (k_f + G_{pv}) s^2 + G_p \cdot G_{pv} \cdot s + G_{pv} \cdot G_i} \tag{7-9}$$

Therefore, the steady state error is

$$e(\infty) = \lim_{s\to 0} s \cdot E(s) \cdot \frac{a}{s^3} = \frac{k_f + G_{pv} - G_{fv} \cdot G_{pv}}{G_{pv} \cdot G_i} \cdot a \tag{7-10}$$

when $G_{fv} = 1$,

$$e(\infty) = \frac{k_f}{G_{pv} \cdot G_i} \cdot a \tag{7-11}$$

The steady state error after the introduction of the velocity feedforward is reduced to 0.04 *mm* in theory.

In addition, an acceleration feedforward term G_{fa} can also be used to reduce the control errors without causing a stability problem. The value of the term depends on the total mass that the motor drives. Since the effective mass varies an average value may be used.

7.3. Internal Model Control

The Internal Model Control (IMC) structure [45] is studied as an alternative to the classical feedback structure. Its main advantage is that closed loop stability is assured simply by choosing a stable IMC controller. Also, closed loop performance characteristics are related directly to controller parameters, which makes on line tuning of the IMC convenient.

The block diagram of the IMC loop is shown in Figure 7.11. The output of the real plant H_p is compared with that of an ideal model of plant p_1 in the controller, the result of which is compared with the input signal. The action of the control regulator is then to adjust and output control signals both to the real plant and to the ideal one.

The IMC design method adopted for the system can be partitioned into two steps [45].

- Nominal Performance. The controller is designed for optimal setpoint tracking without regard for input saturation and model uncertainty, where the regulator q_1 is selected to yield a "good" system response for the input of interest.

- Robust Stability and Performance. The controller is detuned for robust stability and performance, where q_1 is augmented by a low pass filter f $(q = q_1 \cdot f)$.

7.3.1. Nominal Performance

Because the performance in pump stage 3 is more important in the system, the model without the stiffness is used as the nominal plant p_1.

$$p_1(s) = \frac{1}{s \cdot (m \cdot s + k_f) \cdot (\tau_e \cdot s + 1)} \qquad (7\text{-}12)$$

Thus, the nominal regulator q_1 is selected such that it is H_2 optimal for a particular input r. This means that q_1 has to come from

$$\min_{q_1} \|e\|_2 = \min_{q_1} \|(1 - p_1 \cdot q_1) \cdot r\|_2 \tag{7-13}$$

subject to the constraint that q_1 is stable and casual. Because the model described in equation 7-12 is a minimum phase system and there are no constraints on the input saturation, the problem 7-13 reaches its absolute minimum (zero) for

$$q_1 = \frac{1}{p_1} = s \cdot (m_0 \cdot s + k_f) \cdot (\tau_e \cdot s + 1) \tag{7-14}$$

where an optimal value of m_0 will be selected using simulation. Note that the model inverse is an acceptable solution only for minimum phase systems [45].

7.3.2. The IMC Filter

For robustness q_1 has to be augmented by a low pass filter f $(q = q_1 \cdot f)$, because it exhibits undesirable high frequency behaviour. In principle both the structure and parameters of the filter should be determined such that an optimal compromise between performance and robustness is reached. To simplify the design task, the filter structure is fixed and has a format as follows.

$$f(s) = (\beta_2 \cdot s^2 + \beta_1 \cdot s + 1) \cdot \frac{1}{(\lambda \cdot s + 1)^n} \tag{7-15}$$

where λ is the adjustable filter parameter. n is selected large enough to make q proper. The numerator is chosen for the closed loop system to retain asymptotic tracking properties, i.e. zero steady state error; in this case both s and s^2 terms are required, as the following analysis shows.

It is not difficult to obtain the transfer function of the control error from Figure 7.11.

$$E(s) = \frac{1 - p_1 \cdot q}{1 + q \cdot (H_p - p_1)} \tag{7-16}$$

Steady state analysis for an acceleration input gives

$$e(\infty) = \lim_{s \to 0} (s \cdot \frac{1 - p_1 \cdot q}{1 + q \cdot (H_p - p_1)} \cdot \frac{a}{s^3}) \tag{7-17}$$

$e(\infty)=0$ if and only if $(1-p_1\cdot q)$ has 2 zeros at the origin which is the case if and only if

$$\lim_{s\to0}(1-p_1\cdot q)=\lim_{s\to0}(1-f)=0 \tag{7-18}$$

$$\lim_{s\to0}\frac{d}{ds}(1-p_1\cdot q)=\lim_{s\to0}\frac{d}{ds}(f)=0 \tag{7-19}$$

$$\lim_{s\to0}\frac{d^2}{ds^2}(1-p_1\cdot q)=\lim_{s\to0}\frac{d^2}{ds^2}(f)=0 \tag{7-20}$$

Solution of equations 7-18 to 7-20 gives $\beta_1=n\cdot\lambda$ and $\beta_2=n\cdot(n-1)/2$. q is proper when n=6, thus the final structure of the filter is given in equation 7-21

$$f(s)=(15\lambda^2\cdot s^2+6\lambda\cdot s+1)\cdot\frac{1}{(\lambda\cdot s+1)^6} \tag{7-21}$$

and the transfer function of the system is described in equation 7-22.

$$H(s)=\frac{H_p(s)}{[1-f(s)]\cdot p_1(s)+H_p(s)\cdot f(s)}\cdot f(s) \tag{7-22}$$

If the plant and ideal models are exactly equal then the poles of the filter at $-\lambda^{-1}$ are the closed loop system poles. Adjusting λ is equivalent to adjusting the time constant of the closed loop response. It is conceivable that λ is left for on line adjustment, either through simulation or on the real system.

7.3.3. Selection of Control Parameters

The control parameters are selected through frequency domain analysis using SIMBOL. Two parameters, m_0 in the equation 7-14 and λ in the equation 7-21, are determined based on the design requirement such as bandwidth and stability as well as robustness. It has been found that the best compromise for the system is obtained when $\lambda=0.02$ and $m_0=2400$.

The performance of the controller using these gains is also analysed in the frequency domain. The procedure is similar to that for cascade control and the following performance is obtained:

- The bandwidth of the closed loop control varies between 8 and 18 *Hz* when the mass changes from m=1400 *kg* to m=4135 *kg*, as shown in Figures 7.12 and 7.13.

- The controller is stable within the uncertainty bounds. Gain margin 5.58 *db* and the phase margin 24^0 are obtained.

- Minimum disturbance reduction of the controller is 1.78×10^{-4} *m/N*.

7.4. Optimal Tracking Control

As mentioned in the chapter 2, an optimal tracking control [42] was attempted in the early stage of the project using the Linear Quadratic Regulator (LQR) method. Optimal control is concerned with obtaining a system which is the best possible with respect to a *performance criterion* against which one can measure real performance. Because the optimal control formulates a mathematical problem in the state space form, it has following advantages. Firstly, it solves the problem mathematically with respect to some defined performance criterion and thus less experience is required for the design work. Secondly it is a lot easier to tackle multi input and multi output (MIMO) problems than classic methods. Thirdly, all states are used as feedback signals such that better performance can be achieved for some systems. Hence there is no doubt that optimal control can be very effective for some applications, although the measurement of all the states may be difficult in practice and a state estimator will be necessary.

However, optimal control does not take account of system uncertainties and it requires a sound knowledge of a system. So, unless adaptation is used, it is unpredictable whether the required performance of a system can still be maintained when the system parameters or structure or both are changed. In addition, on line adjustment is difficult as an optimal controller tends to have more control gains than other formulations of controller.

For comparison with the two controllers developed above, optimal control is also included in the thesis. Since the design of the optimal tracking was carried out before [19, 20] and its principle has been well known from many publications [39, 40, 42], only a brief introduction of the controller is given.

The system model was used to design the control is one described by equation 4.1 or 4.2 for the state space form, where the position and velocity are two state variables. The load force was assumed to be constant and thus neglected, i.e. only the mass of the slider and the viscous friction coefficient of the motor were considered. As the controller was designed in the discrete time, the model was transferred to the discrete state space form.

$$X(k+1) = A_p \cdot X(k) + B_p \cdot u_d(k) \tag{7-23}$$

$$Y = C_p \cdot X(k) \tag{7-24}$$

where

state vector $X = \begin{bmatrix} x \\ v \end{bmatrix}$, input $u_d = F$, and output $Y = x$

The cost function of LQR is defined as

$$J_k = \sum_{j=k}^{\infty} \left\{ \left[x(j) - x_{ref}(j) \right]^2 + R \cdot \left[\Delta u_d(j) \right]^2 \right\} \tag{7-25}$$

where R is a weighting factor. The constraints on the R ensure that the control law leads to a finite control. The resulting control law including integral action is given:

$$u_d(k) = G_{px}\left[x_{ref}(k) - x(k)\right] + G_{ix}\sum_{j=0}^{k}\left[x_{ref}(k) - x(k)\right] - G_{vb}v(k) + G_{vf}v_{ref}(k) \tag{7-26}$$

It can be easily converted back to continuous time system for ease of the comparison.

$$u_d(t) = G_p\left[x_{ref}(t) - x(t)\right] + G_i\int_{t=0}^{t}\left[x_{ref}(k) - x(k)\right]dt - G_v v(t) + G_{ff}v_{ref}(t) \tag{7-27}$$

The block diagram of the control structure is given in Figure 7.14. The weighting factor is selected by using simulation. When R is decreased, the gains all increase which should provide better regulation, although there is a limit because in practice at some point the system becomes unstable. It has been shown that a value of R=0.001 is the best compromise between the stability and control accuracy, which lead G_p=1599200, G_i=20781600, G_v=67470 and G_{ff}=44900.

7.5. Initial Evaluation

It has been shown that the stability of these controllers is guaranteed during the design procedure and the performance of the first two controllers have mainly been accessed in the frequency domain. Now it is necessary to evaluate and compare the performance of all the controllers in the time domain, especially the response speed and the robustness against system uncertainty during pump stage 3 due to the importance of the system performance in the stage. An initial simulation of the designed control laws is performed by means of the SIMBOL package and using the simplified system model.

The step responses of these three control laws are firstly simulated to give a clear indication of dynamic performance. Figure 7.15 gives the responses of the cascade control for the lowest and the highest bounds, where the mass varies from 1400 *kg* to 4135 *kg*. Figure 7.16 is the result for the cascade control plus velocity feedforward term. Figures 7.17 and 7.18 show the responses of the internal model controller and the optimal tracking controller respectively.

From these simulation results,

- The cascade control shows a good robustness against parameter variations. The transient period remains almost unchanged when the mass changes from the lowest bound to the highest. The overshoot is increased with increasing of the mass.

- When a velocity feedforward term in added onto the cascade control, the transient period is improved and it also very robust. The response at the lowest bound starts to show some oscillation and the overshoot is increased compared with the one without the feedforward term.

- The performance of the IMC is worse than the cascade control. It shows a reasonable robustness, but the transient period at the highest bound is too long. In addition, it has the largest overshoot of the three controllers.

- The optimal tracking controller shows a good performance when the mass is at the lowest bound. However, it is very under damped at the highest bound and the transient period is not acceptable.

To further investigate the performances, the second simulation is carried out using a quadratic position and triangular velocity as the input reference signal. Figure 7.19 shows the waveforms of these two trajectories. Clearly the responses of the system, especially steady state error, will be different from those seen with the step responses due to the different input signals.

- Figure 7.20 shows the control errors of the cascade control. Again it shows a little sign of change with the parameter variation. However, the steady state error in both cases reaches about 70 *mm*, as predicted in the design.

- The introduction of the velocity feedforward term is very effective for eliminating the steady state error. Figure 7.21 gives the results when the term is added. The error is reduced to virtually zero and the transient period of the response is about 0.3 *s*.

- If an acceleration feedforward term is added on top of the velocity feedforward, the overshoot can be reduced as well. This is because of the prediction of the required extra force when the acceleration changes sign. However, the acceleration term is dependent upon the mass. This is a physical parameter which cannot be known precisely, and in this case it is affected by the mixture being pumped. A possible compromise is to use an average value. Figure 7.22 shows the results where a mass of 2000 *kg* is used to calculate the acceleration feedforward control signal.

- Figures 7.23 and 7.24 give the control errors of the IMC and the optimal tracking control respectively. Both controllers are not robust enough to tackle the parameter variations in the system and start to oscillate at the highest bound. Moreover, the optimal tracking control as described always has a steady state error regardless of the system parameters. Extensions are possible to reduce this, but this has not been tackled here.

The results obtained so far show that the cascade controller is very robust against the defined parameter variations and has reasonable response speed. It also has desirable control accuracy when feedforward terms are introduced. So further studies are mainly carried out based on the Cascade Controller.

7.6. Selection of Sample Period

The selection of sample period for the current loop has been studied in the last chapter. The sample period of the current loop sets up a minimum value for the outer loops, since it is pointless for the outer loops to have a smaller sample period than the inner loop. But this does not automatically mean that the sample period of the position / velocity loops should be the same as the current loop, although it is desirable to have a sample period as short as possible for fast response, better disturbance rejection and system stability etc. However one has to examine very carefully other factors in the entire system which may require relatively larger but sufficient sample period. In fact there are some elements in this system which limit the maximum size of the sample period.

- <u>Bandwidth of Position and Velocity Loops.</u> From these two points of view, it is not necessary to make the sample frequency too high. The Sampling Theorem states that a signal can be restored from sampled data if the sample frequency is equal to or higher than twice of frequency of the sampled signal, but in practice for control systems this criterion causes unacceptable phase lag due to sampling, and it is commonly recognised that a sample frequency of at least 5 to 10 times loop bandwidth is needed. In this system the bandwidths of the position and velocity loops are about 6 and 15 *Hz* respectively. A sample frequency above 100 *Hz* would be sufficient for this respect.

- <u>Response Speed of Inner Loop.</u> The bandwidth of the innermost current loop is about between 20 and 40 *Hz*, depending on the control gains used. A further improvement of the bandwidth and therefore the response speed is not realistic for the current system configuration, which is restricted by many factors such as the voltage supply and switching frequency of the inverter. As seen from the step response of the current loop given in Figures 6.5 and 6.6, the response speed is between 5 to 10 *ms*. This requires that the outer loops should allow the inner loop to respond in that time period for the demanded force.

Truncation Error of Position Sensor. The position sensor used in the system is a digital incremental transducer with accuracy of 0.25 *mm*. The velocity feedback is derived from the position sensor signals. Therefore a truncation error is inevitably introduced into the system. Since the velocity trajectory of the system is triangular and the actual velocity is quite low at the both ends of each stroke, the error would be considerably increased when the sample period is reduced. This error would produce extra control noise, which is within the audio frequency range, and thus would not be helpful to the system performance. For instance, the instantaneous control signal, and therefore the instantaneous voltage from the inverter, might be higher than expected as a consequence. Note that size of the applied voltage is limited by the d.c. link voltage.

So a sample period 3 to 5 times of the inner loop has been chosen for the position and velocity loops, i.e. the sample period $T_s = 4.5\ ms$ to $T_s = 7.5\ ms$ and the sample frequency $f_s = 222\ Hz$ and $f_s = 133\ Hz$ respectively.

7.7. Summary

This chapter has presented the design of the outer position / velocity loops. Three different approaches have been introduced. Cascade control and internal model control are designed using conventional frequency domain methods. Velocity and acceleration feedforward terms are used in the cascade control to improve the control accuracy. Optimal tracking control is presented for comparison.

The step responses and quadratic position responses of the three controllers have been studied to evaluate the system performances by using the SIMBOL package, initially with the simplified model. It has been shown that the cascade control has the best performance as well as robustness against system uncertainty compared with the other two controllers. A sample period of 4.5 to 7.5 *ms* has been selected for the outer loops.

It has been also shown that the cascade control plus feedforward terms can meet the design requirement and an adaptive control may not be necessary for the application. Therefore further studies using full computer simulation and real time implementation will be mainly concentrated on the cascade control.

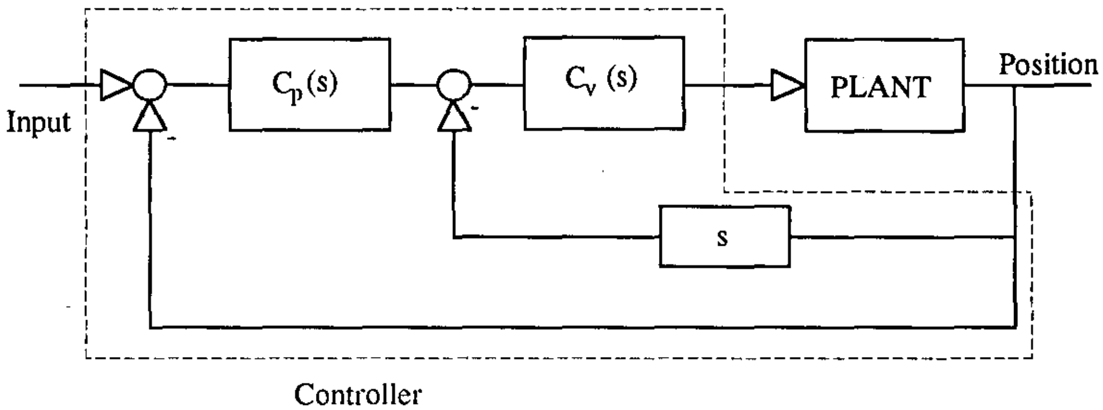

Figure 7.1. Cascade Control.

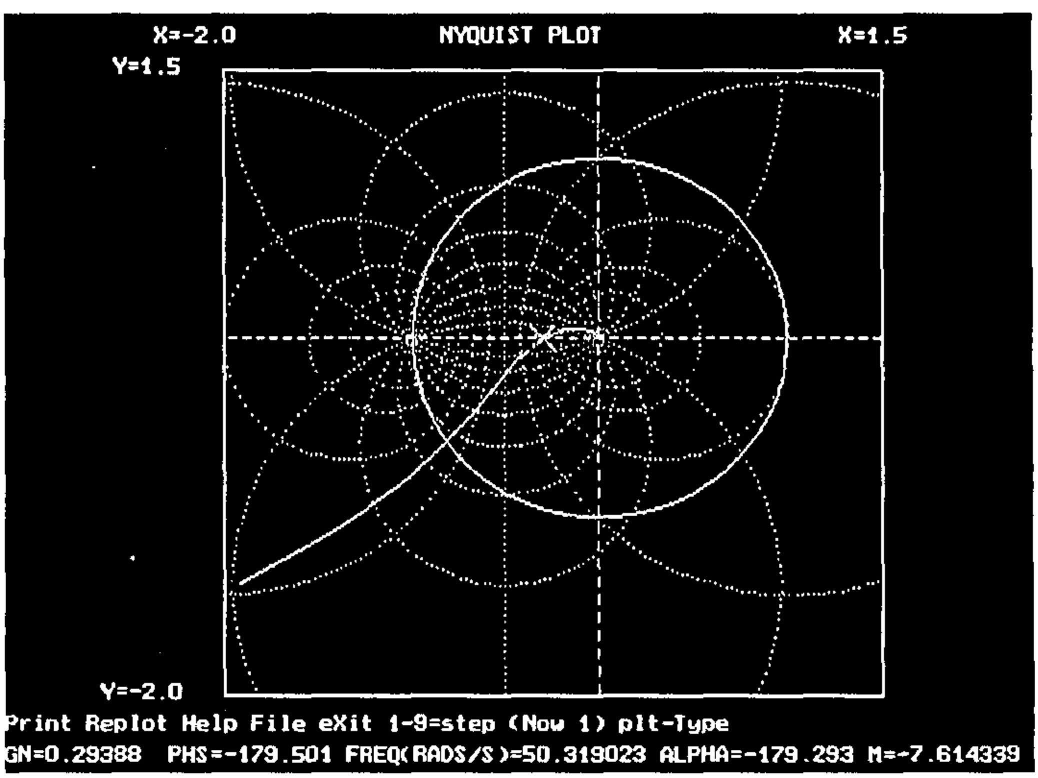

Figure 7.2. Open Loop Nyquist Plot (m=4135kg)

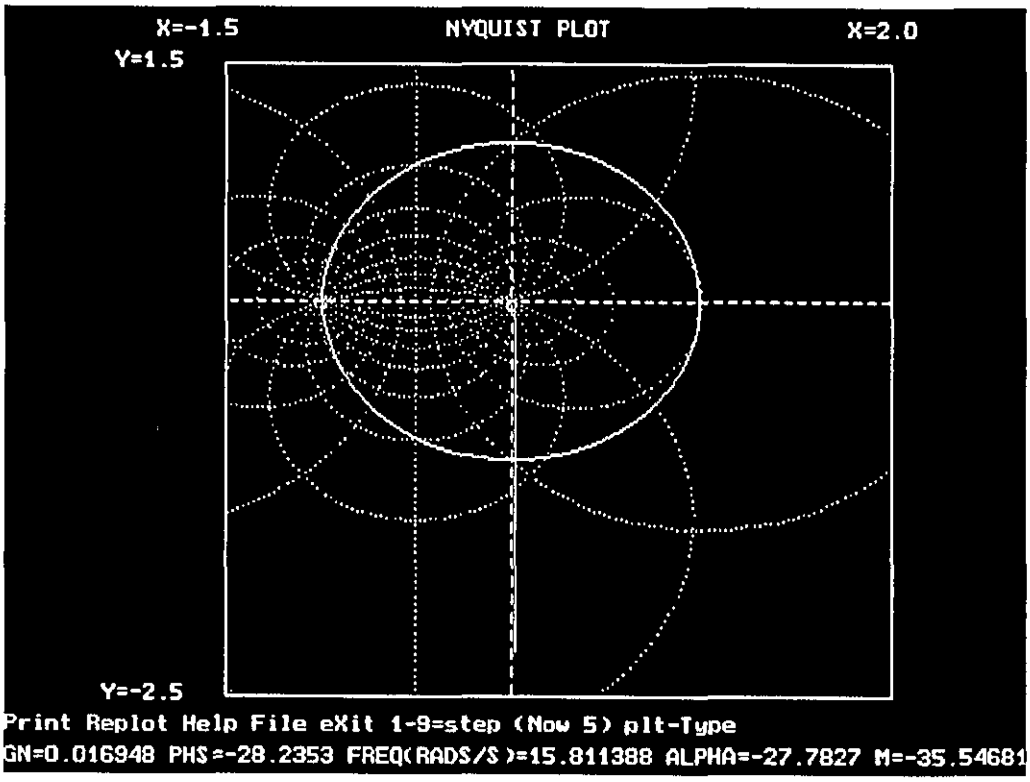

Figure 7.3. Open Loop Nyquist Plot ($m = 1400kg, k_0 = 2 \cdot 10^8$)

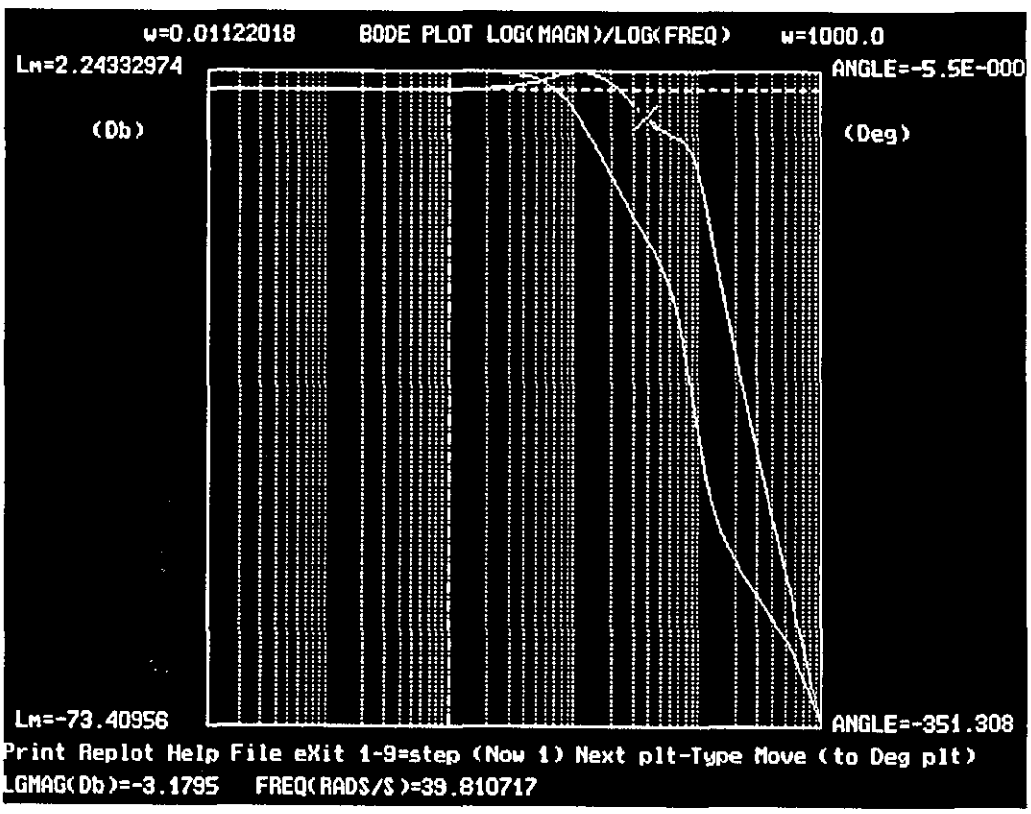

Figure 7.4. Close Loop Bode Plot ($m = 1400$)

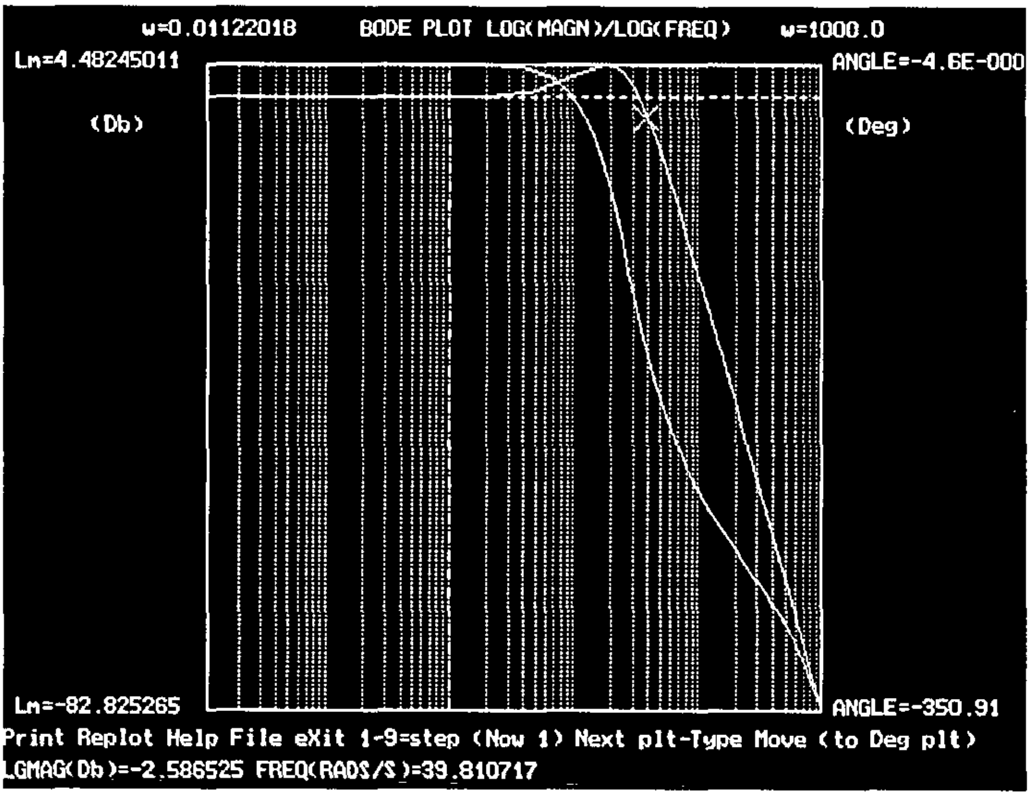

Figure 7.5. Close Loop Bode Plot ($m = 4135$)

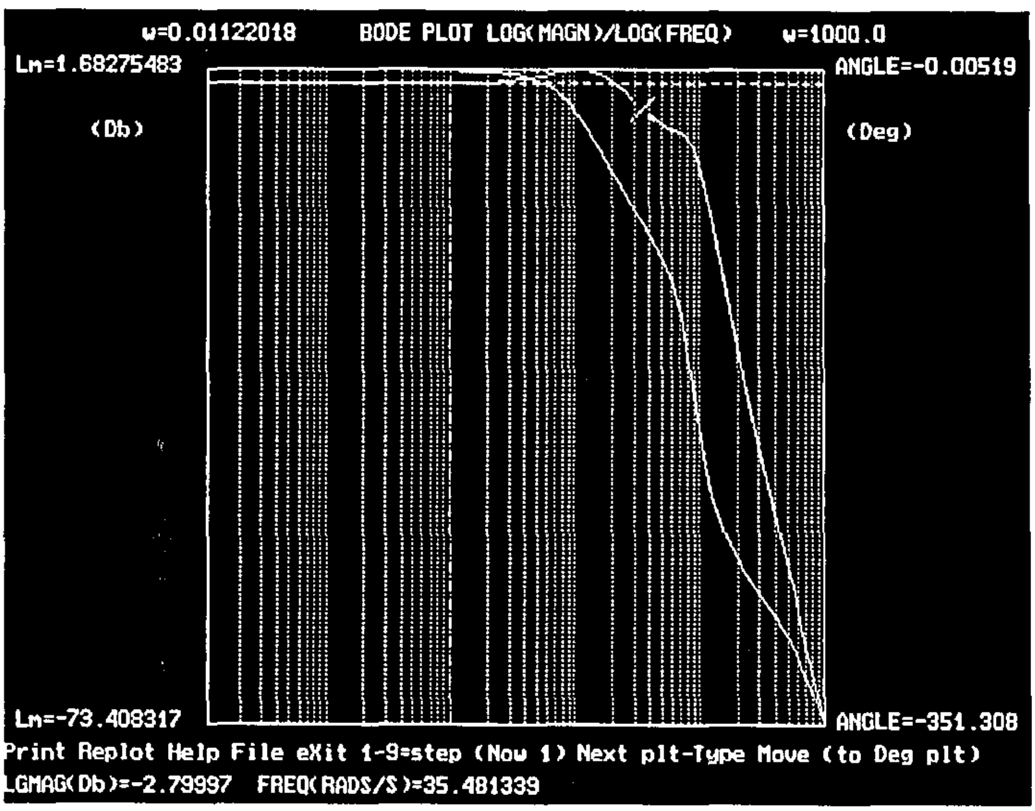

Figure 7.6. Close Loop Bode Plot ($k_0 = 2 \times 10^5$)

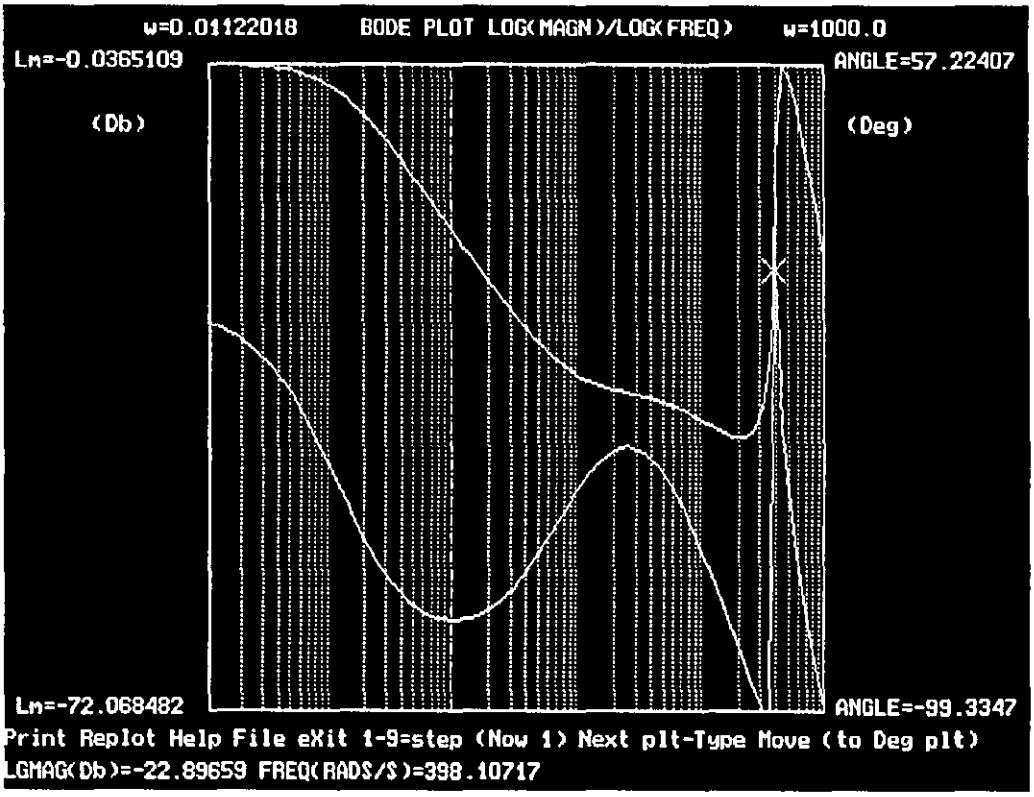

Figure 7.7. Close Loop Bode Plot ($k_0 = 2 \times 10^8$)

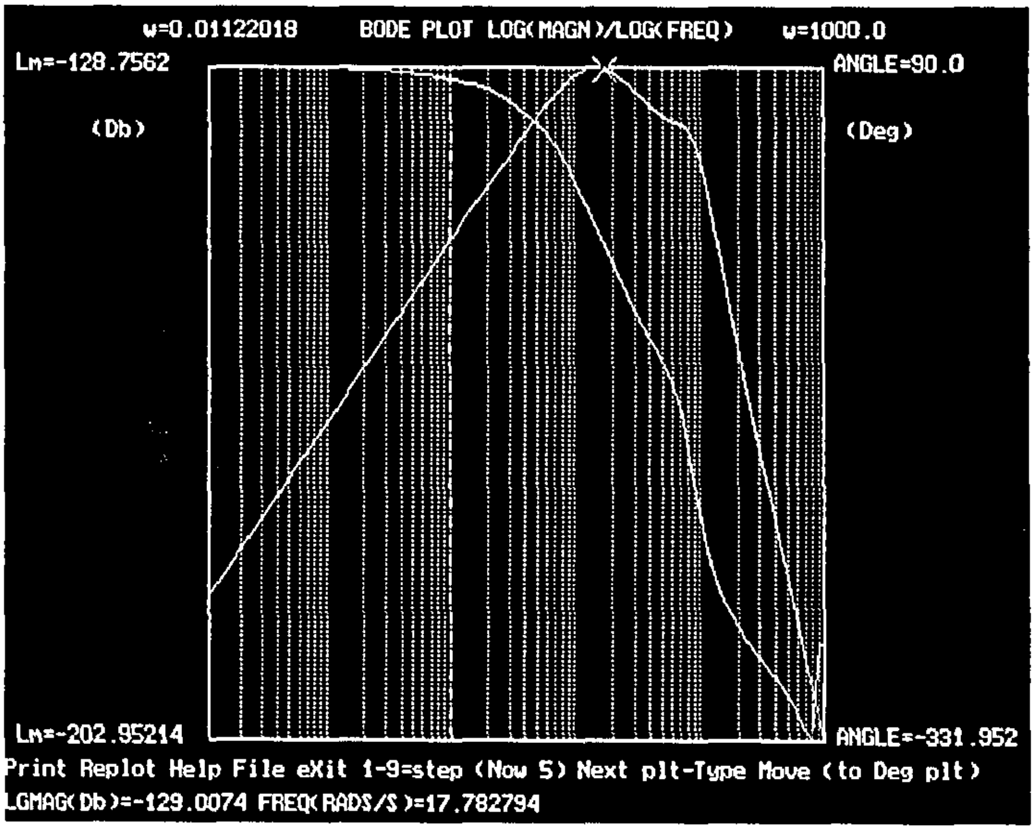

Figure 7.8. Disturbance Rejection ($m = 1400$)

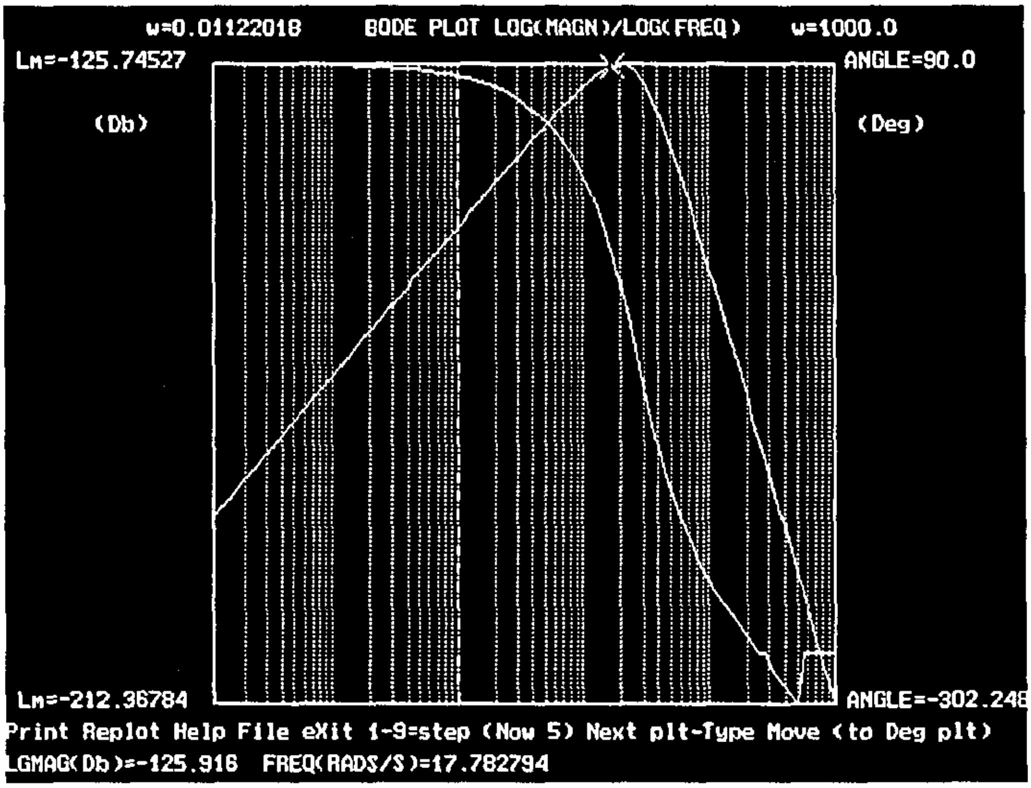

Figure 7.9. Disturbance Rejection ($m = 4135$)

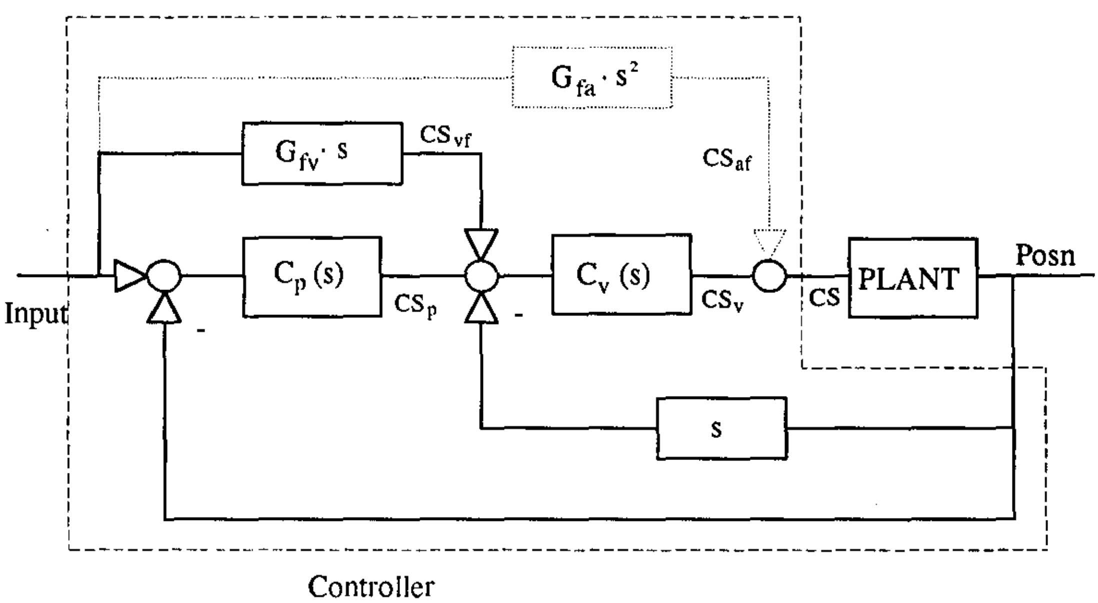

Figure 7.10. Cascade Control With Feed Forward Terms.

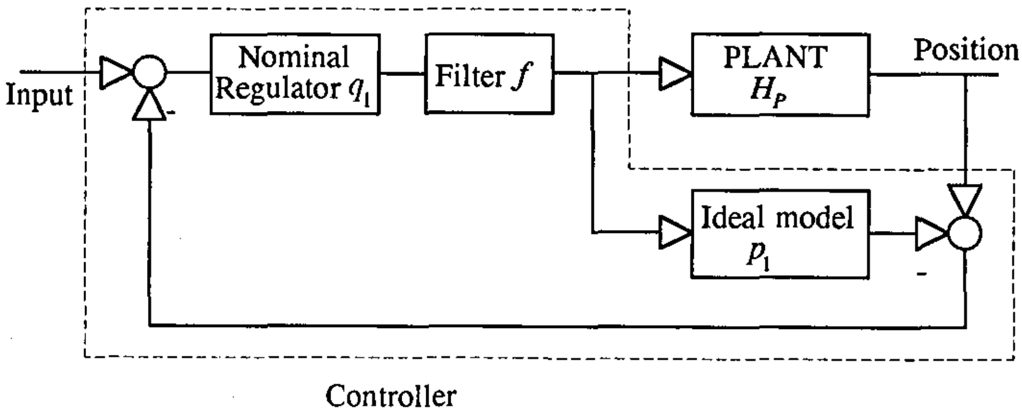

Figure 7.11. Internal Model Control

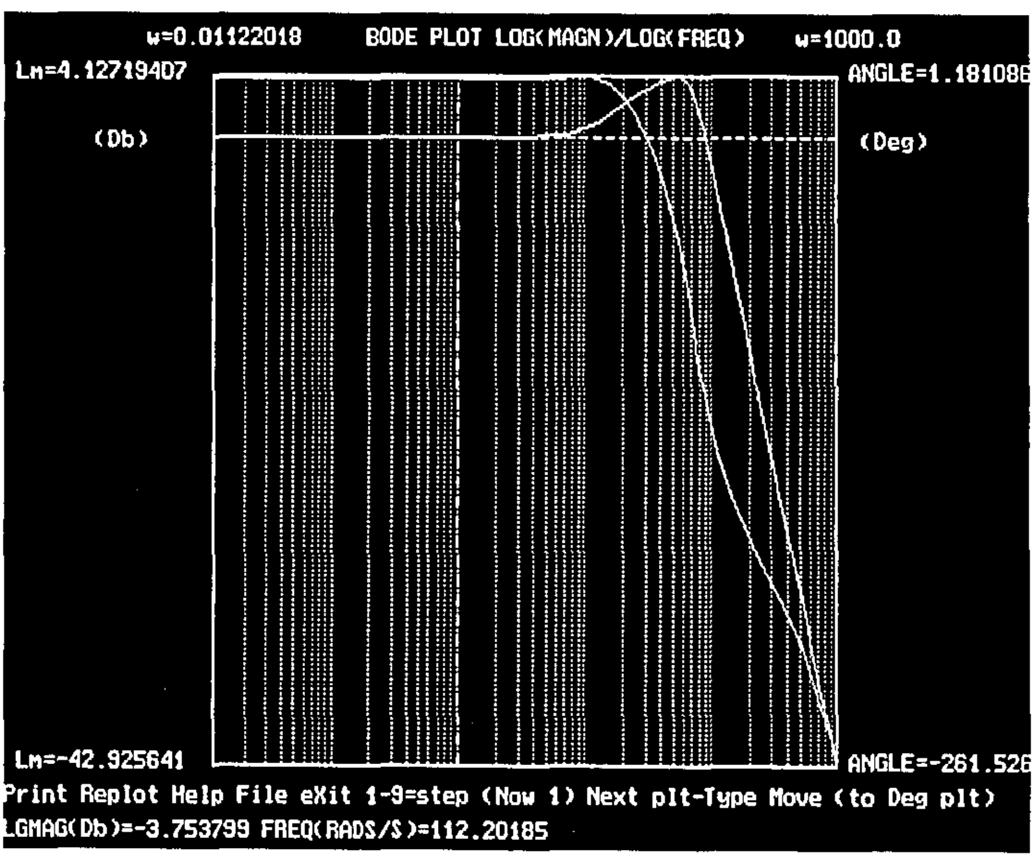

Figure 7.12. Closed Loop Bode Plot of IMC ($m = 1400$)

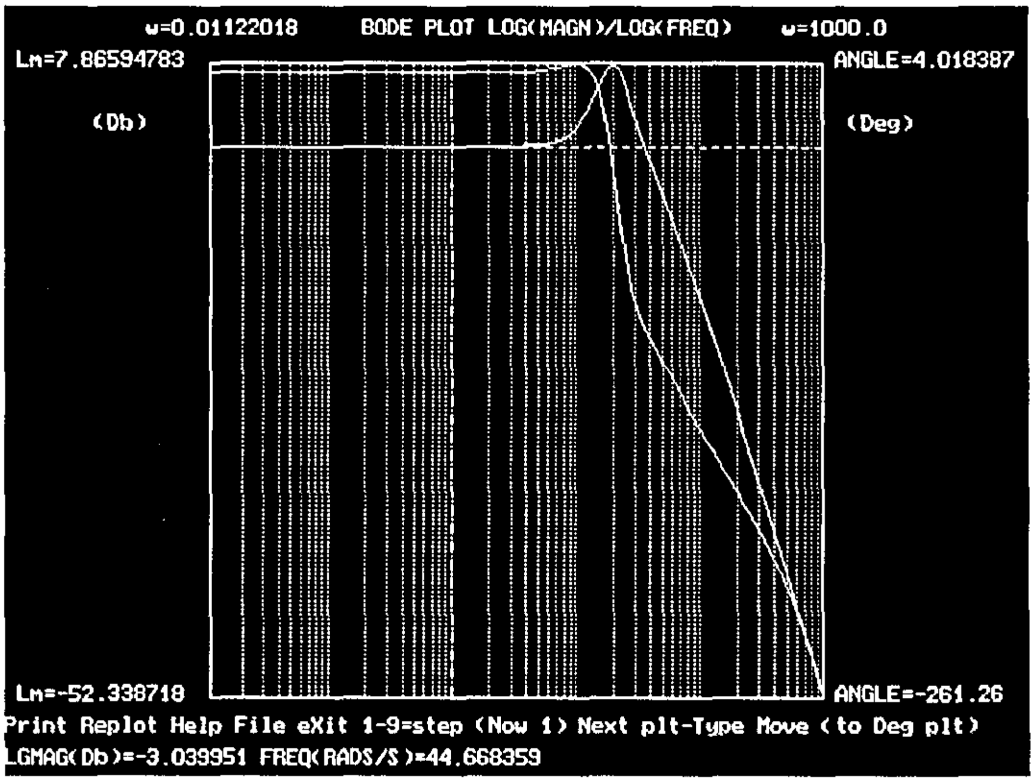

Figure 7.13. Closed Loop Bode Plot of IMC (m=4135)

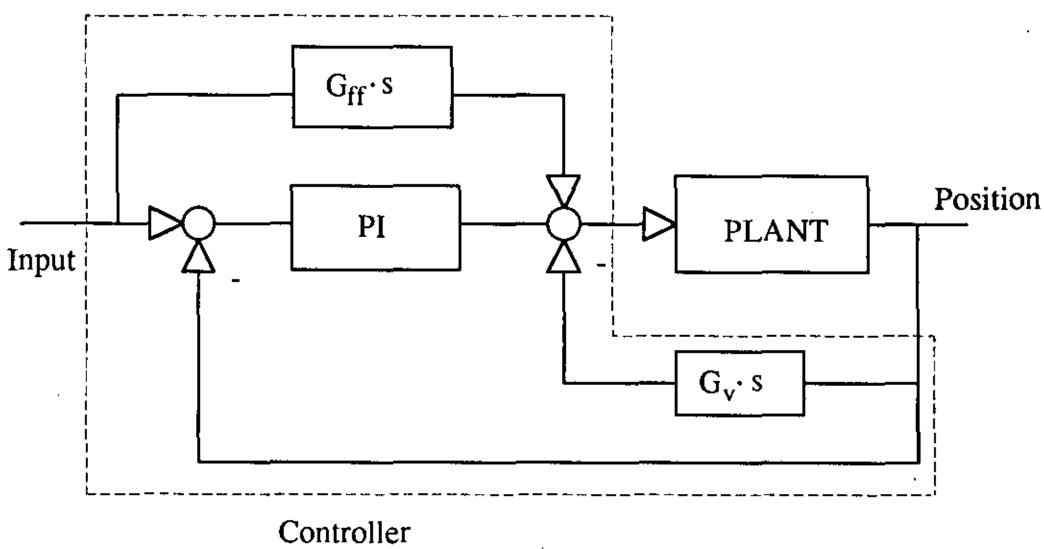

Figure 7.14. Optimal Tracking With I term.

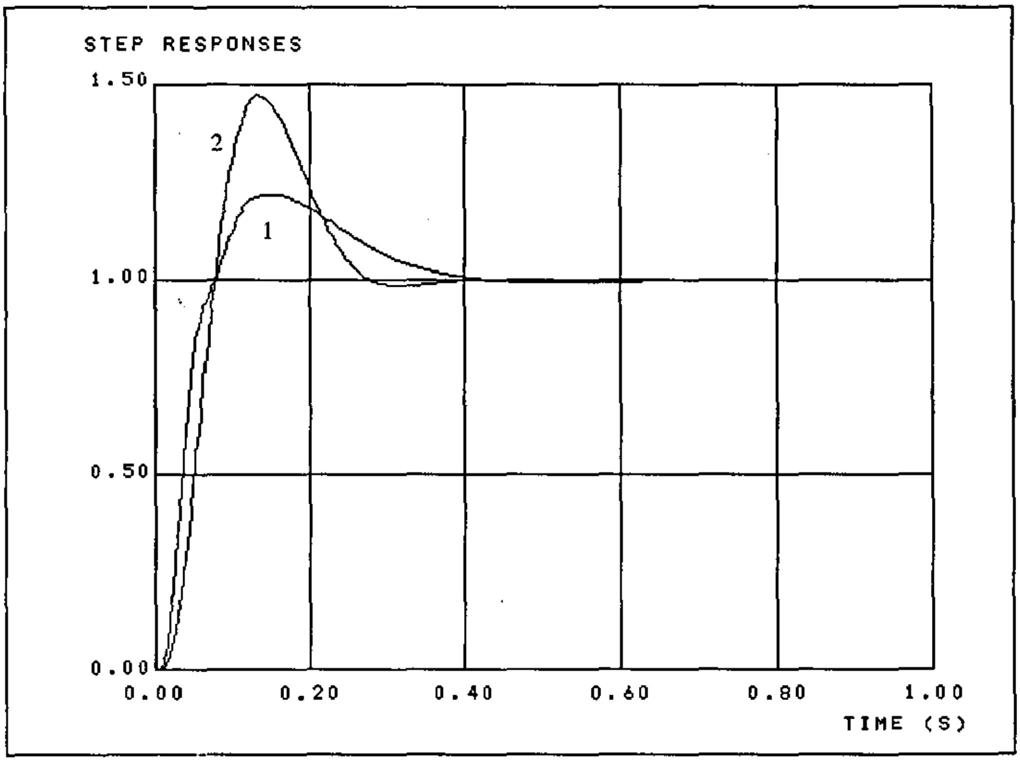

Figure 7.15. Step Response Of Cascade Control
(1. $m = 1400$, 2. $m = 4135$)

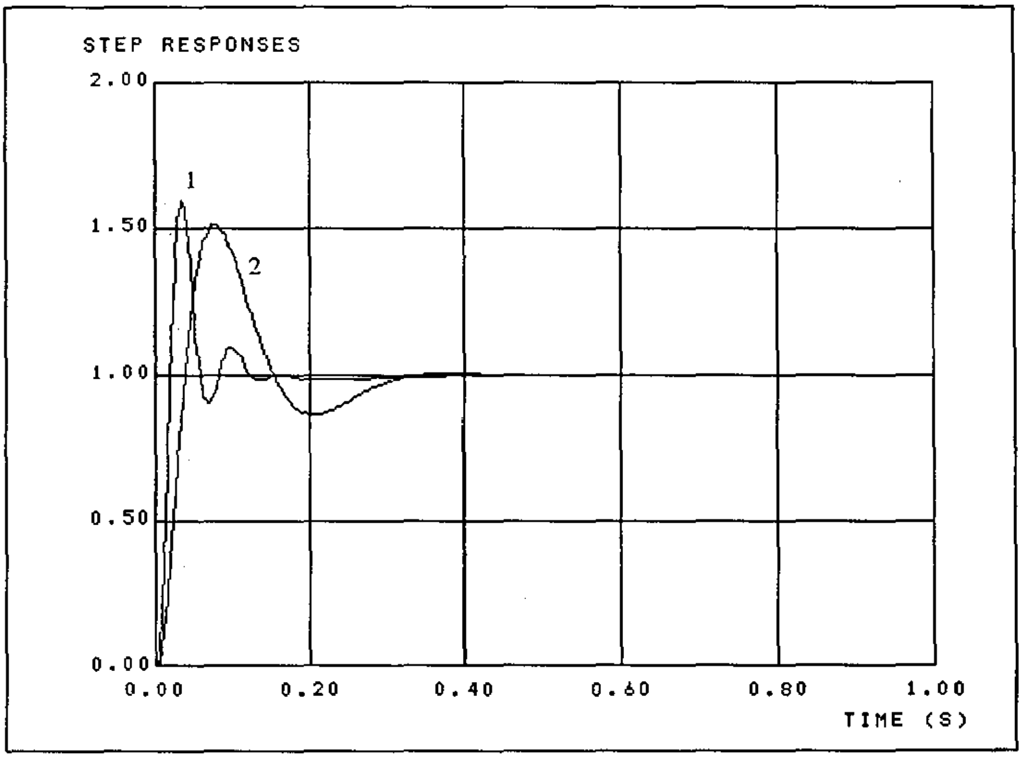

Figure 7.16. Step Response Of Cascade Plus Velocity Feedforward
(1. $m = 1400$, 2. $m = 4135$)

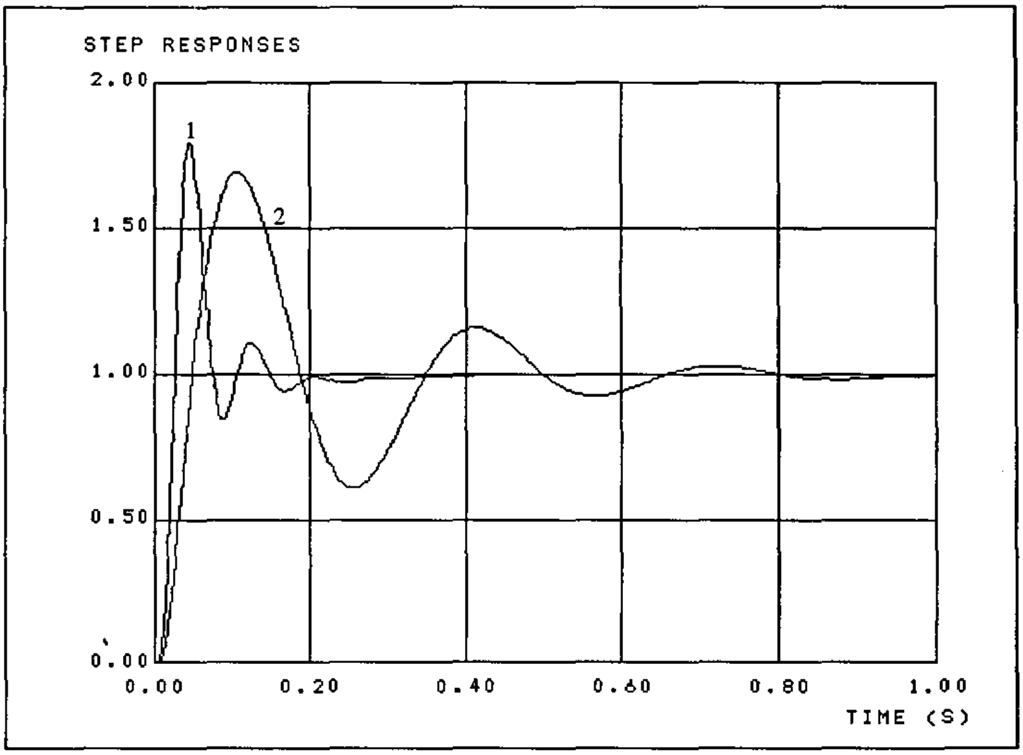

Figure 7.17. Step Response Of IMC
(1. $m = 1400$, 2. $m = 4135$)

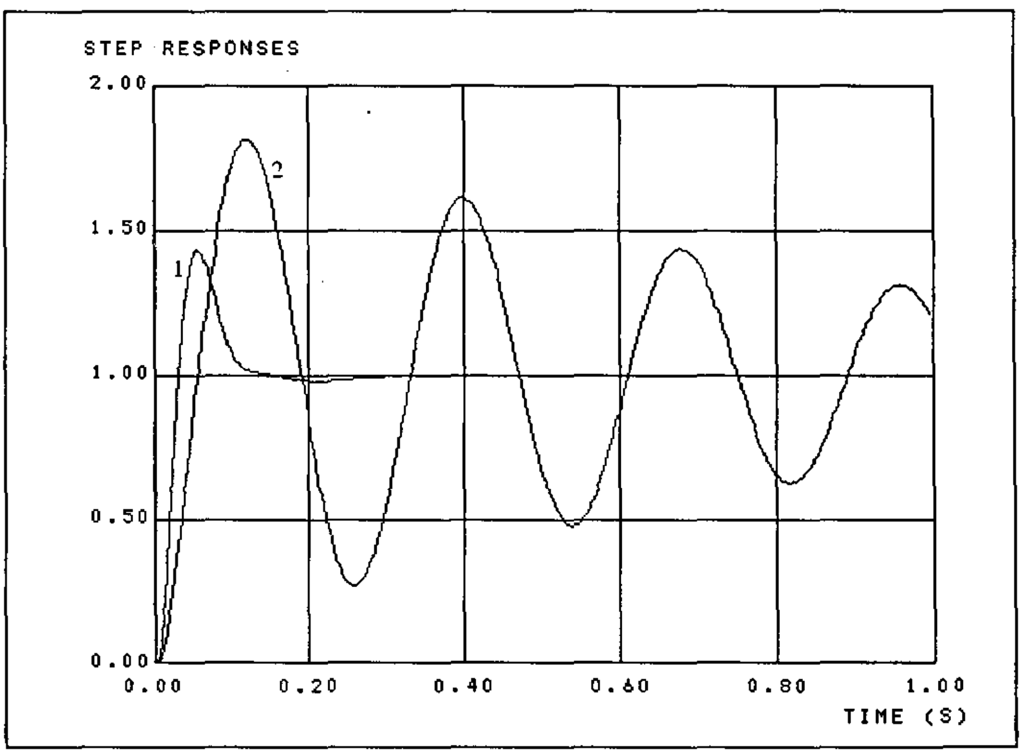

Figure 7.18. Step Response Of Optimal Tracking Control
(1. $m = 1400$, 2. $m = 4135$)

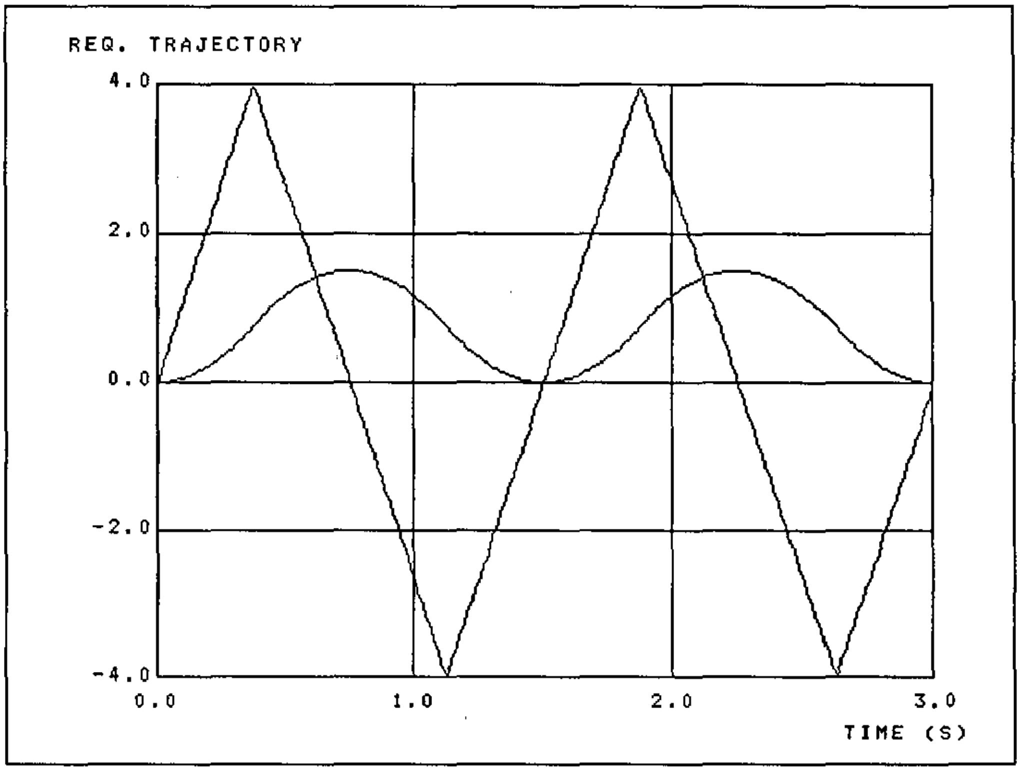

Figure 7.19. Position and Velocity Trajectory

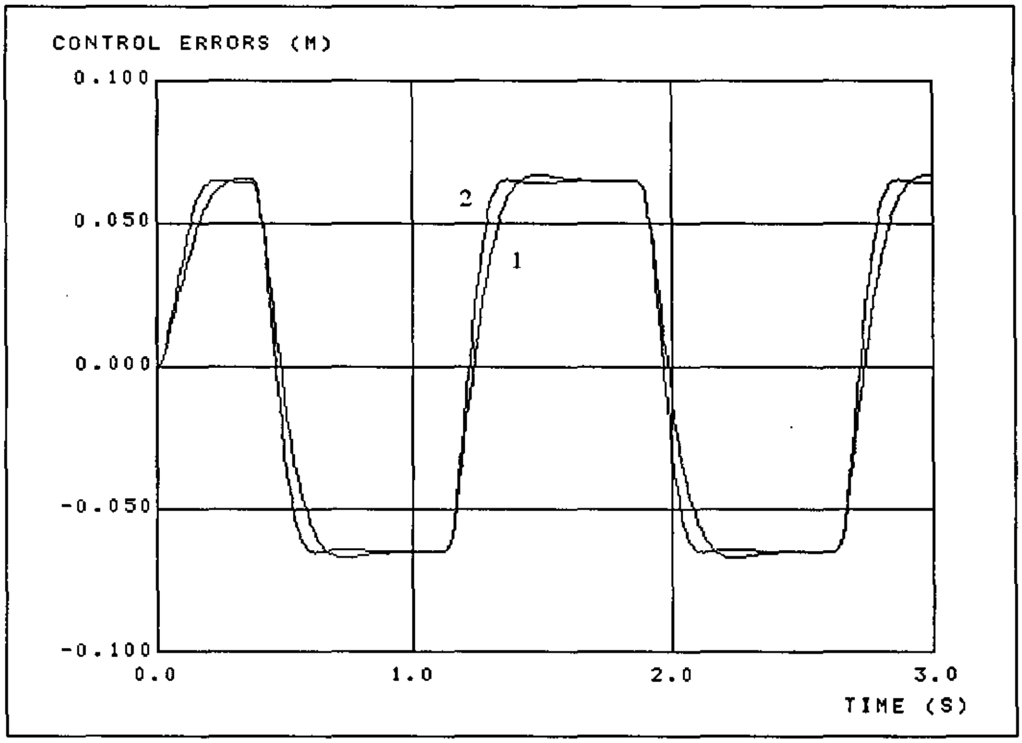

Figure 7.20. Control Error Of Cascade Control
(1. $m = 1400$, 2. $m = 4135$)

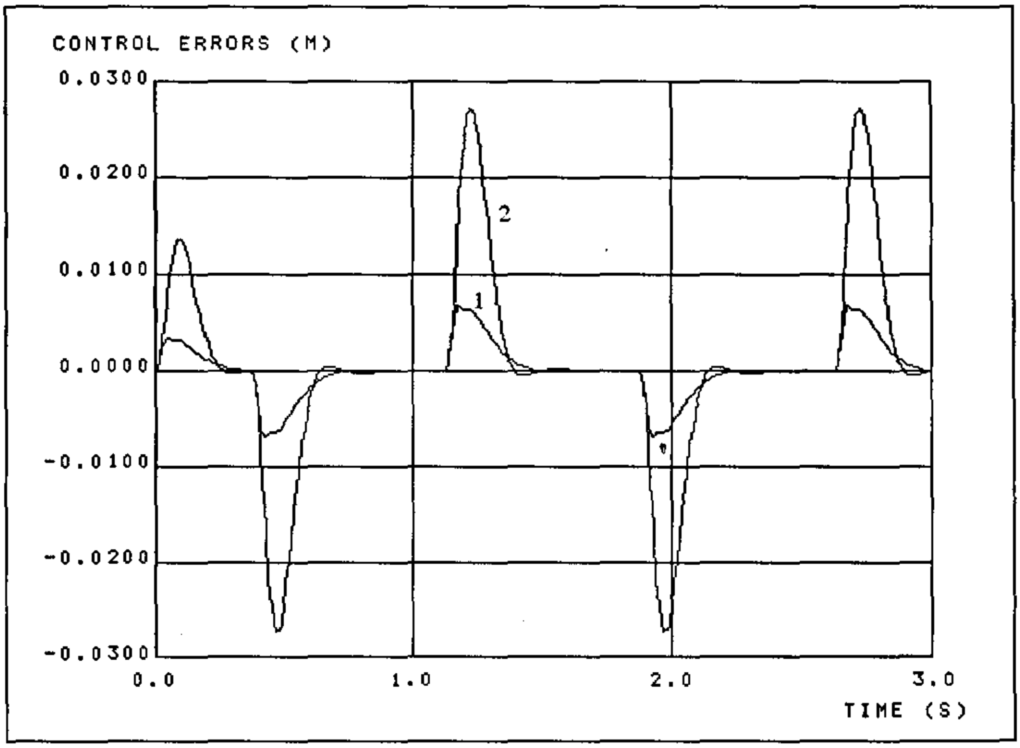

Figure 7.21. Control Error of Cascade Plus Velocity Feedforward (1. $m = 1400$, 2. $m = 4135$)

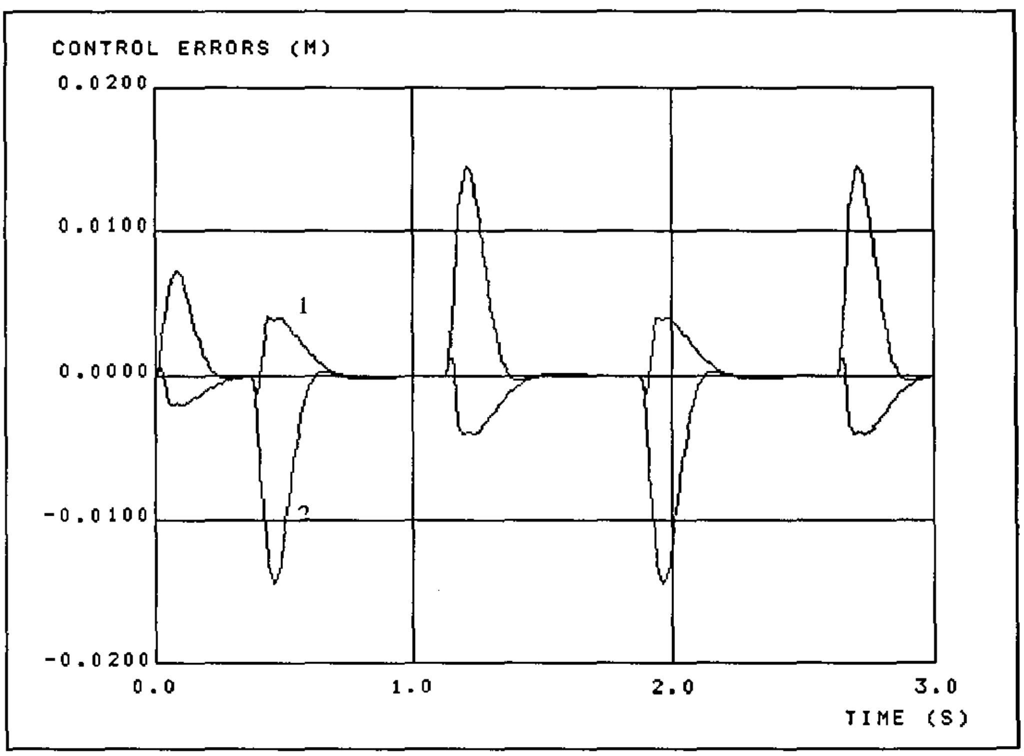

Figure 7.22. Control Error Of Cascade Control Plus Velocity and Acceleration Feedforward Terms(1. $m = 1400$, 2. $m = 4135$)

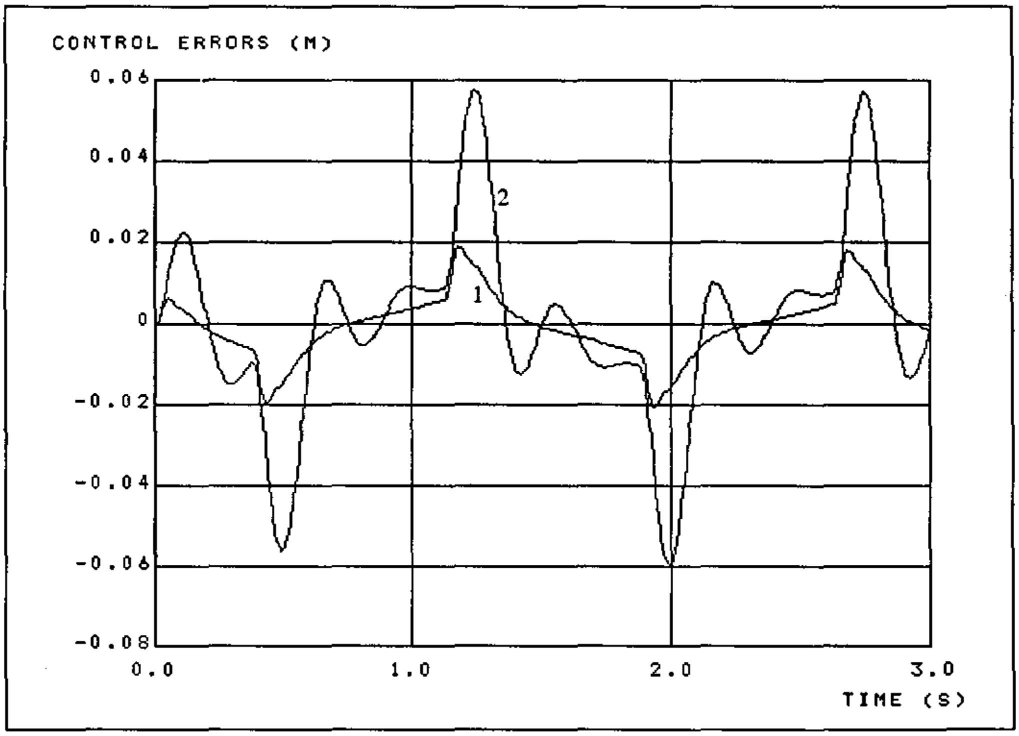

Figure 7.23. Control Error of IMC
(1. $m = 1400$, 2. $m = 4135$)

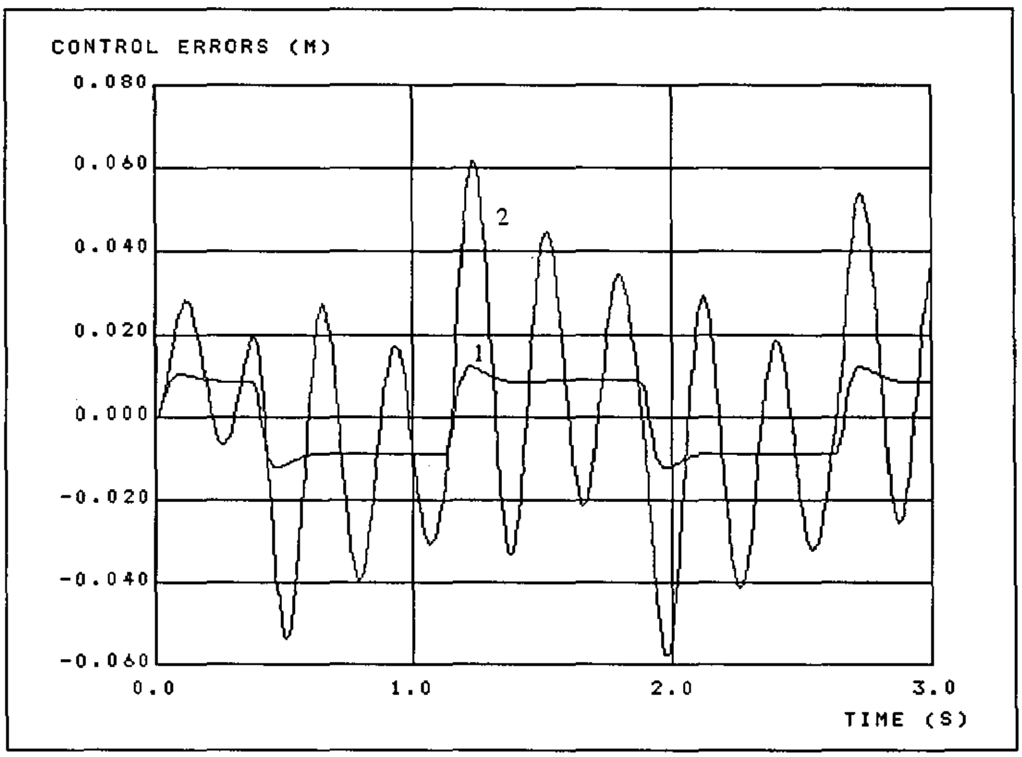

Figure 7.24. Control Error Of Optimal Tracking Control
(1. $m = 1400$, 2. $m = 4135$)

CHAPTER 8.

COMPUTER SIMULATIONS

Because of the great advancement of digital computers and their software, computer simulation techniques have been widely used in the last two decades. It has become a very powerful tool for academic research and industrial applications as well as military uses. Simulations can predict what would happen to a real system if some faulty or extreme conditions occur in the system; prove designs and improve design outcomes and efficiencies; assess the performances of systems in a simpler manner; and reduce costs and risks of training drivers, pilots and other system operators.

This chapter presents the full computer simulation of the subsea pump system, which consists of the models of the system developed in the chapters 4 and 5. The current controller and the cascade controller designed in the chapters 6 and 7 respectively are used in the simulation. Design of the simulation programme is conducted by using the flow chart diagrams. Digital control is implemented for all control loops in the simulation. The sample period and the control gains for the current loop are selected and evaluation of the control system is carried out based on the simulation.

In this chapter, section 8.1 presents the design and structure of the simulation programme. Open loop simulation, current and vector control simulation used in the chapters 4 and 5 respectively are derived from the full simulation programme. Simulation results for the pure gas and pure oil cases are presented and analysed in sections 8.2 and 8.3 respectively. Simulation of the load angle control is presented in section 8.4. A summary of the chapter is given in section 8.5.

8.1. Simulation Programme

The programme is written in C language, which can be run either on a SUN station or a PC and its compatibles, and can easily be adapted for other computer systems. The programme consists of a main programme and number of functions for the different parts of the system.

8.1.1. Main Programme

The main programme performs the interfacing with data files, initialisation of the simulation, calculation of the outer loop control signals, generation of the reference trajectories and connection between the functions.

A flow chart presenting the execution sequence of the program is given in Figure 8.1. It calculates the outer loop control signal once in every outer loop control period, which is several inner loop periods. The number of the periods is defined in the data file. The algorithms of the cascade control plus feedforward actions can be obtained by transferring the control law from the continuous time to the discrete time.

$$CS_p(n) = G_p \cdot \left[x_{ref}(n) - x(n)\right] + G_i \cdot T_s \cdot \sum_{i=0}^{n}\left[x_{ref}(i) - x(i)\right] \tag{8-1}$$

$$CS_{vf}(n) = G_{fv} \cdot v_{ref}(n) \tag{8-2}$$

$$CS_{af}(n) = G_{fa} \cdot a_{ref}(n) \tag{8-3}$$

$$CS_v(n) = G_{pv} \cdot \left[CS_p(n) + CS_{vf}(n) - \frac{1}{T_s}\left(x(n) - x(n-1)\right)\right] \tag{8-4}$$

$$CS(n) = CS_{af}(n) + CS_v(n) \tag{8-5}$$

where, as shown in Figure 7.10, $CS_p(n)$ and $CS_v(n)$ are control signals from the position loop and the velocity loop respectively, $CS_{vf}(n)$ and $CS_{af}(n)$ are output signals of the velocity and acceleration feedforward terms respectively and $CS(n)$ forms the command input to the inner current loop. T_s (4.5-7.5 *ms*) is the sample period of the outer control loops.

The reference position, velocity and acceleration input signals are generated once every outer loop period. The algorithms to compute the reference trajectories are:

$$x_{ref}(n) = x_{ref}(n-1) + v_{ref}(n-1) \cdot T_s + \frac{1}{2} \cdot a_{ref}(n-1) \cdot T_s^2 \tag{8-6}$$

$$v_{ref}(n) = v_{ref}(n-1) + a_{ref}(n-1) \cdot T_s \tag{8-7}$$

$$a_{ref}(n) = \begin{cases} a & 0 \le n \cdot T_s < T/4 \\ -a & T/4 \le n \cdot T_s < T/2 \\ a & T/2 \le n \cdot T_s < T \end{cases} \tag{8-8}$$

where T is period of the pumping cycle and $a = 24 / T^2$ is the acceleration.

The main programme also checks and changes the pump stages of the operation for both sides of the pump according to the pressures in the cylinders and the direction of the piston movement. When the pump stage changes from one status to another, the programme sets up initial conditions for the new stage such that the gas or oil function can respond to the changes correctly.

The 0.25 *mm* resolution of the position sensor is simulated by the integer and float functions of the C language. Velocity used for inner loop current control is derived from the position signals using the sample periods for the inner loop.

$$v_1(k) = \frac{x(k) - x(k-1)}{t_s} \tag{8-9}$$

where $t_s = 1.5\ ms$ is the sample period of the inner loop.

All functions in the simulation are called by the main programme. The current control function is used to simulate the vector control and the closed current loop. Function "rk6_7" is a function used to solve differential equations for the model of the motor. The "gas" and "oil" functions are used to simulate the dynamics of the gas and oil in the cylinders and pipes respectively. Results of the simulations are saved into a data file for analysis.

8.1.2. Current Control Function

The current control function is used to implement the inner closed loop, which is called by the main programme every sample period of the inner loop (1.5 *ms*). A flow chart of the function is presented in Figure 8.2. The motor currents are firstly transferred into the d - q axis currents according to the equations 5-33 and 5-34. The electrical angle of the motor is derived from the current slider position.

$$\gamma = \frac{\pi}{P} \cdot x(k) \tag{8-10}$$

The reference q axis current is calculated from the force demanded by the outer loop controller as given in Equation 5-40. The current is limited by a maximum value to avoid saturation and overload, as well as to provide the protection. The reference d axis current is set to be zero for minimum motor current or proportional to the reference q axis current for load angle control. The ratio is read from the data file in the main programme.

Real and reference currents are used for the current controller to compute the corrective d - q axis voltages. The controller consists of two parts, the command feedforward terms and the closed loop PI action. The feedforward terms are calculated according to equations 6-4 and 6-5 and the PI action is described as follow:

$$v_{d\_pi}(k) = K_{p\_vec} \cdot \left[i_{d\_ref}(k) - i_d(k)\right] + K_{i\_dvec} \cdot t_s \cdot \sum_{i=0}^{k}\left[i_{d\_ref}(k) - i_d(k)\right] \quad (8\text{-}11)$$

$$v_{q\_pi}(k) = K_{p\_vec} \cdot \left[i_{q\_ref}(k) - i_q(k)\right] + K_{i\_vec} \cdot t_s \cdot \sum_{i=0}^{k}\left[i_{q\_ref}(k) - i_q(k)\right] \quad (8\text{-}12)$$

The final d - q axis voltages are the sum of the feedforward signals and the PI actions. Because the voltages in the system are limited by the d.c. link voltage, the two voltages are checked against their maximum values.

Next the d-q voltages are transferred back to three phases by the inverse Park Transformation described in the equation 6.1. A time delay of 1.5 *ms* is simulated at the end of the function in order to represent the computation delay.

8.1.3. Function rk6-7

The function rk6_7 is one of the functions embedded in the C scientific library, which uses the well known Runge Kutta algorithm for solving a set of first order differential equations. In this simulation programme the function is used to solve the equations of the motor model. Figure 8.3 shows a flow chart of sub-function of the rk6_7, which defines the motor model given in equations 4-2 and 5-14. The motor inductances are calculated from equations 5-15 to 5-22 and the load force is obtained from the gas or oil function. Force produced by the motor is also calculated in the function according to equation 5-25.

8.1.4. Gas Function

The gas function is quite straightforward. It is used to calculate the pressures in the two cylinders for the pure gas case. Figure 8.4 gives a flow chart of the function. The function uses equation 4-44 for the calculation when the relevant valve closes. When a valve opens, the pressure in the relevant cylinder is set to constant. Initial conditions in the two cylinders are defined in the main programme. Load forces applied on the piston are derived from the calculated pressures.

The motor model and the gas model interact with each other, but since they are described in two different functions, the calculation steps for the two functions must be selected reasonably small to reduce simulation errors. In the simulation, a calculation step equal to 1/20 of the sample period t_s is used.

8.1.5. Oil Function

The oil function is the biggest and the most complicated part in the simulation programme. The flow chart given in Figure 8.5 highlights the structure of the function. There are two modules in the function, which are used for fluid at two sides of the pump. The two modules have the same structure but perform their functions independently. However their results affect each other indirectly via the piston position, as pressures produced at the two sides are applied to the same piston. The initial conditions for every pump stage are defined in the main programme. The simulation step of the oil function is reduced to 1/74 of the sample period in order to maintain the simulation accuracy. Selection of the time step and its relation with the position grid used for computation are decided by equation 4-34.

Each module is portioned into four parts according to the piston directions and status of the relative valves. Assuming that positive direction of the piston movement is from left to right, the four parts for the right side of the pump are:

- Positive Direction and Valve Closed. When all valves are closed, only oil in the cylinder needs to be simulated as far as the pump is concerned. The cylinder is divided into a number of sections along the x axis and equations 4-26 to 4-33 are used in turn to calculate the head H and the flow rate Q for every section in every time step. The discharge flow rate at the piston side equals the piston velocity and its boundary condition is given in equation 4-

45. The flow rate at the valve side is zero and the boundary condition is given in equation 4-49.

- Positive Direction and Valve Open. When the discharge valve opens, oil in both the cylinder and the outlet pipe must be simulated and equations 4-26 to 4-33 are not only applied for the cylinder but the outlet pipe. The boundary condition at the piston side is the same. However the downstream boundary condition is at joint A, which is defined by equation 4-47. The head and the flow rate at the connection point between the cylinder and the pipe are calculated according to equation 4-51.

- Negative Direction and Valve Closed. Immediately the piston direction reverses, the discharge valve is closed and this side of the pump is in suction mode. Again, only oil in the cylinder needs to be simulated, but the boundary conditions are different. At the piston side, the suction flow rate is equal to the piston velocity and the conditions are defined by equation 4-46. The flow rate at the valve side is zero and the boundary condition is defined by equation 4-50.

- Negative Direction and Valve Open. After the suction valve opens, the boundary condition at the piston side is the same as that before it opens. But the downstream boundary condition is at joint B, which is defined by the equation 4-48. The calculation of the head and the flow rate for the series connection still uses equation 4-51.

The pressures and therefore the load forces applied to the piston are derived from the head as shown in equation 4-4.

8.1.6. Open Loop and Current Control Simulation Programmes

The programmes used for the open loop and the current control simulations in chapters 4 and 5 are derived from the full simulation programme by disabling some irrelevant functions.

For the open loop simulation, the current control function and the electrical part of the motor model are not needed. So the current control function is disabled and the dynamic model for the mechanical part of the motor is used to define the sub-function of the rk6_7, which is a second order system as given in equation 4-2. The outer loop controller and the trajectory generation part in the main programme are also disabled. A constant reference force is set to simulate the step input.

For simulation of the current control loop, the gas and oil functions are irrelevant. In the step response simulation, the outer loop controller and the trajectory generation are disabled and a step reference force is used. For the simulation of frequency responses, only the electrical part of the motor model and the current control function are used in the simulation. Sinusoidal input signals are used as the q axis reference current.

8.2. Simulation of Gas Case

By using the simulation programme described above and selecting the gas function, simulation for the pure gas case has been carried out. In the simulation, the peak velocity is set to 4.2 *m/s* and the pumping stroke 1.5 *m*. Pressures at points A and B are set to 70 and 35 *bar* respectively to simulate the subsea conditions. The feedforward terms and the three different gains for the current control loop are used in the simulation respectively to assess their performance. Different sample periods for the outer position / velocity controller are also simulated to examine their effect on the overall performance. The simulation results are given as follows.

- Position and Velocity Outputs. Figure 8.6 shows the outputs of the slider position and velocity, which follow the demanded trajectories well. Transient response periods at the beginning of each stroke and at the midpoint where the acceleration changes sign can be observed on the velocity output. Figure 8.7 shows the load forces in the two cylinders produced by the piston compressing gas. The pressure in one of the cylinders and therefore the force applied on the piston builds up at the beginning of the stroke until the relevant discharge valve opens, after which constant pressure is maintained. When the direction of the slider reverses, it repeats the same procedure in the other cylinder.

- Velocity and Acceleration Feedforward Terms. The cascade controller with velocity and acceleration feedforward terms is compared with that having the velocity feedforward term only. Figure 8.8 gives the simulation results, where the gain 1 of the current control loop is used and the sample period of the outer loops is 5 times that of the inner loop (7.5 *ms*). From the results, it is shown that the acceleration term does not improve the control accuracy in the pure gas case. This is because the pump stage 1 lasts a relatively long period and the control error is mainly caused by the stiffness. The response of the controller with the acceleration term is a bit slower than that without the term, although it seems that it does not affect the overall performance. This is because the stiffness causes a longer transient period and the force reduction at the midpoint of each stroke caused by the acceleration term affects the response speed. It is expected that the acceleration term should improve the performance for the pure oil case, where stage 1 is very short.

- Gains of Inner Current Control Loop. To evaluate the performance of the three gains for the current control loop, simulations using the gains 2 and 3 have also been performed. The results are presented in Figures 8.9 and 8.10 respectively. Again the 7.5 *ms* sample period of the outer loops and velocity feedforward are used. The control error with gain 2 is very similar to that for gain 1 but it starts to show oscillations on the waveform, compared with the results in Figure 8.8. The gain 3 is unstable in this case because it has the slowest response of the three gains. By comparing the outer loop control signals $CS(n)$ for gains 1 and 2 as given in Figures 8.11 and 8.12 respectively, both signals show the oscillations, with gain 1 being slightly better. The cause of the oscillations is that the sample period for the outer control loops is too large, as shown below.

  The difference between the control signal (i.e. the demand force) and the load force (i.e. the total force applied on the piston due to the pressure in both cylinders) is a consequence of the acceleration and deceleration of the slider.

- Sample Period of Outer Control Loops. The oscillations can be improved by reducing the sample period from 5 times the inner loop sample period to 3 times (4.5 *ms*). Figure 8.13 demonstrates the improvement due to the reduction. There are little differences between the three gains as far as the position error is concerned. Only slight oscillations can be observed on the control error for gain 3. Figures 8.14 and 8.15 show the much improved response of the control signals in the gains 1 and 3 cases. However it can be observed that some extra noise is introduced on these control signals, which may cause problems on the inner current loop. The noise is caused by the truncation error of the position transducer. The situation would be worse when the pump operates at the lower speeds, where the truncation error of the velocity is more severe.

- Control Noise. Figures 8.16 to 8.18 compare the effects of the truncation errors on the d - q axis voltages in the simulations using the three current control gains respectively. Gain 1 has the worst noise on the q axis voltage because it has the highest bandwidth; gain 3 has the least noise and the gain 2 is in between. To compromise between the inner and the outer loop performances as well as overall stability, it is sensible to select the gain 2 for the current control loop and 4.5 *ms* as the sample period for the outer control loops.

- D - Q Axis Currents and Response of Inner Loop. Figure 8.19 gives the d-q axis currents, where the outer loop sample period is 4.5 *ms* and the current control loop uses the gain 2. In the figure, the difference between the reference and the real q axis current is hardly visible. The real d axis current is almost zero at all the time because the d axis reference current is set to zero in the simulation. Therefore gain 2 is quite sufficient for the inner control loop.

- Phase Current and Voltage. Figures 8.20 and 8.21 presents the phase current and the phase voltage of the motor respectively. Amplitude of the phase current is basically dependent upon the demanded force and the phase voltage is closely related to the slider velocity.

8.3. Simulation of Oil Case

Simulations of the pure oil case have been performed using the different pipe lengths and diameters in order to assess the system robustness and performance. As before, a peak velocity of 4.2 *m/s* and stroke of 1.5 *m* have been used. Pressures at points A and B are 70 and 35 *bar* respectively. The feedforward terms and gain 2 of the current control loop are used in the simulation. The sample periods for the inner current loop and the outer position / velocity controller are 1.5 *ms* and 4.5 *ms* respectively.

- Position and Velocity Outputs. Figure 8.22 shows the outputs of the slider position and velocity. Compared with that obtained in the pure gas simulation, the velocity in the pure oil case has worse distortion at the beginning of every stroke. This is expected because the high stiffness due to high value of bulk modulus of the oil in the stage 1 opposes the movement of the piston and the control system needs time to respond to the rapid increase of the load force. The Bode diagram presented in Figure 7.7 has shown that the bandwidth in the high stiffness case is relatively low.

- Effect of The Driven Mass. The total mass to be driven by the motor is the mass of the slider and pistons plus the equivalent mass of the oil in the inlet and outlet pipes, where the mass of the slider is a fixed value but that of the oil depends on the length and diameter of the pipes. Higher mass demands higher driving force in the acceleration periods.

  Figure 8.23 shows the forces demanded by the system to deal with different masses, where the pipe lengths of the inlet and outlet pipes are 10+10 *m* and 40+40 *m* respectively and the diameter of the pipes is 100 *mm*. It is clearly shown that the demanded force is increased in the acceleration periods of each stroke when the length of the pipes is increased from 10 *m* to 40 *m*. During deceleration the driving force is reduced with the longer pipes.

  Although reducing the diameter of the pipes decreases the quantity of the oil in the pipes, the equivalent mass is increased as far as the motor drive is concerned, as indicated in equation 4-63. Figures 8.24 and 8.25 demonstrate the effect of the change with pipe lengths of 20+20 *m* and 40+40 *m* respectively. In both diagrams, the required force is increased in the acceleration periods and decreased in the deceleration periods when the pipe diameter is reduced from 150 to 100 *mm*.

- Disturbances In The System. In the pure oil or oil dominant mixture case, the fluid dynamics cause transient pulsating forces. Figure 8.26 shows typical waveforms, where FL1 is the load force applied on the one side of the slider and FL2 is that on the other side. These load forces will affect the performance of the control system. However the pulsating forces can be treated as independent disturbances as their frequencies are mainly related to the length of the pipes and the bulk modulus of the fluid; the amplitudes depend on initial velocity of the fluid. Figures 8.27 to 8.29 show how the forces vary with these parameters over one pump stroke.

In Figure 8.27, the force pulsations have the highest frequency when the pipe length is 10+10 *m*. The frequency for a pipe length of 20+20 *m* is about half of that in the case of 10+10 *m* pipes. It has the lowest frequency when the length is 40+40 *m*, for which the frequency is about halved compared with 20+20 *m*.

Figure 8.28 gives the results when the fluid is changed from the pure oil to 99% oil mixture which reduces the bulk modulus and therefore the stiffness of the fluid, and shows that the frequency is reduced but the amplitude is increased. The increase of the amplitude is caused because the piston achieves higher velocity before the discharge valve opens due to the lower stiffness.

Figure 8.29 shows the results where the diameters of the pipes are different. The frequencies of the two waveforms are basically the same since they are not related to the mass of the fluid, but the amplitude of the force in the smaller pipe is higher. Again, it is caused by the higher piston velocity. In this case, because the diameter of the pipes is a lot smaller than the cylinders, the series connection causes an increase of the speed of the oil in the pipes.

- Stiffness. High stiffness has been shown on the load forces in Figures 8.26 to 8.29. The forces increase rapidly in pump stage 1. The value of the stiffness is dependent on the bulk modulus of the fluid in the cylinders, which is greatly affected by the percentages of the oil mixture. In Figure 8.28, the rate of increase of the load force is clearly lower even though the fluid is only changed from the pure oil to 99% oil and 1% gas.

- Inner Control Loop. Like the pure gas case, the inner current control loop follows the demands from the outer control loops well. Figures 8.30 and 8.31 show the d-q axis currents where the pipe lengths are 10+10 *m* and 40+40 *m*. As expected, the performance of the inner loop is not affected by the variation.

- Acceleration Feedforward Term. Figures 8.32 to 8.34 show the effects of the acceleration term of the outer control loops in the oil case. In Figure 8.32 where the pipe length is 10+10 *m* and the diameter is 100 *mm*, the control error caused by the driven mass at the midpoint of each stroke is reduced when an acceleration feedforward gain m=2000 is added, which helps to smooth the velocity waveforms. However it does not reduce the errors caused by the high stiffness at the beginning of each stroke. In Figure 8.33, where the pipe length is 20+20 *m* and the diameter is 100 *mm*, it also shows a significant reduction of the control error at the midpoint of each stroke when the same acceleration term is introduced.

Figure 8.34 compares the effects of the different acceleration gains when the pipe length is 40+40 *m* and the diameter is 100 *mm*, which is in fact at the highest bound of the system uncertainty. Because the system now has the maximum mass, the gain corresponding to m=4000 shows better effect than the gain corresponding to $m = 2000$, but it will cause over compensation when the system drives less mass, especially in the pure gas case. Therefore a compromise of an average value over the uncertainty bound is preferred for the acceleration feedforward term.

- Stability, Robustness and Control Errors. Stability and robustness as well as performance are the most important issues in the control system. Figure 8.35 gives the control errors in different pipe lengths and Figure 8.36 gives the results with different pipe diameters where the pipe lengths are 10+10 *m* and 40+40 *m* respectively.

  The control system is stable when the pipe length and diameter (and therefore the mass) are changed. This means that the system should also be stable when it pumps the oil-gas mixture where the mass varies with the uncertainty bound.

  The system is robust against system uncertainty. It has been shown that the stability and performance of the system in both the pure gas and the pure oil cases are very little affected by the variations. The peak values of the control errors are increased when the driven mass in the system is increased, but their transient periods and steady state errors are kept about the same. The errors at the end of each stroke are close to zero, which are better than required. No overshoot at the stroke ends has been observed.

  The control system shows excellent disturbance rejection capability. The pulsating forces in all simulations are compensated by the control loops and as expected they have little effect on the control errors.

- Phase Current and Phase Voltage. Figures 8.37 and 8.38 show the phase current and voltage of the motor in one pumping cycle respectively, where the pipe lengths are 10+10 *m* and 40+40 *m*. When the pipe length is increased, the driving force and therefore the motor current is increased in the acceleration periods and decreased in the deceleration periods. The phase voltage is mainly related to the motor velocity but it also has to increase in order to produce higher current when higher force is demanded.

8.4. Simulation of Load Angle Control

As presented in the chapter 6, the power factor of the drive system can be improved and the inverter power capacity can be reduced by controlling the load angle of the motor. A simulation has been carried out to prove the theoretical results. The simulation is performed for the pure oil case. The d - axis current is controlled to be proportional to the q - axis current such that a constant leading angle of 20^0 is achieved. The pipe length of 20+20 *m* and the diameter of 150 *mm* are used in the simulation. For clarity, only the results for one stroke are shown.

- Figure 8.39 gives the d - q axis currents. The q-current produces the motor force and the d-current adjusts the current angle. In the acceleration period, the q axis current is quite high and so is the d axis current. In the deceleration period, the two currents are reduced because the required force is lower.

- Figure 8.40 shows that the magnitude of the phase current is increased when the current angle is changed from 0 to 20^0. Because the d-current is controlled proportional to the q-current, the increase of the phase current is relatively smaller in the deceleration period where the required current is lower.

- Figure 8.41 shows improvement of the power factor. It can be observed that the power factor is increased from about 0.92 to 0.98 in the acceleration period and from less than 0.98 to nearly unity during deceleration. The improvement is not so obvious in the deceleration period as it is already quite high when the d-axis current is zero.

- Figures 8.42 and 8.43 show reductions of the voltage amplitude and VI rating respectively. Again the improvement in the acceleration period is better than that in the deceleration period, because of the higher current in the prior situation. It has also been noted the reduction at lower velocity is less than that at higher velocity. This is because the resistive term in Equation 6-11 is more dominant at the lower velocity.

  The reduction of the peak voltage means that maximum voltage of the inverter output and therefore d.c. link voltage can be reduced. The improvement of the VI rating makes reduction of the inverter power possible.

8.5. Summary

In this chapter, the full computer simulation of the control system has been presented where the main programme, the motor function, the vector control function and gas and oil functions are described by flow chart diagrams. Simulations for the gas and the oil cases have been carried out. In the oil case, different pipe lengths and diameters have been examined in the simulation.

Control gain 2 for the inner current loop and the sample period 4.5 *ms* of the outer loops are chosen with the help of the simulation. Results of the simulations have been used to assess the performance of the control system. The simulation has shown that the dominant factor affecting the system performance is the total equivalent mass, which varies with the mixture of oil and gas. The designed controller is stable in all cases and the system has demonstrated robustness against uncertainty. Control accuracy in all simulations is satisfactory. The acceleration feedforward term improves the performance in the oil case, but it does not improve the accuracy in the pure case due to the longer period of the pump stage 1. An average value of the masses of the highest and the lowest bounds is recommended for the term as a compromise.

The pulsating forces caused by the fluid mechanics can be treated as independent disturbances in the system as they are mainly related to the pipe length and the bulk modulus of the fluid. The system has shown good capability for disturbance rejection and the control errors are virtually unaffected by the disturbances.

Therefore the simplified model developed for the control design is valid and the controller which has been developed meets the requirement according to the simulation results.

Load angle control has been simulated. The simulation results have shown that the power factor can be improved and the voltage and the VI rating can be reduced by adjusting the d axis current. The best results are obtained in the acceleration periods, where the higher driving force and therefore higher motor current are required. It should be noted that this is achieved by the increase of the phase current.

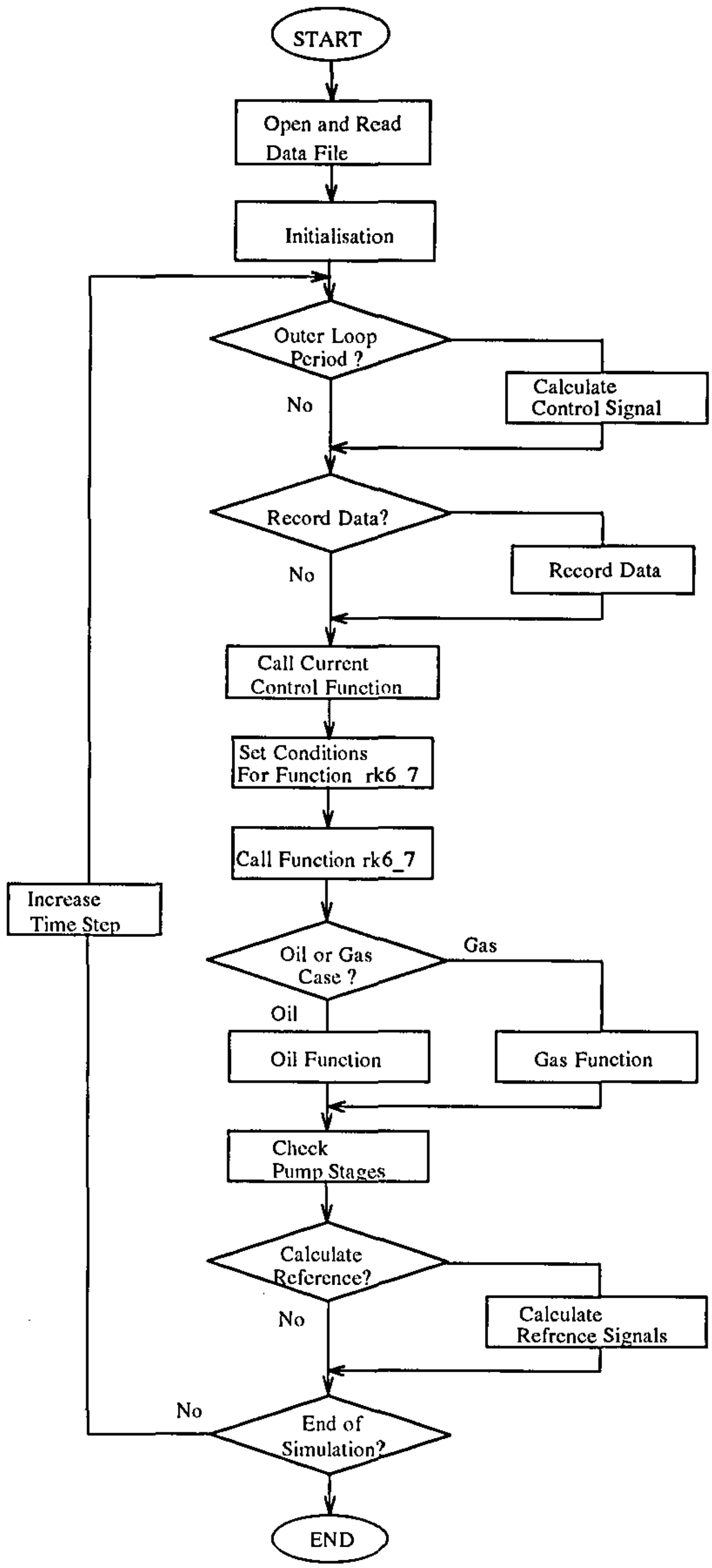

Figure 8.1 Flow Chart of Main Programme

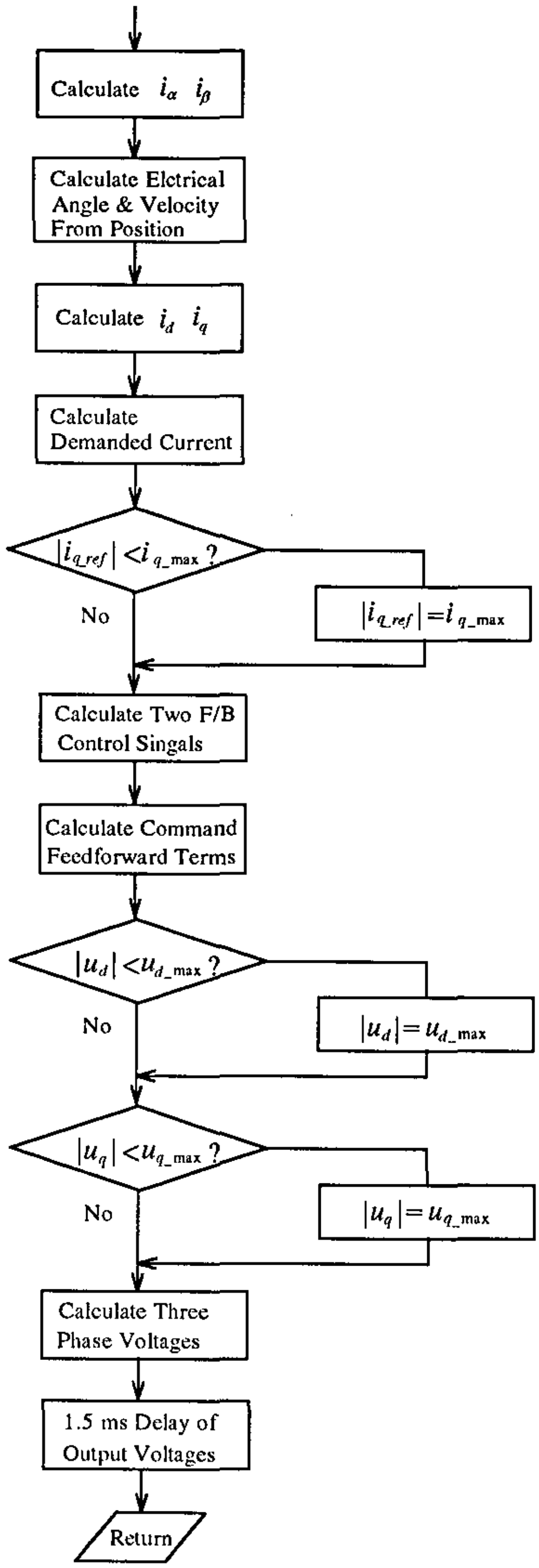

Figure 8.2. Flow Chart of The Current Control Loop

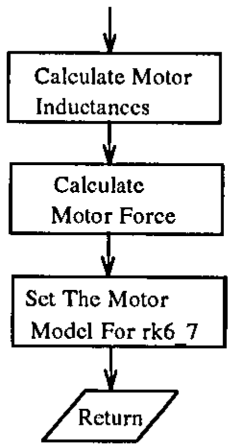

Figure 8.3. Flow Chart of Motor Function

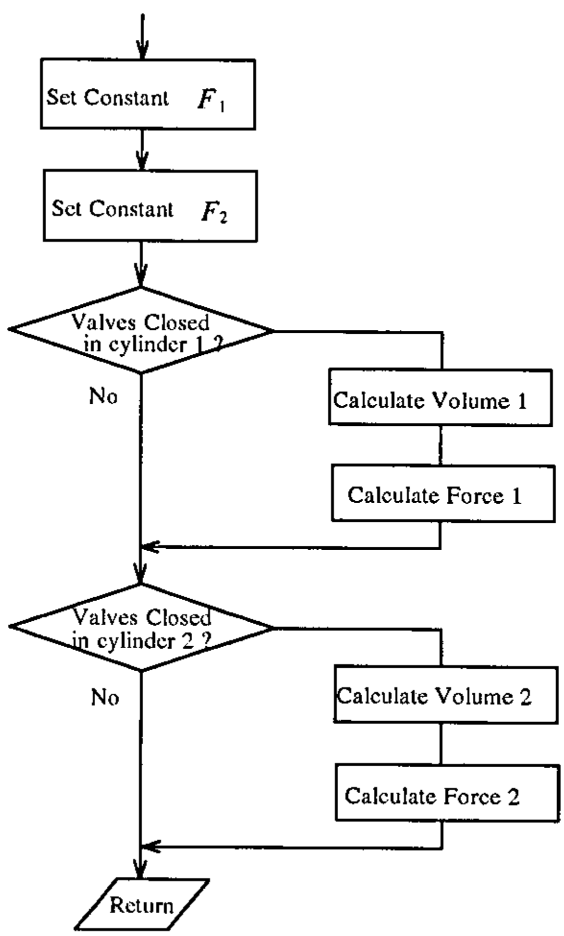

Figure 8.4. Flow Chart of Gas Function

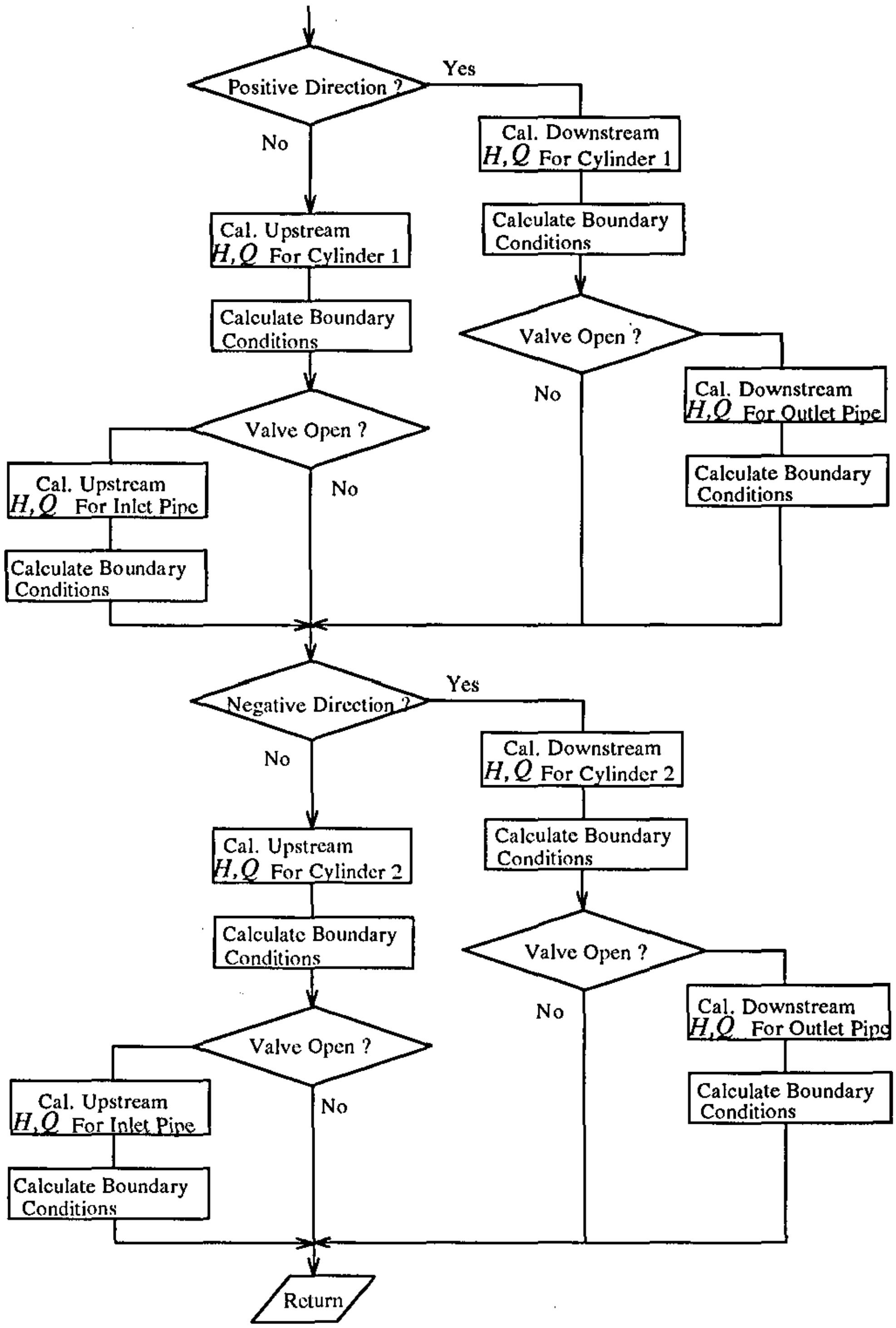

Figure 8.5. Flow Chart of Oil Function

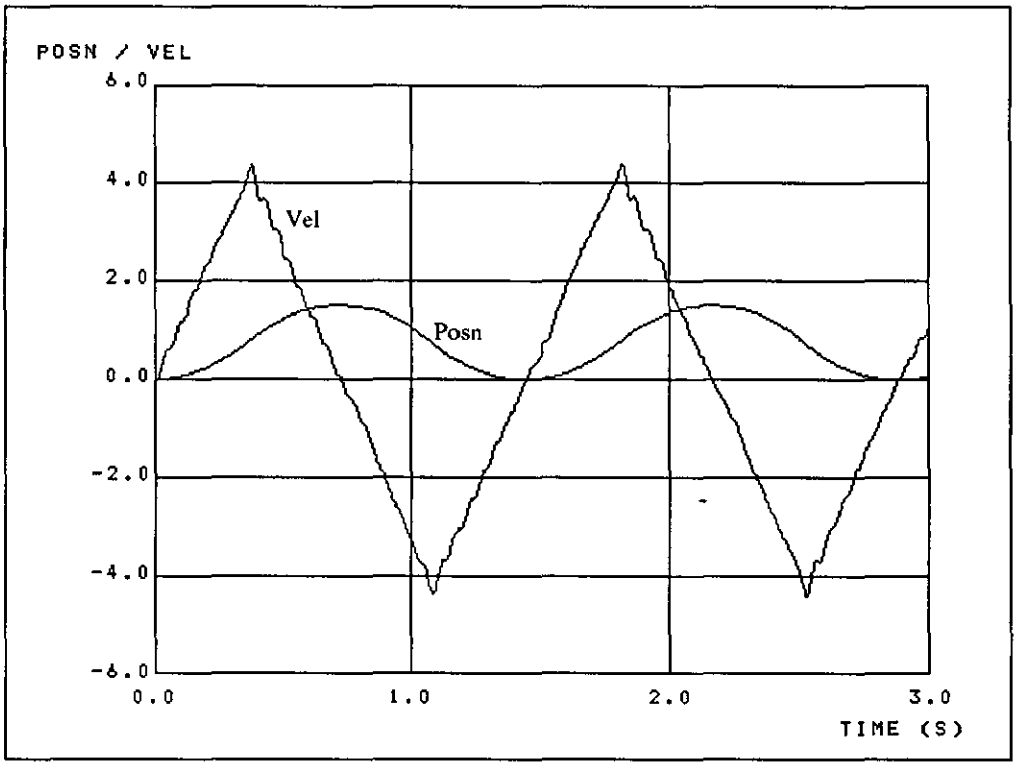

Figure 8.6. Position and Velocity In Pure Gas Case

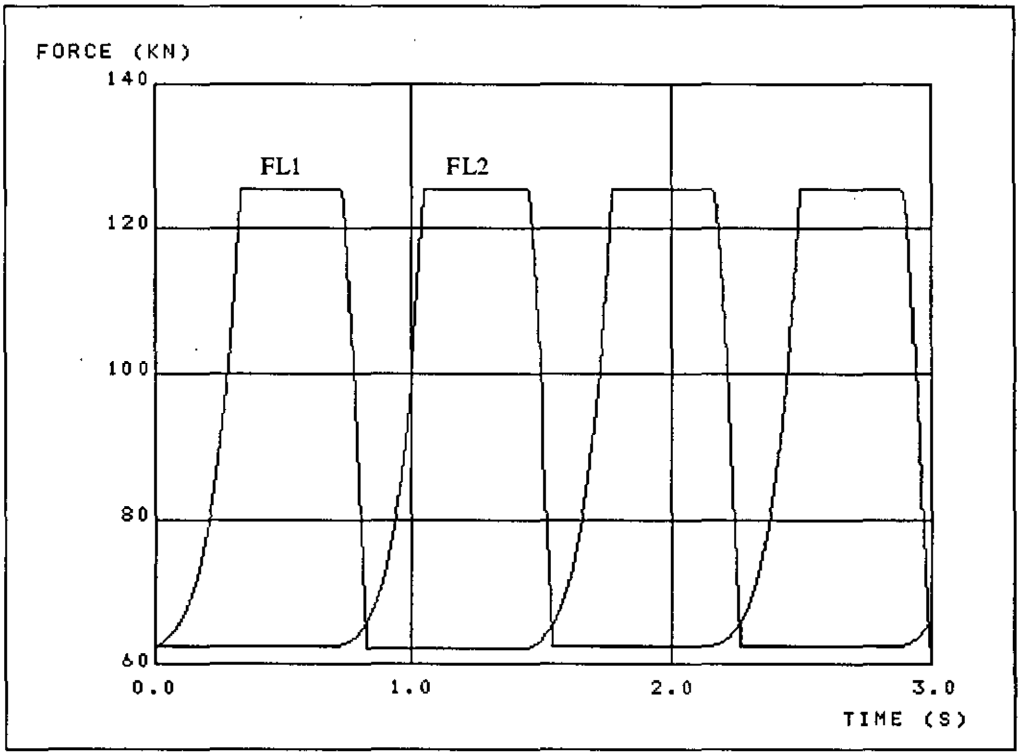

Figure 8.7. Load Forces In Pure Gas Case

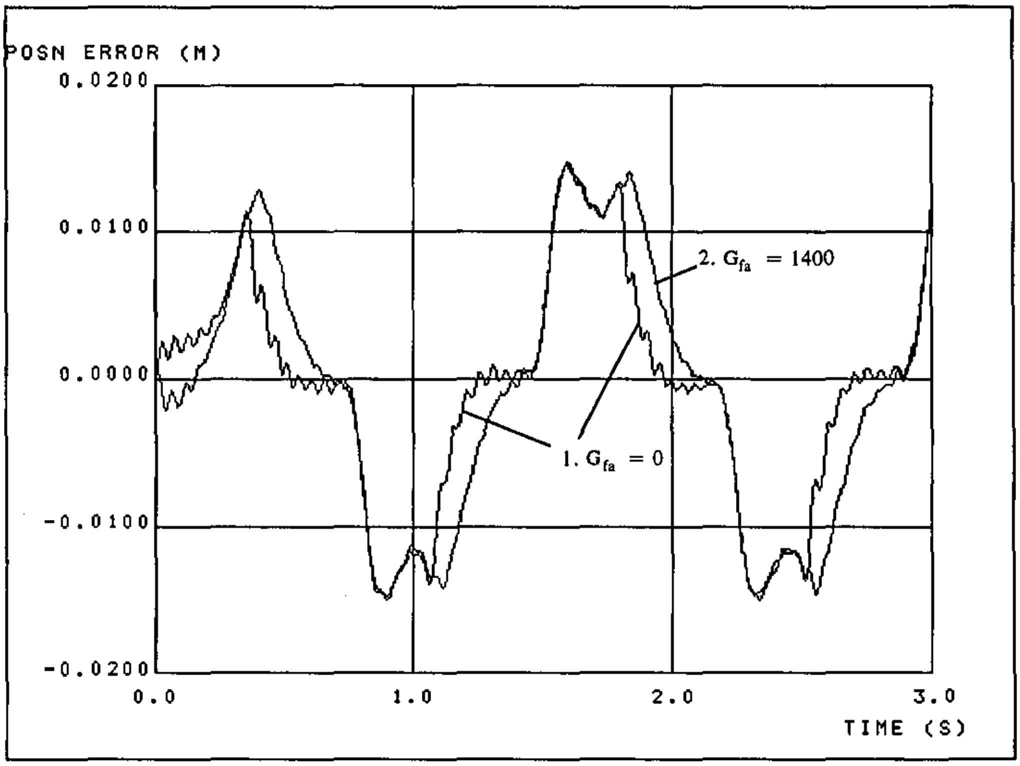

Figure 8.8. Position Errors with Gain 1 of Current Loop

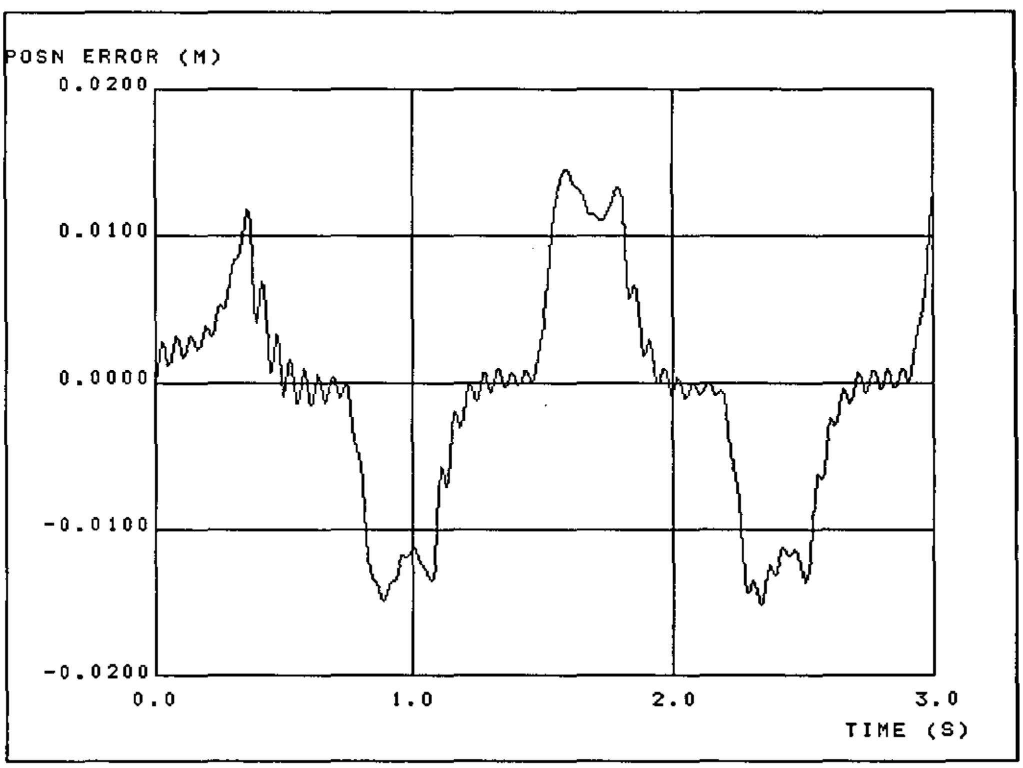

Figure 8.9. Position Error with Gain 2 of Current Loop

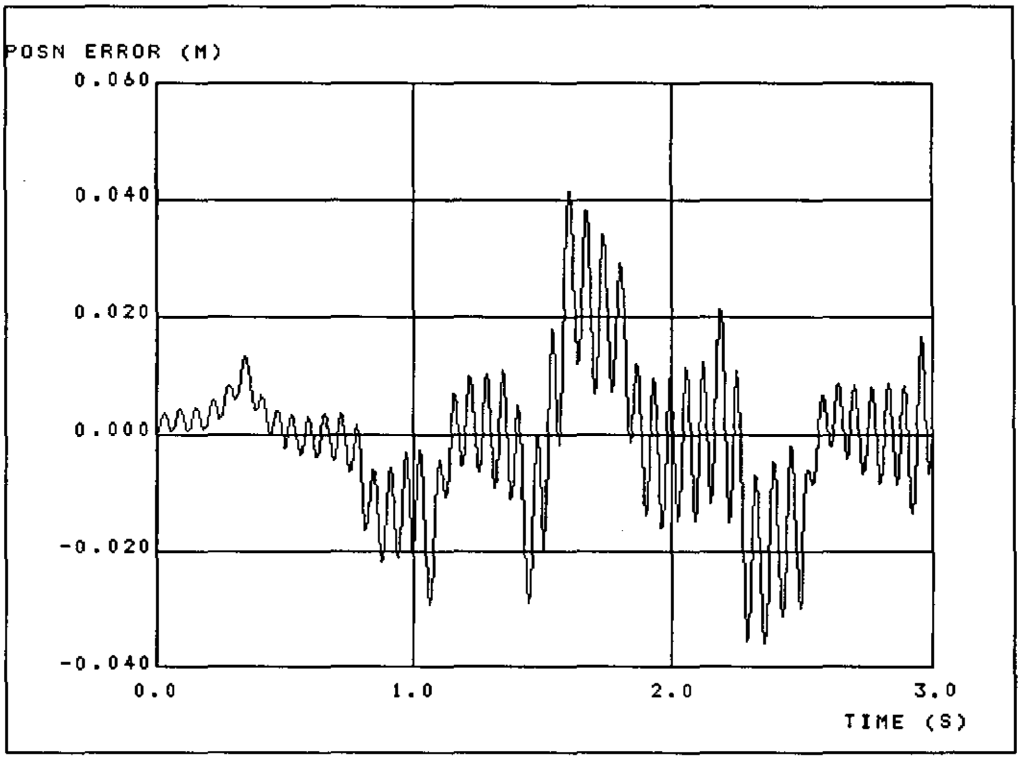

Figure 8.10. Position Errors with Gain 3 of Current Loop

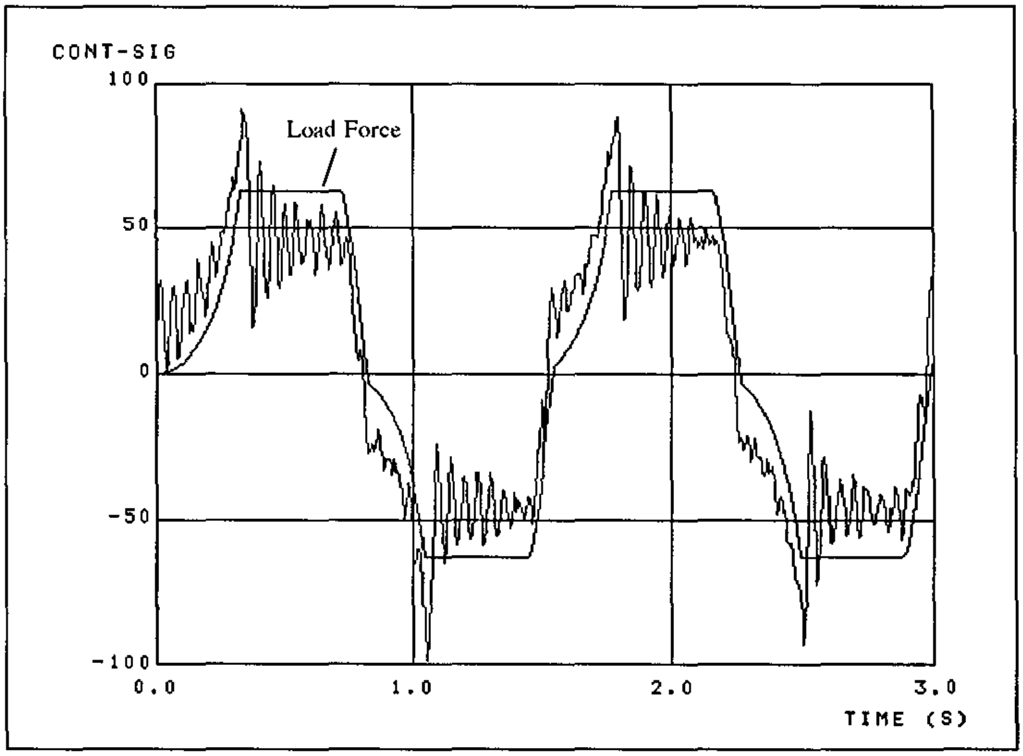

Figure 8.11. Position Control Signal with Gain 1 of Current Loop

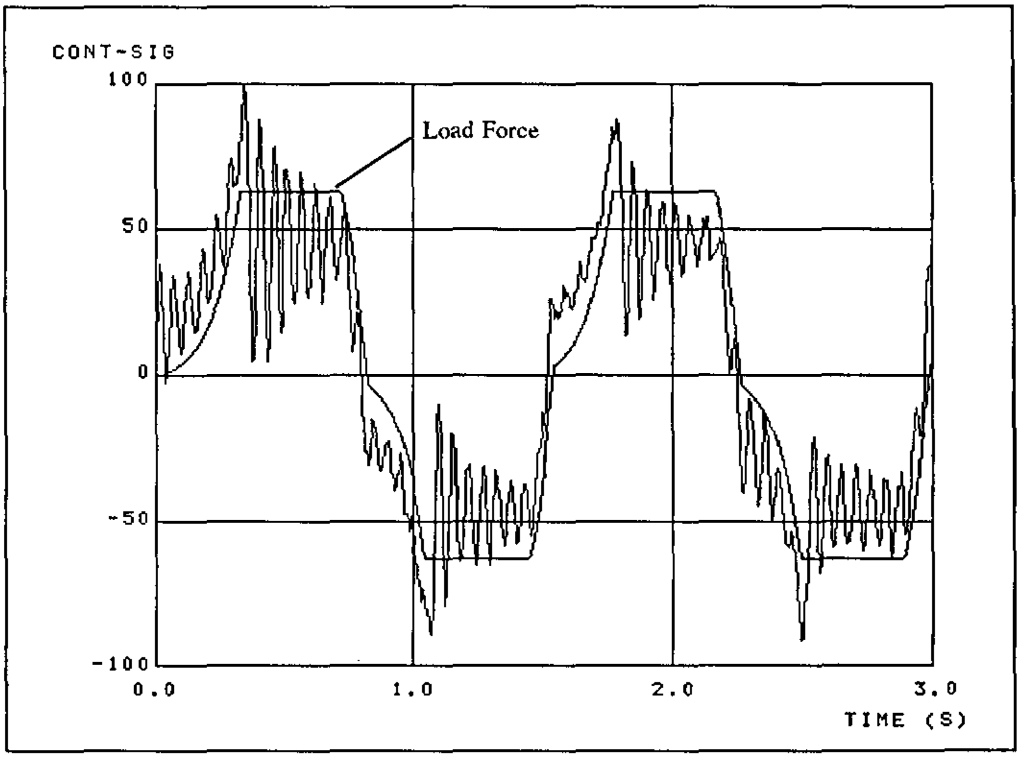

Figure 8.12. Position Control Signal with Gain 2 of Current Loop

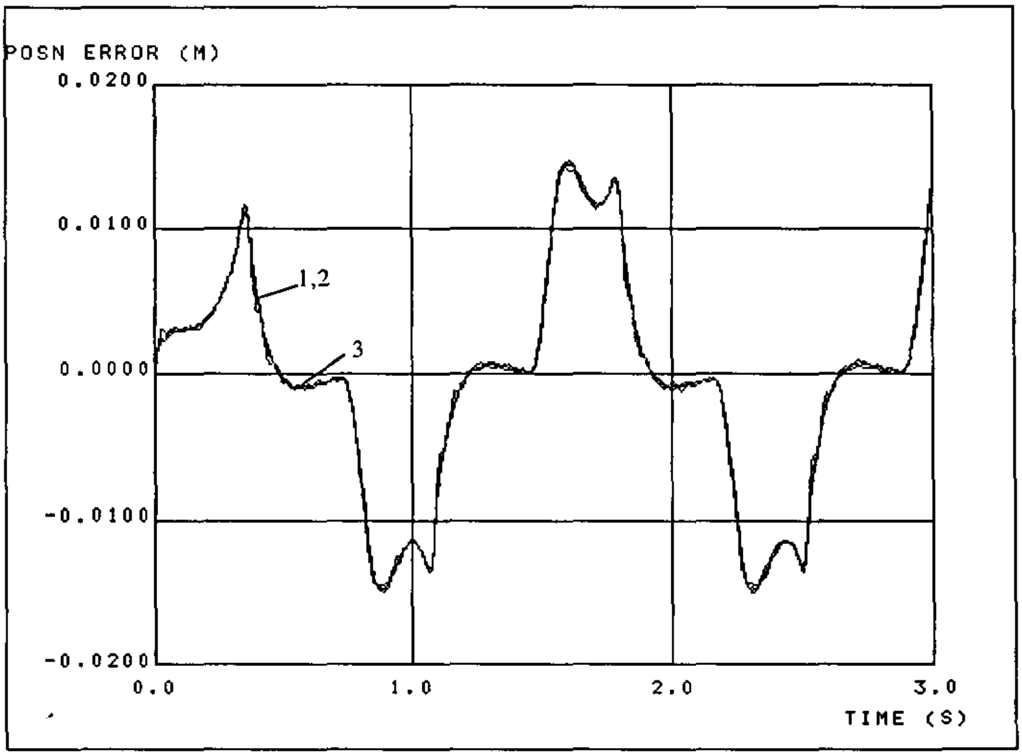

Figure 8.13. Position Errors with Sample Period ($T_s = 3 \cdot t_s$)

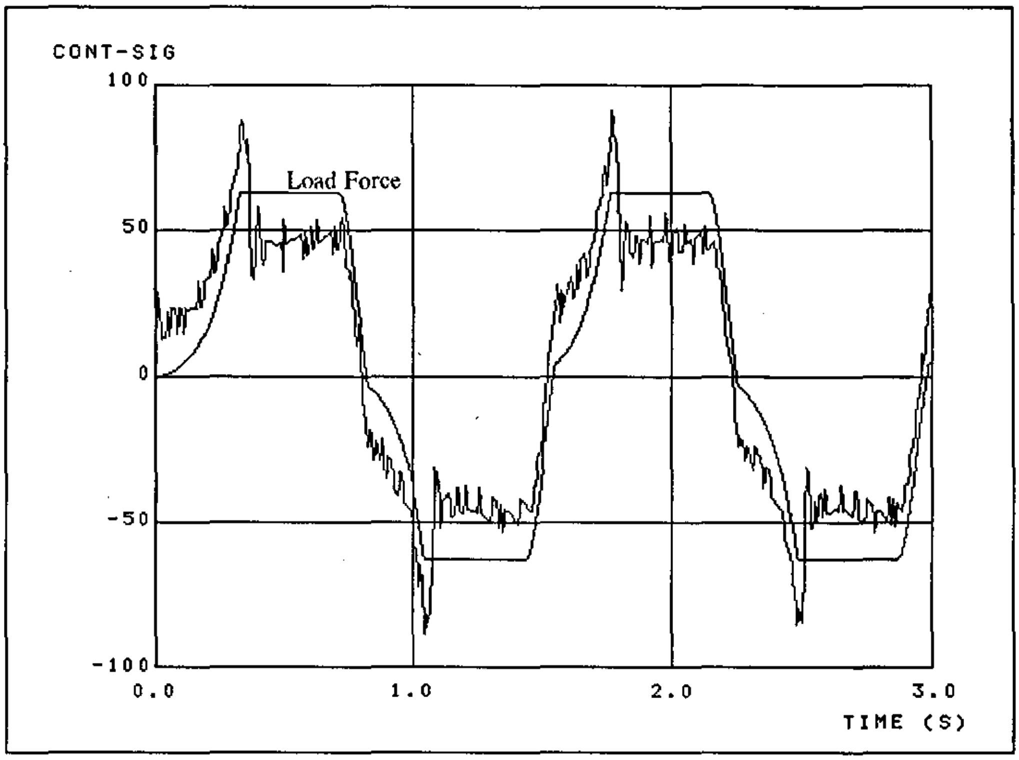

Figure 8.14. Position Control Signal with Gain 1 of Current Loop

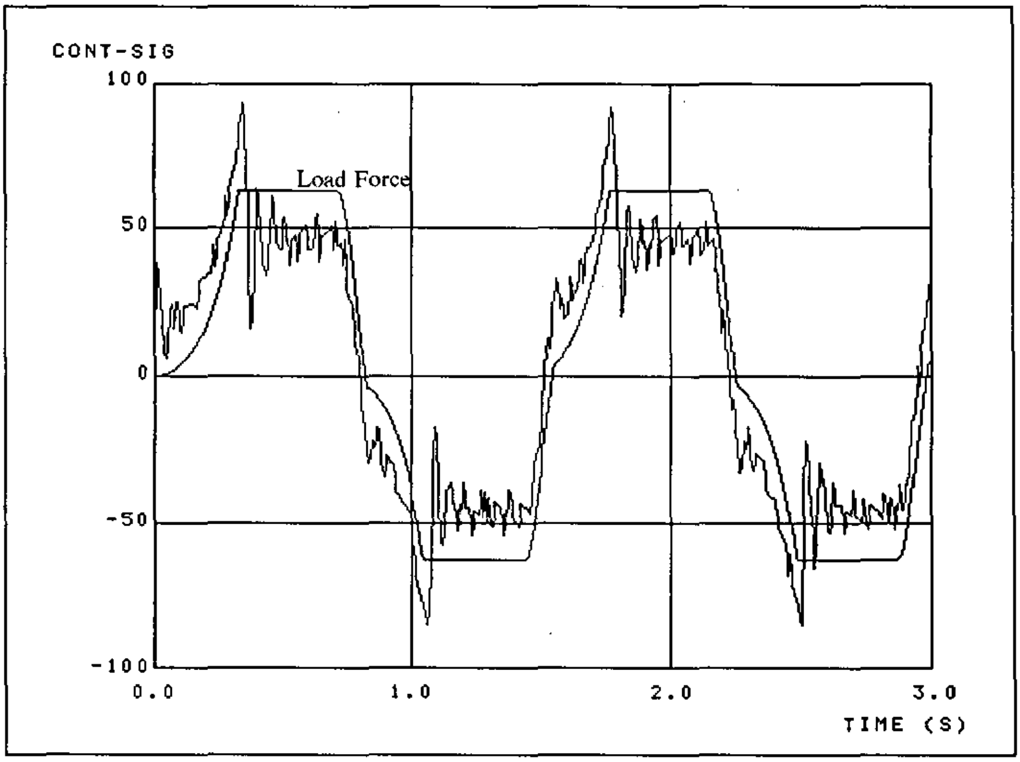

Figure 8.15. Position Control Signal with Gain 3 of Current Loop

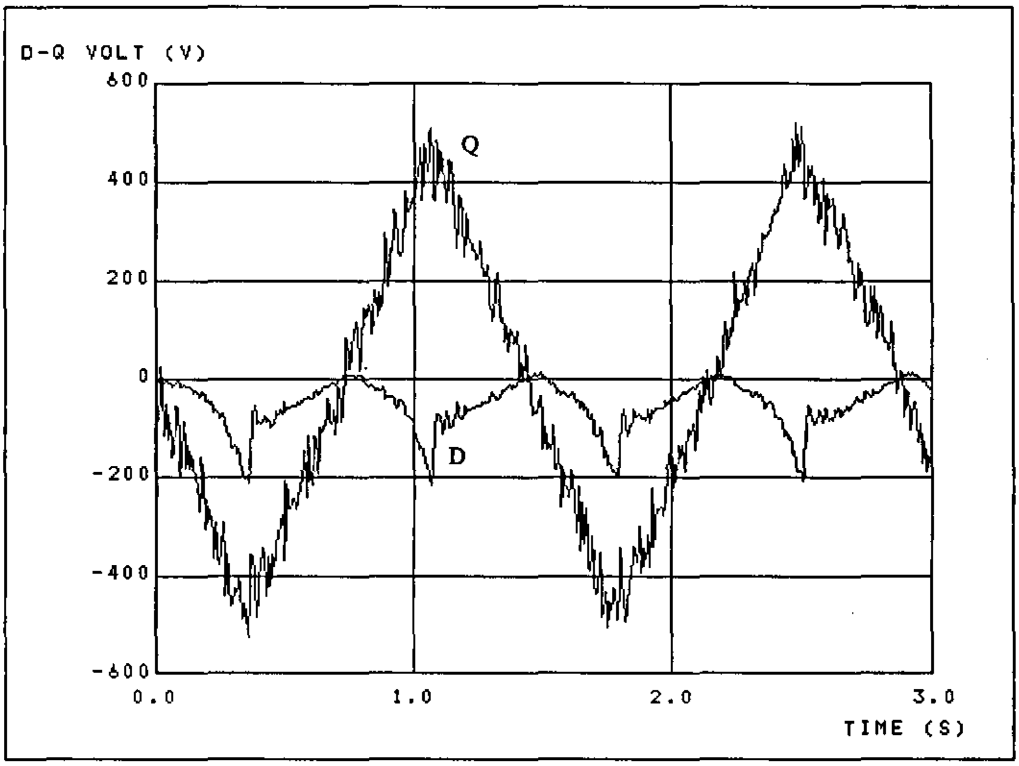

Figure 8.16. D - Q Axes Voltages with Gain 1 of Current Loop

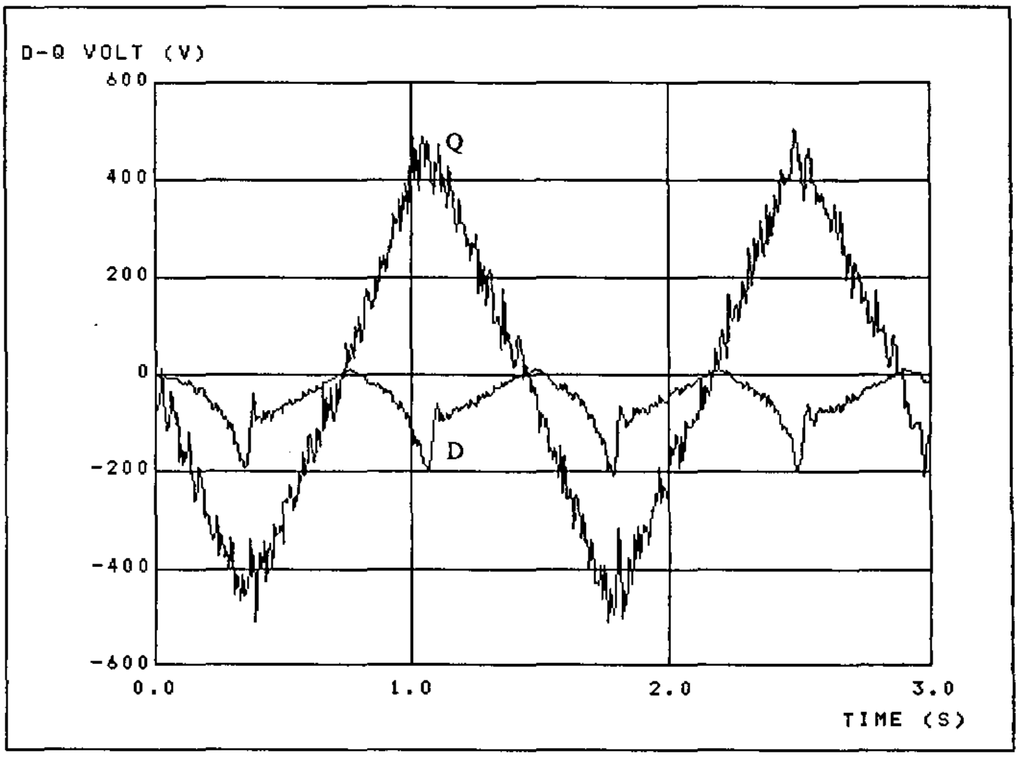

Figure 8.17. D-Q Axes Voltages with Gain 2 of Current Loop

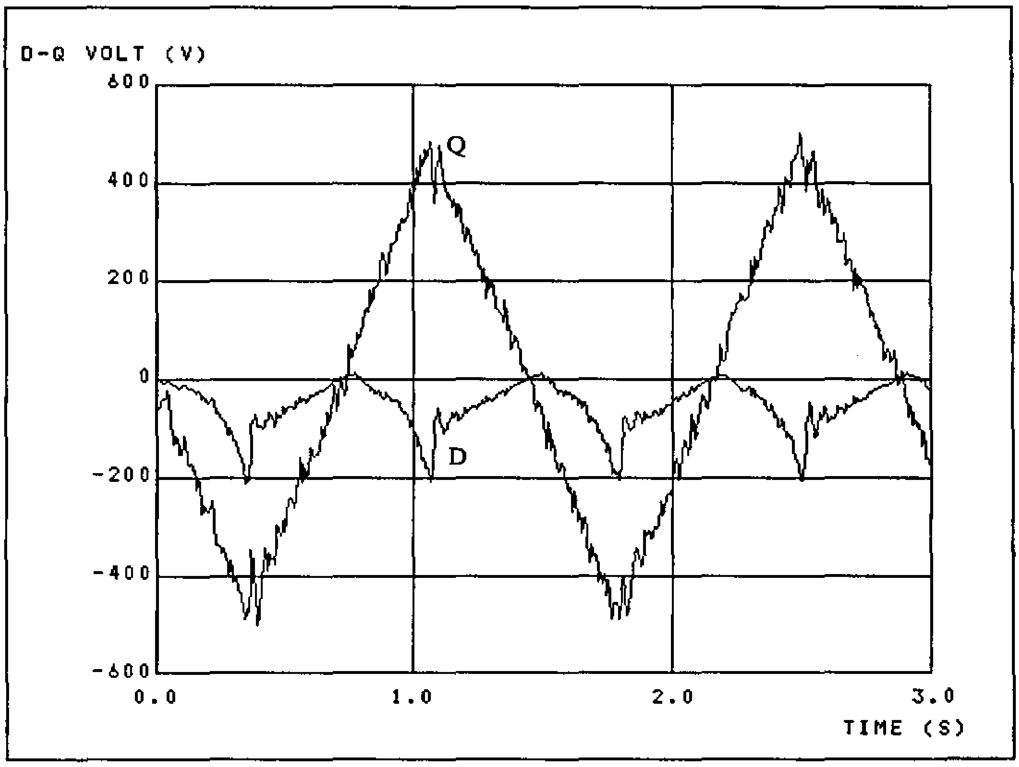

Figure 8.18. D - Q Axes Voltages with Gain 3 of Current Loop

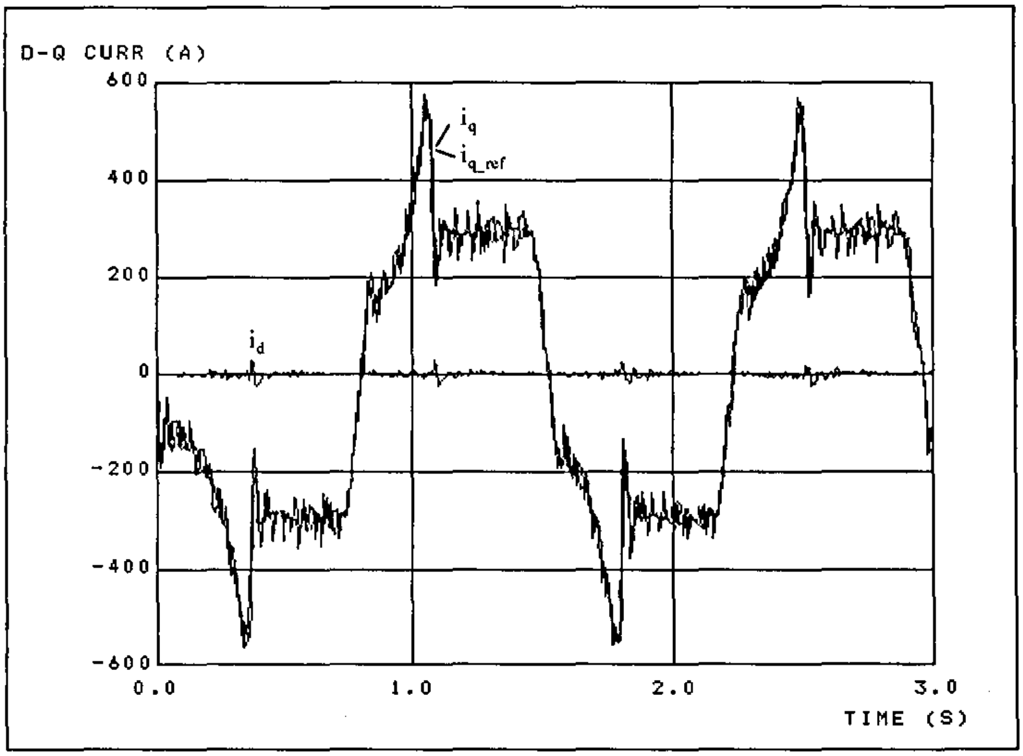

Figure 8.19. D-Q Axes Currents with Gain 2 of Current Loop

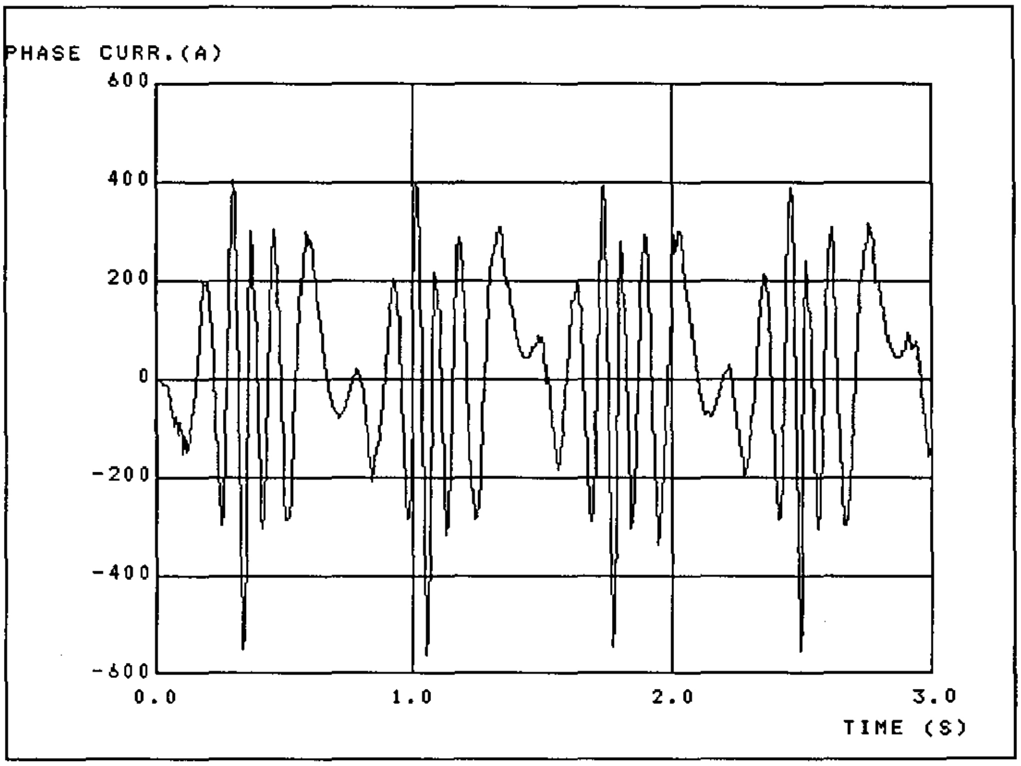

Figure 8.20. Red Phase Current with Gain 2 of Current Loop

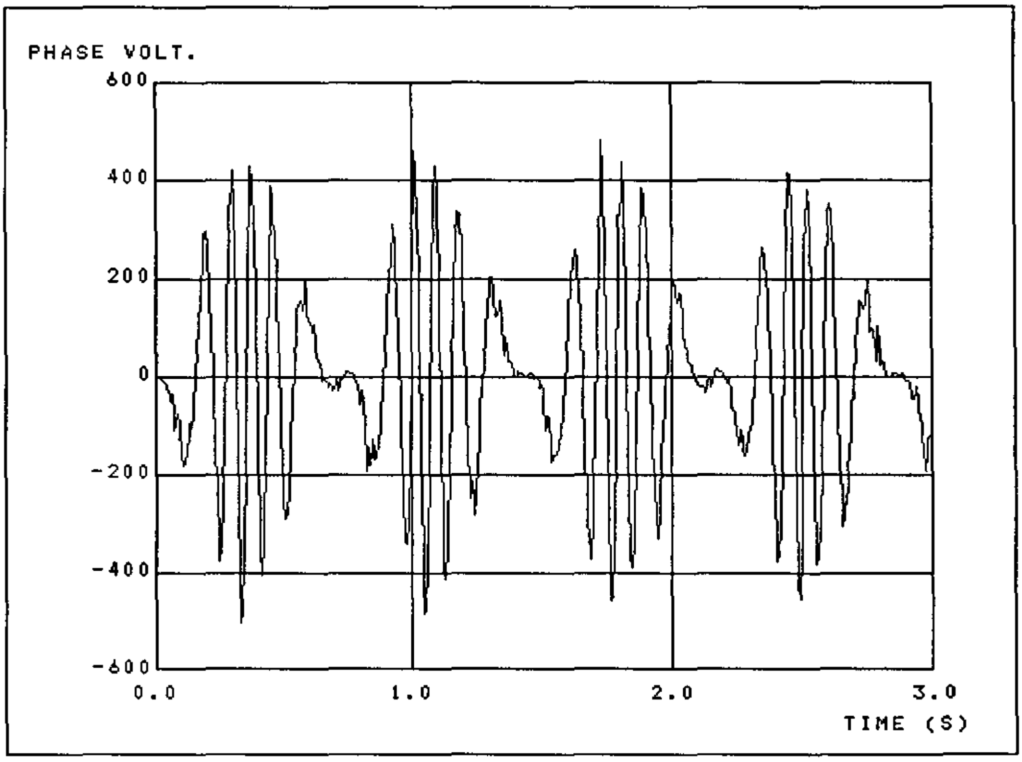

Figure 8.21. Red Phase Voltage with Gain 2 of Current Loop

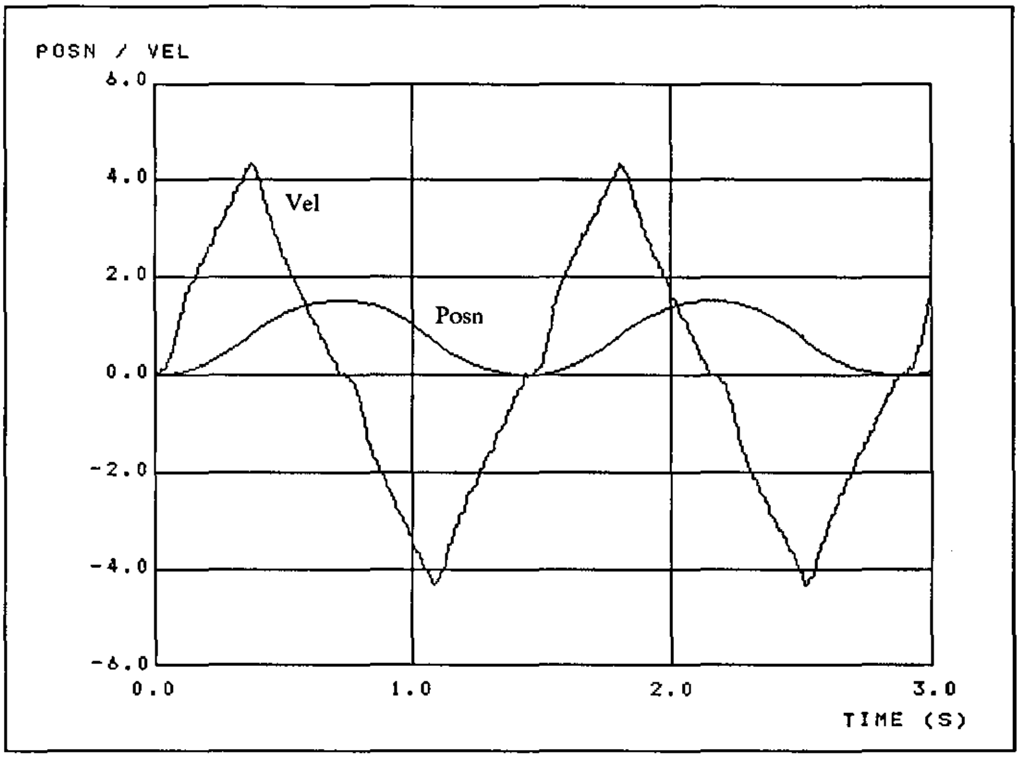

Figure 8.22. Position and Velocity in Oil Case

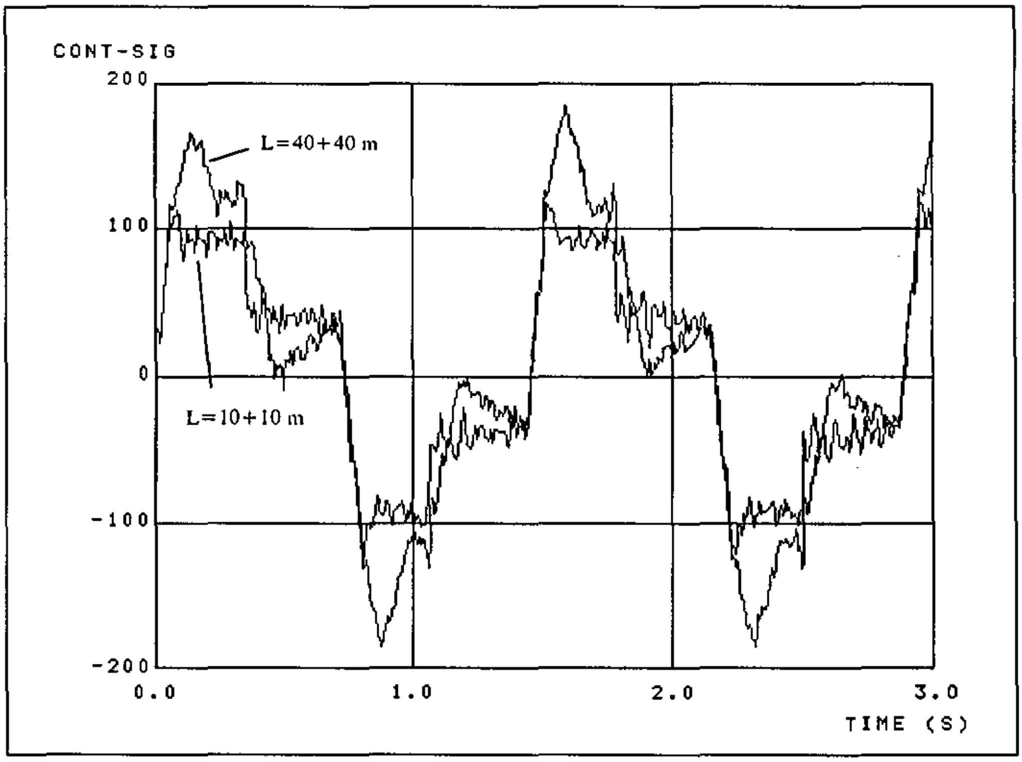

Figure 8.23. Control Signals of Outer Loop (D=100 mm)

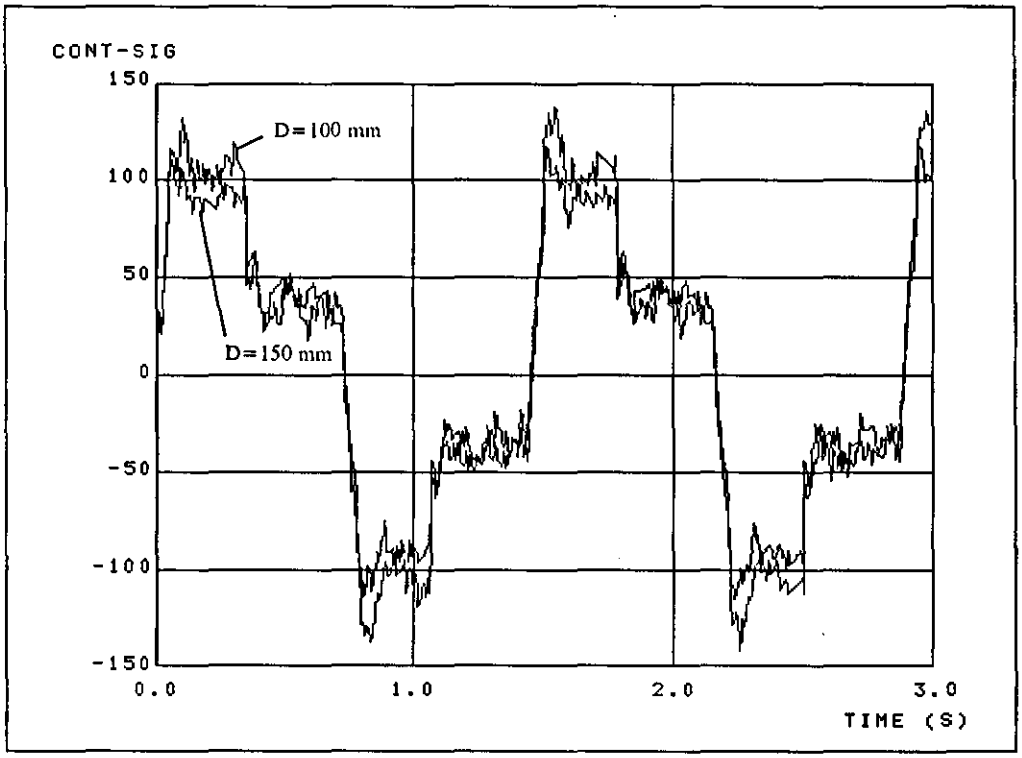

Figure 8.24. Control Signals of Outer Loop (L=20+20 m)

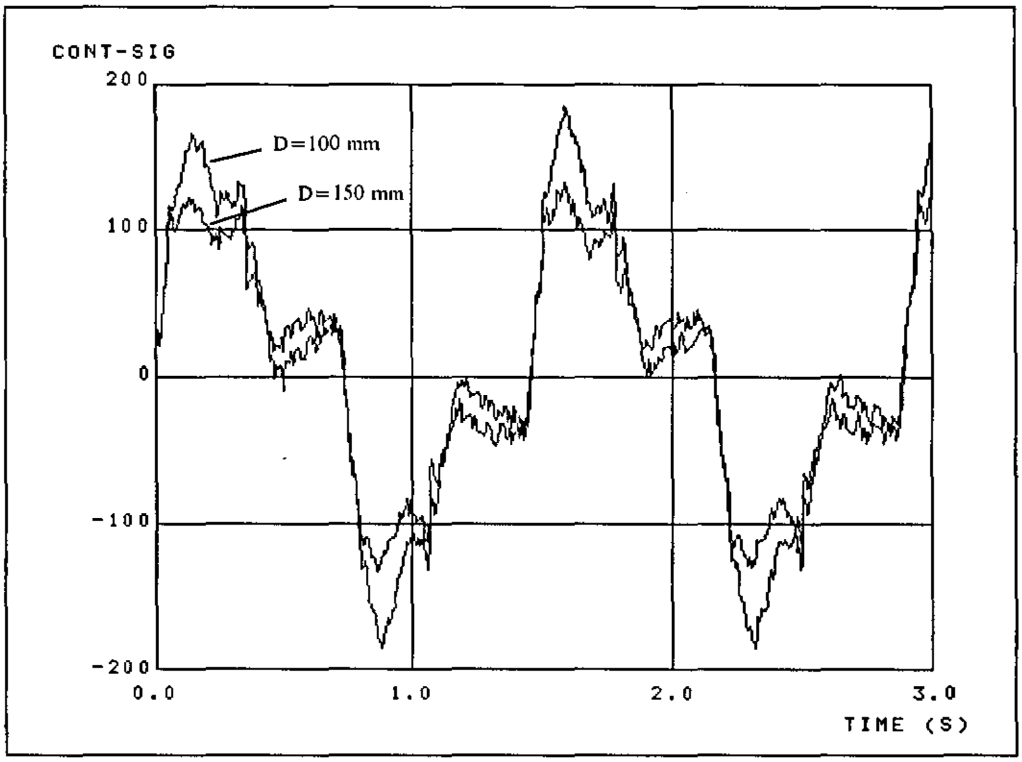

Figure 8.25. Control Signals of Outer Loop (L=40+40 m)

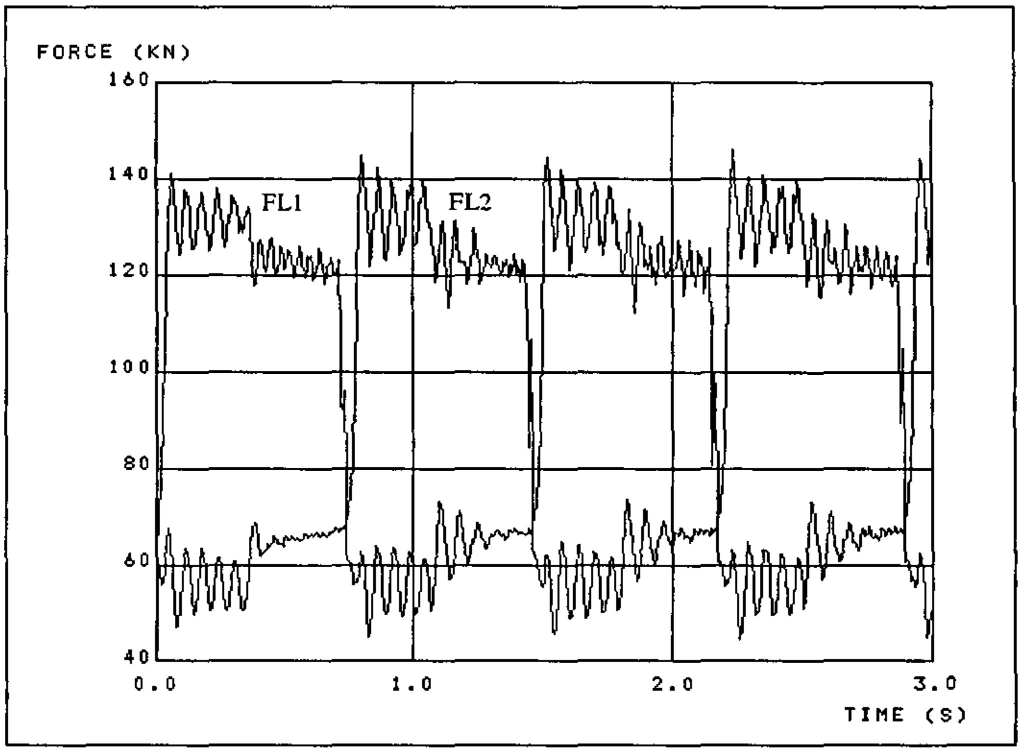

Figure 8.26. Load Forces (L=10+10 m, D=100 mm)

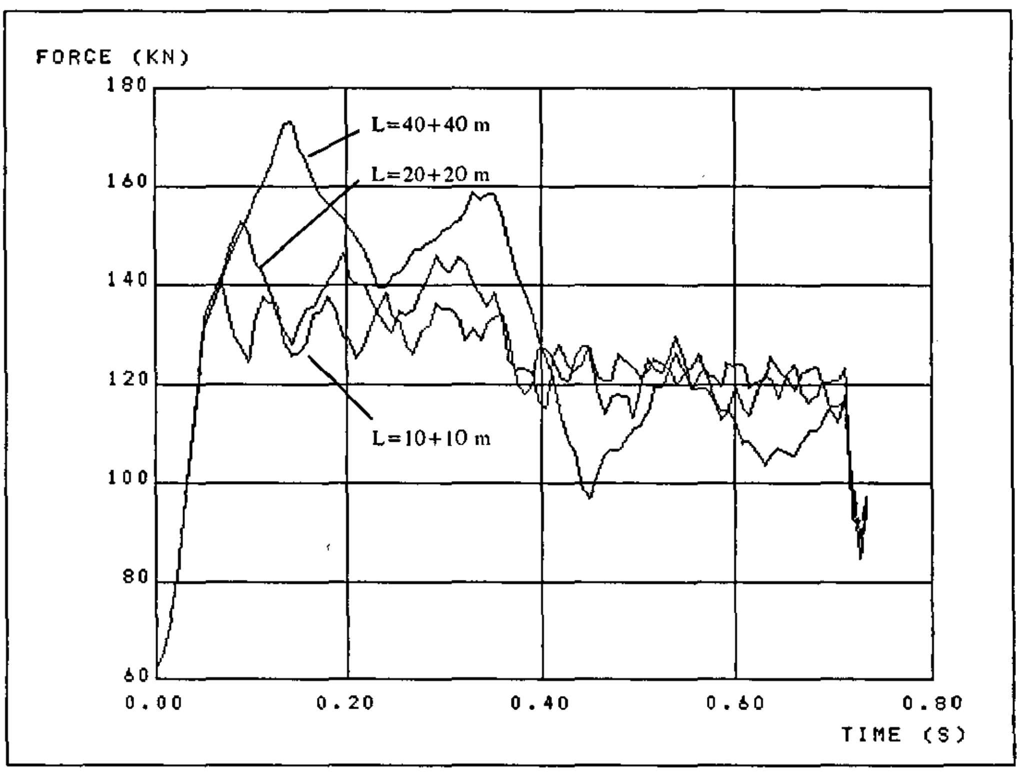

Figure 8.27. Load Forces of Different Pipe Lengths (D=100 mm)

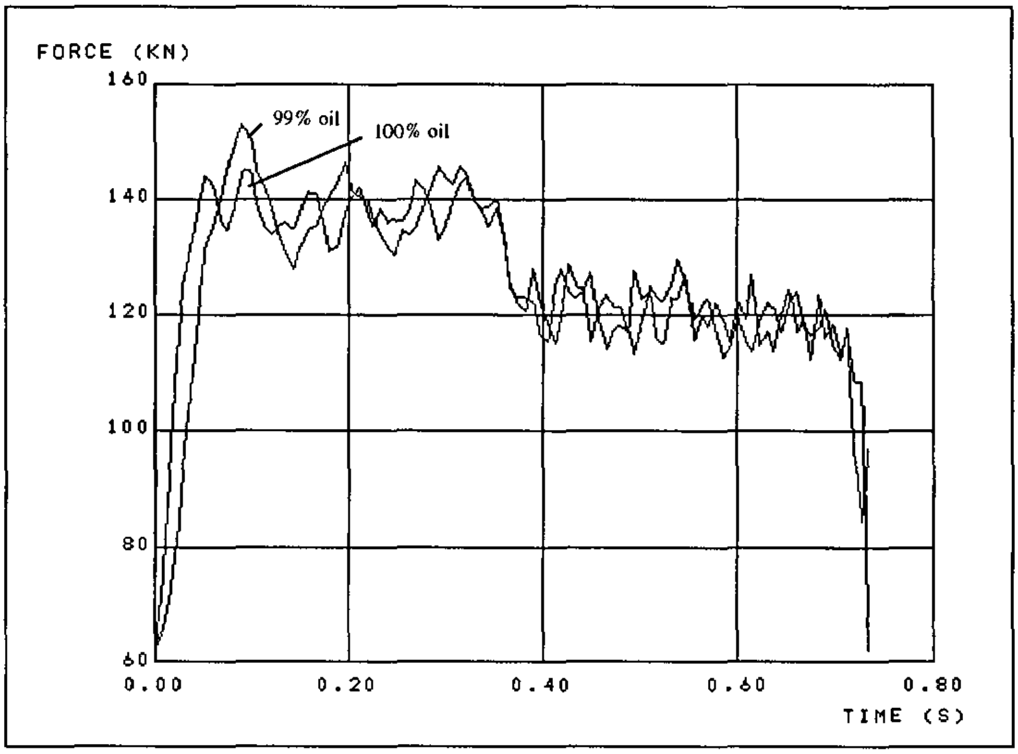

Figure 8.28. Load Forces of Pure and 99% Oil (L=20+20 m)

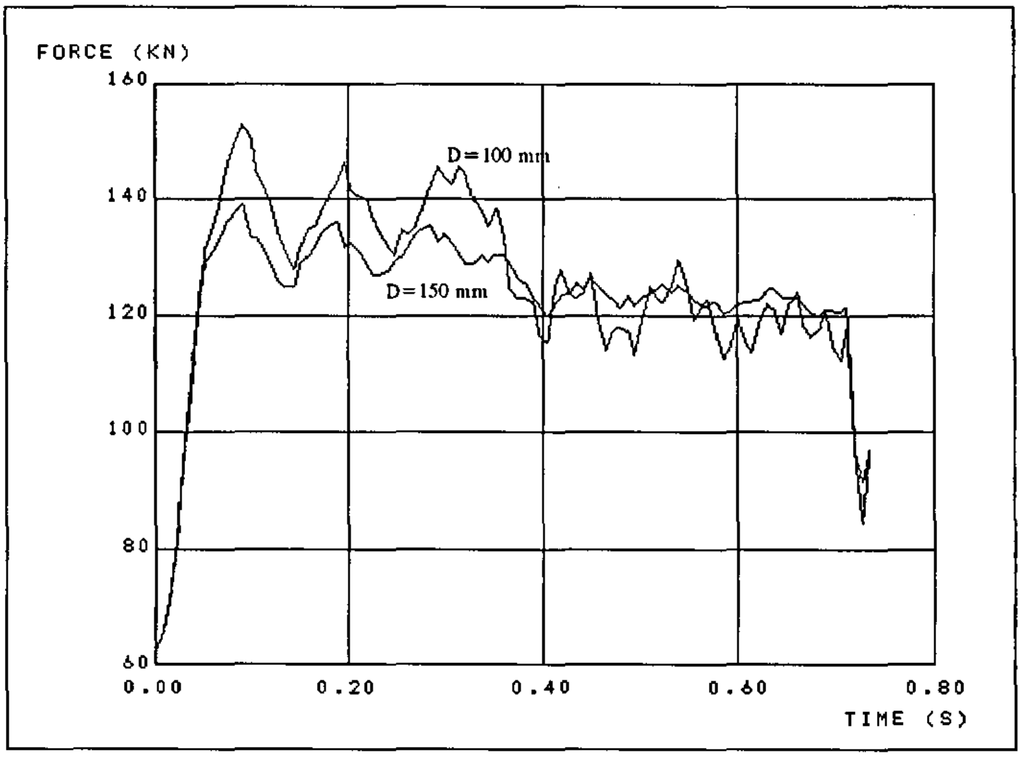

Figure 8.29. Load Forces of Different Pipe Diameters (L=20+20m)

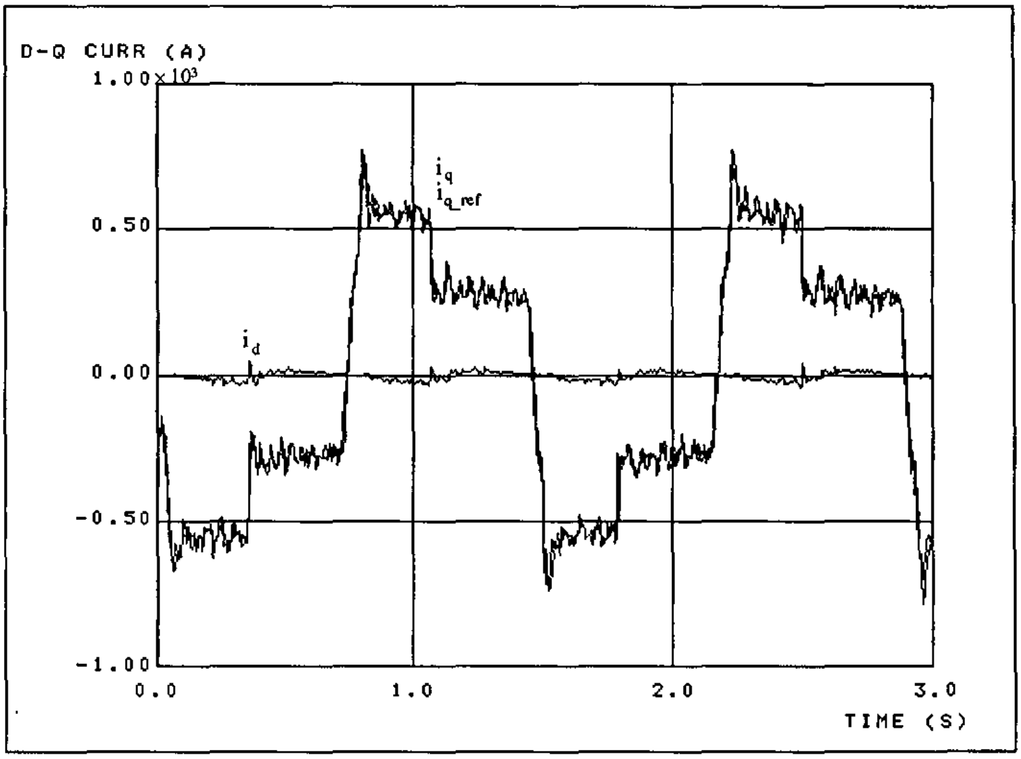

Figure 8.30. D-Q Currents (L=20+20 m, D=150 mm)

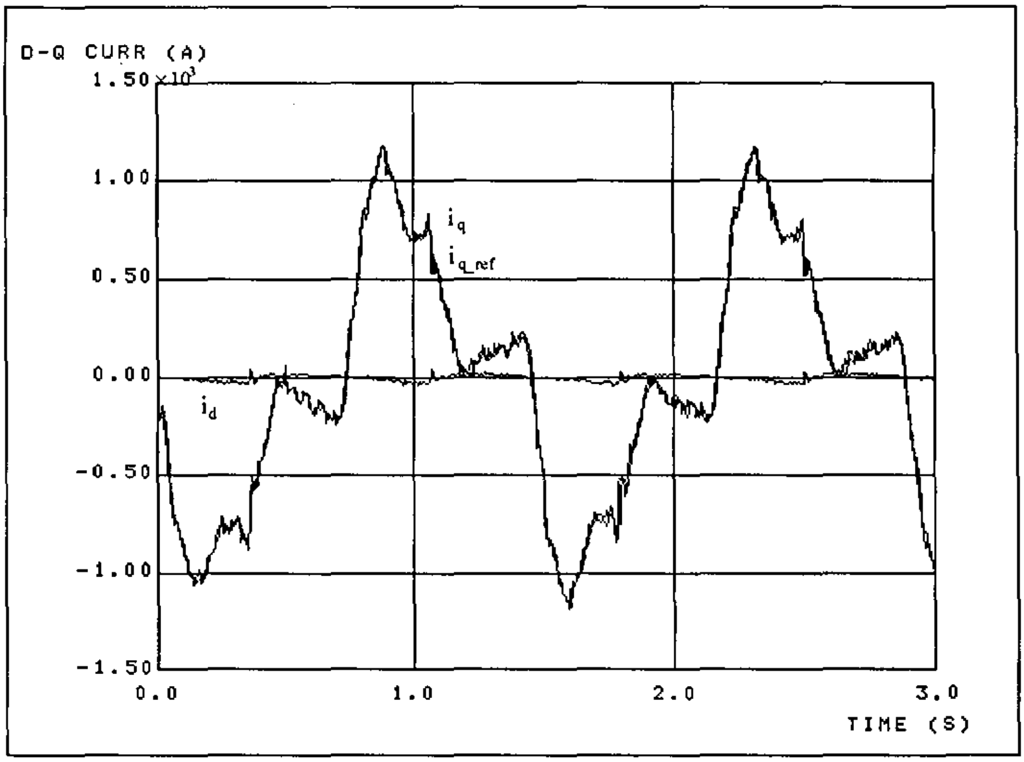

Figure 8.31. D-Q Currents (L=40+40m, D=100 mm)

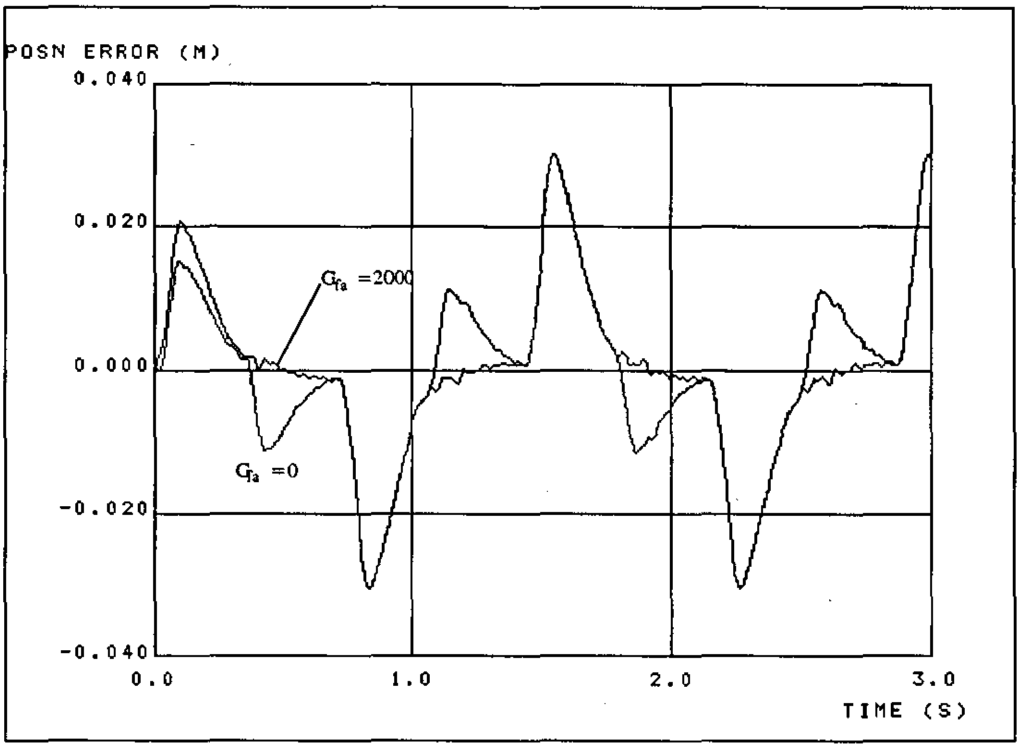

Figure 8.32. Control Errors (L=10+10m, D=100 mm)

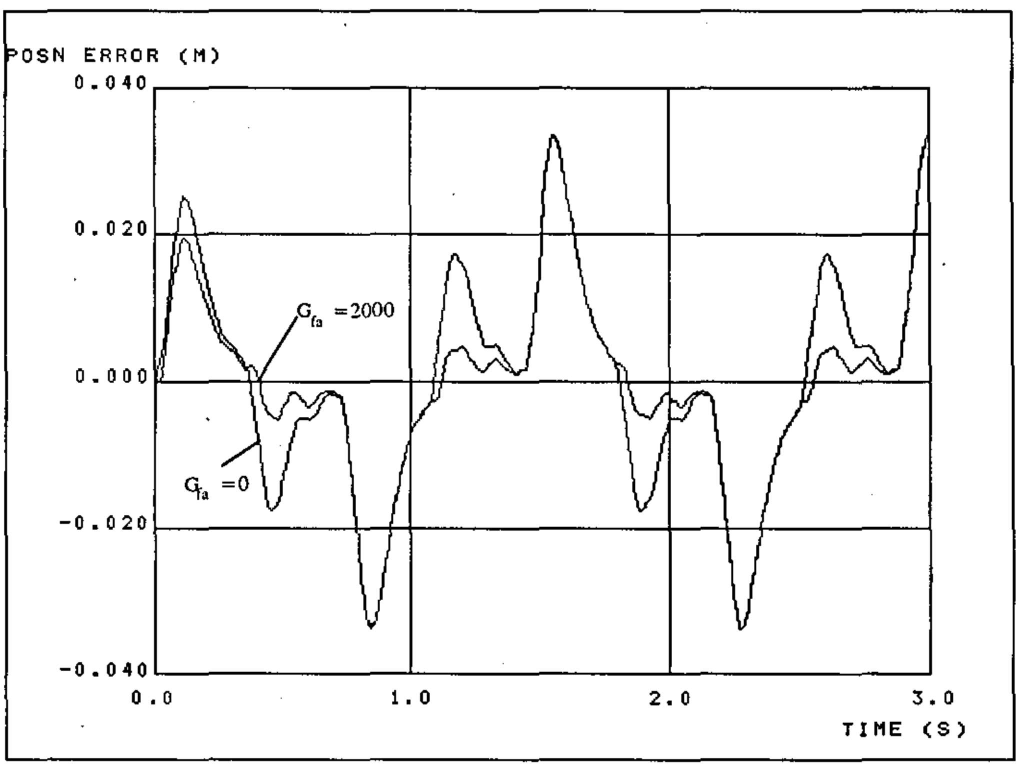

Figure 8.33. Control Errors (L=20+20 m, D=100 mm)

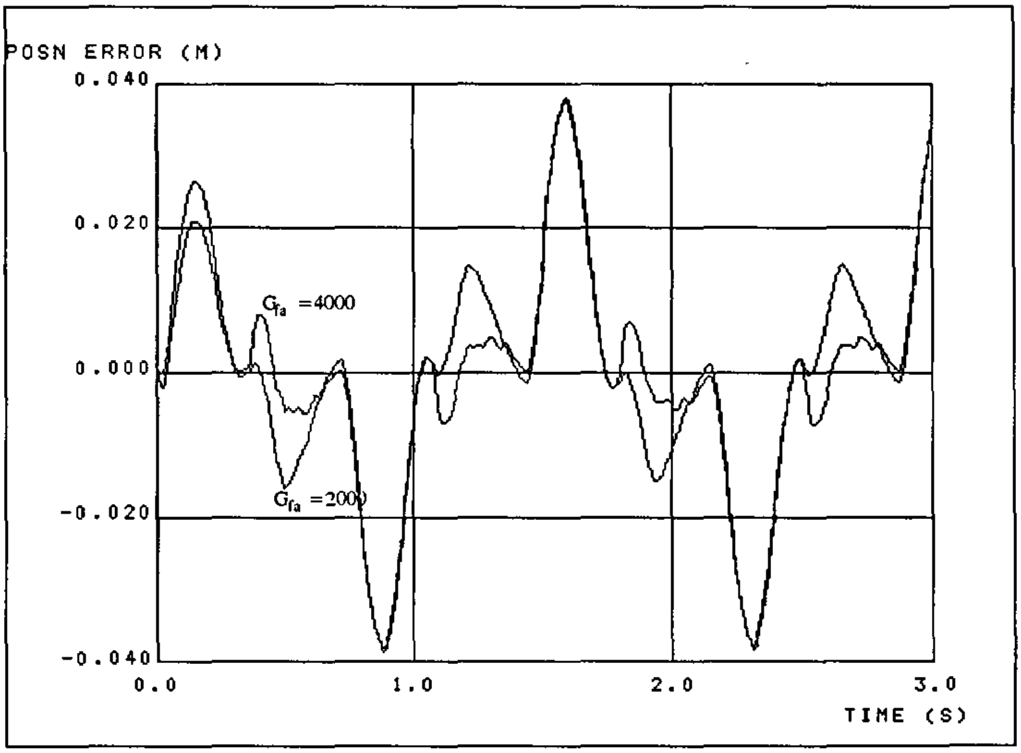

Figure 8.34. Control Errors (L=40+40m, D=100 mm)

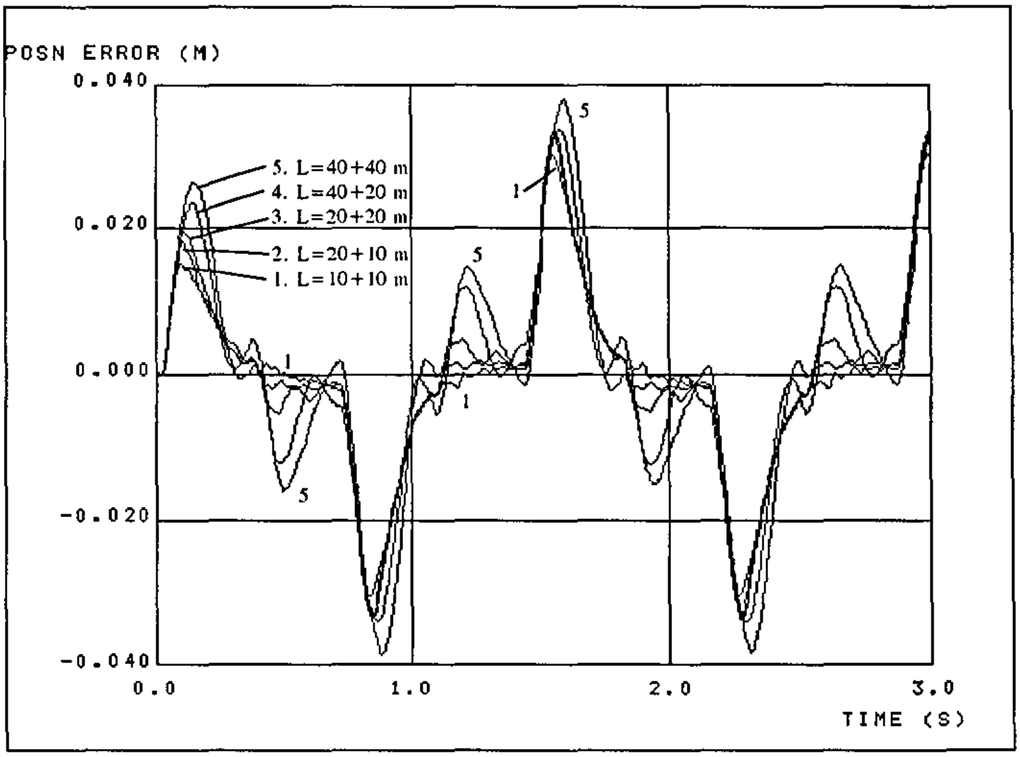

Figure 8.35. Control Errors of Different Pipe Lengths (D=100 mm)

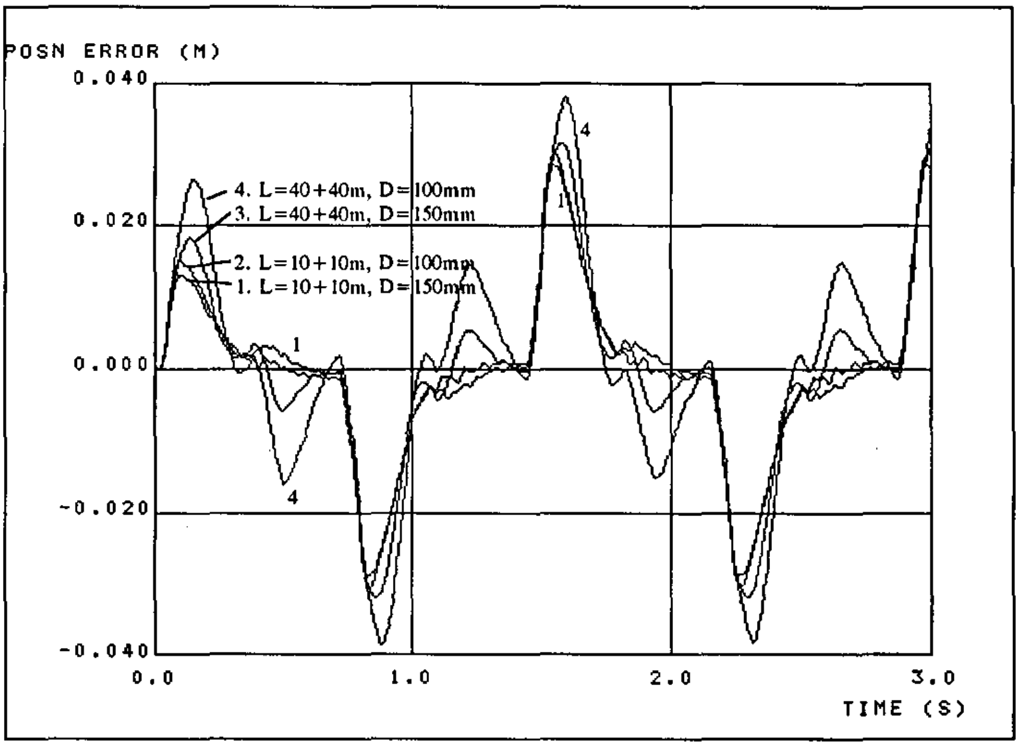

Figure 8.36. Control Errors of Different Pipes

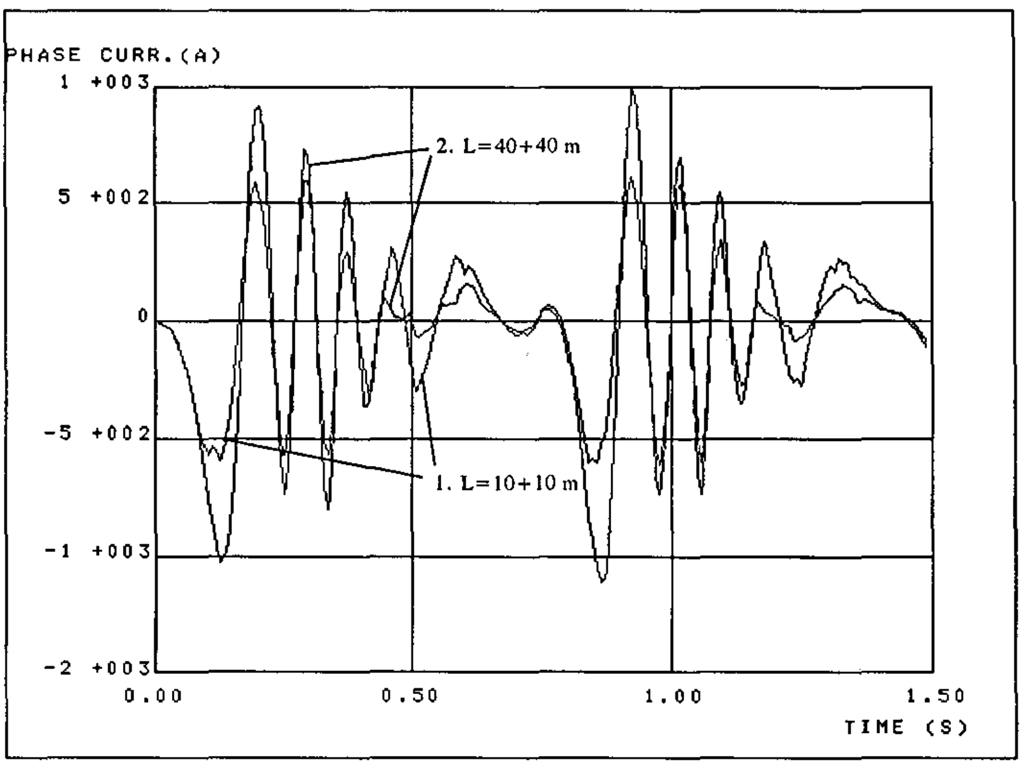

Figure 8.37. Phase Current of The Motor (D=100 mm)

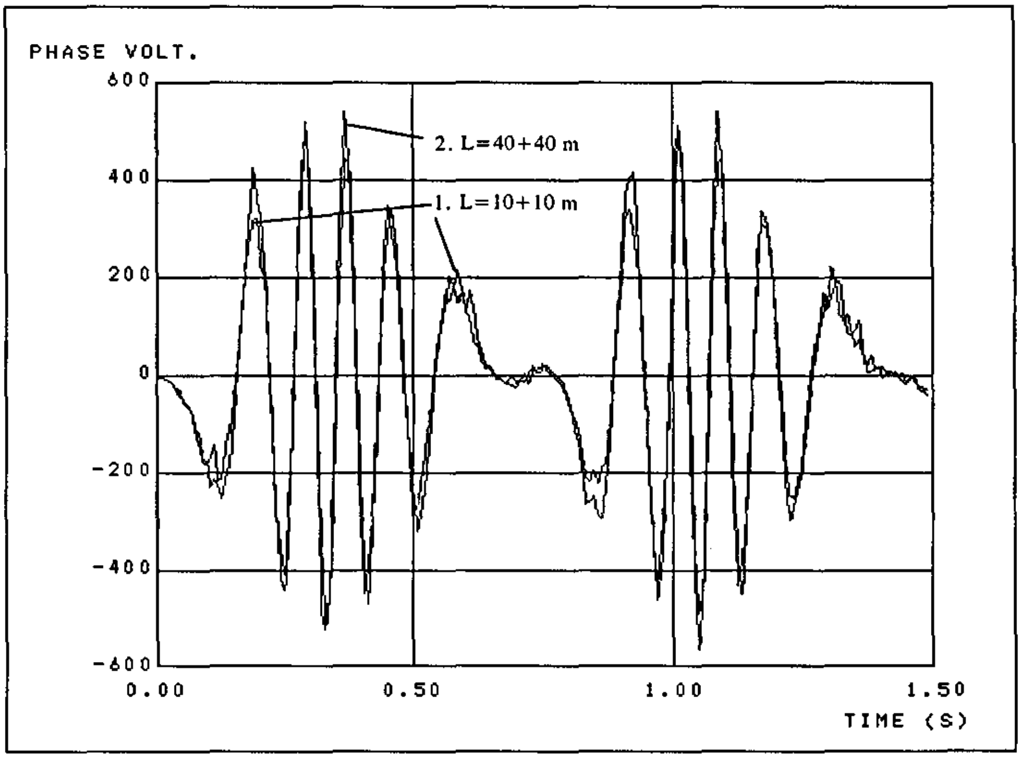

Figure 8.38. Phase Voltage of The Motor (D=100 mm)

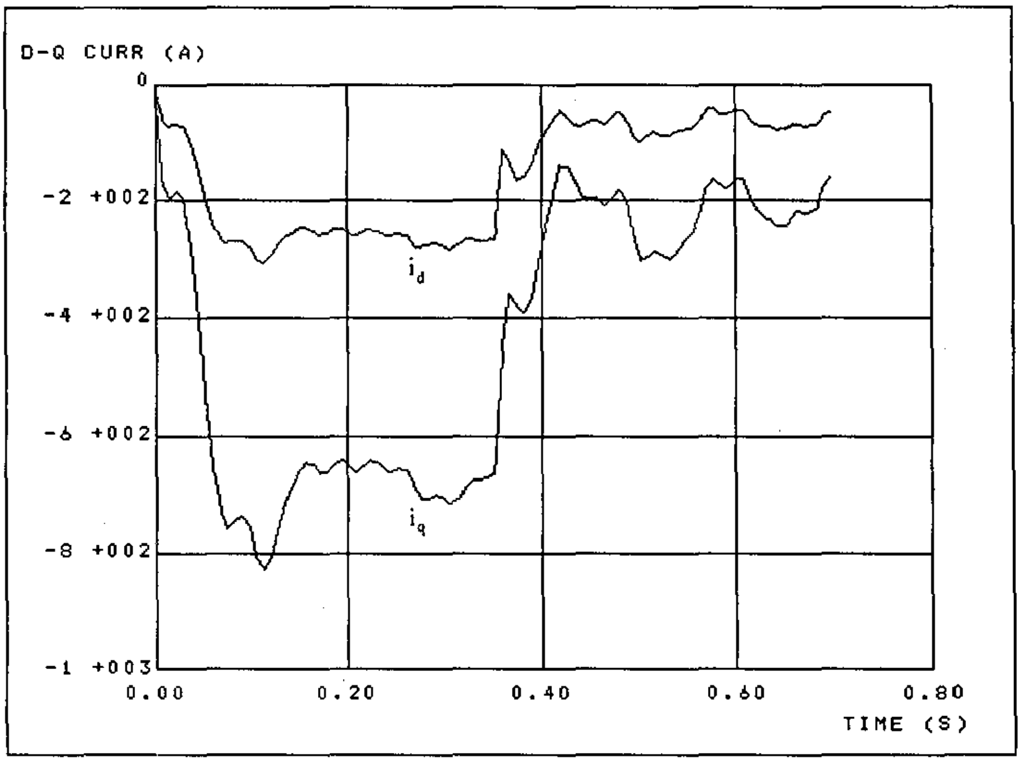

Figure 8.39. D-Q Current When Current Angle is 20°.

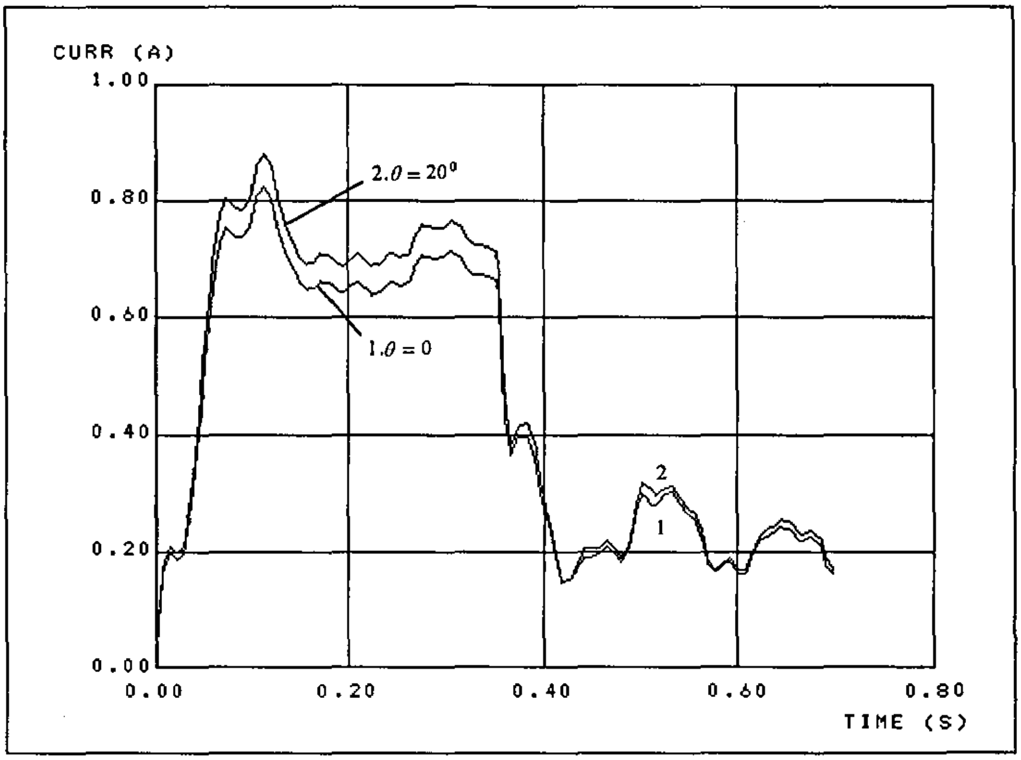

Figure 8.40. Amplitude of Phase Current

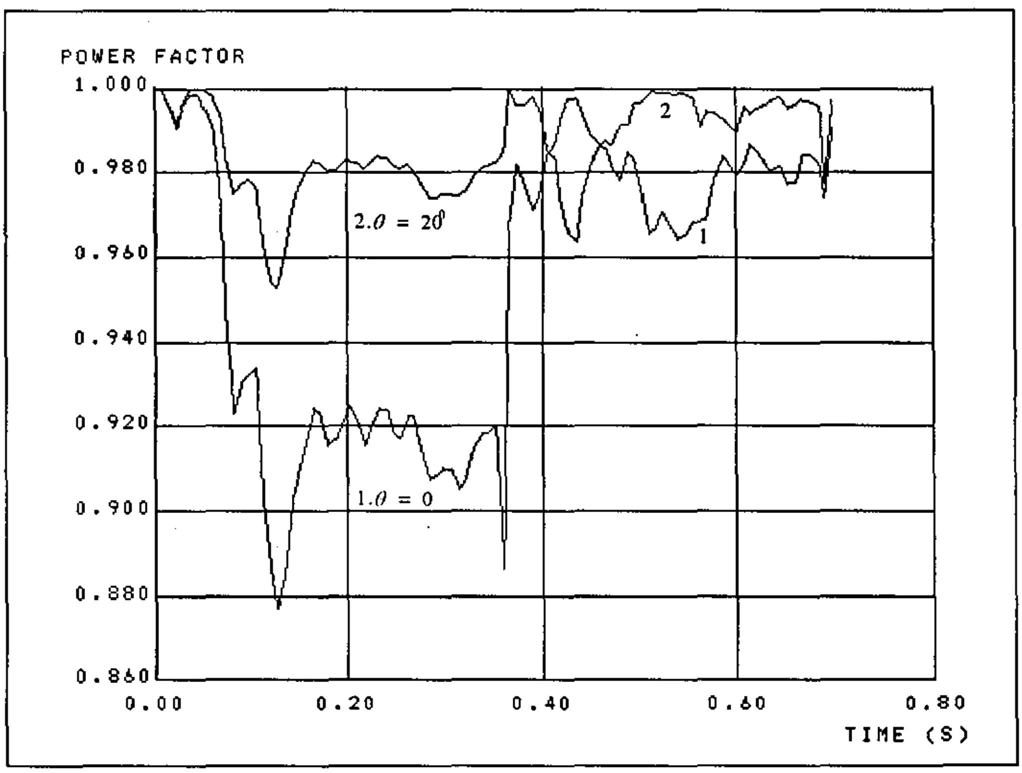

Figure 8.41. Power Factor

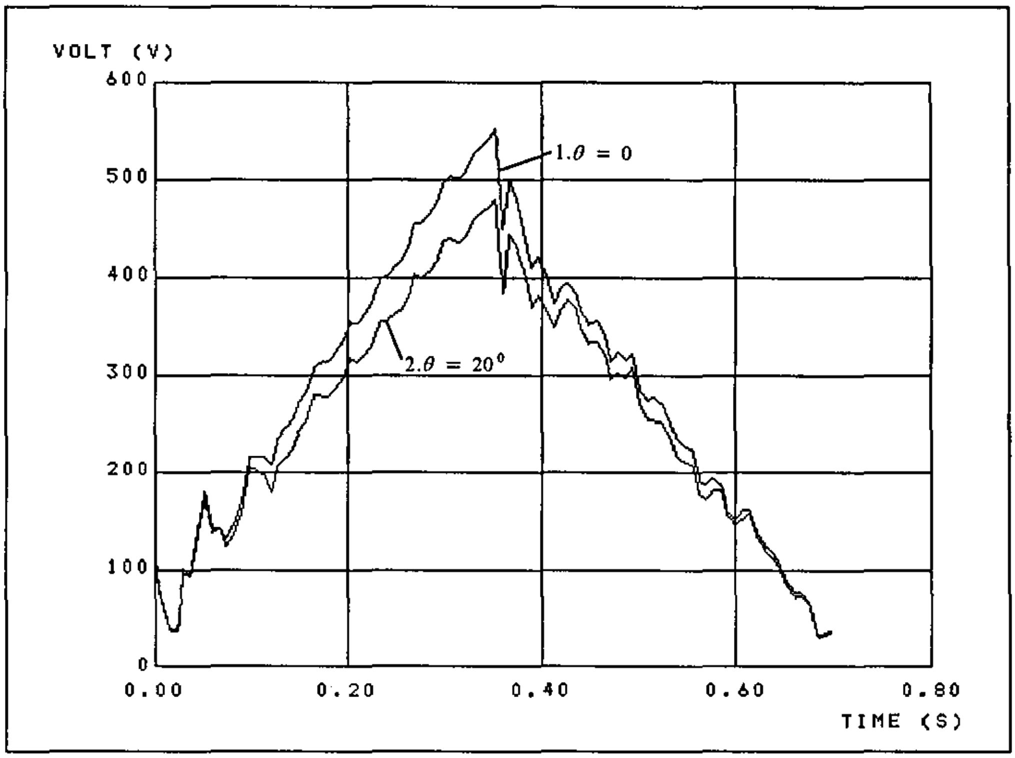

Figure 8.42. Amplitude of Phase Voltage

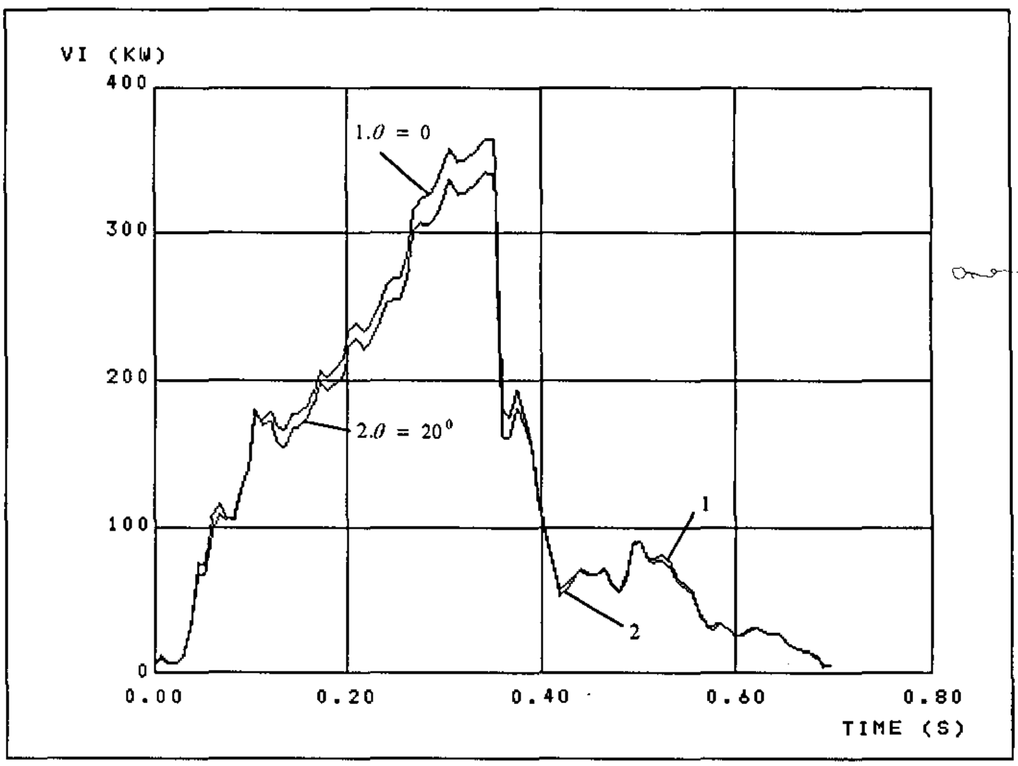

Figure 8.43. VI Rating

CHAPTER 9.

HARDWARE FOR REAL TIME CONTROL

There are two kinds of controllers for real time implementation: analogue and digital. Analogue controllers are relatively simple with low component costs and cheap manufacturing technology, although as the number of functions increases so does the complexity. Digital control is another option for control implementation, which normally consists of central processor unit (CPU) and certain essential features. Advantages of the digital controllers are significant. They improve reliability, eliminate drift and electromagnetic interference problems, and provide cost reduction in control electronics for highly sophisticated systems. They also permit universal hardware and flexible software control. With the rapid advancement of microelectronics technology, cheaper and faster microprocessors are becoming available with better accuracy and more on chip functions.

A digital controller is adopted for the subsea system mainly due to complexity of the control system particularly the vector control, multi-tasks and flexibility required for the system.

This chapter presents the hardware developed for the real time implementation of the system. An overall structure of the entire subsea system is presented in section 9.1. The control microcontroller and its relevant features are described in section 9.2. Section 9.3 gives details of the position transducer and position switches. Current sensors and their interfaces are presented in section 9.4, and the power interface is described in section 9.5, followed by summary of the chapter in section 9.6.

9.1. Overall System

Because the pump system is designed for subsea applications, the conditions and the working environment of the system are totally different from any land based systems. The system must be fully isolated from surrounding sea water. Direct access to the system is impossible as everything will be sealed. As a consequence, it would require that the system is dismantled and lifted from bottom of the sea for any modifications, which would be a very complicated operation. Therefore flexibility and reliability of the overall system are two important design issues.

The entire pump system consists of many units, which are placed in different containers, and the motor drive system is its key element. Communication between these containers are performed by a data communication system (referred to as Data Comm). It is not the objective of this thesis to present the entire pump system in great detail, however the design of the control hardware is closely related to that of the whole system and guided by it. It is thought that presentation of the basic structure of the overall system would be helpful for understanding of the hardware designed for the control.

Figure 9.1 shows a schematic diagram of the system. It includes the main unit on surface, the electronics and control unit, the motor and pump unit, the power transformer and the data communication.

The main unit on the surface consists of a SUN station, a PC computer, an Intel 196 development system (ICE) and a data communication node. The SUN station is responsible for the system management, human-machine interface, analysis and diagnosis as well as simulations. It monitors the status of the entire system; downloads the control software to microprocessors in the subsea via the data communication system; issues commands in defined sequences for required operations; collects data from the subsea units.

The PC is used for the modification and development of the control software, which can be pre-tested by using an Intel 196 development system (ICE) connecting with the PC via a serial link. The connection between the SUN station and the PC is an Ethernet system, where the PC can send or take files from the SUN station and it can also become one of the terminals of the SUN station via the link.

There are several units on the seabed. The motor and the pump are placed in one container, where the position transducer and number of other sensors for temperature and pressures are installed and one of the data communication nodes is used to transmit data. The position transducer signals are processed by a local microprocessor and then transferred to a defined format for transmission.

The control microprocessor and its interfaces together with the power electronics are placed in one container. The control software is downloaded from the SUN station via the data communication before any operations can be carried out, which allows software modifications at any time. The control microprocessor collects phase current data via sensor interface (SIF), where each channel of the current sensors is decoded as a memory location of the control microprocessor. The position feedback signal is sent to the data communication interface (DIF) by the data communication node in the container. The interface uses a dual port RAM (DPR) chip and both sides of the interface can access the DPR in parallel as their own memory locations such that high speed interfacing is achieved.

The control microprocessor fires GTO thyristers of the voltage source inverter via a power interface (PIF). The power interface controls all GTO firing circuits and the d.c. link charging sequences. It also executes the emergency shut down of the system when one of critical faults occurs.

In addition an extra microprocessor (protection processor) is used to monitor the voltage and current sensors for the electronics. It performs a data logging task and checks the status of the electronics as a safeguard in parallel with the control microprocessor. The protection processor may be used to provide redundancy of the control microprocessor in the future.

The hardware related to the control is the control microprocessor, the data communication interface, the position transducer, the current interface and the power interface. Following sections present the details of these hardware.

It should be noted that this chapter mainly concentrates on design strategies of the control hardware based on requirement of the control system, but the actual circuits were designed by other engineers involved in the project.

9.2. Control Microcontroller

It was decided in the early stage of the project that a specially designed microprocessor board rather than a commercial product was to be used for the system due to special conditions in the subsea.

There are generally four types of microprocessors: basic microprocessors, single chip microcontrollers, digital signal processors and transputers. Moreover, there are many many different particular devices in each type and it is a complex procedure to select the right processor for a particular application. First of all, the basic requirement of the processor must be defined according to the functions to be performed by the hardware. Then functionality, reliability, complexity, costs, processing speed and accuracy of available processors are compared against the requirement. The experience of certain microprocessors and preference of the designers also influence the decision making of the selection. In addition, availability of the development tools for the processors play an important role in the selection.

In this system, an Intel 80C196KC has been chosen to perform the control task [68-70]. The 80C196KC is high performance microcontroller with a 16 bit CPU running at 16 MHz clock frequency. A 16x16 multiply takes only 1.75 μs and a 32/16 division takes 3.0 μs. The main functions of the microcontroller are briefly described as follows.

- There are 488 bytes of on chip RAM available to users with register to register architecture such that no accumulator is needed. The RAM can be referenced as byte, word and double word registers. It is much quicker to access these registers than external memory and the RAM is large enough to allow large portions of the processing to be carried out locally and speed up the overall processing. In addition the registers can control many on chip peripherals directly.

- There are two internal 16-bit timers allowing up to four 16-bit software timers. Timer 1 is a free running timer which is incremented every eight state times and is used to synchronise real time events. Timer 2 counts transitions, both positive and negative, on its input. Also timer 2 can be clocked internally every 1 or 8 state times. High accuracy time control can be achieved by these timers, which is important for the sample period of the control loops and accuracy of current data acquisition.

- There are up to six high speed outputs (HSO) and four high speed inputs (HSI), which are all programmable. The HSO can generate events at specified values of the Timer 1 or Timer 2 with minimum CPU overhead. The high speed outputs are very useful for the current application as they can generate pulses to fire the GTO thyristers.

- There are 28 different interrupt sources and 16 vectors on the 80C196KC chip, including hardware interrupts, software interrupts and special interrupts. These interrupts enable flexible and multi functional software design as well as easier and more reliable hardware design.

- There is a serial port on the chip, which can be used for simple communication. An A/D converter with sample/hold facility can be configured to a 8 or 10 bit converter for the input of analogue signals.

A control board has been designed using the 80C196KC as the central processor. Figure 9.2 gives a block diagram of the board. It mainly consists of a 80C196KC chip, EPROM, RAM and decoder. The microcontroller chip is to perform all control tasks and other relevant functions. The decoder is used for mapping all memory locations.

The decode maps the on board memory and memory locations to two interface cards. The first one is the data communication interface card where a Dual Port RAM chip is used for the data exchange between the microcontroller and the data communication system. Via the DPR, the control software and parameters can downloaded into the microcontroller; the microcontroller can collect the position signals, accept operation commands and send recorded data. The second board is the sensor interface card such that the microcontroller acquires current feedback signals by accessing its own memory.

The downloading of the control software is performed by the software embedded in the EPROM of the microcontroller board. In addition, the embedded software performs the initialisation and reset of the microcontroller. A flow chart is presented in Figure 9.3. The downloaded code or data uses HEX format to guarantee the correct transmission, which includes data record, start address record and end of file record. The embedded software reads and checks data against their check sum. If the data is correct, it is sent into RAM. If the data is incorrect, an error message is sent to DPR for re-transmission.

Three HSO channels are connected to the power interface card. The HSO signals are converted to six channels by interlocking logic circuit on the PIF card for firing inverter GTO thyristers. IOPORT1.0, which is controlled by the Timer 2 of the microcontroller, is used for the current sensor timing. The serial link is used for interfacing with the protection microcontroller, which uses a 80C196KC as well.

9.3. Position Transducer and Switches

The position signal is essential to the proper operation of the control system and the accurate position measurement is of great importance to the control performance. The choice of the position transducer to be used in the system depends on levels of precision and the performance required. The cost of the transducer is not a great concern compared with the overall cost of the system. Considerations of the selection are given as follows.

- Since digital control is used for the system, it leads naturally to digital transducers. The digital outputs can be directly interfaced to the digital system and thus simplify the processing procedure. Moreover digital signals can be better transmitted with better inherent noise immunity than analogue signals.

- The control accuracy required by the system is 5 *mm* and a zero error at stroke ends is desirable. In addition, a small truncation error is also necessary to reduce the control noise as demonstrated in chapter 6. It is clear that a transducer with high resolution is required for the system.

- The clearance between the piston heads and the cylinder ends is very critical for high volumetric efficiency, thus repeatability of the measurement is of the same importance as the accuracy for safe and continuous operation.

- As the motor has linear motion with a maximum stroke length of 1500 *mm*, a linear transducer is the best choice for measuring the slider position and the measurement range must be longer than the stroke length.

- The pump runs at peak velocity 4.2 *m/s*. Therefore the dynamic response speed of the transducer must be faster than the peak velocity.

- The pump works in the subsea environment, which requires that the transducer must be able to withstand high pressure.

- Long working life of the transducer is also necessary to avoid the need for replacement.

9.3.1. Linear Incremental Transducer

There are many types of position transducers [41]. Potentiometers are analogue sensors which can be relatively cheap. Optical encoders use a rotating slotted disc to interrupt a light beam for obtaining the angular position of the movement. Inductive type transducers typically consist of one primary winding and two secondary windings on a hollow cylinder. They perform the position measurement via flux variation. Magnet type transducers use a permanent rod magnet attached on the moving part to indicate the position. Absolute position measurement and high accuracy can be achieved. This type of position transducers has only become available recently and its high pressure version in less than one year.

After investigations and tests on several transducers, a linear incremental digital transducer (SACOL) has been chosen, which is a inductive type transducer. The transducer can directly coupled to the motor slider so that no extra mechanics are needed. The position transducer measures displacement of the movement with the best resolution of 0.25 *mm* within measurement range of 2000 *mm*. The dynamic response of the transducer is such that it can maintain the proper measurement at speeds up to 5.0 *m/s*. The mechanical structure is designed to withstand a pressure of 100 *bar* and test results have shown that the transducer has reasonable repeatability.

Signal outputs from the transducer are processed by its interface card which generates pulses. By using a counter to count the number of pulses, determination of the position and speed can be achieved. The transducer outputs two trains of pulses having a 90^0 phase difference as shown in Figure 9.4. Each pulse period of the outputs represents a displacement of 1.0 *mm* with high and low levels of the pulse having an equal width of 0.5 *mm*. The best resolution of 0.25 *mm* can be achieved by using a XOR logic for the two phases as shown in Figure 9.4. The direction of movement can be deduced from the two outputs using well established principles. An interface circuit is used to obtain the resolution of 0.25 *mm* by implementing the XOR logic to the two pulse trains and to eliminate some noises by using D type flip flops [68]. Figure 9.5 gives the diagram of the circuit.

These signals are processed by a microprocessor located in the container of the motor and pump unit and transmitted to the defined DPR location via the data communication. Delays are introduced by the processing and data transmission, but those are no more than 0.15 *ms* in total.

9.3.2. Position Switches

Despite the quality of the position transducer, its major drawback is that it only measures movement and does not give absolute position. This means that there is no position reference and the initial position of the slider will be unknown. Since it was not possible to find an absolute position transducer to meet other specifications required for the system, additional position references were used in the system.

The position references are achieved by using four inductive sensors (referred as position switches) installed along the track of the slider movement. Figure 9.6 gives the arrangement of the position switches. The inner two switches (2 and 3) are used for normal position references. The outer two switches are placed just outside of the stroke length such that protective action can be taken if the slider and piston pass these switches. The status of these switches is also detected by the microprocessor in the motor and pump unit and then transmitted back to a defined location in the DPR. The inductive sensors used in the system have the accuracy of 0.5 *mm*.

9.4. Current Sensor and Interface

In the development of the vector control, it has been shown the phase currents of the motor are required as the feedback signals. Since the motor stator is star connected, only two of the three currents need to be measured. Amongst various methods for measuring the current feedback signal, the Hall effect sensor is preferred for its ability of electrical isolation, measurement of the d.c. and a.c. current, accuracy and reliability.

9.4.1. Current Sensor and V/F Converter

The current sensor is a proprietary feedback measuring system using the Hall effect principle, which has been commonly used for feedback control systems, variable speed drives, power supplies, robotics and over current protection.

There are mainly two methods for converting the analogue measurement to the digital signals, which are analogue to digital (A/D) converters and voltage to frequency (V/F) converters.

Conversion time of an A/D converter can be very short and accuracy of the measurement depends on the number of bits of the converter. For the 80C196KC microcontroller, no extra A/D converter is required as there is a on chip 10-bit converter. However, the disadvantages are obvious as well. It requires a stable power supply with high precision. Tolerance of noise is low: a 10-bit digital A/D converter with a full scale of 5 volts cannot tolerate a noise voltage in excess of 5 mV if the required accuracy is one bit. In the current system, the switching noise of the VSI and the noise of the power supply of the GTO firing circuit can be quite severe. The distance between the microcontroller and the current sensors is relatively long, which means that the noise can be easily introduced in the analogue signals. Although a filter can be used at the receiving end, there is always a conflict between the extra phase lag of the current measurement introduced by the filter and reduction of noise.

As an alternative to the A/D converters, voltage to frequency converters provide a simple and low cost way of converting analogue signals into digital forms, which are an appropriate choice when operating in noisy environments. The combination of high accuracy and linearity, low temperature drift, and monotonicity often provides performance characteristics unattainable with other techniques [71].

Since an analogue quantity represented as a frequency is inherently serial data, it is easily handled in multi-channel systems. Frequency information can be transmitted over long lines with excellent noise immunity using digital line transmitters and receivers. Isolation can be accomplished with optical or transformer couplers without loss in accuracy. High frequency V/F converters are available nowadays, which eliminates problem of the slow response existing in the earlier versions of the V/F converters. Therefore the voltage to frequency converter is chosen for the current measurement of the system.

9.4.2. Interface

A circuit is designed for interfacing between the sensors and the control microcontroller. Three channels are used for measurement of the three phase currents, one of which is for redundancy. The interface circuit of each channel is partitioned into two modules, remote sensor module and sensor interface module. Figure 9.7 gives a schematic diagram of the current sensor interface

The remote sensor module is located beside the current sensor. A burden resistor *R* is used to convert the current input into voltage. An amplifier is used to amplify the input signal and shift it to the positive level for the V/F converter. Input voltage to the converter is 2 - 8 *V* and working frequency range of the converter is 0.8 - 3.2 *MHz* as shown in Figure 9.8. The isolation is achieved by an optical coupler after the converter. A line driver is used for the transmission of the digital signal.

The sensor interface module is located at the microcontroller side. Each channel consists of a receiver, a counter and a latch. A decoder, a timing sequence control and a buffer are shared by all three channels. The timing sequence control is crucial for correct pulse counting and data acquisition. Figure 9.9 shows the sequences. Firstly, the high level of the Gate disables the receiver such that the counting is stopped. Second step is that rising edge of the RCLK enables the data transmission from the counter to the latch. Then low level of the CLR clears the counter and a new counting period is started. The microcontroller can only read the current data after all these steps are completed. The clock for the counting period is provided by the microcontroller, which is a train of one shot low level pulses in every 0.3 *ms*.

Selection of the counting period of 0.3 *ms* is decided due to the required accuracy. A longer counting period of the V/F converter apparently results in higher resolution, but care must be taken because it brings a longer delay which introduces error. When the period of 0.3 *ms* is used, the worst error caused by the resolution occurs at the lowest frequency 0.8 *MHz* which is 0.42% of the measured current.

9.5. VSI and Power Interface

The switching devices used for the VSI are gate-turn-off thyristers (GTO). This is a variant of the thyrister in which the internal structure has been modified to enable the forward current to be turned off by the application of a negative gate current. Recent developments in both device technology and control systems, particularly those employing microprocessors, has led to a growth in GTO applications, particularly in pulse width modulated inverter devices.

A standard structure of the VSI is adopted for the system. Figure 9.10 shows the schematic diagram of the inverter together with its d.c. link circuitry. Six GTO thyristers form three complementary legs of the inverter. Six reverse diodes, which are not shown in the diagram, are connected in parallel with the GTO thyristers in order to accommodate the phase relationship between current and voltage in the inductive load.

The d.c. link circuitry consists of RC filter, a contactor and a GTO charging unit. The GTO is used to isolate the motor and the inverter from power supply. During powering up of the d.c link, the GTO is turned on and the charging current goes through the resistor to avoid current surge and possible oscillations. After the capacitor of the filter is charged to the normal voltage, the contactor comes into action to supply the maximum power.

In addition there is a dynamic braking unit employing a series connected GTO and a resistor in parallel with the d.c. link. This unit is included for locking the motor slider and dissipating regenerated power from the motor when a fast stop of the motor is demanded in emergency situations.

The switching sequences for the power up / down of the d.c. link are performed by the power interface circuitry and the firing the GTO thyristers of the VSI is controlled by the microcontroller via the PIF. A schematic diagram of the power interface board is given in Figure 9.11. The PIF consists of an interlocking unit, a gate control, a sequence control, an emergency shut down (ESD) unit, a watchdog monitor of the microcontroller and an optical coupler unit. These functions are mainly achieved by employing programmable array logic (PAL) components instead of the glue logic. The PAL enables the high flexibility of the system design and provides all required functions in much smaller space than the glue logic.

The interlocking unit is used to convert the three firing signals for the three complementary legs into six channels for the six GTO thyristers respectively. Since each GTO thyrister needs a time period to be turned on and turned off and thus the switching signals for the two GTO of each complementary leg must have a time difference, the interlocking logic is designed to have a time delay between these two as shown in Figure 9.12. The optical couplers are used to isolate the power interface circuit from the possible high voltage from the power inverter. Outputs of the interlocking logic can be disabled by the switching sequence unit.

The sequence logic unit is used to control the switching sequences of the d.c. link powering up and down, as shown in Figure 9.13. The commands of the power up and down are issued by the protection microcontroller.

The emergency shut down (ESD) logic unit is used for protection of the system. It can be tripped by the microcontrollers, the SIF and the output of the position switches. When the control microcontroller detects an fatal error in the control loops, it can request an ESD by sending a message to the protection microcontroller or simply failing to serve its own watchdog. The SIF checks outputs of sensor measurement against their limit thresholds and trips the ESD if one of the thresholds is reached. In addition, the ESD can be tripped by the two outer position switches if the slider position moves to outside of the stroke range.

9.6. Summary

This chapter has presented the structures and designs of the hardware for the control system, which are the microcontroller and data communication, the position transducer and switches, the current sensor and its interface, the power interface.

The 80C196KC microcontroller has been chosen and a dedicated circuit has been designed to implement the digital control. The Dual Port RAM is used for handshaking with the data communication system. The SACOL incremental displacement transducer is used for the position measurement. The current sensors and the voltage to frequency converters are used for the current measurement and the analogue to digital conversion respectively. The remote sensor module and the sensor interface module have been designed for the interfacing with the microcontroller. The power interface circuit has been developed for converting switching logic of the microcontroller to fire the GTO thyristers of the VSI. The PIF also performs the protection of the system and controls the switching sequences of the d.c. link powering up and down.

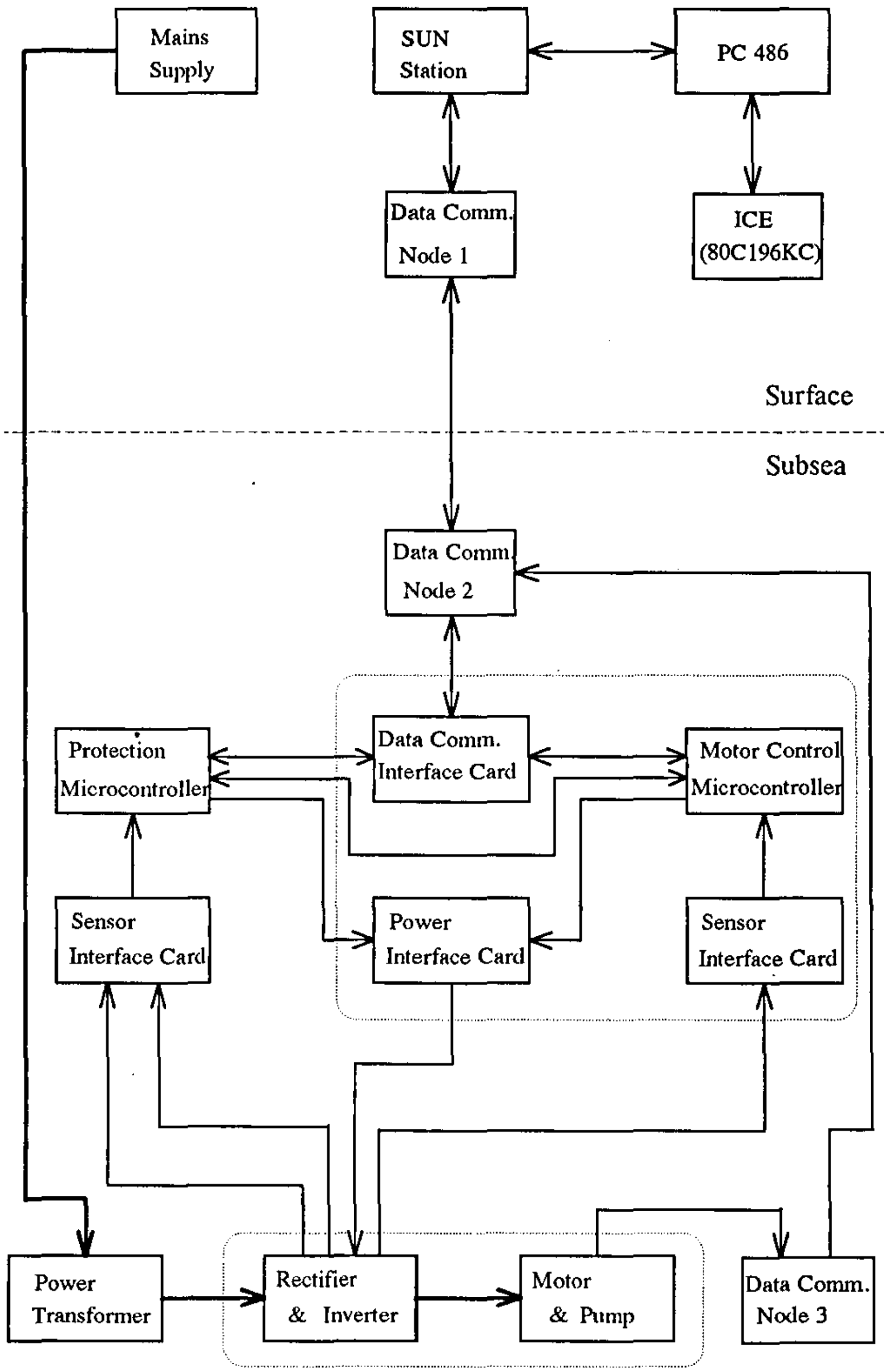

Figure 9.1. Schematic Diagram of The Subsea Pump System.

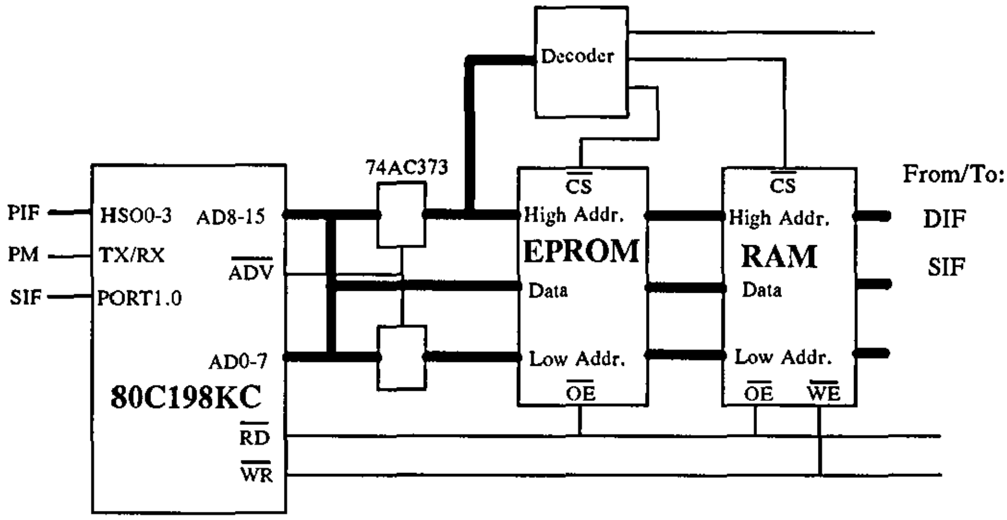

Figure 9.2. Block Diagram of Control Microcontroller.

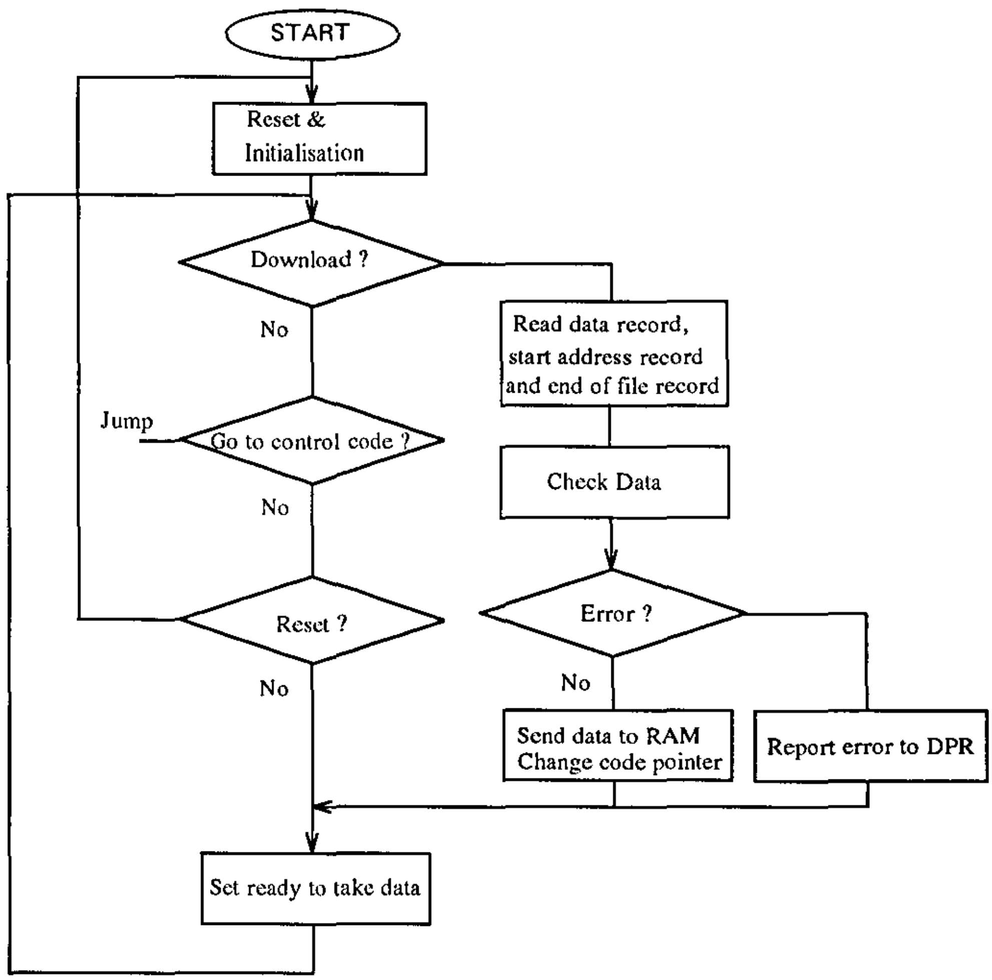

Figure 9.3. Flow Chart of Embedded Initialisation Code.

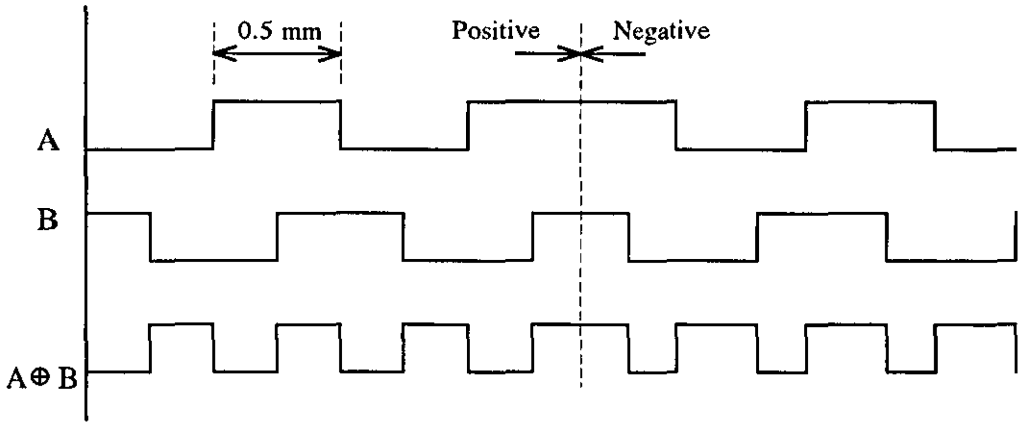

Figure 9.4. Incremental Quadrature Outputs of Position Transducer

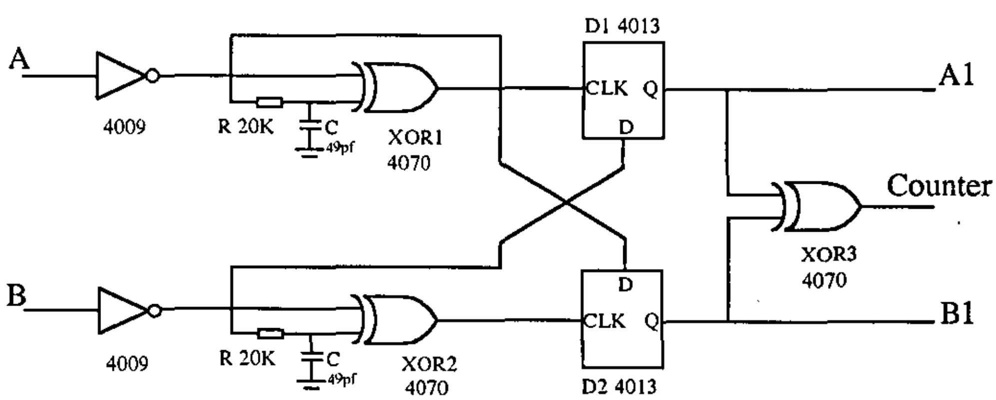

Figure 9.5. Interface of Position Transducer.

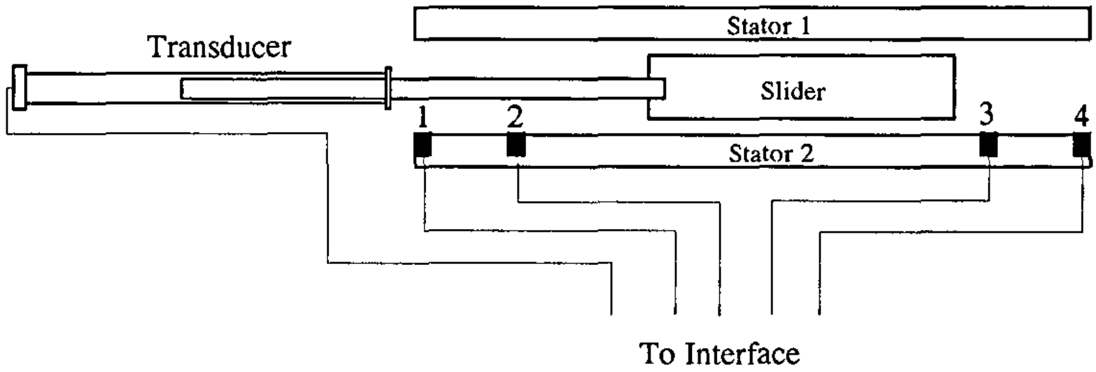

Figure 9.6. Mechanical Arrangement of Position Switches

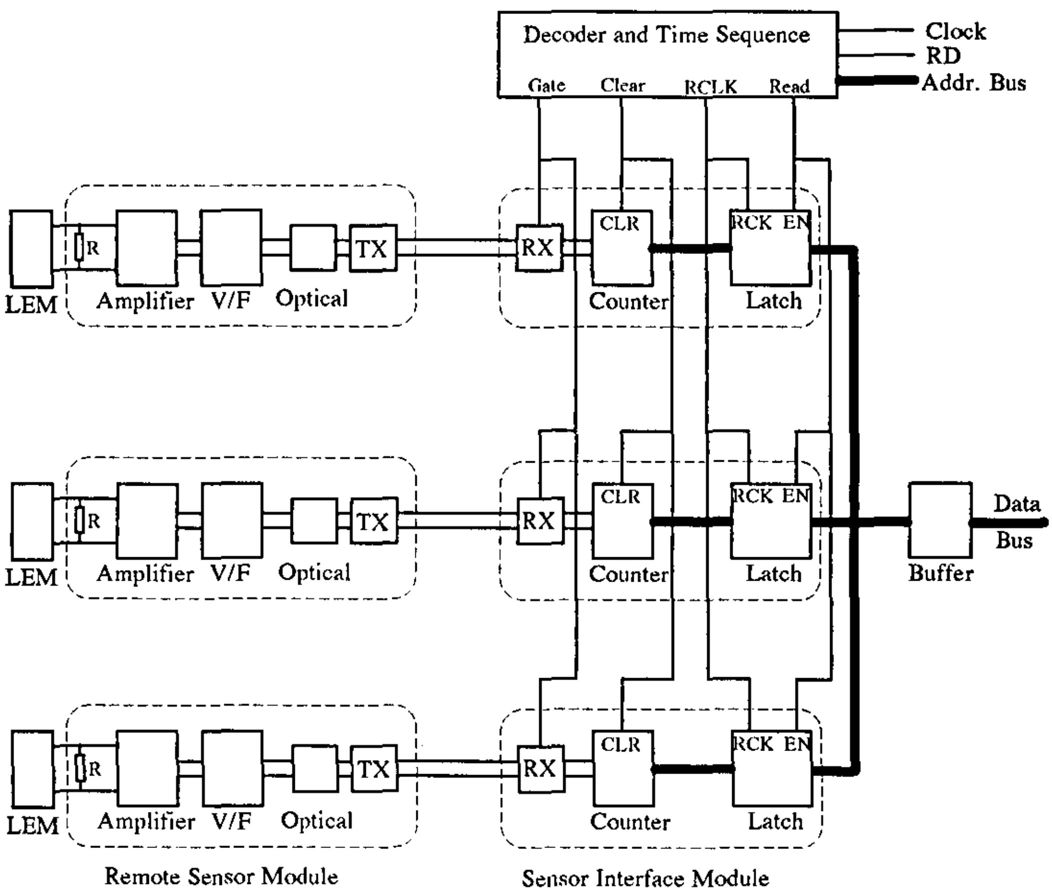

Figure 9.7. Schematic Diagram of Current Sensor Interface

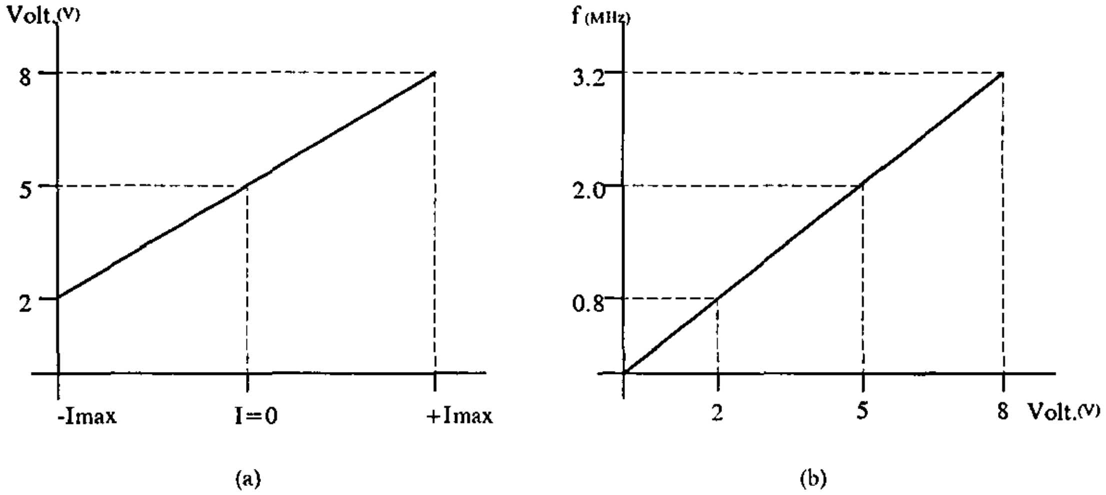

Figure 9.8. Signal Processing Diagram of Current Sensor Interface

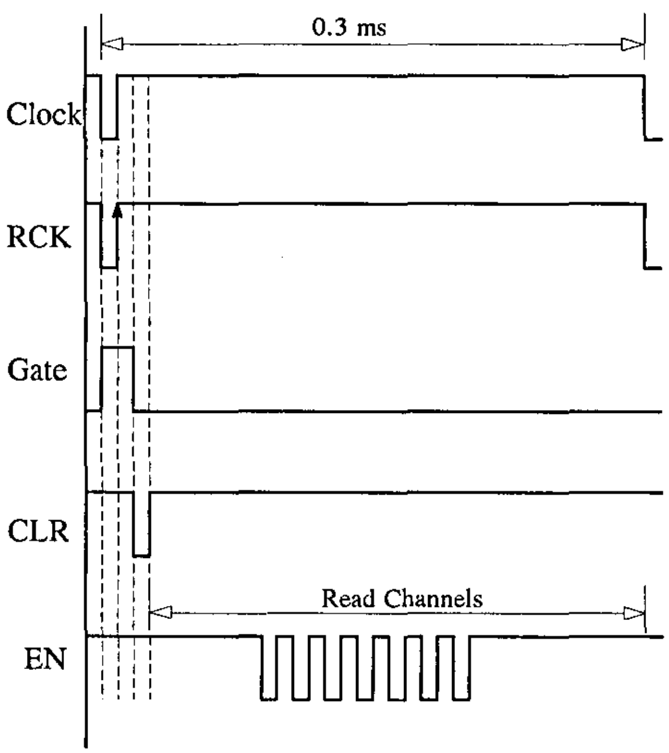

Figure 9.9. Timing Diagram of Current Sensor Interface

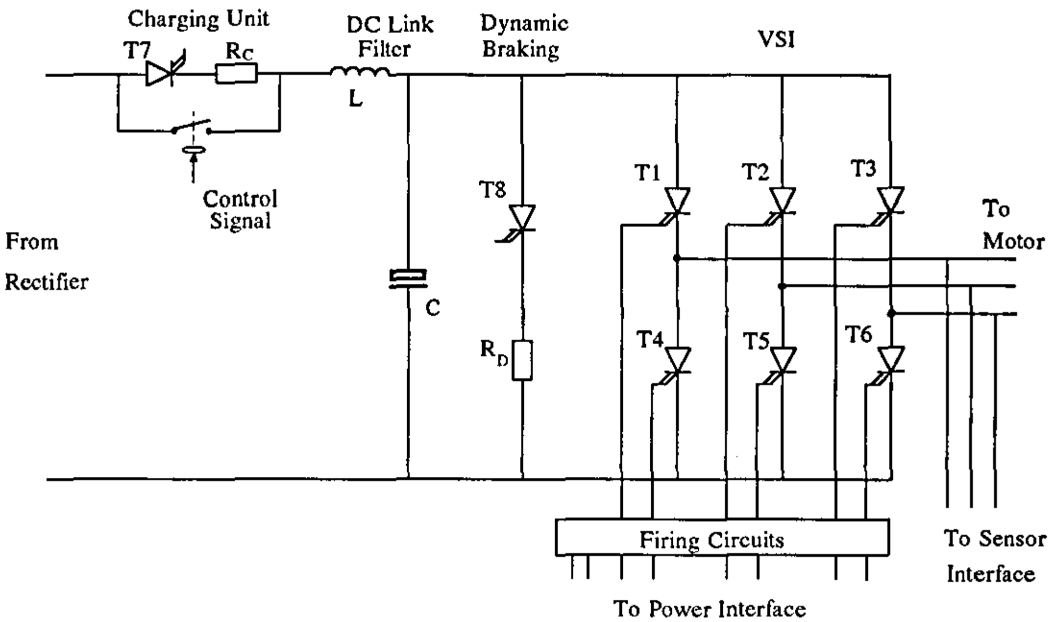

Figure 9.10. Schematic Diagram of VSI and D.C. Link

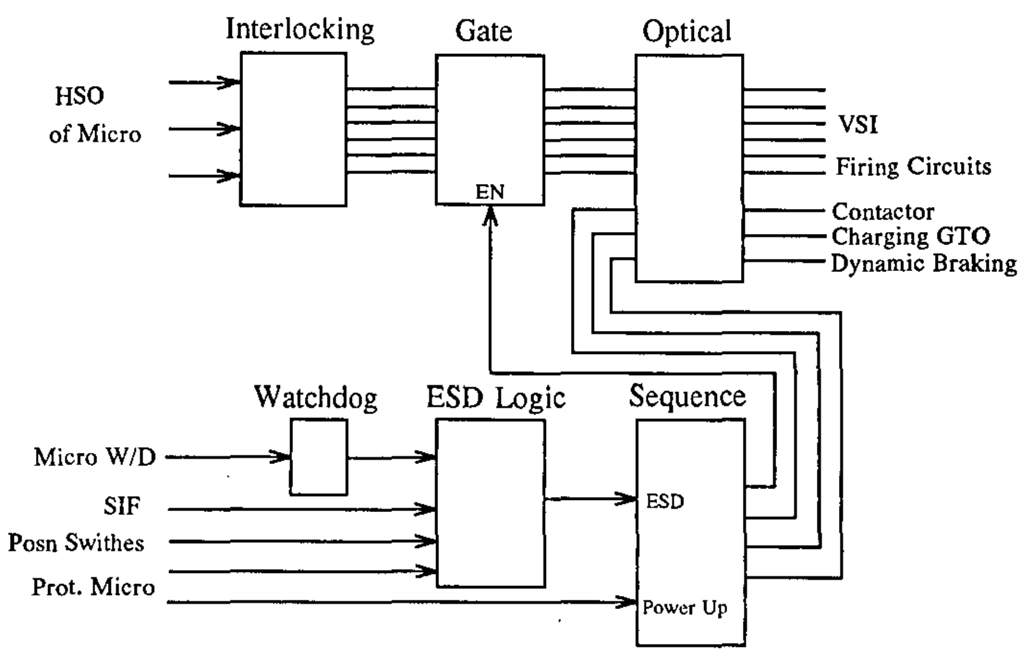

Figure 9.11. Schematic Diagram of Power Interface

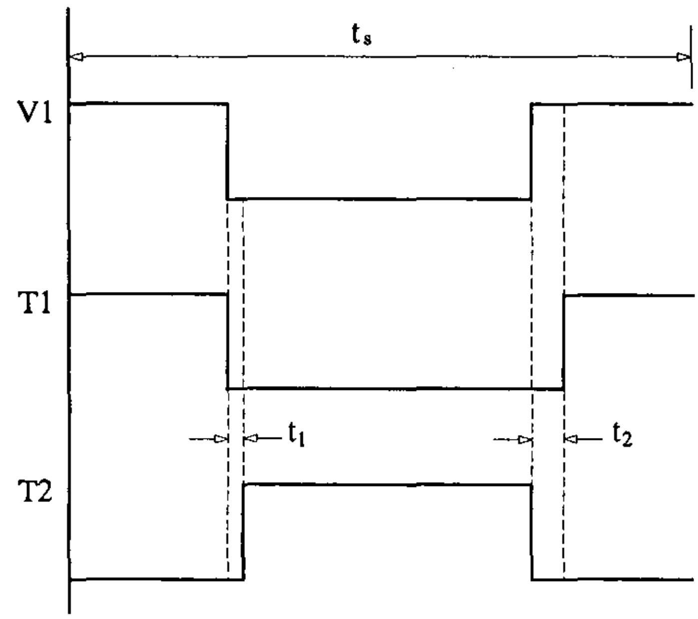

Figure 9.12. Switching Sequences of Each GTO Leg

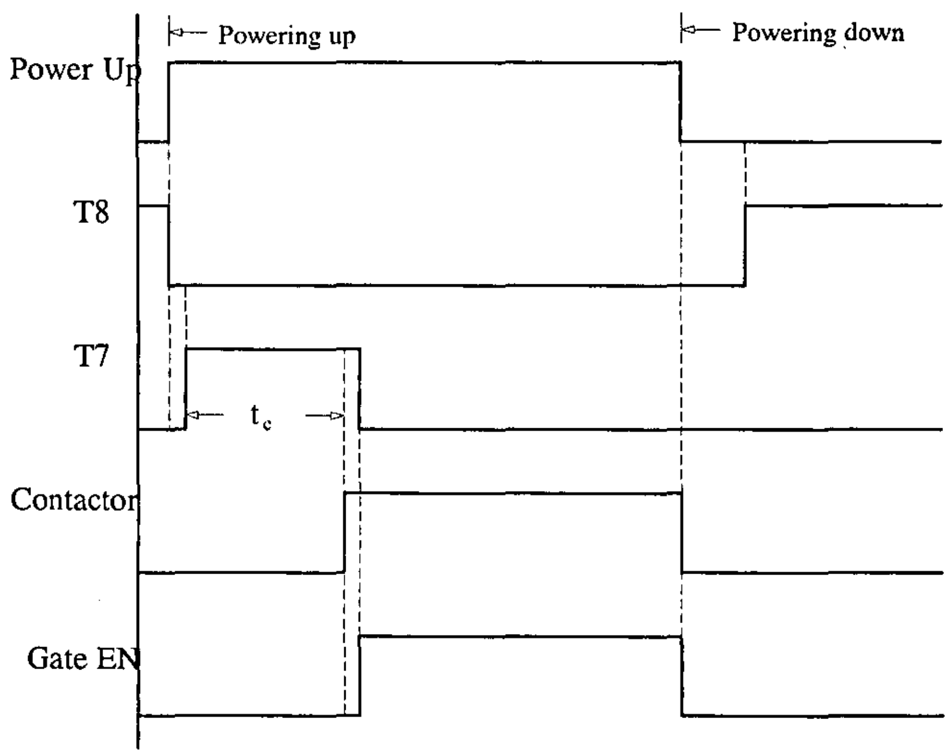

Figure 9.13. Switching Sequences of d.c. Link

CHAPTER 10.

SOFTWARE FOR REAL TIME CONTROL

Digital control normally employs a microprocessor and implementation software plays a very important role. High efficiency of the software is of priority as computation time affects the performance of a control system. Control accuracy is inevitably affected by the wordlength of the processor. A constant sample period for a control loop must be maintained. Above all, a proper structure and appropriate algorithms used to perform the control tasks in the software are essential for achieving desirable performance.

This chapter presents the design of the control software for the subsea pump system. It is not intended to go through every detail of the software, but to highlight some important design issues and the main algorithms used in software. A list of the source code of the programme can be found in the appendices.

In this chapter, an overall structure of the control software is presented in section 10.1. Programme languages and number formats are presented in section 10.2. The PWM module for controlling GTO thyristers of the VSI is described in section 10.3. The vector control module is described in section 10.4, where on-line calculations of sine and cosine functions are included. Section 10.5 presents the outer loop control module which includes implementation of position / velocity control algorithms and reference on-line generation. Section 10.6 presents the auto positioning module, which is used for searching initial position of the motor slider. Software timing and memory requirement are presented in section 10.7. Finally, a summary of the chapter is given in section 10.8.

10.1. Overall Structure.

The structure of software may vary from one application to another, depending on various tasks to be performed and features of the processor employed. The main functions of the control system are the three control loops; PWM generation; auto positioning; motor current measurement and data interfacing. The sample period of the current control loop is 1.5 *ms*, with the velocity and position loops being executed every three of the inner loop samples. Three PWM signals for switching the GTO thyristers of the VSI are required every 1.5 *ms*. As mentioned in chapter 9, the clock signal for the current measurement is every 0.3 *ms*. These sample periods and the GTO switching signals all require precise time control, which must be carefully considered in the software design.

Figure 10.1 shows an overall structure of the control software, which consists of a main programme, a timer 1 interrupt routine, a timer 2 interrupt routine and some other interrupt service routines.

The main programme is used to handle commands and data via the data communication system. It reads commands from the Dual Port Ram (DPR) to decide whether it should remain holding, implement auto positioning or normal pumping operation, or jump back to the software embedded in the EPROM. As the maximum speed and stroke length of the pumping operation are defined by the master computer via the data comm, the main programme checks these values before implementation to ensure safe and correct operation. The main programme also checks the position and velocity of the slider against their references. If the control errors become excessive, emergency action will be taken by the software. The main programme can jump back to the embedded software when demanded, because the control software is downloaded from the master computer and it must allow redownloading for system flexibility.

Using the internal clock of the microcontroller, the timer 1 software interrupt period is set for 1.5 *ms*, in which the three control loops and PWM generation module are implemented. The vector control module executes the inner control loop and outputs the required three phase voltages, which form the inputs to the PWM module. The PWM generation module calculates three logic signals for switching the GTO thyristers, which are timed by using HSOs. The HSO pins are connected to the power interface (PIF) card. The sample period of the outer position and velocity loops is achieved by using a byte variable to count number of inner sample periods. The outer loop module generates the reference trajectories and perform the control algorithms.

A data logging subroutine is also included in the timer interrupt routine. The internal variables and the control outputs can be recorded every 1.5 *ms* or integer multiples for evaluation of the system performance.

The Timer 2 software interrupt is used to clock the V/F converter for the current measurement and to collect the current feedback signals, which means that synchronisation between the microcontroller and the SIF is achieved without any extra hardware.

Non Maskable Interrupt (NMI), External Interrupt and Serial Interrupt are also used in the microcontroller. The former two are used for emergency cases, such as loss of power and failure of the microcontroller. The latter is used for communication with the protection microcontroller.

10.2. Programme Language and Numbers

Software languages can be fundamentally classified into two groups: high level compiled languages with instructions and syntax which are independent of the processor, and low level Assemble languages using an instruction set which is specific to the processor.

High level languages have the advantages of compact program code and ease of development. The disadvantage is inefficiency, which results in significantly increased computation time and program memory space. Moreover high level instructions are not generally well suited to handle peripheral devices of the processor. These drawbacks severely affect their use for real time applications.

Low level Assembler languages have been used for many real time systems. The advantage of using Assembler is that the code is written directly in the instructions which the processor executes, which gives the highest possible efficiency both in execution speed and memory requirements. Dealing with peripherals is usually very straightforward and precise sample periods can be achieved by internal timers. The disadvantage is that it is generally more difficult to write a programme using the Assembler, and software development will take longer. An Assembler language program is normally less readable which means that the associated documentation must be carefully written.

The differences between fixed point and floating numbers are similar to those between low and high level languages. For fixed point processors, higher speed, less memory space and lower cost can be achieved by using fixed point numbers, but at the expense of lower accuracy and restricted dynamic range. Considering floating point numbers, the opposite is true as the accuracy is increased while the speed is reduced.

For the current control system, the microcontroller must execute sophisticated algorithms in a relatively short time period. Therefore program efficiency is the priority, which leads naturally to the Assembler language, even though the programming work is increased. The Assembler language for the 80C196KC microcontroller mainly uses 16 bit variables, but 8-bit or 32-bit variables are also available. The required accuracy can be achieved by selecting proper scaling coefficients for the variables used in the software. There is not a unique method for selection of scaling factors and it is very much dependent upon individual applications and personal experience of the designers. The key issues are to avoid overflow and excessive signal quantisation errors.

10.3. PWM Module

The heart of any PWM inverter control scheme is the way in which the switching edges of the triggering pulses are generated. The main switching strategies described in literature are naturally sampled PWM, regular sampled PWM and optimal PWM. Naturally sampled PWM is based on the comparison between required modulating signal and a triangular waveform, which can be easily implemented using an analogue circuit. Regular sampled PWM is very easy to be implemented by digital control. It is based on the comparison of a triangular carrier wave with a stepped waveform obtained by regularly sampling the required modulating signal and holding its value until next sampling instant. The so called optimal PWM strategies are used to optimise certain specific performances of systems.

The type of the PWM used in the system is the symmetric regular sampled PWM As shown in Figure 10.2, the value of the modulating signal (a) at a sampling instant is maintained at the same level until the next sampling instant producing signal (c). Comparison of the triangular carrier waveform (b) with the stepped signal produces the intersection points defining the switching instants for the width modulated pulse. Note that the stepped modulating wave has a constant value while an intersection point is being determined. Consequently, the widths of the output pulses are proportional to the value of the modulating wave at each sampling instant, and the centres of the pulses are spaced uniformly in time, leading to the term regular sampling.

Since the sampling instants and the sampled values of the modulating signal are defined unambiguously, both the width and the position of the output pulses produced by this strategy can be predicted easily.

For the current system the three phase voltages will be compared with a fixed frequency triangular signal to generate three PWM output signals. These pulse signals will be used for timing the firing circuits to switch on or off six GTO thyristers of the inverter in order to supply the required voltages to the motor. In the sampling period $t_s = 1.5\ ms$, the on / off times of upper GTO thyrister of the red phase are calculated according to following equations:

$$T_{on\_R} = 2 \cdot t_s \cdot \frac{v_R}{V_{dc}} \tag{10-1}$$

$$T_{off\_R} = t_s - T_{on\_R} \tag{10-2}$$

where V_{dc} is the d.c. link voltage. Similar equations are used for the yellow and blue phases.

However the values obtained in equations 10-1 and 10-2 are not the final switching times, because delays caused by finite switching time of the GTO thyristers and the interlocking logic are not included. These delays would cause zero current crossing distortions [13]. To compensate, polarities of the three phase currents are needed for the software to adjust the on/off timing, as the delays are related to the directions of the current flows in the phases. The actual delay time of the GTO thyristers can be obtained either from testing or their data sheet, and the dead time of the interlocking logic is known from the PAL logic.

The actual timing control of GTO thyristers' on and off is achieved by using the High Speed Output of the microcontroller. Three pins of the HSO are used for the three phases respectively. The timing of each channel is programmed by setting two registers, HSO_COMMAND and HSO_TIME. The resolution of the timing control is 1 μs, which is 1/1500 of the sample period. Finally, the software computing time must be added into all three switching signals. This is because the PWM signals could have switching instants at any time during every sample period and it is impossible to output them while they are being calculated and therefore all the timing must be delayed by the computation time. The implementation sequences of the module can be described as follows.

- Calculate switching times for the three phases according to equations 10-1 and 10-2.

- Check polarities of the three phase currents and deduct delay times from the switching times.

- Add computation delay into both on and off times of the switching signals.

- Output the signals using HSO. The pins HSO0, HSO1 and HSO2 are used to output switching signals for the red, yellow and blue phases respectively.

10.4. Vector Control Module

The real time implementation of the vector control is similar to that in the simulation programme, and mainly includes following steps.

- Acquisition of phase currents. This is achieved by reading values of two phase currents from the sensor interface board and calculating the third one. As the output of the current sensors is shifted to a positive level by the SIF, the current offset of each phase is then deducted from the data.

- Calculation of the d-q axis currents. The slider position feedback is obtained from the defined memory location of the DPR. The position signal is converted into the electrical angle of the motor and a subroutine is used to calculate the sine and cosine functions of the angle. The d-q axis currents are then calculated by using inverse Park transformation.

- Calculation of the inner loop control signals. The control signals are calculated according to equations 6-4, 6-5, 8-11 and 8-12. The reference input is provided from the outer control loop and the output signal defines the d-q axis voltages.

- Calculation of the three phase voltages. Firstly, the slider velocity is derived from the position signals using equation 8-9. Then angle compensation is added on the angle obtained in step 2 according to the velocity and computation time delay. Finally, the three phase voltages are calculated using equation 6-1. The three phase voltages are used by the PWM generation module as its input signals.

The reference q-axis current is updated every 4.5 *ms*. The current and the d-q axis voltages are limited to their maximum values such that saturation of the motor is minimised.

In calculating the d-q axis currents, the sine and cosine functions are involved. To obtain the best possible speed and accuracy within the memory space available, a look-up table of a quarter cycle of the cosine function in steps of 0.045 degrees and resolution of 1/1500 is used. The sine function and the other three quarters of the cosine function can be derived from the table. A subroutine has been developed to calculate these two functions at any angle.

10.5. Outer Loop Control Module

10.5.1. Outer Loop Controller

Compared with the other parts of the software, the implementation of the outer control loops is relatively simple. The control signals are calculated using equations 8-1 to 8-5. A byte register is used to count the number of Timer 1 interrupts such that the control sample period can be easily obtained. A long word register has to be used for the control signal in order to maintain the necessary accuracy. The position feedback is obtained from the DPR. Reference trajectories are obtained using a trajectory generation subroutine, which is explained in the next sub-section.

For comparison, the optimal tracking controller has also been implemented by using the controller presented in the chapter 7.

10.5.2. Trajectory Generator

The maximum speed and stroke length required for the pumping operation are downloaded from the SUN work station via the data communication system. The speed is defined in cycles per minute and its possible range is between 1 and 42 cycles/minute, which is equivalent to a peak velocity of 0.1 - 4.2 *m/s* for the stroke length of 1.5 m. In addition, a rapid increase or decrease of the pumping speed is not acceptable for the system, as it would cause severe pressure surges of the fluids to be pumped in the transportation pipes. The speed must be changed gradually when the required speed is changed. Therefore the trajectory generation module not only provides references for every control period, but also performs the Ramp Up and Ramp Down of the maximum pump speed as required.

The first step of the trajectory module is to generate reference positions and velocities at a very low speed for the motor to drive the slider from its position to the start point of the pumping stroke according to the stroke length defined, which is achieved by a small increase or decrease of position steps, i.e. a slow constant speed.

The second step is to generate the trajectories for the normal pumping cycle. Since the slowest speed is 1 cycle/minute, a look-up table of one quarter period of the reference position for the speed is used and a subroutine with an internal counter has been developed to calculate reference positions, velocities and accelerations. The internal counter is used as the pointer of the look-up table. A byte variable is used as an incremental step for the pointer, the value of which depends upon the current speed required. The reference position in every sample period is calculated from the data located by the pointer in the look-up table. The velocity is proportional to the value of the pointer and the acceleration is constant in each pumping cycle with either a positive or a negative sign.

The pumping is always started at 1 cycle/minute. The Ramp Up and Ramp Down are achieved by using a variable as reference. It is initially set to 1 and then it is compared at starting point of each stroke with the speed required by the SUN station. A small speed step will be added or deducted, depending upon whether it is less or more than the required value.

The Ramp Down is also useful for system protection. In the vector control, a variable is used to count the number of times which the q-axis current exceeds its saturation value. If the number exceeds a defined value in one pumping cycle, this information will be passed to the trajectory generation module to implement the Ramp Down until the number drops to an allowed level.

10.6. Auto Positioning Routine

As mentioned earlier, the system employs an incremental transducer for position measurement. The disadvantage of the transducer is that the initial position, which has to be given to start the motor, is not available. In order to obtain a reference position, four position switches at fixed points are employed as shown in Figure 9.6. The four sensors divide the stroke length into three parts, i.e. those between 1 and 2, 2 and 3, 3 and 4 respectively. Because they are inductive type sensors and distance between 1 and 2 or 3 and 4 is less than the length of the slider, it is known in which part the slider is located at the beginning. Figure 10.3 shows the responses of these sensors to the slider position. When a sensor is covered by the slider, it outputs a high level signal; otherwise a low level signal is given from the sensor. The transition edges of the output signals indicate the position of the slider. In order to eliminate the errors caused by the hysteresis characteristics of the sensors, only edges in one direction are used.

The problem now is how to drive the motor slider to 'find' the transition edges. In finding the position, large sudden jumps of the slider must be avoided as it may cause the piston to crash into one of the cylinder ends. In this section, a method is developed to solve the problem.

10.6.1. Principle of Auto Positioning

The stroke length of the pump system is 1.5 *m* and the electrical pole pitch of the motor is 0.15 *m*, i.e. the stroke length covers 5 electrical periods. The electrical angle at which the motor slider is located has to be obtained before any scheme can be used to control motor. This is achieved by using a technique which will be called 'Phase Locking'.

According to the inverse d-q axis transformation, the d-q axis currents can be represented by the three phase currents.

$$\begin{bmatrix} i_d \\ i_q \end{bmatrix} = \frac{2}{3} \cdot \begin{bmatrix} \cos(\gamma) & \cos(\gamma - 2\pi/3) & \cos(\gamma + 2\pi/3) \\ \sin(\gamma) & \sin(\gamma - 2\pi/3) & \sin(\gamma + 2\pi/3) \end{bmatrix} \cdot \begin{bmatrix} i_R \\ i_Y \\ i_B \end{bmatrix} \qquad (10\text{-}3)$$

and therefore

$$i_q = \frac{2}{3}\cdot\left[\sin(\gamma)\cdot i_R + \sin(\gamma - 2\pi/3)\cdot i_Y + \sin(\gamma + 2\pi/3)\cdot i_B\right] \tag{10-4}$$

If the motor is excited with $i_Y = i_B = -i_R / 2$, then

$$i_q = i_R \cdot \sin(\gamma) \tag{10-5}$$

and from equation 5-40, the force produced by the motor is

$$F_R = -\frac{3}{2}\cdot M_{fM}\cdot\frac{\pi}{P}\cdot i_R \cdot \sin(\gamma) \tag{10-6}$$

Similarly,

$$F_Y = -\frac{3}{2}\cdot M_{fM}\cdot\frac{\pi}{P}\cdot i_Y \cdot \sin(\gamma - 2\pi/3) \tag{10-7}$$

when the motor is excited with $i_R = i_B = -i_Y / 2$ and

$$F_B = -\frac{3}{2}\cdot M_{fM}\cdot\frac{\pi}{P}\cdot i_B \cdot \sin(\gamma + 2\pi/3) \tag{10-8}$$

when the motor is excited with $i_R = i_Y = -i_B / 2$.

For the red phase, the force F_R is equal to zero only when $\gamma = 0$, π and 2π, which means that the force drives the slider towards the 0 (2π) or π electrical degrees of the phase. The direction in which the slider moves depends on sign of the current i_R and present position of the slider. Figure 10-4 shows the force waveform along the motor when i_R is positive. If the position is between 0 and 180 degrees, the slider moves towards 0 degrees. If the position is between 180 and 360 degrees, the slider moves towards 2π degrees. So position location of the slider in one electrical period can be divided into two sections by the direction of the slider movement.

Once the slider starts moving, the power can be shut down to avoid any overshoot. Then the same principle can be applied by injecting positive current to the yellow and blue phases of the motor respectively such that one electrical period can be divided into six sections. By combination of the three directions, a range of the position location can be detected with slight movement of the slider. Resolution of the detection is a third of the pole pitch, i.e. 50 *mm*. There are possibilities that the slider might not move at all when it is located at or close to 0 or π degrees of one of the phases. In this case, the position can be easily obtained by using the other two lockings. Table 10.1 shows logic relations between the slider location and the three directions, where zero represents no movement.

Table 10.1. Position Range and Directions of Phase Locking

	Red Phase			Yellow Phase			Blue Phase		
	Pos.	Neg.	Zero	Pos.	Neg.	Zero	Pos.	Neg.	Zero
0			1	1				1	
0-60		1		1				1	
60		1		1					1
60-120		1		1			1		
120		1				1	1		
120-180		1			1		1		
180			1		1		1		
180-240	1				1		1		
240	1				1				1
240-300	1				1			1	
300	1					1		1	
300-360	1			1				1	

If two of the three or all three are non movements, that means that there is a fault in the system, the operation will go no further and an error status will be reported to the DPR.

Having detected the position range, the slider can be locked into one of two nearest poles of the motor with a maximum movement of 50 mm.The position switches are used at this stage to decide which pole can be locked into. If the slider is located between the switches 2 and 3, it can be locked into either of these two, otherwise the slider should be locked into the one closer to the midpoint of the stroke length such that the piston will not crash into the cylinder ends.

From equation 10-6 and Figure 10-4, it is noted that the locking force is being decreased while the slider moves towards the poles. Because of the friction and load forces existing in the pump, there are dead areas near 0 and 180 degrees as shown shaded in Figure 10-4. Therefore the slider can not be locked exactly into the poles, which means that the information obtained so far will not be sufficient to implement the closed loop control schemes since the absolute position still remains unknown. However there is enough information to control the motor in an open loop scheme, and so the slider can be driven to trigger the position switches. The motor controller will create three phase sinusoidal currents at a very low frequency, which the slider will follow.

The slider is driven in both directions to trigger the switches 2 and 3. Switch 2 is used to reset the position to the switch's predefined value and switch 3 is used to check the distance between these two. To ensure a correct reference position, the distance is checked repeatedly until two consecutive outcomes agree with the physical distance.

10.6.2. Implementation Software

The tasks for the software to perform can be divided into three steps.

- Find the initial position range by implementing the Phase Locking algorithm. The three phase voltages are supplied with relations $v_Y = v_B = -v_R / 2$ using the PWM module. An internal variable is incremented to increase the amplitude of the voltages gradually. The slider starts to move when the force exceeds the total load force. The software detects the movement and its direction from feedback signal of the position transducer, and the GTO thyristers are switched off until the movement stops. If the slider movement is detected when the voltage v_R reaches its limit, the software records a message of no movement. The same procedure is then implemented for the other phases, so three direction signals are detected. The position range, where the slider is located, is obtained by implementing table 10.1.

- Lock the slider into the pole. The pole to which the slider is locked can be determined from information of the position range and the position switches. Then the PWM module is used to supply sufficient power to lock the slider.

- Drive the slider and check position switches. The following voltages are supplied via the PWM module.

$$\begin{aligned} v_R &= V_m \cdot \cos(\gamma_1) \\ v_Y &= V_m \cdot \cos(\gamma_1 - 2\pi / 3) \\ v_B &= V_m \cdot \cos(\gamma_1 + 2\pi / 3) \end{aligned} \qquad (10\text{-}9)$$

The rate of the angle γ_1 is much lower than the electrical dynamics of the motor, such that slow sinusoidal currents are obtained. Increasing and decreasing the angle will drive the slider in different directions.

10.7. Software Timing and Memory

The real time control software has been written and tested using a scaled down motor. Details of the motor and testing will be presented in next chapter. The entire programme consists of about 1500 Assembly language instructions, which require about 5.4 Kbytes of memory space. In addition the look up tables require about 8 Kbytes of the memory. On the microcontroller board, there are total 16K bytes of RAM which meet the requirement.

Computation times for the major routines in the software are given in table 10.2. It is shown that the maximum execution time in the Timer 1 interrupt routine is about 500 μs (i.e. 1/3 of the sample period) and this must be allowed for in the output signals of the PWM module.

Table 10.2. Computation of Major Routines of Software

	Computation time min / max. (μs)
Outer loop controller	22.5
trajectory generator	58/64
PWM generation module	68.75/69.13
Vector control module	194.25/259.25
Total time of normal pump operation in TIMER 1	325.88/501.75
Total time of auto positioning in TIMER 1	89/420
Time of Main Programme	6/40
TIMER 2 Interrupt	9.25

The Timer 2 interrupt routine has priority over the Timer 1 routine. Since it takes less than 10 μs to process data there is no problem for the microcontroller to respond the Timer 2 in the middle of processing the Timer 1.

About 2/3 of the sample period and 3000 bytes of RAM space have not been used, which gives the flexibility for modification and improvement of the control software. In addition, it is possible that the protection tasks could be taken over by the control microcontroller, and the protection microcontroller is used to provide redundancy of the former one.

10.8. Summary

This chapter has presented the design of the real time control software. Assembler language programming with fixed point numbers have been used to develop the software to give the high processing speed and lower memory requirement, but this has increased the programming work.

The software uses various modules for different functions to allow more flexibility. The Timer 1 interrupt routine is used to perform the main control tasks and the PWM switching. Timer 2 is used for clocking the SIF and collecting the current feedback signals. A scheme for searching the initial position of the slider has been developed using the Phase Locking and open loop drive.

The software has covered all functions required for the sub-sea operations. Reasonable margins of the computation time and memory space are obtained so that additional tasks or future modifications can be added.

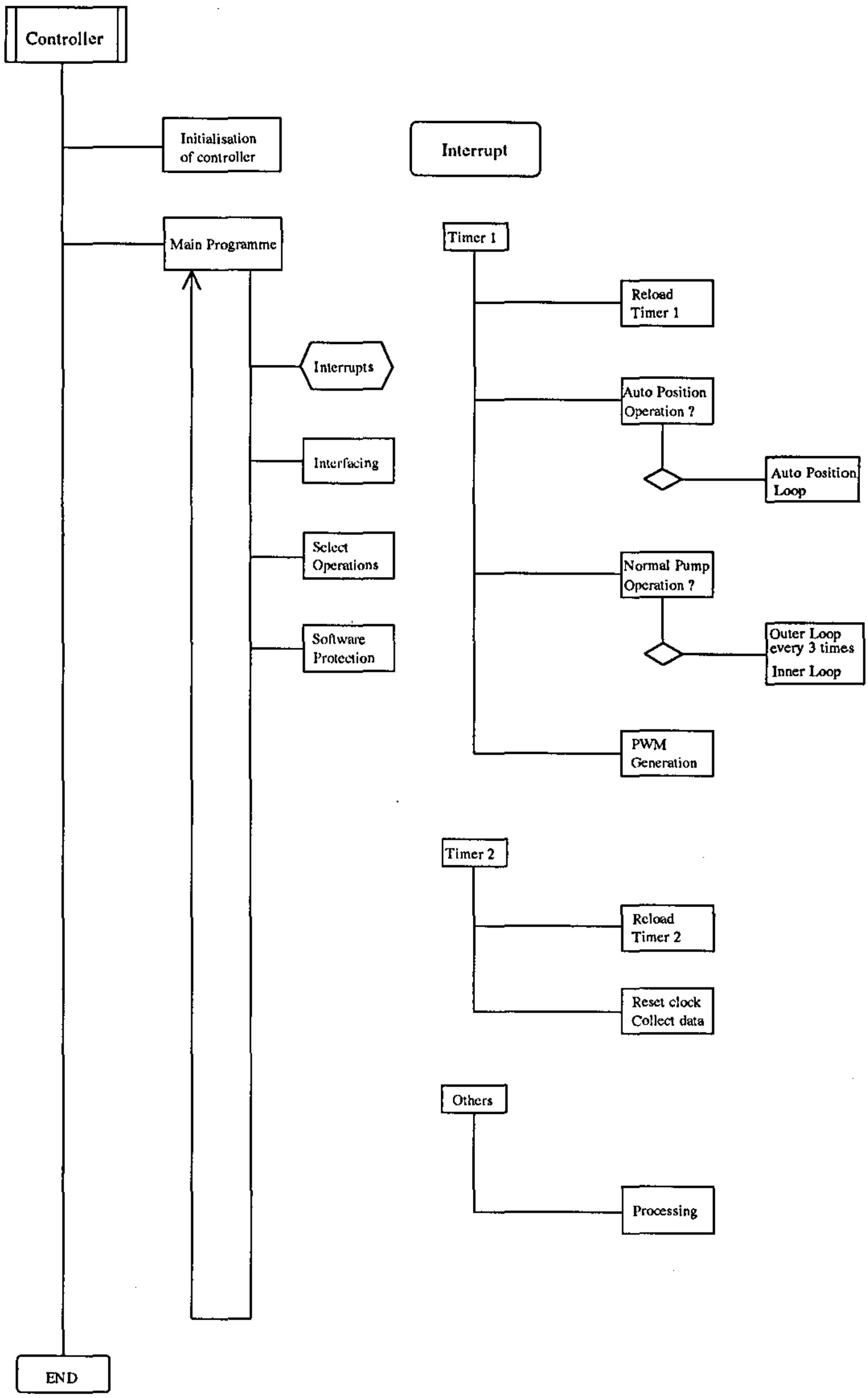

Figure 10.1 Overall Structure of Control Software

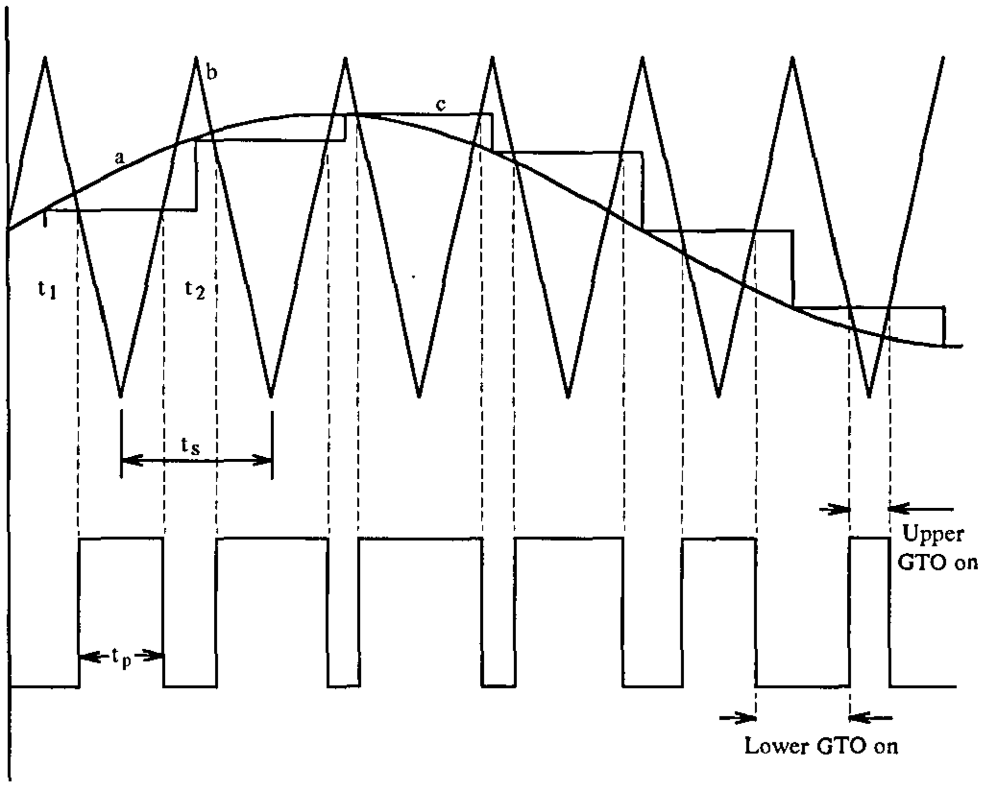

Figure 10.2. Symmetric Regular Sampled PWM

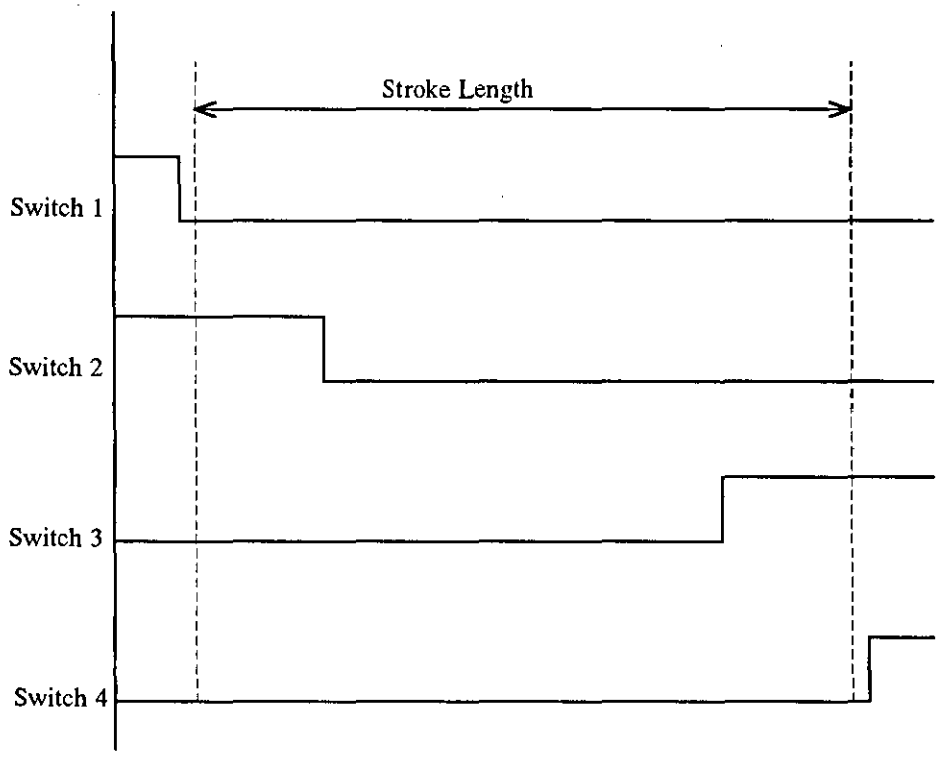

Figure 10.3. Responses of Position Switches.

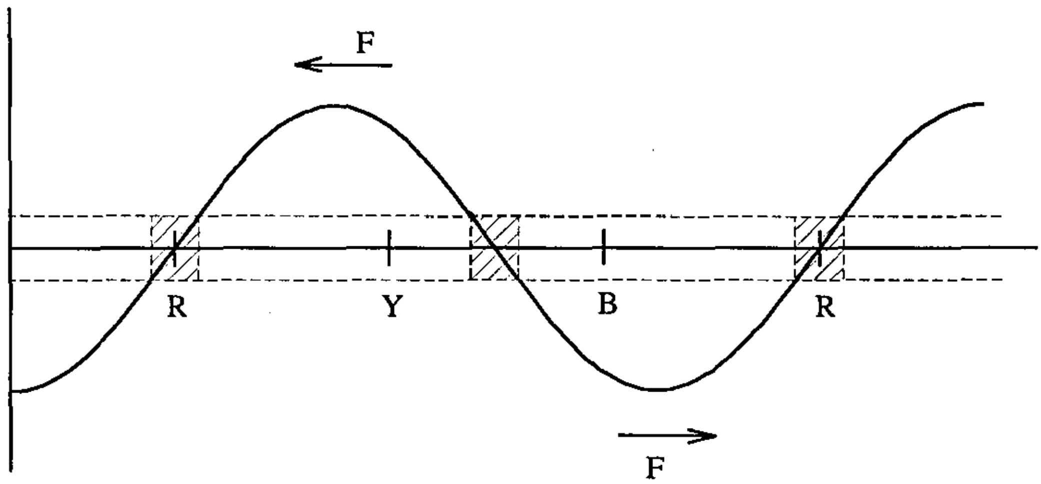

Figure 10.4. Motor Force When $i_Y = i_B = -i_R / 2$, $i_R > 0$

CHAPTER 11.

SCALED DOWN MODEL AND TESTS

In order to further study the control system being developed, a test rig has been designed and built. A double sided PLSM is used, specifications for which have been selected as close to the full scale one as possible such that the desired performance evaluation can be achieved. One side (referred as side A) of the motor is used to drive the slider, for which the hardware presented in chapter 9 has been implemented. The other side (referred as side B) of the motor is controlled to simulate the load conditions. An additional frequency converter (referred as AFC), its control microcontroller and required interface circuits has been developed for the load simulation.

In this chapter, the test rig is firstly presented in section 11.1. Section 11.2 explains how the controller developed in previous chapters has been adapted for the test rig. Section 11.3 shows how the additional converter is controlled to give the load simulation. Test results are presented and analysed in section 11.4 and a summary of the chapter is given in section 11.5.

11.1. Test Rig

11.1.1. Scaled Down Motor

The design of the motor was derived from the full scale motor with appropriate scaling in order to verify the control principles. It was decided to have one double sided motor instead of the two as in the pump. Each side of the motor produces a thrust of 2000 N and the design of the electrical and magnetic circuits was kept as close to the full scale motor design as possible. Figure 11.1 gives a photograph of the motor with the position transducer and switches installed. The main parameters of the machine are listed as follows:

Stroke length	1500 mm
Minimum time per cycle	1.429 s

Maximum velocity	4.20 m/s
Average velocity	2.10 m/s
Acceleration	11.76 m/s^2
Total mass of moving part	95 kg
Viscous friction coefficient	5 - 40 $N \cdot s/m$
Length of slider	1060 mm
Number of the magnet poles	6
Pole pitch	150 mm
Slot width	13 mm
Tooth width	12 mm
Slot depth	40 mm
Air gap	3.0 mm
Winding:	3 phase
	2 slots per pole per phase
	5/6 chorded
Armature resistance per phase (each side)	1.3 Ω
Self inductance per phase (each side)	32.0 ± mH
Mutual inductance per phase (each side)	-11.0 ± mH
Assumed equivalent current in slider	1.0 A
Peak mutual inductance between stator coil and equivalent circuit	1.61 H
Nominal Current (each side)	30 A
Frequency	0 - 14.0 Hz

11.1.2. Hardware of Control System

Chapter 9 has presented hardware design of the control system. Full implementation of the design has been realised on the test rig, where some of the components have also been scaled down accordingly.

Six GTO thyristers with their dedicated freewheel diodes, snubber capacitors, snubber resistors, snubber diodes and di/dt chokes as well as associated GTO firing circuits form the voltage source inverter. A d.c. link filter is connected to the output of a rectifier to provide a d.c. voltage of 600 V for the inverter. The main parameters of the inverter are:

Input:	3 phase, 50 Hz, 415 V
Output:	3 Phase, 0-14 Hz, 0-100A (max.), 0-400 V (line-line), 50 kW

A microcontroller card using the Intel 80C196KC chip has been made for implementation of the control algorithm. Its interfaces such as PIF, SIF and DIF cards have all been built as presented in the chapter 9. Figure 11.2 gives a picture of a rack with these electronic cards installed.

As the phase current of the motor is much smaller than that of the full size motor, current sensors with a lower range (LEM Module LC 100-S) were selected to give a similar accuracy of measurement. The sensor has a measurement range of $\pm 200A$ and turns ratio of 1:1000. By selecting a proper burden resistor ($R = 15\Omega$) for the sensor and adjusting the amplifier gain of the remote sensor module, the same sensor interface circuit can be used for the test rig.

Fibre optic links have been used between communication nodes for elimination of the effect of noise in the system. System management software has also been developed in a SUN workstation to supervise the operations.

11.1.3. Additional Frequency Converter

Because the additional frequency converter is used for testing in the laboratory only, the main approach for the hardware design was for simplicity, speed and effectiveness.

A BRUSH TOPDRIVE PWM transistor inverter was selected for the AFC. The inverter is a standard commercial product, which generates a sine-wave output with a frequency range of 0 - 381 *Hz* mainly used for open loop speed control of induction motors. The main parameters of the inverter are given as:

Input: 3 phase, 50 *Hz*, 415 *V*
Output: 3 Phase, 0-381 *Hz*, 0-87 *A* (max.), 0-400 *V* (line), 45 *kW*

This inverter can not be directly used for the test rig and some modifications have been performed to disable the original control unit and to incorporate customised circuitry which provides the power transistor switching logic interface and the sensor signal processing interface to a new dedicated control card. Figure 11.3 and 11.4 give a photograph of the inverter after modification and a block diagram of the AFC respectively.

An Intel EV80C196KC microcontroller evaluation board was selected for controlling the inverter rather than using the original control unit. It has an 80C196KC chip, 8K words and 8K bytes of user code or data memory, a UART for host communications, analogue input filtering and a precision voltage reference. Also included is programmable chip-select, bus-width and wait-state-counter logic. The board provides communications between the microcontroller's monitor program and a personal computer serving as a low cost development system. Object code can be downloaded from PC to the RAM of the emulator, and RAM variables and CPU registers can be monitored or changed from the PC.

In order to reduce truncation errors in deriving velocity and in particular acceleration from the position signals, it would be desirable to have a position transducer with better resolution. At the time when the AFC was being worked on, there was an incremental encoder (Hohner 6500 series hollow shaft encoder) available and thus it was adopted. The encoder together with a rack and pinion, installed on the motor as shown in Figure 11.1, performs a linear measurement. Like the linear transducer, the encoder has two output signals with a 90 degree difference. It gives 800 pulses per revolution and a complete rotation of the encoder covers 188.4 *mm* of the rack. By using the interface circuit given in Figure 9.5, the resolution is quadrupled to give:

$$\text{Resolution of position encoder} = 800 \times 4 / 0.1884 = 16985 \text{ pulses/meter}$$

Timer 2 of the 80C196 is used to count the pulses for the measurement, and the two encoder outputs are connected to two pairs of High Speed Input (HSI) in order to detect every rising and falling edge of the pulses and to set an interrupt request which is served to detect moving directions for the Timer 2 counting up or counting down.

The same current sensors as those for side A are used for current measurement, however the on-chip A/D converter of the 80C196 is used to convert the analogue signals into digital format. An interface circuit consisting of an amplifier, a second order low pass active filter and a level shift for each channel is used in order to reduce the noise effect and to transfer the input signal into a proper level for the A/D converter. Figure 11.5 gives a diagram of the interface.

Interlocking logic interface was designed to allow switching delays for each transistor complementary leg, as shown in Figure 11.6. The inverter can be disabled by either the embedded current protection unit or a manually controlled switch. The dynamic brake unit is used to absorb regenerated power when the side B of the machine works in generation mode, which is controlled via HSO.3 of the microcontroller.

To synchronise the operation of the two sides of the motor, a serial link with RS-422 drive is used for communications between the two microcontrollers. Modification of the control software for the side A was also necessary in order to send start and stop commands to the microcontroller of the AFC side via the serial link.

11.2. Controllers

As some parameters of the scaled down motor are different from those of the full size one, the gains of all control loops have to be re-tuned in order to achieve the same bandwidth and performance of the pump system.

11.2.1. Current Loop

It has been demonstrated in the computer simulation that the controller with the closed loop time constant of 5 *ms*, i.e. bandwidth 30 *Hz*, appears to be the best choice for the current loop. To obtain the same characteristics for the scaled down system, PI gains G_p=4.0 and G_i=66.67 have been selected. Table 11.1 gives the frequency response of the current loop when these two gains are applied. Again it is compared with an ideal first order model with the time constant of 5.0 *ms* as given in the right hand side column of the table.

Table 11.1. Frequency Responses of Current Loop

	$v =$ 0		$v =$ 4 *m/s*		First order
	Amp. (*db*)	Phase (°)	Amp. (*db*)	Phase (°)	(5.0 *ms*)
1	0.108	0	0.11	0	0.0 (-1.8°)
5	0.496	-8.1	0.348	-5.4	-0.11 (-8.93)
10	0.217	-18.0	0.19	-14.4	-0.41 (-17.4)
20	-1.085	-32.4	-0.439	-28.8	-1.44 (-32.1)
40	-3.954	-51.84	-3.233	-51.84	-4.12 (-51.5)
100	-10.586	-72.0	-11.363	-72.0	-10.4 (-72.3)
500	-24.26	-84.6	-24.41	84.6	-23.9 (-86.4)

11.2.2. Position and Velocity Loops

The position control gains do not need to be changed if the characteristics of velocity loop are maintained. This can be achieved with G_{vp}=4.0 and G_{vi}=66.67. The velocity feedforward term is still 1 and the acceleration feedforward term depends on the sum of the slider and the simulated masses.

Since the bandwidth of every loop follows the previous design, it is reasonable to use the same sample periods, i.e. 1.5 *ms* for the current loop and 4.5 *ms* for the position and velocity loops.

11.3. Control Strategy of Load Simulation

In order to simulate the load conditions of the pump system, side B of the linear motor is used to generate load forces. The control of the force is equivalent to the control of the motor current, because the force produced by the PLSM is proportional to the q axis current. On the other hand, a current controller has been designed for the inner loop of side A and both sides of the motor are identical, therefore the controller was directly adopted for side B and no additional work was required in this respect. The remaining work was to generate force references as input signals of the controller, which depend on the load characteristics to be simulated. Two kinds of the load have been implemented in the test:

- Stiffness. In stages 1 and 2 of the pumping operation, high stiffness appears in the system due to the compressibility of the gas and oil, the values of which depend on the ratio of the gas and oil mixture. To simulate the stiffness, the position measurement is used to generate the input signals. At the beginning of each stroke, the reference input is proportional to the position until a defined maximum value is reached where the input is set to be constant to simulate the load in stage 3. The different increase rate of the opposing force represents the different ratio of the gas and oil mixture.

- Mass of Fluids. This is to simulate the effect of the mass of the fluids being pumped. In this case, the load force is controlled proportional to the acceleration of the slider, where the proportional ratio represents the value of the mass. The acceleration is derived from the position encoder. Although the encoder has better resolution than that used for side A, truncation noise still appears in the acceleration signals and a low pass digital filter with bandwidth of 30 *Hz* is used in the software to reduce the noise.

It should be noted that for two reasons the test rig can only partly simulate the load conditions. Firstly, the power of the motor is limited such that the load force has to be scaled down. Secondly, a delay is introduced by the current controller due to the limited bandwidth of the controller and the effect of the low pass filter. However, the work can prove the design of the real time control system, both software and hardware, and support the results obtained in the computer simulation.

11.4. Test Results and Evaluation

The test is started from the auto positioning operation every time the power of the system is switched on in order to find the initial position of the slider. The outcome is satisfactory and the software does 'find' the position successfully as expected. In the normal pumping operation, the speed is ramped up to the required speed when a start command is received or a higher speed is requested (note that the speed is defined as number of cycles per minute in the system). Figure 11.7 is a diagram showing the slider velocity and position during the ramp up. When a stop or a lower speed is requested, the speed is ramped down.

The test results of the closed loop control are presented in following sequence. Firstly, the test is carried out with no load applied. The results of the cascade controller with feedforward term(s) and the optimal tracking controller are presented and the performances of the different controllers are compared. The test results are also compared with the computer simulation. Secondly, the stiffness is generated by using the additional frequency converter and the performance of the designed controller is assessed. Finally, the mass of the fluids is simulated and test results are presented and compared.

11.4.1. Test Results with No Load

Figure 11.8 shows the position and velocity of the slider where the peak velocity is 2.0 *m/s*, which follow the trajectories well. At the same speed, Figures 11.9 to 11.11 compare the control errors of three controllers. In Figure 11.9, the controller with the velocity feedforward term shows a reasonable tracking performance with the maximum position error of 2.5 *mm* and near zero steady state error. The maximum error occurs at the midpoint of every stroke where the sign of the acceleration reference changes. This error can be improved by introduction of the acceleration feedforward as shown in Figure 11.10. For a comparison, the control error of the optimal tracking is also given in Figure 11.11. The optimal controller has larger errors and in particular presents a steady state error.

From these diagrams, it can be observed that the control errors are not symmetrical; larger errors occur on the second half of the stroke length, which is in fact the physical centre of the motor. This extra error is caused by a mechanical design fault. The body of the stator is not rigid enough to resist the attractive force of the magnetic field produced by both the permanent magnet and the stator current, which attracts both sides of the stator and bends the stator to press the slider. This problem becomes more severe when the slider is at the centre of the stator and an extra load force is applied on the slider as a consequence. The test results show that this extra load force has more effect on the optimal controller and less effect on the cascade controller. This means that the disturbance rejection capability of the cascade controller is better. However, this problem is not expected on the full size motor as it has been considered in the design and manufacture.

The test has also been carried out at the maximum speed, i.e. the peak velocity 4.2 *m/s*. Figure 11.12 presents the measured position and velocity of the slider, which shows a good tracking performance. Figures 11.13 and 11.14 give the reference q axis current and the q axis feedback current respectively to assess the performance of the current control loop. Except for the high frequency noise, little difference between the two can be observed and the response of the controller is very satisfactory. As the reference q axis current is proportional to the control signal of the outer position and velocity loops and the motor q axis current is proportional to the force produced by the motor, the preciseness of the inner controller ensures the performance of the outer loops.

Figures 11.15 to 11.17 are the control errors at the maximum speed, which show similar patterns to those in Figures 11.9 to 11.11. Cascade control with a velocity feedforward term gives a maximum error of 12 *mm*, and the error at every stroke end is near zero. The error of the cascade controller with the velocity and acceleration feedforward terms is less than 4.0 *mm*. The control error of the optimal tracking controller is around 10 *mm* and this large error at the stroke end is not acceptable for the system.

To verify the simulation models developed in previous chapters, the parameters of the scaled down motor have been input into the simulation program instead of the full size motor and the simulation results have been used to compare with the practical results given in Figures 11.18 to 11.22, where a peak velocity of 4.2 *m/s* and cascade control with velocity feedforward term were used in the simulation. At this point, it should be emphasised that the simulation represents more or less an ideal situation although some practical factors such as truncation errors of the feedback signals have been included.

Figure 11.18 is the control error obtained from the simulation. Compared with that given in Figure 11.15, the two position errors agree closely and the performances are basically the same: the maximum error occurs at the midpoint of every stroke with the simulation error slightly lower, the transient period is the same and the steady state error is near zero. The mechanical problem of the motor was not included in the simulation and thus its effect does not appear on the simulation result.

Figure 11.19 and 11.20 give the q axis currents obtained from the test and simulation respectively and Figure 11.21 and 11.22 show the red phase currents of the motor from the test and simulation respectively. Except for the extra current required to overcome the load force caused by the mechanical problem, these waveforms are virtually the same. Therefore it is fair to conclude that the developed simulation models can effectively represent the real system.

11.4.2. Test Results in Presence of Load

As mentioned earlier, the power of the scaled down motor is very limited. To perform the test in the presence of load, the maximum velocity of the slider was reduced to 3.0 *m/s*. The simulation has shown that only the cascade controller would have a reasonable performance under load, and so the test was only carried out for this controller.

The second frequency converter and the relevant software have been developed to generate various load forces via controlling the currents in the motor side B. Figures 11.23 to 11.24 show the currents with different rates of increase at the beginning of every stroke to simulate different stiffness (these are referred to as Force 1 and Force 2 respectively). Just as that for side A, the current controller shows a good performance and the current follows the required trajectories well. The proportional ratio between the q axis current and the motor force is 50 and therefore the opposing force at the peak of the waveforms is 1000 *N*. In Figure 11.25 the load force was made proportional to the slider acceleration, which simulates a mass of 100 *kg*. It can be seen that an oscillation on the acceleration signal occurs at the first half of every stroke in Figure 11.25. The reason has not yet been identified and further study is needed. The same oscillation is not seen on the other half stroke, and so the control system design and its implementation software can be excluded as the cause.

Figure 11.26 shows the control error with no load, and Figures 11.27 and 11.28 show the control errors where Force 1 is applied by the second frequency converter with maximum forces of 500 and 1000 *N* respectively. Because the load force has a relatively rapid increase at the beginning of every stroke, the control error increases with the load. The transient period lasts for about 0.33 *s* and the steady state error at the stroke ends is not affected by the load force.

Figure 11.29 gives the control error where Force 2 is applied. The increase of the load force is slower and its period is longer, thus the peak error is smaller but the transient period of the controller is longer. The controller reaches the steady state and the error is near zero before the stroke ends, which meets the design requirement.

Figure 11.30 shows the test result where the mass of the fluids is simulated. This time, the error at the midpoint of every stroke is increased due to the increased mass. The control error is compensated by the controller and reduced to zero in a short transient period of about 0.3 *s*.

11.5. Summary

This chapter has presented the implementation of the real time control carried out on the scaled down double sided permanent magnet linear motor, where one side of the motor has been used to drive the slider and the other side has been used to simulate the various load conditions. A second frequency converter has been developed to perform the task of load simulation.

The test was firstly performed with load force. The cascade controller with velocity feedforward, the controller with both velocity and acceleration feedforward terms, and the optimal tracking controller have been implemented. The results have indicated that the cascade controller has better performance than the optimal tracking one, and that acceleration feedforward improves the control accuracy.

In the presence of the loads, the position errors of the control system are increased but compensated by the controller before the slider reaches the stroke ends. Near zero position errors at the stroke ends have been achieved by the controller. The overall performance of the system is satisfactory and meet the design specification.

The performance of the inner current control loop has been evaluated by the test, which has shown that a tight inner loop has been achieved by the PI control with the command feedforward. The test results have also been compared with those from the simulation in order to verify the simulation models developed in the previous chapters, and these have demonstrated the validity of the simulation model.

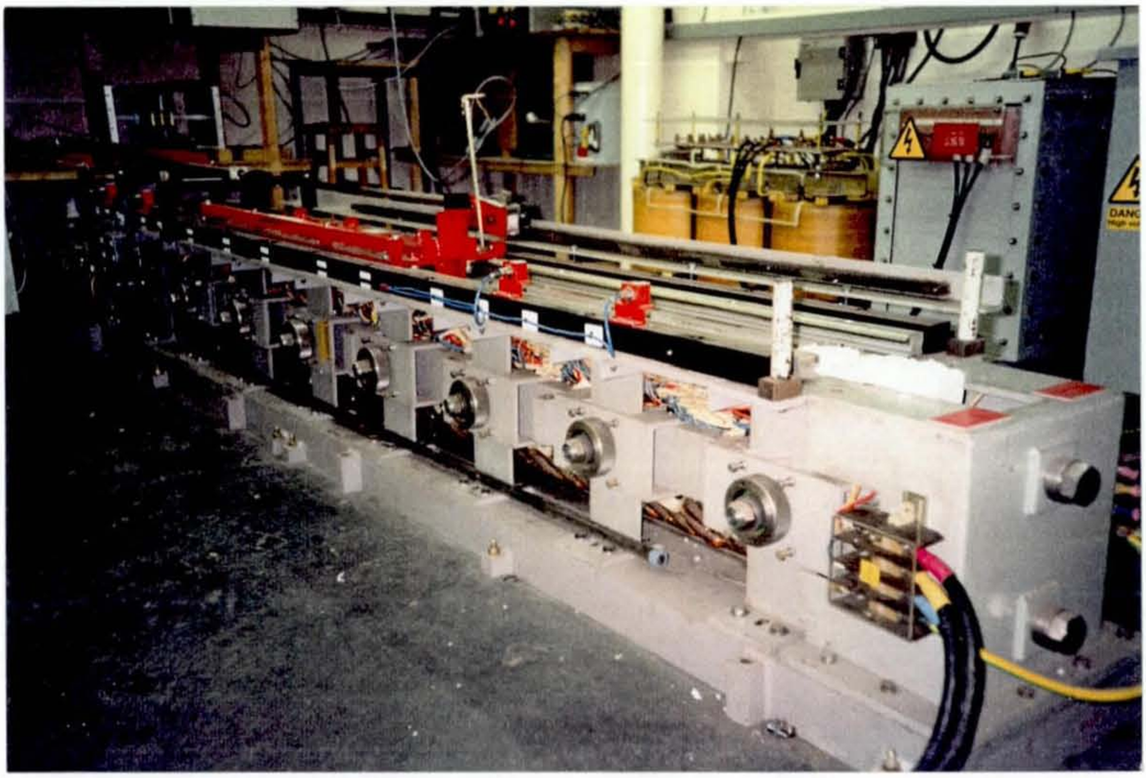

Figure 11.1. A Picture of Scaled Down Motor

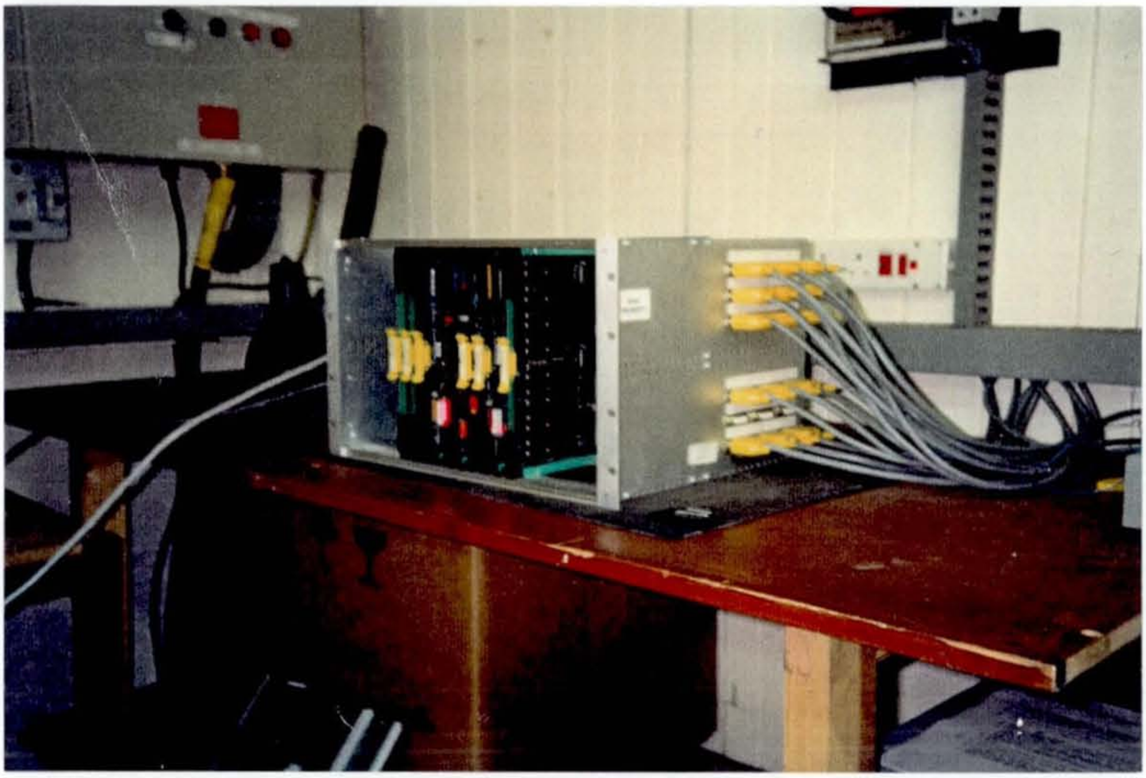

Figure 11.2. A Picture of Electronics Rack

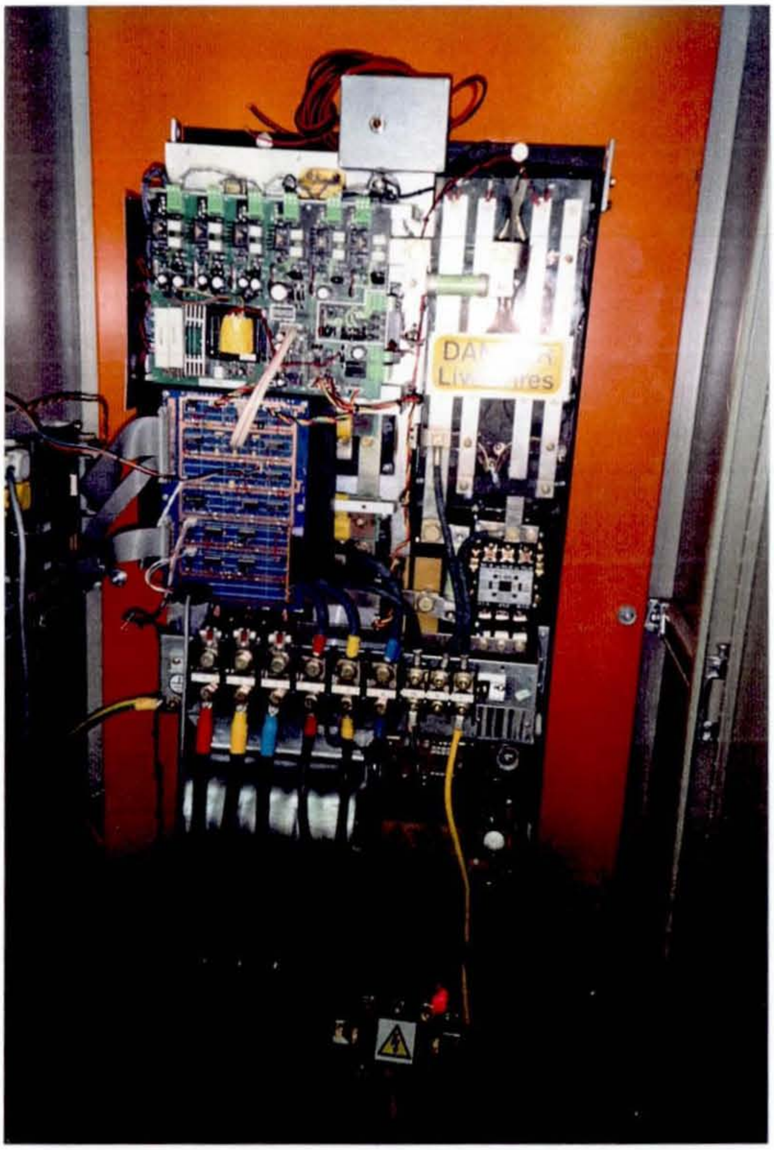

Figure 11.3. A Picture of AFC

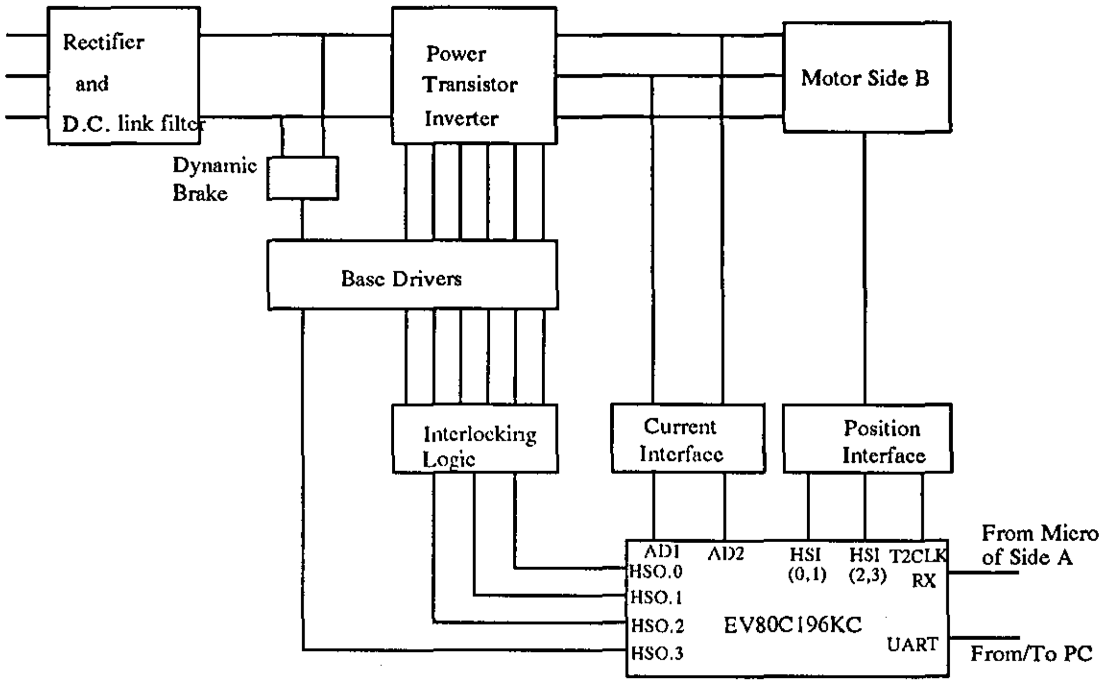

Figure 11.4. Block Diagram of AFC

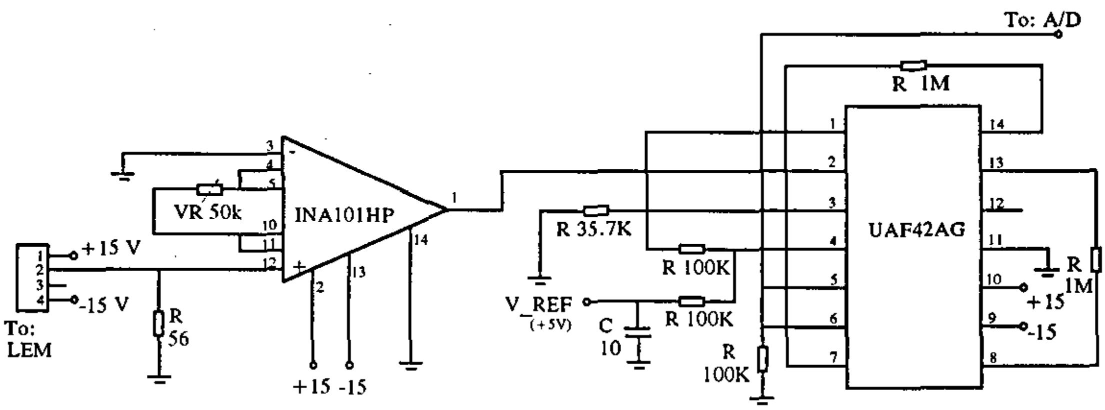

Figure 11.5. Diagram of Current Sensor Interface

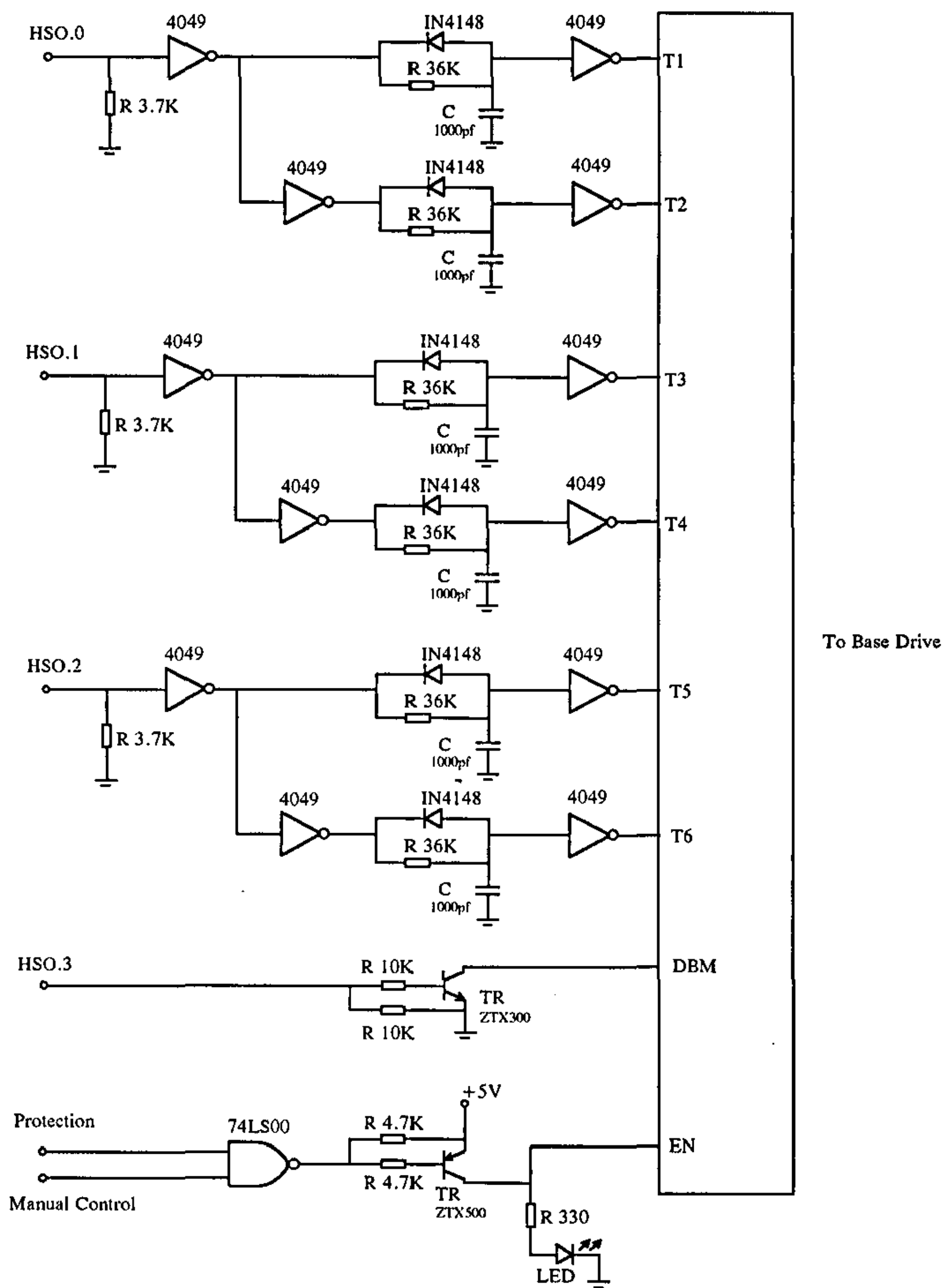

Figure 11.6. Diagram of Interlocking Logic Interface

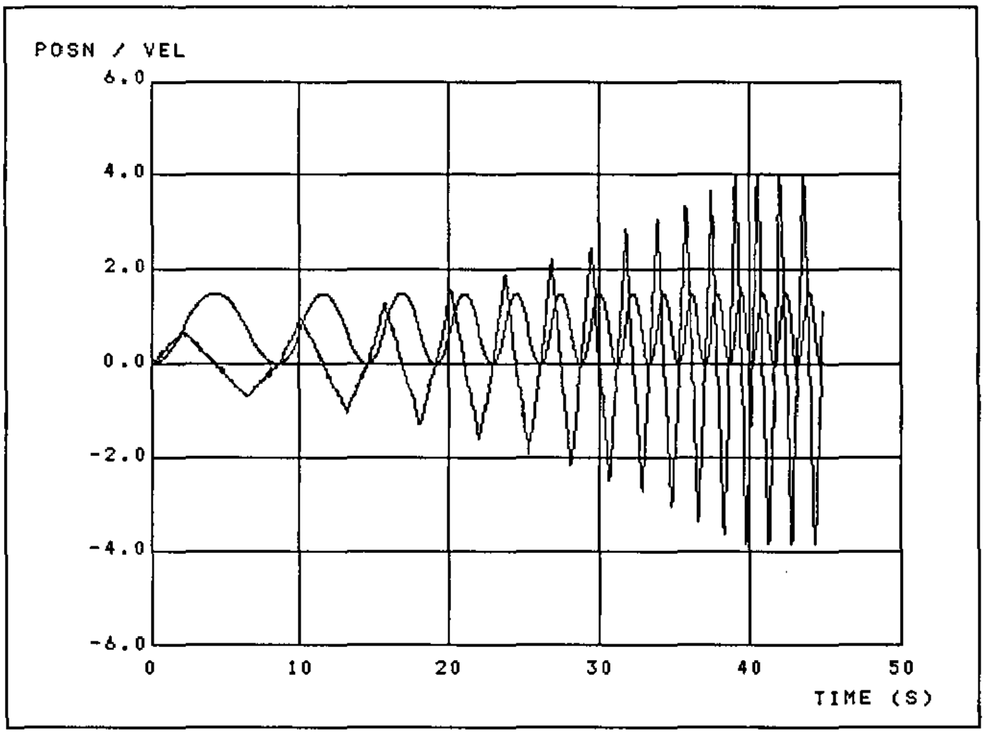

Figure 11.7. Ramp Up of The Pump Speed

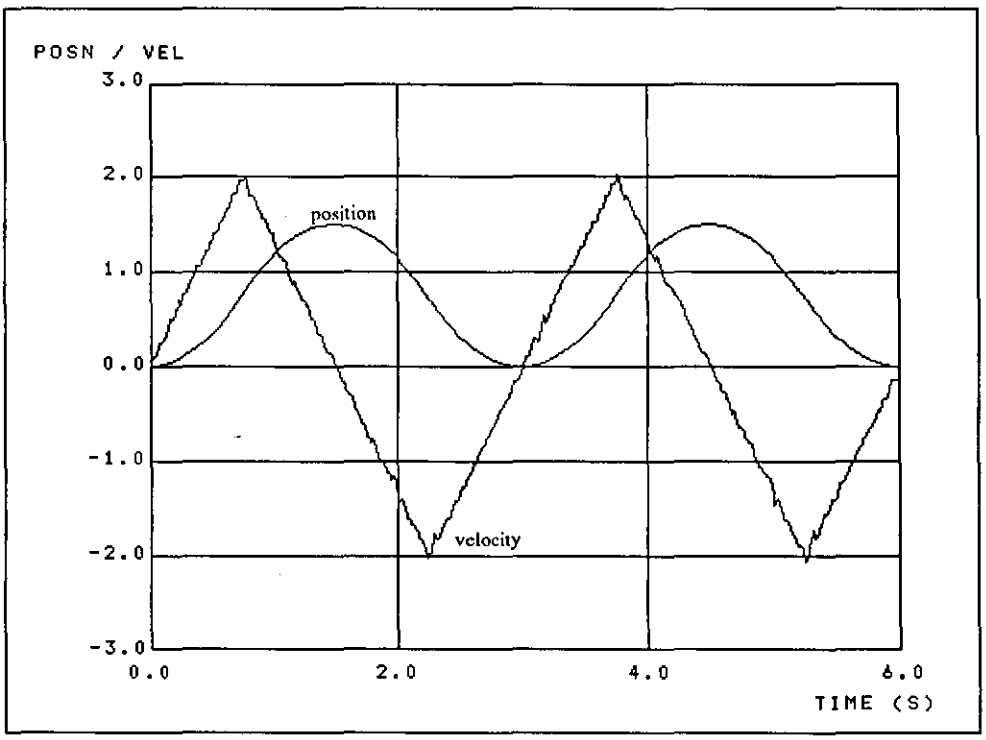

Figure 11.8. Test Results ($v_{TOP} = 2.0 m/s$)

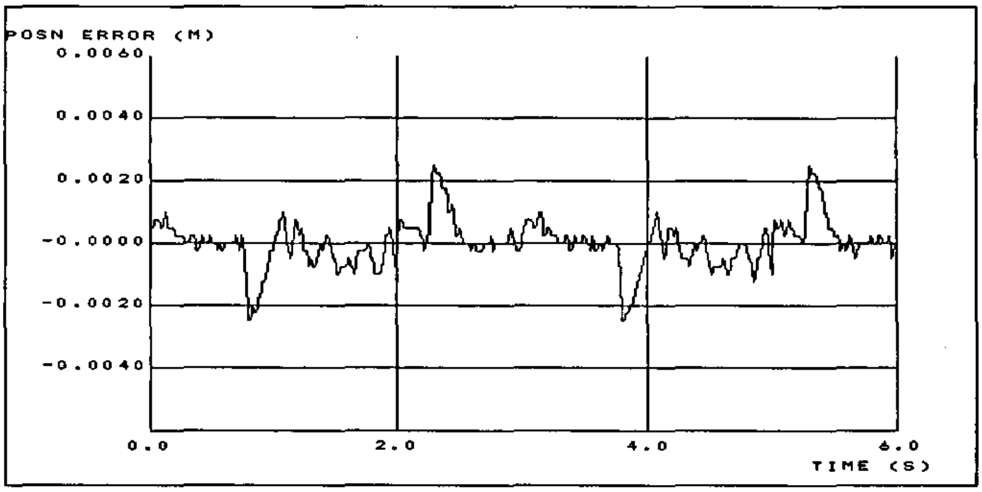

Figure 11.9. Control Error ($G_{af} = 0$)

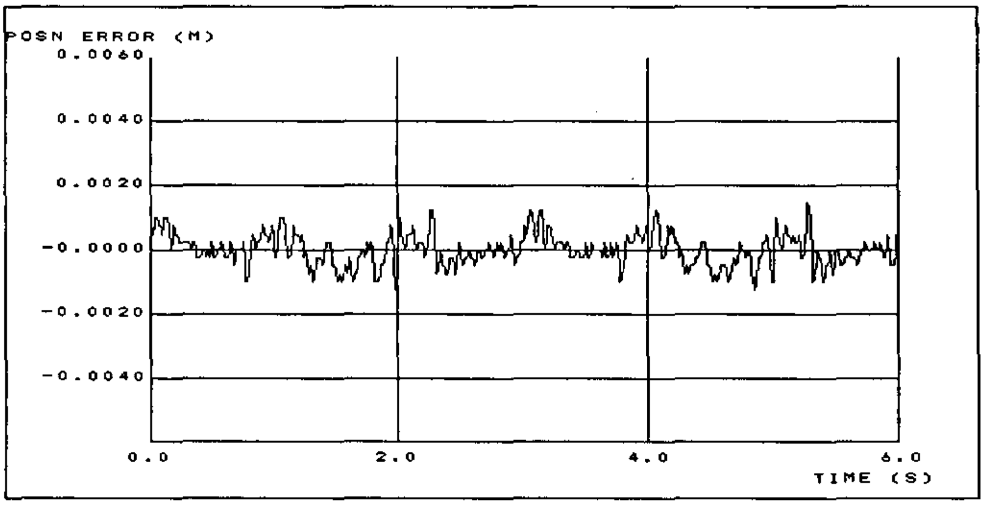

Figure 11.10. Control Error ($G_{af} = 100$)

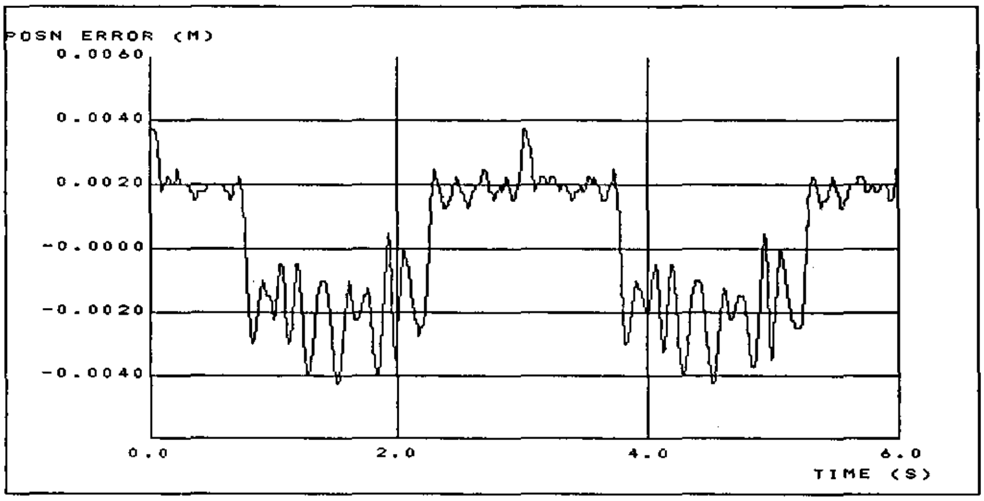

Figure 11.11. Control Error (Optimal Tracking)

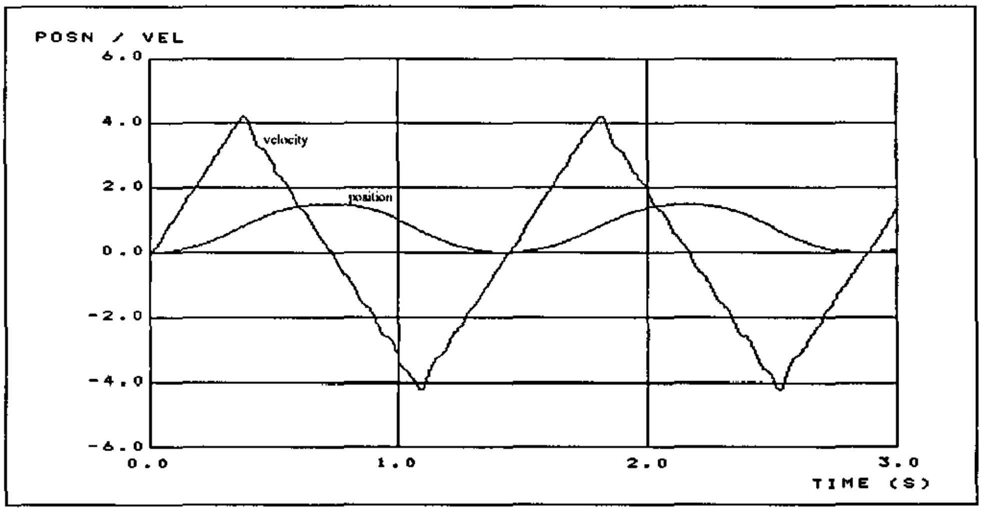

Figure 11.12 Test Results ($v_{TOP} = 4.2m/s$)

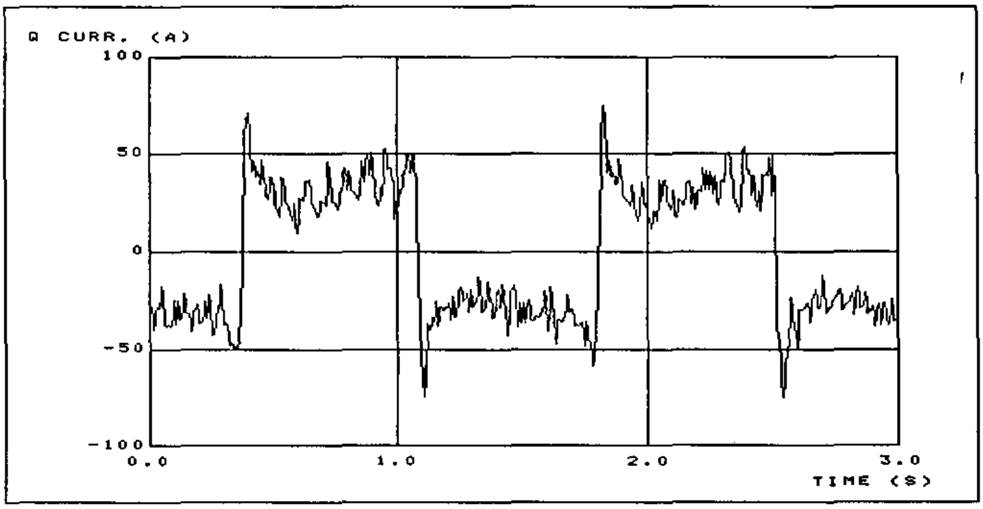

Figure 11.13. Reference Q Axis Current

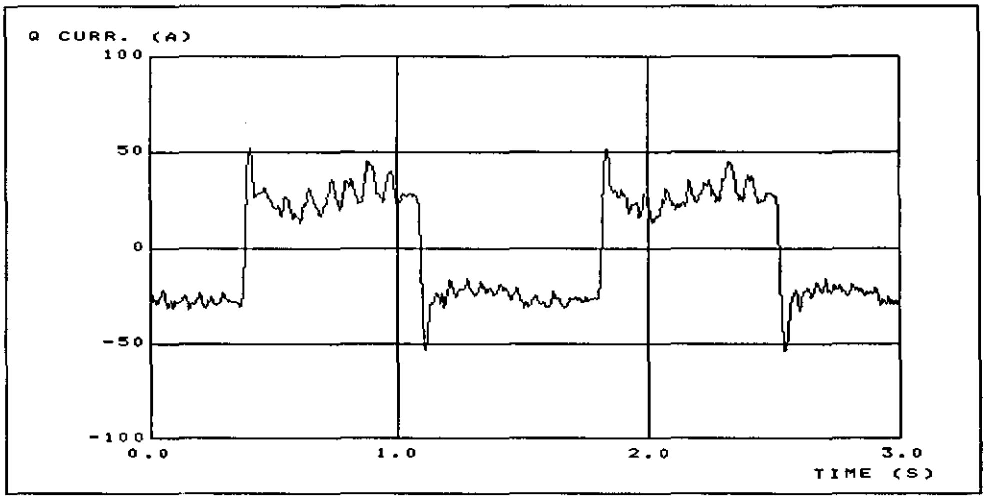

Figure 11.14. Q Axis Current

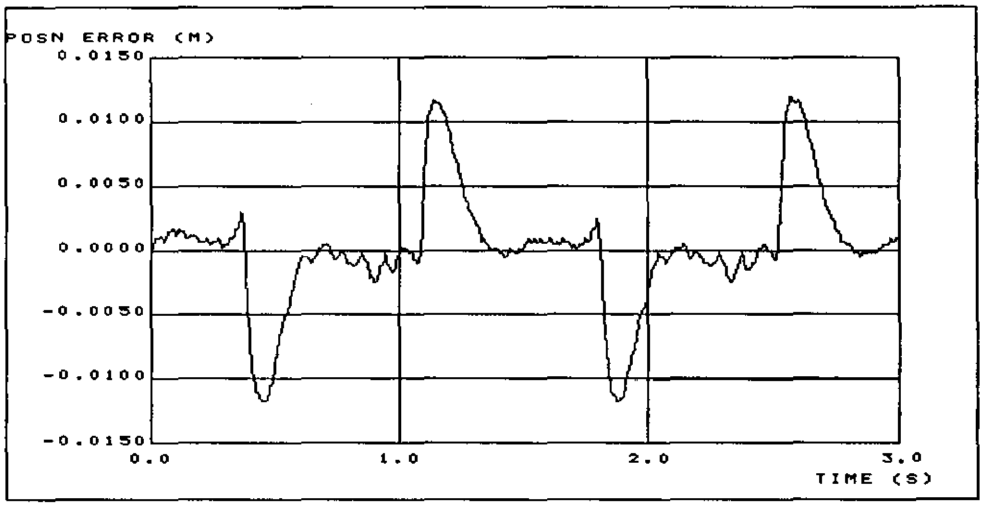

Figure 11.15. Control Error ($G_{af} = 0$)

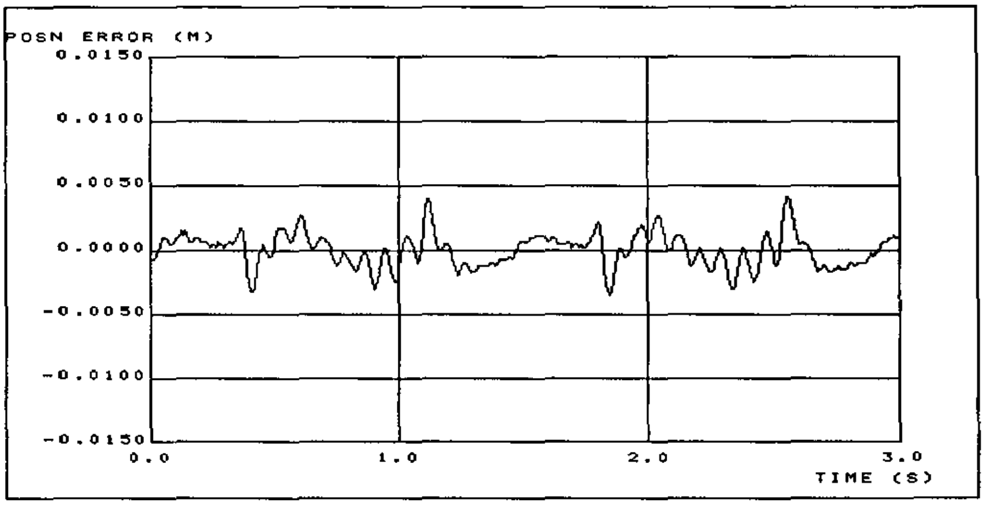

Figure 11.16. Control Error ($G_{af} = 100$)

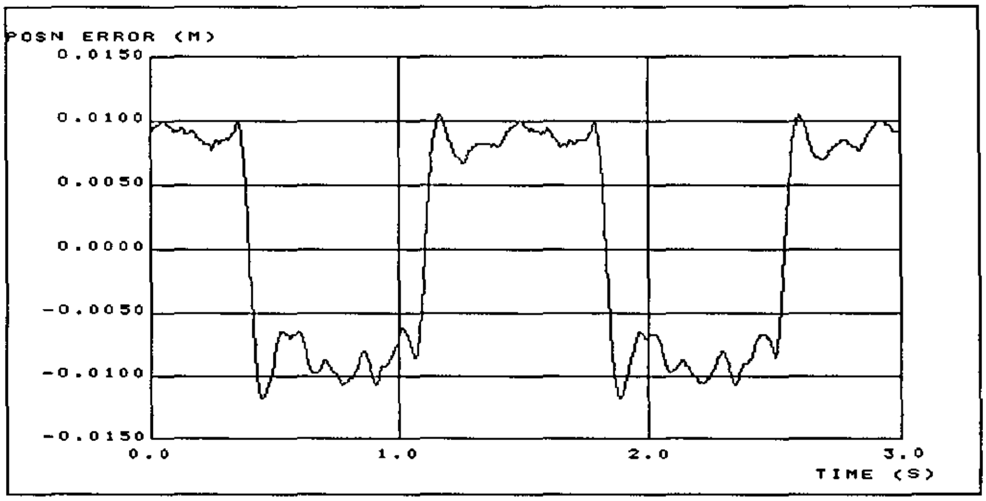

Figure 11.17. Control Error (Optimal Control)

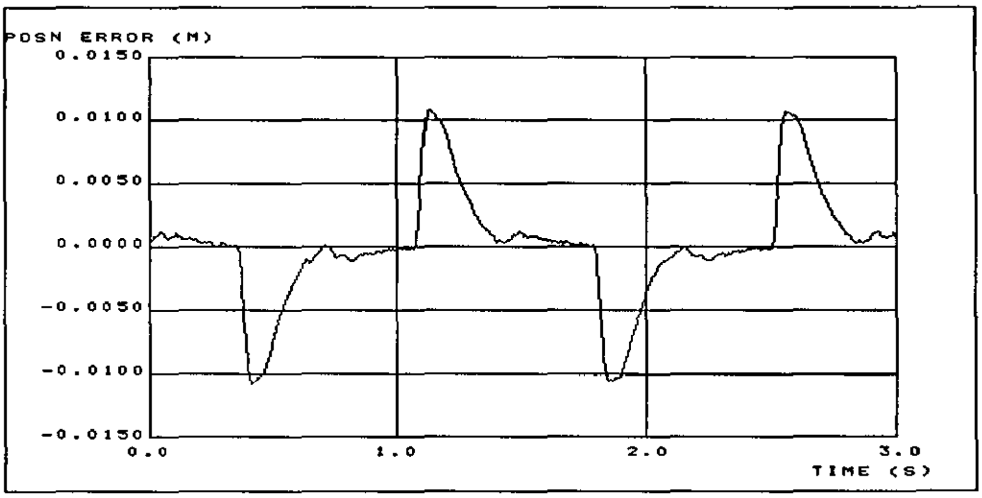

Figure 11.18. Control Error (Simulation Result)

Figure 11.19. Q Axis Current (Test Result)

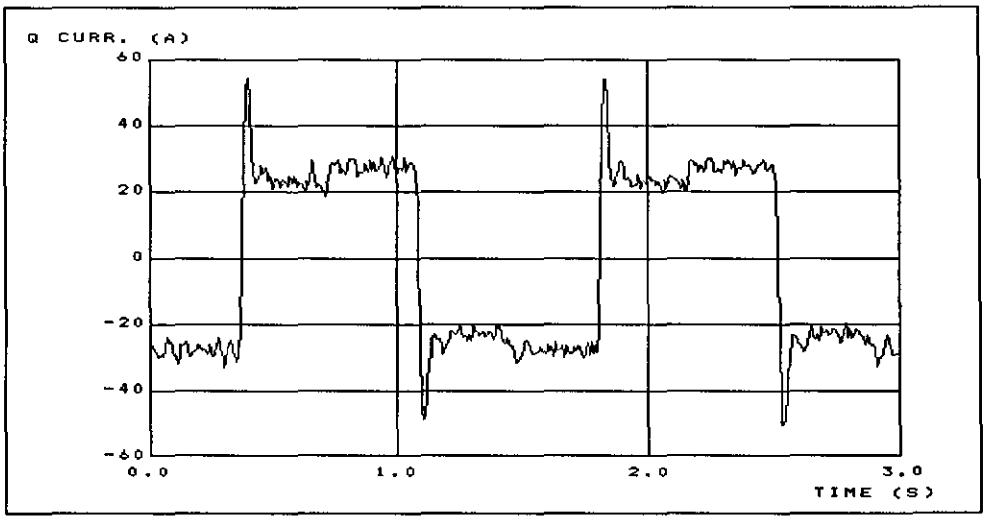

Figure 11.20 Q Axis Current (Simulation Result)

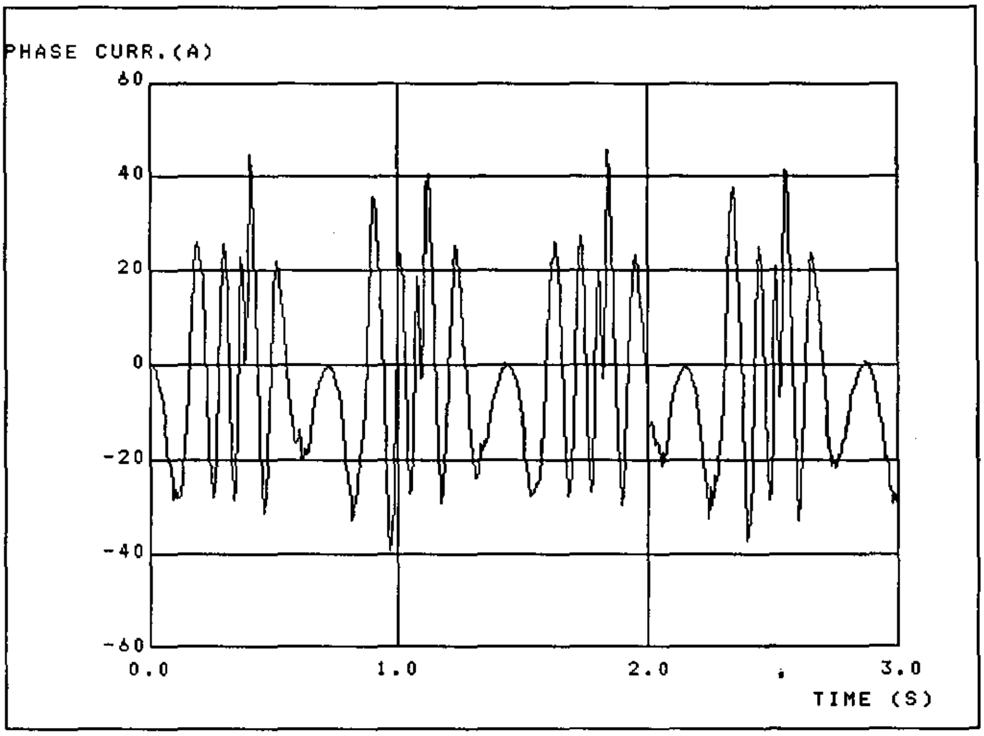

Figure 11.21. Red Phase Current (Test Result)

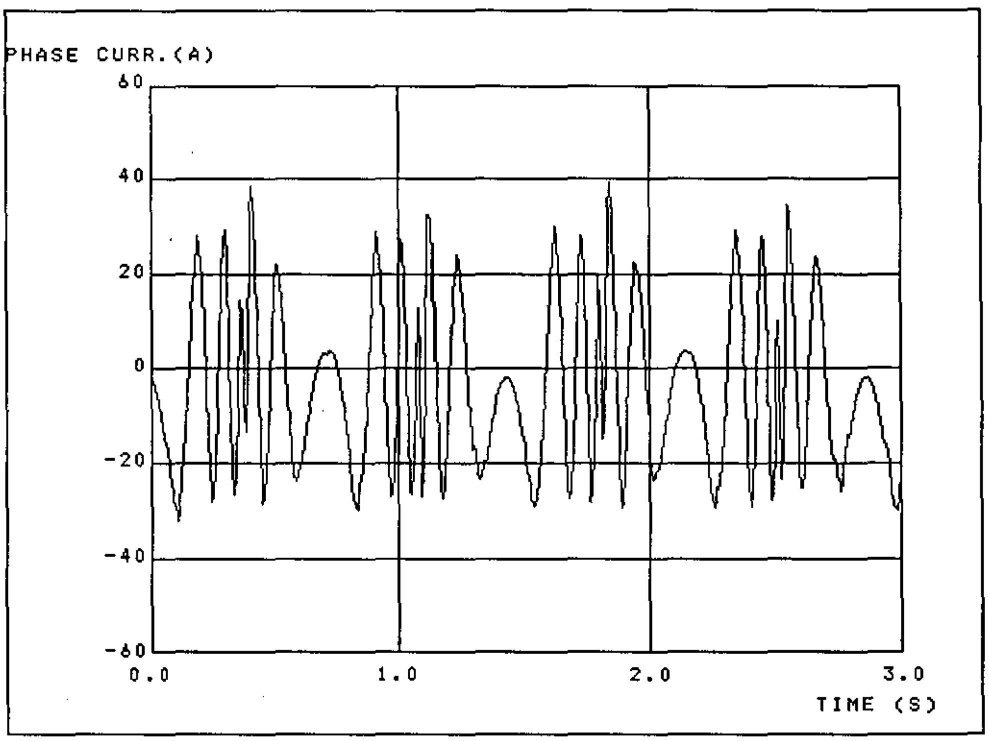

Figure 11.22. Red Phase Current (Simulation Result)

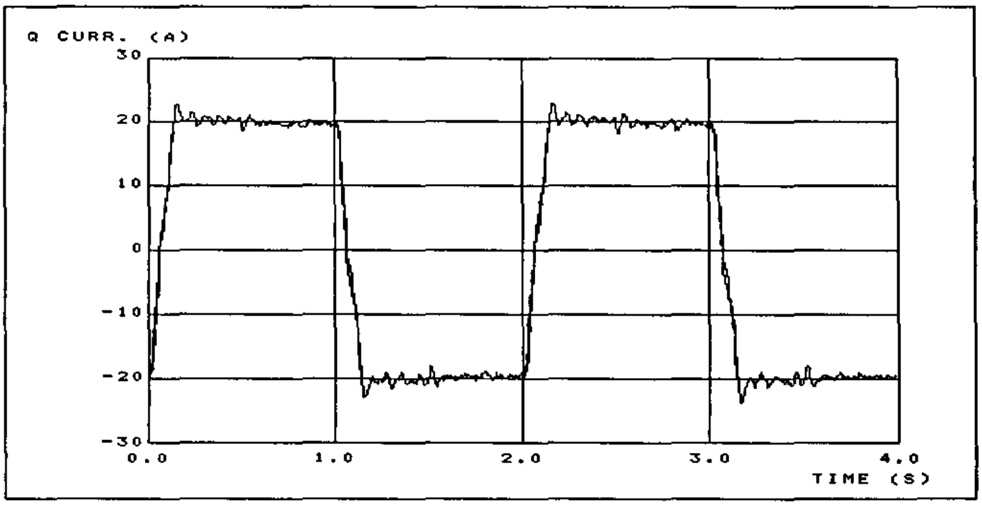

Figure 11.23. Q Axis Current of AFC (Load Force 1)

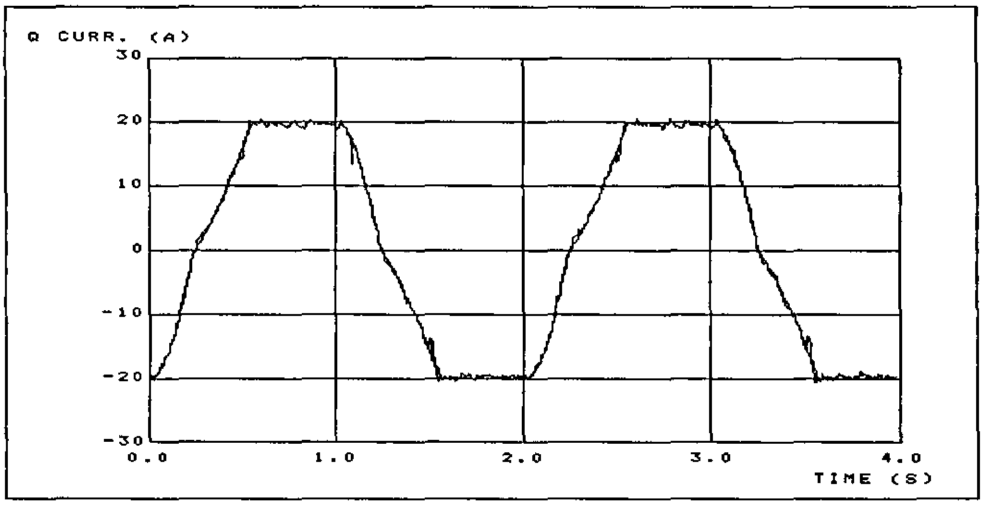

Figure 11.24. Q Axis Current of AFC (Load Force 2)

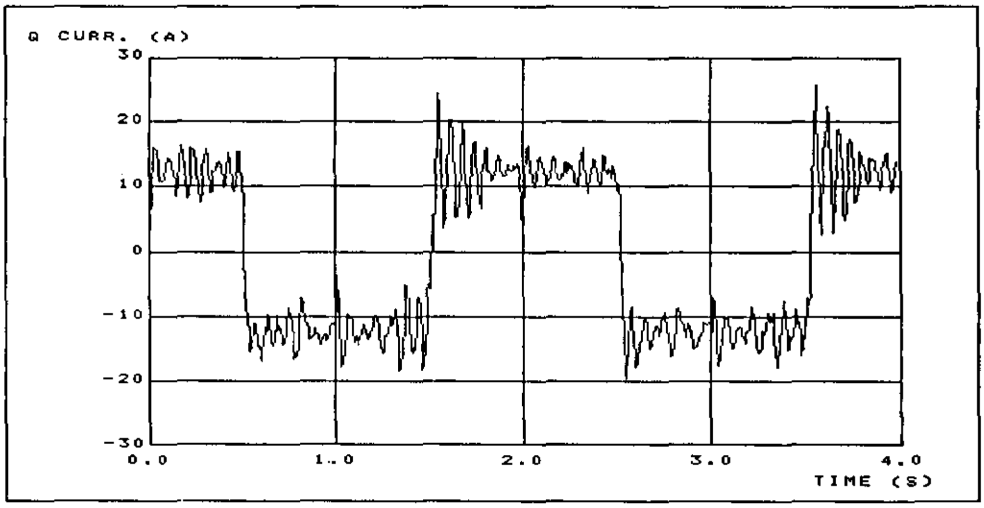

Figure 11.25. Q Axis Current of AFC (Load Force 3)

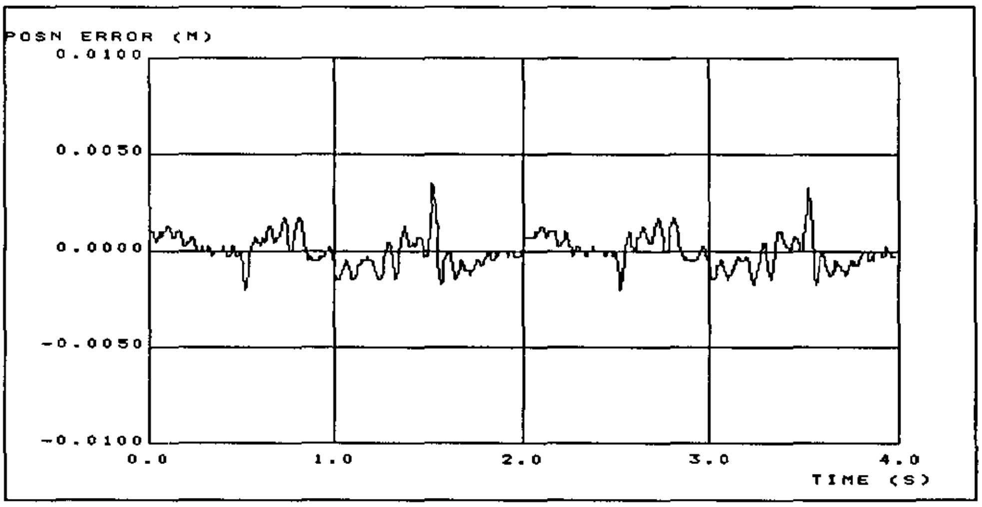

Figure 11.26. Control Error (No Load)

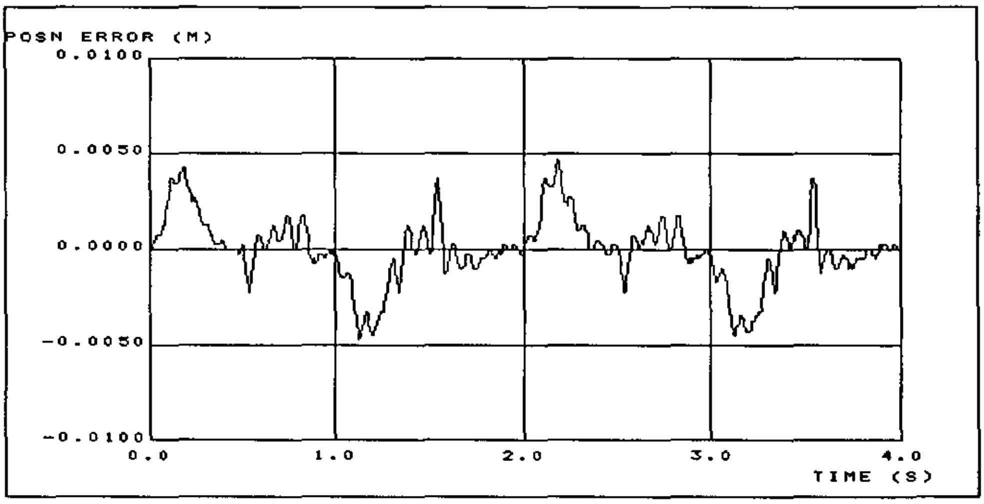

Figure 11.27. Control Error ($F_1 = 500N$)

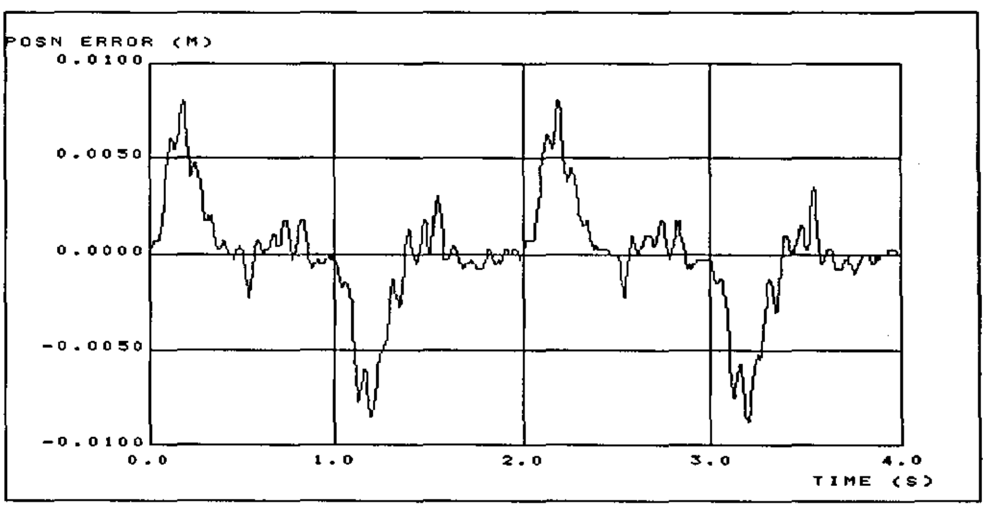

Figure 11.28. Control Error ($F_1 = 1000N$)

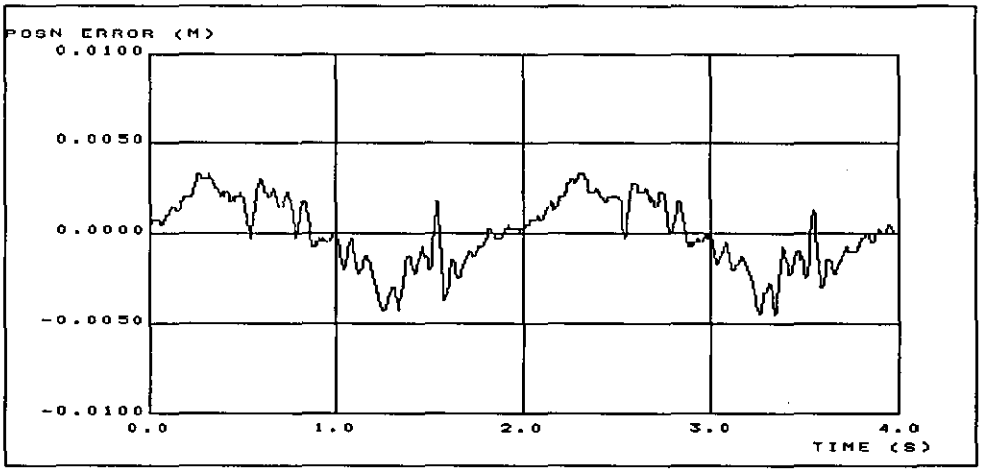

Figure 11.29. Control Error ($F_2 = 1000N$)

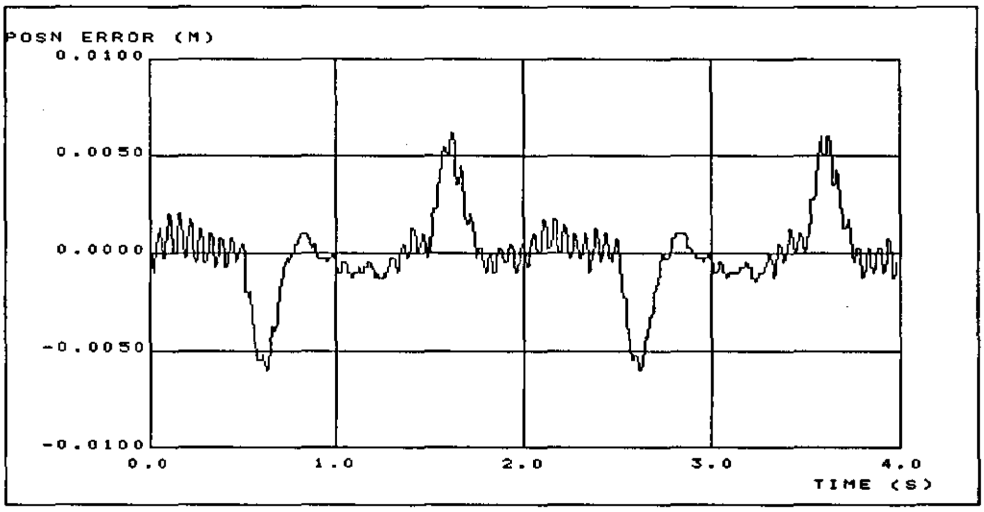

Figure 11.30. Control Error ($m = 95 + 100kg$)

CHAPTER 12.

CONCLUSION AND FURTHER WORK

This thesis has presented the simulation and design of the control system for the subsea electric pump driven by double sided permanent magnet linear synchronous motors, and it has demonstrated that the required performance of the system has been achieved by designing a conventional cascade controller with feedforward terms and an inner vector control scheme. The real time implementation of the system has been performed based on a scaled down motor to prove the validity of the controller. Using the work presented in the thesis, a prototype system using the full size motor is under development, and testing of the system is expected to be carried out in Texas, USA, later in 1994.

In this thesis, the simulation model of the pump and the motor has been developed. The modelling of the pump is based on the fundamental theory of fluid mechanics, where a non linear model and a distributed parameter model have been established for the pure gas and the pure oil cases respectively. The two models are necessary for the computer simulation in order to assess the characteristics of the system, however the non linear and distributed parameter models are not preferred for the control design as most design methods are based on linear models. Thus the open loop simulation using these two models has been carried out and a linear second order model with bounds on its parameters has been derived from the simulation results. Since these two models represent the two extreme cases of the system and the characteristics of any mixture of the gas and oil are in between, the bounds of the simplified model have also been obtained.

In the modelling of the linear motor, a parameter test has firstly been carried out. Two models have been developed using the test results, which are the three phase model and the d-q axis model. The three phase model represents the motor in a way directly related to the physical machine and demonstrates the relationships between the three phase voltages, the three phase currents and the permanent magnets. The d-q axis model using the Park transform exposes the relationship between the motor current, flux and produced force such that the design of the current control loop becomes more apparent.

Having obtained the system models, the design of the control system was partitioned into two steps: firstly the current control as it is the innermost loop, and then the position and velocity loops. A PI controller with command feedforward term has been designed for the inner loop, where the computer simulation was used to help the design of the control gains for the required bandwidth of the inner loop and to assess the performances. It has been shown that a 30 *Hz* bandwidth for the current loop is a reasonable choice. As part of the vector control, the effect of the load angle on the performance of the system has also been studied. By controlling d axis current appropriately, the voltage, VI rating and power factor of the motor can be improved with little increase in the motor current.

Three controllers have been studied for the position and velocity loops: cascade control, internal model control and optimal tracking control. The former two controllers have been designed in the frequency domain, and the latter in the time domain. The stability, robustness and overall performance of the three controllers were initially evaluated using a design package SIMBOL. It has shown that the cascade controller with feedforward terms is the best choice for the system.

It must be stressed that the aim of this thesis was to find a solution for the system, and the outcome has been very successful. However the preference for the cascade controller does not necessarily deny the usefulness of the other two or any other controllers. The methods presented in this thesis for the designs of the internal model and the optimal tracking controllers are two of many design methods, and it is always possible to find a controller with a different structure to achieve the same task. In addition, since H^∞ control shows a general robustness to both the structure and the parameter uncertainties and it has not been studied in the thesis due to the limited time, it is thought worthwhile to study the possibility of using such a controller for the system in the future.

Full computer simulation has been carried out to examine the performance of the entire control system in detail. Selection of the sample periods for the inner and outer control loops was finalised by using the simulation. It has been shown that the sample periods of 1.5 *ms* for the inner current loop and 4.5 *ms* for the outer position and velocity loops seem to be the best compromise for the system. The simulation has shown that the dominant factor affecting the system performance is the total equivalent mass, which varies with the actual mixture of oil and gas. The derived controller has demonstrated stability in all cases and robustness against the uncertainty. The control accuracy in all simulations is better than required. The acceleration feedforward term improves the performance and a value based upon the average of the masses of the highest and the lowest bounds is recommended.

Real time control software and hardware for implementation of the designed controller have been developed. A test rig using a scaled down double sided PLSM has been built, where one side of the motor was used for driving the motor and the other side was used to simulate the load conditions. The test has proved the design of the control system and the test results have shown the general agreement with the simulation. When the load is applied on the motor, the position error is increased but compensated by the controller very quickly, and the near zero steady state error has been achieved before the slider reaches the stroke ends.

The practical test has proved that both speed of the microcontroller and accuracy of the software algorithms are good enough to handle the control task. The performance of the system is very close to that predicted in the computer simulation. Therefore there is no need to change either the processor or the fundamental algorithms, although some improvement of the software would be useful in the future to make it more readable and efficient.

The accuracy of the feedback signals is of vital importance for the system performance. Measurement of the motor current is not a problem and high accuracy can be easily achieved, but care must be taken with the position measurement. The resolution of 0.25 *mm* seems sufficient, but the transducer itself is not ideal although the problem of the initial position has been resolved by the development of an auto positioning operation. Firstly, noise and possible loss of output pulses may be integrated to cause position drift and an extra datum may be needed to solve the problem. An alternative solution could be the use of an absolute position sensor, because high resolution absolute position transducers for a high pressure environment have recently become available. Secondly, the position of the slider is measured and processed by a dedicated microprocessor and then transmitted to the microcontroller of the motor control, so it requires a fast and reliable data communication system, otherwise false messages or excessive delays of the feedback would cause system instability.

A number of recent publications have shown the possibility of controlling permanent magnet type motors without position sensing [72-75]. By using a state observer, two line to line voltages and two stator currents of a motor are sensed and processed to obtain the necessary position and speed information to replace the mechanical sensor. The principle has been implemented on some speed controls in laboratories, but its performance has been less than desirable. However it gives a prospect for the motor drive systems in the future and indicates one direction for future work.

In summary, this thesis has covered a number of aspects of the system and the design requirement has been achieved. The future prospects for the project are very promising and successful results are expected from the USA tests. In addition, the work presented in the thesis has demonstrated the feasibility of high performance control of permanent magnet linear motors which could apply to a number of other applications.

References:

[1] Ranney, M.W. < Offshore Oil Technology - Recent Development > , Noyes Data Corporation, 1979.

[2] Morphy, J.M.D. < Power Electronic Control of AC Machines >, Pergamon, 1988

[3] Edwards, J.D. < Electrical Machines & Drives >, Macmillan, 1991

[4] Leonhard, W. < Control of Electrical Drives >. Springer-Verlag, 1985.

[5] McLean, G.W. " Review of Recent Progress in Linear Motors " Proc. IEE Vol. 135, pt.B, No.6, Nov. 1988, pp. 380 - 416.

[6] Eastham, J.F, "Novel Synchronous Machines: Linear and Disc", Proc. IEE, Pt.B, Vol 137, 1990, pp. 49 - 58.

[7] Lipo, T.A. " Recent progress in the development of solid-state ac motor drives ", IEEE Trans. PE-3, 1988, pp. 105 - 107

[8] Barton, T.H. " Variable Frequency Variable Speed AC Drives", Electrical Machine and Power Systems, 1987, pp 143 - 163.

[9] Bowes, S.R. et al, "Microprocessor Control of PWM inverters", Proc. IEE, Pt.B, Vol 137, 1981, pp. 293 - 305.

[10] Fukuda, S. et al, "PWM Technique for Inverter with Sinusoidal Output Current", IEEE Trans., PE - 5, 1990, pp. 54 - 61.

[11] Joos, G. et al, " A Model Reference Adaptive PWM Technique", IEEE Trans. PE - 5. 1990, pp. 485 - 494.

[12] Heinz Willi Van Der Broeck, et al, "Analysis and Realization of a Pulsewidth Modulator Based on Voltage Space Vectors", IEEE. Trans, IA - 24, 1988, pp. 142 - 149.

[13] Handley, P.G. et al, "Space Vector Modulation: An Engineering Review", 4th Intern. Conf. on Power Electronics and Variable Speed Drives, 17 - 19, July 1990. pp. 87 - 97.

[14] Taniguchi, K. et al, "PWM Technique for Power MOSFET Inverter", IEEE, Trans. PE - 3, 1988, pp. 328 - 334.

[15] Sen, P.C. " Electric Motor Drives and Control - Past, Present, and Future ", IEEE Trans. IE-37, No. 6, December, 1990, pp. 562 - 575.

[16] Ogasawara, S. et al. " The Generalised Theory of Indirect Vector Control for AC Machines ", IEEE Trans. IA - 22, 1986, pp 117 - 123.

[17] Acarnley, P.P. et al. " Field Orientation in AC Drives: State Of The Art and Future Prospects ", Third International Conference on Electrical Machines and Drives, November, 1987, pp 285 - 289.

[18] Verster, J.P. et al, "Practical Design Procedure for PWM Torque Controllers in The Application of Permanent Synchronous Machine (PMSM) Drives", 4th Intern. Conf. on Power Electronics and Variable Speed Drives, 17 - 19, July 1990. pp. 40 - 46.

[19] McLean, G.W. et al. " Design of a Permanent Linear Synchronous Motor Drive for a Position / Velocity Actuator " International Conference on Electrical Machines, Boston, USA, August 1990, pp. 1136 - 1141.

[20] Afshar A, " Optimal Digital Control of Permanent Magnet Linear Synchronous Motor for Cyclic Tracking ", Ph. D Thesis, Manchester University, 1991

[21] Roos, J.G. et al, " Analysis, Simulation and Practical Evalution of Torque Vector Control Strategies for Medium Power Highly Responsive PMSM Drives ", 4th Intern. Conf. on Power Electronics and Variable Speed Drives, 17 - 19, July 1990. pp. 34 - 39.

[22] Pilly, P. et al, " Modelling, Simulation, and Analysis of Permanent-Magnet Motor Drives, Part I: The Permanent-Magnet Synchronous Motor Drive ", IEEE. Trans, IA-25, 1989, pp. 265 - 272.

[23] Rekioua, T. et al, "A New Approach for The Field-Oriented Control of Brushless, Synchronous, Permanent Magnet Machines", 4th Intern. Conf. on Power Electronics and Variable Speed Drives, 17 - 19, July 1990. pp. 46 - 50.

[24] Matsui, T. et al, " A High Accuracy Current Component Detection Method for Fully Digital Vector Controlled PWM VSI-Fed AC Drives", IEEE Trans. PE - 5. 1990, pp. 62 - 68.

[25] Pillay, P. et al " Application Characteristics of Permanent Magnet Synchronous and Brushless d. c. Motors for Servo Drives ", IEEE Trans. IA-27, 1991, pp. 986- 996.

[26] Pillay, P. et al. " Control Characteristics and Speed Controller Design for a High Performance Magnet Synchronous Motor Drive ", IEEE Trans. PE - 5, 1990, pp. 151 - 159.

[27] Liu, T. H et al, " A Multiprocessor-Based Fully Digital Control Architecture for Permanent Magnet Synchronous Motor Drives", IEEE Trans. PE - 5. 1990, pp.413 - 423.

[28] Naunin, D. et al " Completely Digital Position Feedback Control for Synchronous Servo Drives ", IEEE Trans. PE - 5, 1990, pp. 495 - 502.

[29] Matsui, N. et al " DSP Based Adaptive Control of A Brushless Motor ", IEEE Trans. IA-28, 1992, pp. 448 - 454.

[30] Sepe, R.B. " Real Time Adaptive Control of A Permanent Magnet Synchronous Motor ", IEEE Trans. IA-27, 1991, pp. 706 - 714.

[31] Clausen V. et al, " Microprocessor Controlled Linear Synchronous Motor As Positioning Drive ", Proc ICEM. 1978, pp.L5 / 2- 1- 8.

[32] Maresca, R. L. "A 400-W Tri-State Switching Controller for Reciprocating Linear Motors", IEEE, Trans. PE - 3, 1988, pp. 3 - 9.

[33] Goldberg L.F., " The Design and Simulation Investigation of A Linear Alternator Dynamometer Coupled To A Free Piston Stirling Engine ", Proc. 10th Intersociety Energy Conversion Eng. Conf. 1985, pp 218 - 233

[34] Lessmeier, R. et al, "Microprocessor-Controlled AC-Servo Drives with Synchronous or Induction Motors: Which is Preferable?", IEEE, Trans. IA - 22, 1986, pp. 812 - 818.

[35] Mei, T. X, "Studies of Vector Control Optimisation, Control Stability and Auto-Start of A Linear Synchronous Machine", M. Sc. Thesis, Manchester University, 1991.

[36] Moromoto, S. et al, "Current Phase Control Methods for Permanent Magnet Synchronous Motors", IEEE. Trans, PE - 5, 1990, pp. 133 - 139.

[37] He, Y. K. et al, "The State-Space Analysis of Excitation Regulation of Self-Controlled Synchronous Motor with Constant Margin-Angle Control", IEEE. Trans, PE - 5, 1990, pp. 269 - 275.

[38] Wallace, A.K et al, "The Effects of Motor Parameters on the Performance of Brushless DC Drives", IEEE. Trans, PE - 5, 1990, pp. 2 - 7

[39] Shinners, S M, < Modern Control System Theory and Application >, Addison-Wesley, 1978

[40] Doyle, J, < Feedback Control Theory >, Macmillan, 1992

[41] Bollinger, J.G. < Computer Control of Machines and Processes >, Addison-Wesley, 1988

[42] Anderson, B.D.O. and Moore, J.B. < Optimal Control - Linear Quadratic Methods >, Prentice-Hall, Inc., 1990

[43] Warwick, K. "Adaptive Control: An Insight", Computing & Control Engineering Journal, 1990, pp. 35 - 39.

[44] Astrom, K.J. < Adaptive Control >, 1989

[45] Morari, M, < Robust Process Control >, Prentice - Hall, Inc.1989

[46] Lunze, J. < Robust Multivariable Feedback Control >, Prentice - Hall, Inc. 1989

[47] Billings, S.A. et al, < Nonlinear System Design >, IEE Contrrol Engineering Series 25, Peter Peregrinus Ltd. 1984

[48] Tzafestas, S.G. < Distributed Parameter Control Systems >, International Series on Systems and Control, Volume 6, Pergamon Press. 1989

[49] Rafael T. Yanushevsky, "Aspects of Robust Control". Control and Dynamic Systems, Vol 50, Part 1, 1992, pp. 55-78

[50] Altug Iftar etc., "Techniques in Modelling Uncertain Dynamics for Robust Control System Design" Control and Dynamic Systems, Vol 50, Part 1, 1992, pp. 255-296.

[51] Altugiftar A. et al, "Modelling of Uncertain Dynamics for Robust Controller Design in State Space", Automatica, Vol 27, No 1, 1991, pp. 141 - 146.

[52] Bhattacharyya, D.P. etc.,"Robust Stability and Control of Linear and Multilinear Interval Systems", Control and Dynamic Systems, Vol 51, Part 2, 1992.

[53] Wang, D. H, "Robust Tracking Control of Non-linear Systems with Uncertain Dynamics". Control and Dynamic Systems, Vol 50, Part 1, 1992, pp. 119-174.

[54] Nader Sadegh, "Robustness Techniques in Nonlinear Systems with Applications to Manipulator Adaptive Control". Control and Dynamic Systems, Vol 50, Part 1, 1992, pp. 223-254.

[55] Horowitz I.M. "A Synthesis Theory for Linear Time Varying Feedback Systems with Plant Uncertainties", IEEE Trans. AC-20,1975, pp. 454 - 463.

[56] Lunze J. "The Design of Robust Feedback Controllers in The Time Domain", Intern. J. Control, Vol 39, 1984a, pp 1243 - 1260.

[57] Kathryn Lenz et al, "Frequency Domain Analysis and Robust Control Design for an Ideal Flexible Beam", Automatica, Vol 27, No 6, 1991, pp. 947 - 961.

[58] Brian D.O. etc. "Trade-offs among Conflicting Objectives in Robust Control Design", Control and Dynamic Systems, Vol 50, Part 1, 1992, pp. 1-54.

[59] Chen M.J. et al, "Necessary and Sufficient Conditions for Robust Stability of Linear Distributed Feedback Systems", Intern. J. Control, Vol 35, 1982, pp. 255 - 267.

[60] Evans R.J. et al, "Robust Regulator Design" Intern. J. Control, Vol 41, 1985, pp. 461 - 476

[61] Lunze J. "The Design of Robust Feedback Controllers for Partly Unknown Systems by Optimal Control Procedures" Intern. J. Control, Vol 36, 1982c, pp 611 - 630.

[62] Davison E.J. et al "The Robust Control of A Servomechanism Problem for Linear Time-Invariant Multivariable Systems.", IEEE Trans. AC-21,1976a, pp. 25 - 34.

[63] Gu D.W. "H^∞ Super-Optimal Solutions", Control and Dynamic Systems, Vol 51, Part 2, 1992, pp. 183-246.

[64] Kreider, J.F. < Principles of Fluid Mechanics >, Allyn and Bacon, Inc. 1985

[65] Streeter, V.L. < Fluid Mechnics >, McGraw-Hill, 1985

[66] Wylie, E.B. & Streeter, V. L. < Fluid Transients >, McGraw-Hill, 1978

[67] Fox, J.A. < Transient Flow in Pipes, Open Channels and Sewers >, Ellis Horwood Limited. 1989

[68] < Embeded Microcontrollers and Processors >, Intel Corporation. 1992

[69] < EV80C196KC Microcontroller Evaluation Board - User's Manual >, Intel Corporation. 1992

[70] < 80C196KC - User's Manual >, Intel Corporation. 1990

[71] < B-B Integrating Circuits Data Book >, Volume 33, Burr-Brown Corporation 1989.

[72] Kulkarni, A.B. et al, " A Novel Position Sensor Elimination Technique for The Interior Permanent Magnet Synchronous Motor Drive", IEEE Trans, IA-28, 1992, pp 448 - 454.

[73] Sepe, M.B. et al, "Real Time Observer Based (Adaptive) Control of A Permanent Magnet Synchronous Motor Without Mechanical Sensors", IEEE Trans, IA-28, 1992, pp 1345 - 1352.

[74] Wu, R.S et al, "A Permanent Magnet Motor Drive Without A Shaft Sensor", IEEE Trans, IA-27, 1991, pp 1005 - 1011.

[75] Schroedl, M. "Operation of The Permanent Magnet Synchronous Machine without a Mechanical Sensor", 4th Intern. Conf. on Power Electronics and Variable Speed Drives, 17 - 19, July 1990. pp. 51 - 56.

APPENDIX 1:

List of The Simulation Program

```c
/*****************************************************/
/*****************************************************/
/** This is program of motor-pump system simulation   **/
/** Motor is simulated by three phase model           **/
/** Oil is simulated by a disrtibuted parameter model **/
/** Gas is simulated by a non linear model            **/
/** Three control loops as well as vector control     **/
/** sheme are implemented in the simulation program   **/
/** A resolution of 0.25 mm of position transduer is  **/
/** also simulated                                    **/
/*****************************************************/
/*****************************************************/

               /*C language*/

/*****************************************************/

#include <stdio.h>
#include <math.h>
#include <csl2.h>

#define SQ1(z)        (z)*(z)
#define PI            3.141592654
#define AND            &&
#define OR             ||
#define EQU            ==
#define ABS(z)        ((z<0.0) ? -(z) : (z))


/************** Define Global Variables ***************/
/*****************************************************/


int ij,k,n,ii,c_1=1,c_2=3,km1,km2,kdi,ksu,nt;

double H3[10000],Q3[10000],H4[10000],Q4[10000],ht[10000],
       qt[10000],H1[100],Q1[100],H2[100],Q2[100];
double cont_sig=0.0,fl1=0.0,fl2=0.0,ff=0.0,s11=0.0,
       marg1,marg2,Hr,Qr,Qs,Hs,Cp,Cm,Pr1,P0,Pop,kb,
       dett,B10,B11,B12,S,s1,s2,a33,a1,a2,seg1,seg2,
       Pc,B20,B21,B22,lo1,lo2,kb1,kb2,p11=0.0,s22=0.0,
       t=0.0,cont_p, cont_i, cont_vb, cont_vf, cont_af;
double preu1=0.0,preu2=0.0,preu3=0.0,pr1_p11=0.0,
       u4_d1=0.0,u5_d1=0.0,u1=0.0,u2=0.0,u3=0.0,
       i1=0.0,i2=0.0,i3=0.0,i4,i5,u4,u5,i5_r1,u4_d,
       u5_d,ff1=0.0,ff2=0.0,ff3=0.0;

float  fsat,p11,p12,deltat,u4_m,u5_m,tha,rs,ls1,ms,p,
       mfp,fstick,k2,gvf,gaf,ls10,ms10,g,mu,lo,D,d1,d2,
       L,L1,L2,kc,detx,f,tt1,kf,mass,te,ka,per;

/*****************************************************/

double
fnx(x, y, i)
  double  x;
```

```
  double   *y;
  int      i;
   {
     double dy = 0.0;
     double yy3,dmf1,dmf2,dmf3,c11,c12,c21,c22,d11,d12,
            d21,d22,dd,ga1;

     ga1 = PI*y[3]/p;
     c11 = -rs-2.0*PI*y[2]*(ls10+2.0*ms10)
              *sin(2.0*ga1)/p;
     c12 =  rs+2.0*PI*y[2]*(ls10+2.0*ms10)*sin(2.0*ga1
              +2.0*PI/3.0)/p;
     c21 = -rs-2.0*PI*y[2]*(ls10+2.0*ms10)
              *sin(2.0*ga1-2.0*PI/3.0)/p;
     c22 = -2.0*rs+2.0*PI*y[2]*(ls10+2.0*ms10)
              *sin(2.0*ga1)/p;
     d11 =  (ls1+ms)-(ls10+2.0*ms10)*cos(2.0*ga1);
     d12 = -(ls1+ms)+(ls10+2.0*ms10)*cos(2.0*ga1
              +2.0*PI/3.0);
     d21 =  (ls1+ms)-(ls10+2.0*ms10)*cos(2.0*ga1
              -2.0*PI/3.0);
     d22 = 2.0*(ls1+ms)+(ls10+2.0*ms10)*cos(2.0*ga1);
     dd  = d11*d22-d12*d21;

     dmf1 = -mfp*PI*(sin(PI*y[3]/p))/p;
     dmf2 = -mfp*PI*(sin(PI*y[3]/p-2.0*PI/3.0))/p;
     dmf3 = -mfp*PI*(sin(PI*y[3]/p+2.0*PI/3.0))/p;

    yy3 = -(y[0]+y[1]);
    ff1 = y[0]*dmf1+y[1]*dmf2+yy3*dmf3;
    ff2 = ls10*2.0*PI*(y[0]*y[0]*sin(2.0*ga1)
            +y[1]*y[1]*sin(2.*ga1+2.*PI/3.)
            +yy3*yy3*sin(2.*ga1-2.*PI/3.))/p;
    ff3 = ms10*4.0*PI*(y[0]*y[1]*sin(2.0*ga1
            -2.*PI/3.)+y[1]*yy3*sin(2.*ga1)
            +yy3*y[0]*sin(2.*ga1+2.*PI/3.))/p;

    ff = ff1 + ff2 + ff3;

switch(i)
{
   case 0:
       dy = ((c11*d22-c21*d12)*y[0]+(c12*d22-c22*d12)
              *y[1]+d22*(u1-u2)-d12*(u2-u3)+y[2]*d22
              *(dmf2-dmf1)-y[2]*d12*(dmf3-dmf2))/dd;
   break;
   case 1:
       dy = ((c21*d11-c11*d21)*y[0]+(c22*d11-c12*d21)
              *y[1]-d21*(u1-u2)+d11*(u2-u3)-y[2]*d21
              *(dmf2-dmf1)+y[2]*d11*(dmf3-dmf2) )/dd;
   break;
   case 2:
       dy = (ff-kf*y[2]-fl1+fl2)/mass;
   break;
   case 3:
       dy = y[2];
   break;    }
    return(dy);
```

```
   }

/*****************************************************/
/*****************************************************/

cont_1()
   {
      double i6,i7,i4err,i5err,tstart,a331,u4_s,
             u5_s,w,diff,a11,demf,psips,ur1,a44,
             i4_r1=0.0,s221=0.0;

      i6 = 2.0*(i1-((i2+i3)/2.0))/3.0;
      i7 = (i2-i3)/(sqrt(3.0));
      a11  = (PI/p)*p11;
      s221 = (p11-pr1_p11)/tt1;
      pr1_p11 = p11;

      if (ABS(a11) < 0.09)
       {
        i4 = i6 + i7*a11;
        i5 = i6*a11 - i7;  }
      else
       {
        i4=i6*cos(a11)+i7*sin(a11);
        i5=i6*sin(a11)-i7*cos(a11);}

     if((i4 EQU 0.0) AND (i5 EQU 0.0))
            a331 = 0.0;
     else
            a331 = atan2(i4,i5)*180.0/PI;
      demf = ka*cont_sig;
      if(demf > fsat)  demf = fsat;
      if(demf < -fsat) demf = -fsat;

      psips = 3.0*mfp*PI/(2.0*p);
      i5_r1 = -demf/psips;
      i4err = i4_r1-i4;
      i5err = i5_r1-i5;
      u4_d1 = u4_d1+p12*i4err;
      u5_d1 = u5_d1+p12*i5err;
      u4_d  = p11*i4err+u4_d1;
      u5_d  = p11*i5err+u5_d1;
      u4_s  = rs*i4_r1+(ls1-ms)*s221*i5_r1*PI/p;
      u5_s  = (-(ls1-ms))*PI*s221*i4_r1/p+rs*i5_r1
                   -mfp*s221*PI/p;

      u4 = u4_s + u4_d;
      u5 = u5_s + u5_d;
      if(u4 >  u4_m) u4 =  u4_m;
      if(u4 < -u4_m) u4 = -u4_m;
      if(u5 >  u5_m) u5 =  u5_m;
      if(u5 < -u5_m) u5 = -u5_m;

      ur1 = sqrt(u4*u4+u5*u5);
      if((u4 EQU 0.0) AND (u5 EQU 0.0))
        a44=a11+s221*deltat*PI/p;
      else
        a44=atan2(u4,u5)+a11+s221*deltat*PI/p-PI/2.0;
```

```
    u1 = ur1*cos(a44);
    u2 = ur1*(cos(a44)*(-0.5)+(sqrt(3.0))*sin(a44)/2.0);
    u3 = ur1*(cos(a44)*(-0.5)-(sqrt(3.0))*sin(a44)/2.0);

     if (tha != 0.0)
      {
        w=preu1;  preu1=u1;    u1=w;
        w=preu2;  preu2=u2;    u2=w;
        w=preu3;  preu3=u3;    u3=w;    }
  }

/******************************************************/
/******************************************************/

load_ch(c_1,c_2)
     int c_1;
     int c_2;
{
  if((c_1 == 1) OR (c_1 == 2))
   {
     for(ii = 1; ii <= km1; ++ii)
      { qt[ii] = Q1[ii];
        ht[ii] = H1[ii];  }

     for(ii = 2; ii <= km1-1; ++ii)
      {
       Qr = (qt[ii]-seg1*(qt[ii]-qt[ii+1]))
               /(1+a33*(qt[ii]-qt[ii+1])/S);
       Qs = (qt[ii]-seg1*(qt[ii]-qt[ii-1]))
               /(1-a33*(qt[ii]-qt[ii-1])/S);
       Hr = ht[ii]-(Qr*a33/S+seg1)*(ht[ii]-ht[ii+1]);
       Hs = ht[ii]+(Qs*a33/S-seg1)*(ht[ii]-ht[ii-1]);
       Cp = Hr+Qr*B10*(1.0-f*dett*ABS(Qr)/(2.0*D*S));
       Cm = Hs-Qs*B10*(1.0-f*dett*ABS(Qs)/(2.0*D*S));
       H1[ii] = (Cp+Cm)/2.0;
       Q1[ii] = (Cp-Cm)/(B10*2.0);    }

       Qs = (qt[km1]-seg1*(qt[km1]-qt[km1-1]))
               /(1-a33*(qt[km1]-qt[km1-1])/S);
       Hs = ht[km1]+(Qs*a33/S-seg1)*(ht[km1]-ht[km1-1]);
       Cm = Hs-Qs*B10*(1.0-f*dett*ABS(Qs)/(2.0*D*S));
       Q1[km1] = s11*S;
       H1[km1] = B10*Q1[km1]+Cm;
                 /* discharge slider end */

       Qr = (qt[1]-seg1*(qt[1]-qt[2]))/(1+a33*(qt[1]
                -qt[2])/S);
       Hr = ht[1]-(Qr*a33/S+seg1)*(ht[1]-ht[2]);
       Cp = Hr+Qr*B10*(1.0-f*dett*ABS(Qr)/(2.0*D*S));

    if(c_1 == 1)
     { Q1[1] = 0.0;
       H1[1] = Cp;
       Pc    = Cp*g*lo1;
       if(Pc < 0.0) Pc = 0.0;
            kb1 = kb/(1.0+per*(kb/(1.4*Pc)-1.0));
            lo1 = lo*(1.0-per)+pow(Pc*1.0e-5
```

```
                    /1.01325,1.0/1.4)*1.5*per;
          a1   = sqrt(kb1/lo1);
          seg1= a33*a1;
          B10 = a1/(g*S);
          B11 = a1/(g*s1);
          B12 = a1/(g*s2); }
               /* discharge and dead end */

   if(c_1 == 2)
    {
   for (ii = 1; ii <= kdi; ++ii)
    { qt[ii] = Q3[ii];
      ht[ii] = H3[ii];  }

      Qs=(qt[kdi]-seg1*(qt[kdi]-qt[kdi-1]))
                    /(1-a33*(qt[kdi]-qt[kdi-1])/s1);
      Hs=ht[kdi]+(Qs*a33/s1-seg1)*(ht[kdi]-ht[kdi-1]);
      Cm=Hs-Qs*B11*(1.0-f*dett*ABS(Qs)/(2.0*d1*s1)
                    -2.0*kc*dett);
      H1[1]   = (Cp*B11+Cm*B10)/(B10+B11);
      H3[kdi] = H1[1];
      Q1[1]   = (Cp-Cm)/(B10+B11);
      Q3[kdi] = Q1[1];
    /*discharge valve opens and series connection*/

      Qr = (qt[1]-seg1*(qt[1]-qt[2]))/(1+a33*(qt[1]
                    -qt[2])/s1);
      Hr = ht[1]-(Qr*a33/s1+seg1)*(ht[1]-ht[2]);
      Cp = Hr+Qr*B11*(1.0-f*dett*ABS(Qr)/(2.0*d1*s1)
                    -2.0*kc*dett);
      H3[1] = Pr1/(lo1*g);
      Q3[1] = (Cp-H3[1])/B11;
              /* open end with P_r1 */

    for(ii = 2; ii <= kdi-1; ++ii)
     {
      Qr = (qt[ii]-seg1*(qt[ii]-qt[ii+1]))
                    /(1+a33*(qt[ii]-qt[ii+1])/s1);
      Qs = (qt[ii]-seg1*(qt[ii]-qt[ii-1]))
                    /(1-a33*(qt[ii]-qt[ii-1])/s1);
      Hr = ht[ii]-(Qr*a33/s1+seg1)*(ht[ii]-ht[ii+1]);
      Hs = ht[ii]+(Qs*a33/s1-seg1)*(ht[ii]-ht[ii-1]);
      Cp = Hr+Qr*B11*(1.0-f*dett*ABS(Qr)/(2.0*d1*s1)
                    -2.0*kc*dett);
      Cm = Hs-Qs*B11*(1.0-f*dett*ABS(Qs)/(2.0*d1*s1)
                    -2.0*kc*dett);
      H3[ii] = (Cp+Cm)/2.0;
      Q3[ii] = (Cp-Cm)/(B11*2.0);    }
    }
 }
             /* end of discharge */

 if((c_1 == 3) OR (c_1 == 4))
  {
   for(ii = 1; ii <= km1; ++ii)
     { qt[ii] = Q1[ii];
       ht[ii] = H1[ii];  }
```

```
for(ii = 2; ii <= km1-1; ++ii)
 {
   Qr = (qt[ii]-seg1*(qt[ii]-qt[ii-1]))
              /(1+a33*(qt[ii]-qt[ii-1])/S);
   Qs = (qt[ii]-seg1*(qt[ii]-qt[ii+1]))
              /(1-a33*(qt[ii]-qt[ii+1])/S);
   Hr = ht[ii]-(Qr*a33/S+seg1)*(ht[ii]-ht[ii-1]);
   Hs = ht[ii]+(Qs*a33/S-seg1)*(ht[ii]-ht[ii+1]);
   Cp = Hr+Qr*B10*(1.0-f*dett*ABS(Qr)/(2.0*D*S));
   Cm = Hs-Qs*B10*(1.0-f*dett*ABS(Qs)/(2.0*D*S));
   H1[ii] = (Cp+Cm)/2.0;
   Q1[ii] = (Cp-Cm)/(B10*2.0);    }

   Qr = (qt[km1]-seg1*(qt[km1]-qt[km1-1]))
              /(1+a33*(qt[km1]-qt[km1-1])/S);
   Hr = ht[km1]-(Qr*a33/S+seg1)*(ht[km1]-ht[km1-1]);
   Cp = Hr+Qr*B10*(1.0-f*dett*ABS(Qr)/(2.0*D*S));
   Q1[km1] = -s11*S;
   H1[km1] = Cp-B10*Q1[km1];
            /* slider end, suction */

   Qs = (qt[1]-seg1*(qt[1]-qt[2]))/(1-a33*(qt[1]
              -qt[2])/S);
   Hs = ht[1]+(Qs*a33/S-seg1)*(ht[1]-ht[2]);
   Cm = Hs-Qs*B10*(1.0-f*dett*ABS(Qs)/(2.0*D*S));

 if(c_1 == 3)
  { Q1[1] = 0.0;
   H1[1] = Cm;
   Pc     = Cm*lo1*g;
   if(Pc < 0.0) Pc = 0.0;
      kb1    = kb/(1.0+per*(kb/(1.4*Pc)-1.0));
      lo1    = lo*(1.0-per)+pow(Pc*1.0e-5/1.01325,
                   1.0/1.4)*1.5*per;
      a1     = sqrt(kb1/lo1);
      seg1   = a33*a1;
      B10    = a1/(g*S);
      B11    = a1/(g*s1);
      B12    = a1/(g*s2);   }
     /*suction with dead end, suction valve closed*/

if(c_1 == 4)
 {
   for (ii = 1; ii <= ksu; ++ii)
  { qt[ii] = Q3[ii];
   ht[ii] = H3[ii];   }

   Qr=(qt[ksu]-seg1*(qt[ksu]-qt[ksu-1]))
            /(1+a33*(qt[ksu]-qt[ksu-1])/s2);
   Hr=ht[ksu]-(Qr*a33/s2+seg1)*(ht[ksu]-ht[ksu-1]);
   Cp=Hr+Qr*B12*(1.0-f*dett*ABS(Qr)/(2.0*d2*s2)
            -2.0*kc*dett);
   H1[1]    = (Cp*B10+Cm*B12)/(B10+B12);
   H3[ksu] = H1[1];
   Q1[1]    = (Cp-Cm)/(B10+B12);
   Q3[ksu] = Q1[1];
     /* suction valve open and series connection */
```

```
        Qs = (qt[1]-seg1*(qt[1]-qt[2]))/(1-a33*(qt[1]
                -qt[2])/s2);
        Hs = ht[1]+(Qs*a33/s2-seg1)*(ht[1]-ht[2]);
        Cm = Hs-Qs*B12*(1.0-f*dett*ABS(Qs)/(2.0*d2*s2)
                -2.0*kc*dett);
        H3[1] = P0/(lo1*g);
        Q3[1] = (H3[1]-Cm)/B12;
               /* reservoir at upstream end */

     for(ii = 2; ii <= ksu-1; ++ii)
      {
        Qr = (qt[ii]-seg1*(qt[ii]-qt[ii-1]))
                  /(1+a33*(qt[ii]-qt[ii-1])/s2);
        Qs = (qt[ii]-seg1*(qt[ii]-qt[ii+1]))/(1-a33
                  *(qt[ii]-qt[ii+1])/s2);
        Hr = ht[ii]-(Qr*a33/s2+seg1)*(ht[ii]-ht[ii-1]);
        Hs = ht[ii]+(Qs*a33/s2-seg1)*(ht[ii]-ht[ii+1]);
        Cp = Hr+Qr*B12*(1.0-f*dett*ABS(Qr)/(2.0*d2*s2)
                  -2.0*kc*dett);
        Cm = Hs-Qs*B12*(1.0-f*dett*ABS(Qs)/(2.0*d2*s2)
                  -2.0*kc*dett);
        H3[ii] = (Cp+Cm)/2.0;
        Q3[ii] = (Cp-Cm)/(B12*2.0);  }
      }
   }

/*************************************************/

  if((c_2 == 1) OR (c_2 == 2))
   {
     for (ii = 1; ii <= km2; ++ii)
      { qt[ii] = Q2[ii];
        ht[ii] = H2[ii];  }

     for(ii = 2; ii <= km2-1; ++ii)
      {
        Qr = (qt[ii]-seg2*(qt[ii]-qt[ii+1]))
                 /(1+a33*(qt[ii]-qt[ii+1])/S);
        Qs = (qt[ii]-seg2*(qt[ii]-qt[ii-1]))/(1-a33
                 *(qt[ii]-qt[ii-1])/S);
        Hr = ht[ii]-(Qr*a33/S+seg2)*(ht[ii]-ht[ii+1]);
        Hs = ht[ii]+(Qs*a33/S-seg2)*(ht[ii]-ht[ii-1]);
        Cp = Hr+Qr*B20*(1.0-f*dett*ABS(Qr)/(2.0*D*S));
        Cm = Hs-Qs*B20*(1.0-f*dett*ABS(Qs)/(2.0*D*S));
        H2[ii] = (Cp+Cm)/2.0;
        Q2[ii] = (Cp-Cm)/(B20*2.0);   }

        Qs = (qt[km2]-seg2*(qt[km2]-qt[km2-1]))
                 /(1-a33*(qt[km2]-qt[km2-1])/S);
        Hs = ht[km2]+(Qs*a33/S-seg2)*(ht[km2]-ht[km2-1]);
        Cm = Hs-Qs*B20*(1.0-f*dett*ABS(Qs)/(2.0*D*S));
        Q2[km2] = -s11*S;
        H2[km2] = B20*Q2[km2]+Cm;
                 /* discharge slider end */

        Qr = (qt[1]-seg2*(qt[1]-qt[2]))/(1+a33*(qt[1]
                  -qt[2])/S);
        Hr = ht[1]-(Qr*a33/S+seg2)*(ht[1]-ht[2]);
```

```
        Cp = Hr+Qr*B20*(1.0-f*dett*ABS(Qr)/(2.0*D*S));

    if(c_2 == 1)
     {  Q2[1] = 0.0;
        H2[1] = Cp;
        Pc    = Cp*g*lo2;
        if(Pc < 0.0) Pc = 0.0;
            kb2 = kb/(1.0+per*(kb/(1.4*Pc)-1.0));
            lo2 = lo*(1.0-per)+pow(Pc*1.0e-5/1.01325,
                      1.0/1.4)*1.5*per;
            a2  = sqrt(kb2/lo2);
            seg2= a33*a2;
            B20   = a2/(g*S);
            B21   = a2/(g*s1);
            B22   = a2/(g*s2);
}
                /* discharge and dead end */

    if(c_2 == 2)
     {
     for (ii = 1; ii <= kdi; ++ii)
      { qt[ii] = Q4[ii];
        ht[ii] = H4[ii];   }

        Qs=(qt[kdi]-seg2*(qt[kdi]-qt[kdi-1]))/(1-a33
                   *(qt[kdi]-qt[kdi-1])/s1);
        Hs=ht[kdi]+(Qs*a33/s1-seg2)*(ht[kdi]-ht[kdi-1]);
        Cm=Hs-Qs*B21*(1.0-f*dett*ABS(Qs)/(2.0*d1*s1)
                   -2.0*kc*dett);
        H2[1] = (Cp*B21+Cm*B20)/(B20+B21);
        H4[kdi] = H2[1];
        Q2[1] = (Cp-Cm)/(B20+B21);
        Q4[kdi] = Q2[1];
      /*discharge valve opens and series connection*/

        Qr = (qt[1]-seg2*(qt[1]-qt[2]))/(1+a33*(qt[1]
                   -qt[2])/s1);
        Hr = ht[1]-(Qr*a33/s1+seg2)*(ht[1]-ht[2]);
        Cp = Hr+Qr*B21*(1.0-f*dett*ABS(Qr)/(2.0*d1*s1)
                   -2.0*kc*dett);
        H4[1] = Pr1/(lo2*g);
        Q4[1] = (Cp-H4[1])/B21;
                /* open end with P_r1 */

     for(ii = 2; ii <= kdi-1; ++ii)
      {
       Qr = (qt[ii]-seg2*(qt[ii]-qt[ii+1]))
                   /(1+a33*(qt[ii]-qt[ii+1])/s1);
       Qs = (qt[ii]-seg2*(qt[ii]-qt[ii-1]))
                   /(1-a33*(qt[ii]-qt[ii-1])/s1);
       Hr = ht[ii]-(Qr*a33/s1+seg2)*(ht[ii]-ht[ii+1]);
       Hs = ht[ii]+(Qs*a33/s1-seg2)*(ht[ii]-ht[ii-1]);
       Cp = Hr+Qr*B21*(1.0-f*dett*ABS(Qr)/(2.0*d1*s1)
                   -2.0*kc*dett);
       Cm = Hs-Qs*B21*(1.0-f*dett*ABS(Qs)/(2.0*d1*s1)
                  -2.0*kc*dett);
       H4[ii] = (Cp+Cm)/2.0;
       Q4[ii] = (Cp-Cm)/(B21*2.0);    }
```

```
    }
 }
            /* end of discharge */

if((c_2 == 3) OR (c_2 == 4))
 {
   for(ii = 1; ii <= km2; ++ii)
     { qt[ii] = Q2[ii];
       ht[ii] = H2[ii];  }

   for(ii = 2; ii <= km2-1; ++ii)
    {
      Qr = (qt[ii]-seg2*(qt[ii]-qt[ii-1]))
                 /(1+a33*(qt[ii]-qt[ii-1])/S);
      Qs = (qt[ii]-seg2*(qt[ii]-qt[ii+1]))
                 /(1-a33*(qt[ii]-qt[ii+1])/S);
      Hr = ht[ii]-(Qr*a33/S+seg2)*(ht[ii]-ht[ii-1]);
      Hs = ht[ii]+(Qs*a33/S-seg2)*(ht[ii]-ht[ii+1]);
      Cp = Hr+Qr*B20*(1.0-f*dett*ABS(Qr)/(2.0*D*S));
      Cm = Hs-Qs*B20*(1.0-f*dett*ABS(Qs)/(2.0*D*S));
      H2[ii] = (Cp+Cm)/2.0;
      Q2[ii] = (Cp-Cm)/(B20*2.0);    }

      Qr = (qt[km2]-seg2*(qt[km2]-qt[km2-1]))
                  /(1+a33*(qt[km2]-qt[km2-1])/S);
      Hr = ht[km2]-(Qr*a33/S+seg2)*(ht[km2]-ht[km2-1]);
      Cp = Hr+Qr*B20*(1.0-f*dett*ABS(Qr)/(2.0*D*S));
      Q2[km2] = s11*S;
      H2[km2] = Cp-B20*Q2[km2];
             /* slider end, suction */

      Qs = (qt[1]-seg2*(qt[1]-qt[2]))/(1-a33*(qt[1]
                  -qt[2])/S);
      Hs = ht[1]+(Qs*a33/S-seg2)*(ht[1]-ht[2]);
      Cm = Hs-Qs*B20*(1.0-f*dett*ABS(Qs)/(2.0*D*S));

 if(c_2 == 3)
   {  Q2[1]   = 0.0;
      H2[1]   = Cm;
      Pc      = Cm*g*lo2;
      if(Pc < 0.0) Pc = 0.0;
          kb2 = kb/(1.0+per*(kb/(1.4*Pc)-1.0));
          lo2 = lo*(1.0-per)+pow(Pc*1.0e-5/1.01325,
                    1.0/1.4)*1.5*per;
          a2  = sqrt(kb2/lo2);
          seg2= a33*a2;
          B20 = a2/(g*S);
          B21 = a2/(g*s1);
          B22 = a2/(g*s2);
}
    /*suction with dead end, suction valve closed*/

   if(c_2 == 4)
    {
     for (ii = 1; ii <= ksu; ++ii)
    { qt[ii] = Q4[ii];
      ht[ii] = H4[ii];  }
```

```
        Qr=(qt[ksu]-seg2*(qt[ksu]-qt[ksu-1]))
                    /(1+a33*(qt[ksu]-qt[ksu-1])/s2);
        Hr=ht[ksu]-(Qr*a33/s2+seg2)*(ht[ksu]-ht[ksu-1]);
        Cp=Hr+Qr*B22*(1.0-f*dett*ABS(Qr)/(2.0*d2*s2)
                    -2.0*kc*dett);

        H2[1]    = (Cp*B20+Cm*B22)/(B20+B22);
        H4[ksu]  = H2[1];
        Q2[1]    = (Cp-Cm)/(B20+B22);
        Q4[ksu]  = Q2[1];
            /*suction valve open and series connection*/

        Qs = (qt[1]-seg2*(qt[1]-qt[2]))/(1-a33*(qt[1]
                    -qt[2])/s2);
        Hs = ht[1]+(Qs*a33/s2-seg2)*(ht[1]-ht[2]);
        Cm = Hs-Qs*B22*(1.0-f*dett*ABS(Qs)/(2.0*d2*s2)
                    -2.0*kc*dett);
        H4[1] = P0/(lo2*g);
        Q4[1] = (H4[1]-Cm)/B22;
               /* reservoir at upstream end */

    for(ii = 2; ii <= ksu-1; ++ii)
     {
        Qr = (qt[ii]-seg2*(qt[ii]-qt[ii-1]))
                     /(1+a33*(qt[ii]-qt[ii-1])/s2);
        Qs = (qt[ii]-seg2*(qt[ii]-qt[ii+1]))/(1-a33
                     *(qt[ii]-qt[ii+1])/s2);
        Hr = ht[ii]-(Qr*a33/s2+seg2)*(ht[ii]-ht[ii-1]);
        Hs = ht[ii]+(Qs*a33/s2-seg2)*(ht[ii]-ht[ii+1]);
        Cp = Hr+Qr*B22*(1.0-f*dett*ABS(Qr)/(2.0*d2*s2)
                     -2.0*kc*dett);
        Cm = Hs-Qs*B22*(1.0-f*dett*ABS(Qs)/(2.0*d2*s2)
                     -2.0*kc*dett);
        H4[ii] = (Cp+Cm)/2.0;
        Q4[ii] = (Cp-Cm)/(B22*2.0);  }
      }
    }
 }

/*******************************************************/
/*******************************************************/
/*******************************************************/

main()
  {
     float gp,gvb,gi,g_pr[6],peak_s22,stroke,end_time,
           Pr11,P01,Pop1,kb0,dett1;

     double r1_s22=0.0,r1_acc=0.0,r1a_set=0.0,piout=0.0,
            pre_piout=0.0,errp=0.0,errv=0.0, r1_p11=0.0,
            p11_pre[6],s22_pre[6],acc,err=0.0,nn1,errp1,
            force=0.0,x,xmax,h,y[4],tol,pre_p11=0.0,
            p111=0.0;

     int    count=0,count2=0, nn;

/* open files for reading and writing*/
```

```
    FILE *in_file, *out_file, *fopen();

    in_file = fopen("da.in","r");
     if(in_file == NULL)
       printf ("***data_in could not be opened.\n");
    out_file = fopen("da_out","w");
     if (out_file EQU NULL)
       printf ("*** data_out could not be opened.\n");

/* input parameters required for simulation */

  fscanf(in_file,"%f %f", &peak_s22, &end_time);
  fscanf(in_file,"%f %f %f %f %f", &stroke,&tt1,&gp,
                  &gvb,&gi);
  fscanf(in_file,"%f %f %f %f",&kf, &mass, &ka, &te);
  fscanf(in_file,"%f %f %f %f %f %f %f %f",&Pr11,&Pop1,
                  &P01,&kb0,&lo,&mu,&f,&kc);
  fscanf(in_file,"%f %f %f %f %f %f %f %f %f",&L,&L1,
                  &L2,&D,&d1,&d2,&detx,&dett1,&per);
  fscanf(in_file,"%f %f %f %f %f %f %f %d, %d",&fsat,
                  &p11,&p12,&deltat,&u4_m,&u5_m,
                  &tha,&nn,&fun1);
  fscanf(in_file,"%f %f %f %f %f %f %f %f %f %f %f",&rs,
                  &ls1,&ms,&p,&mfp,&fstick,&k2,&gvf,&gaf,
                  &ls10,&ms10);

/*******************************************************/

    r1a_set = (peak_s22*peak_s22)/stroke;
    r1_acc  = r1a_set;
    nn1     = (float)(nn);
    g       = 9.8;
    kb      = kb0*1.0e+9;
    Pr1     = Pr11*1.0e+6;
    P0      = P01*1.0e+6;
    Pc      = P0;
    Pop     = Pop1*Pr1;
    dett    = dett1*1.0e-6;
    marg1   = (L+stroke)/2.0;
    marg2   = (L-stroke)/2.0;
    S       = PI*D*D/4.0;
    s1      = PI*d1*d1/4.0;
    s2      = PI*d2*d2/4.0;
    a33     = dett/detx;

    kb1     = kb/(1.0+per*(kb/(1.4*Pc)-1.0));
    lo1     = lo*(1.0-per)+pow(Pc*1.0e-5/1.01325,
                1.0/1.4)*1.5*per;
    a1      = sqrt(kb1/lo1);
    seg1    = a33*a1;
    B10     = a1/(g*S);
    B11     = a1/(g*s1);
    B12     = a1/(g*s2);

    kb2     = kb1;
    lo2     = lo1;
    a2      = a1;
    seg2    = seg1;
```

```
    B20     = B10;
    B21     = B11;
    B22     = B12;

    kdi     = (int)(L1/detx);
    ksu     = (int)(L2/detx);
    nt      = (int)(tt1/dett);
    km1     = (int)(marg1/detx)+1;
    km2     = (int)(marg2/detx)+1;
    fl1     = S*P0;
    fl2     = S*P0;

    for(ii = 1; ii <= km1; ++ii)
     { H1[ii] = P0/(g*lo1);    Q1[ii] = 0.0;   }
    for(ii = 1; ii <= km2; ++ii)
     { H2[ii] = P0/(g*lo2);    Q2[ii] = 0.0;   }

/*******************************************************/

start:

    count2 = count2 + 1;
    if(count2 >= nn)
      {  count2 = 0;
         piout  = pre_piout+gi*errp1*nn1;
         pre_piout = piout;
         cont_sig  = gvb*(gp*errp1+errv+piout)
                          +r1_acc*gaf; }
         count = count + 1;
         if(count >= 5)
          { count = 0;
            fprintf(out_file,"\n%e %e %e %e %e\n%e %e %e
                    %e %e",t,r1_p11,r1_s22,p11,s22,errp,
                    errv,cont_sig*ka,fl1-fl2,fl1);
            fprintf(out_file,"\n%e %e %e %e %e\n%e %e %e
                    %e %e\n",fl2,i1,i5_r1,i4,i5,u4_d,
                    u5_d,u4,u5,u1);
      }

/*******************************************************/

     cont_1();
     x = t-dett;

for(ij = 1; ij <= nt; ++ij)
{
      x    = x + dett;
      xmax = x + dett;
      h    = dett/50.0;
      tol  = 1.0e-12;
      n    = 4;
      y[0] = i1;
      y[1] = i2;
      y[2] = s11;
      y[3] = p111;

      rk6_7(fnx, y, x, xmax, h, n, tol);
```

```
    i1 = y[0];
    i2 = y[1];
    i3 = -(i1+i2);
    s11 = y[2];
    p111 = y[3];
    p11 = p111;

/***************************************************/

  if(fun1 == 1)
   {
    H1[km1+1] = H1[km1];
    Q1[km1+1] = Q1[km1];
    H2[km2+1] = H2[km2];
    Q2[km2+1] = Q2[km2];
    km1 = (int)((marg1-p111)/detx)+1;
    km2 = (int)((marg2+p111)/detx)+1;

    load_ch(c_1,c_2);

    fl1 = H1[km1]*lo1*g*S;
    fl2 = H2[km2]*lo2*g*S;

    if((c_1 == 1) AND (H1[1] >= Pop/(lo1*g)))
      { c_1 = 2;
        kb1 = kb/(1.0+per*(kb/(1.4*Pr1)-1.0));
        lo1 = lo*(1.0-per)+pow(Pr1*1.0e-5/1.01325,
                 1.0/1.4)*1.5*per;
        a1  = sqrt(kb1/lo1);
        seg1= a33*a1;
        B10 = a1/(g*S);
        B11 = a1/(g*s1);
        B12 = a1/(g*s2);
        for(ii = 1; ii <= kdi; ++ii)
        { H3[ii] = Pr1/(g*lo1);  Q3[ii] = 0.0; } }

    if((c_1 == 2) AND (s11 < -0.01)
                  AND (p111 >= stroke/2.0))
     {  c_1 = 3; c_2 = 1;
        for(ii = 1; ii <= km1+1; ++ii)
              Q1[ii] = -Q1[ii];
        for(ii = 1; ii <= km2+1; ++ii)
              Q2[ii] = -Q2[ii];   }

    if((c_1 == 3) AND (H1[1] <= P0/(lo1*g)))
      { c_1 = 4;
        kb1 = kb/(1.0+per*(kb/(1.4*P0)-1.0));
        lo1 = lo*(1.0-per)+pow(P0*1.0e-5/1.01325,
                 1.0/1.4)*1.5*per;
        a1  = sqrt(kb1/lo1);
        seg1= a33*a1;
        B10 = a1/(g*S);
        B11 = a1/(g*s1);
        B12 = a1/(g*s2);

        for(ii = 1; ii <= ksu; ++ii)
          { H3[ii] = P0/(g*lo1);  Q3[ii] = 0.0;  } }
```

```
if((c_1 == 4) AND (s11 >= 0.01)
              AND (p111 <= stroke/2.0))
    { c_1 = 1;
      c_2 = 3;
     for(ii = 1; ii <= km1+1; ++ii)
          Q1[ii] = -Q1[ii];
      for(ii = 1; ii <= km2+1; ++ii)
          Q2[ii] = -Q2[ii];    }

if((c_2 == 1) AND (H2[1] >= Pop/(lo2*g)))
     { c_2 = 2;
       kb2 = kb/(1.0+per*(kb/(1.4*Pr1)-1.0));
       lo2 = lo*(1.0-per)+pow(Pr1*1.0e-5/1.01325,
                  1.0/1.4)*1.5*per;
       a2  = sqrt(kb2/lo2);
       seg2= a33*a2;
       B20 = a2/(g*S);
       B21 = a2/(g*s1);
       B22 = a2/(g*s2);

       for(ii = 1; ii <= kdi; ++ii)
        { H4[ii] = Pr1/(g*lo2); Q4[ii] = 0.0; } }

if((c_2 == 3) AND (H2[1] <= P0/(lo2*g)))
     { c_2 = 4;
       kb2 = kb/(1.0+per*(kb/(1.4*P0)-1.0));
       lo2 = lo*(1.0-per)+pow(P0*1.0e-5/1.01325,
                  1.0/1.4)*1.5*per;
       a2  = sqrt(kb2/lo2);
       seg2= a33*a2;
       B20 = a2/(g*S);
       B21 = a2/(g*s1);
       B22 = a2/(g*s2);

      for(ii = 1; ii <= ksu; ++ii)
        { H4[ii] = P0/(g*lo2); Q4[ii] = 0.0; } }
}

/**************************************************/

  if(fun1 == 2)
    {
       if((c_1 == 1) OR (c_1 == 3))
          { s1  = pow(marg1-p111,sc);
            fl1 = kb1/s1;  }

       if((c_2 == 1) OR (c_2 == 3))
          { s2  = pow(marg2+p111,sc);
            fl2 = kb2/s2;   }

       if((c_1 == 1) AND (fl1 >= Pop*S))
          { c_1 = 2;  fl1 = Pr1*S; }

       if((c_1 == 2) AND (s11 < -0.01)
                     AND (p111 >= stroke/2.0))
          {  c_1 = 3;     c_2 = 1;
             a1  = p111;
             kb1 = fl1*pow(marg1-a1,sc);
```

```
                kb2 = fl2*pow(marg2+a1,sc);    }

           if((c_1 == 3) AND (fl1 <= P0*S))
              { c_1 = 4;  fl2 = P0*S; }

           if((c_1 == 4) AND (s11 >= 0.01)
                          AND (p111 <= stroke/2.0))
              {  c_1  = 1;
                 c_2  = 3;  a1 = p111;
                 kb1  = fl1*pow(marg1-a1,sc);
                 kb2  = fl2*pow(marg2+a1,sc);   }

           if((c_2 == 1) AND (fl2 >= Pop*S))
              {  c_2 = 2;  fl2 = Pr1*S;  }

           if((c_2 == 3) AND (fl2 <= P0*S))
              { c_2 = 4;  fl2 = P0*S;   }
        }

/****************************************************/

     if(fun1 == 0)
       {  fl1=0.0; fl2=0.0; }

/****************************************************/

     p11=(float)((int)(p11*4000.0))/4000.0;

     if(count2 == nn-1)
      {
       s22      = (p11 - pre_p11)/(tt1*nn1);
       pre_p11 = p11;
       errp     = r1_p11 - p111;
       errv     = r1_s22 - s22;
       errp1    = r1_p11 - p11;
       r1_p11   = r1_p11 + nn1*tt1*r1_s22 + nn1*nn1
                     *r1_acc*tt1*tt1/2.0;

       r1_s22 =r1_s22+r1_acc*tt1*nn1;
       if (r1_s22 >= peak_s22)
        {
         r1_s22 = peak_s22;
         r1_acc = -r1a_set;  }
       if (r1_s22 <= -peak_s22)
        {
         r1_s22 = -peak_s22;
         r1_acc = r1a_set;    }
      }

      t = t + tt1;
      if (t < end_time )
           goto start;
      fclose(in_file);
      fclose(out_file);
}
```

APPENDIX 2:

The Source Code of Real Time Control Software

```
;;;;;;;;;;;;;;;;;;;;;;;;;;;;;;;;;;;;;;;;;;;;;;;;;;;;;;;;;;;
;;;; CONTROL PRGRAM OF A PERMANENT MAGNET LINEAR      ;;;;
;;;; SYNCHRONOUS MOTOR FOR SUBSEA PUMP APPLICATION    ;;;;
;;;;;;;;;;;;;;;;;;;;;;;;;;;;;;;;;;;;;;;;;;;;;;;;;;;;;;;;;;;
;;;; THE REAL TIME CONTROL IS IMPLEMENTED BY USING    ;;;;
;;;; ASSEMBLE LANGUAGE DOWNLOADED TO A SPECIALLY      ;;;;
;;;; DESIGNED MICRO BOARD ENGAGING INTEL 80C196KC     ;;;;
;;;; MICROCONTROL CHIP. CLOCK FREQUENCY IS 16 MHZ.    ;;;;
;;;;;;;;;;;;;;;;;;;;;;;;;;;;;;;;;;;;;;;;;;;;;;;;;;;;;;;;;;;
;;;; It Includes Three Main Functions:                ;;;;
;;;; 1) Autopos. To Search Initial Slider Position.   ;;;;
;;;;    It Includes Three Steps: Initial Phase Serch,;;;;
;;;;    Phase Locking, Open Loop Drive and Position   ;;;;
;;;;    Search.                                       ;;;;
;;;; 2) Normal Ope. To Drive The Slider To Demanded   ;;;;
;;;;    Trajectiries.                                 ;;;;
;;;;    Closed Loops And Trajectory Generate Are      ;;;;
;;;;    Involved To Control The Motor.                ;;;;
;;;;    The Current Loop Engages A PI Controller      ;;;;
;;;;    The Position Loop Engages A Cascade           ;;;;
;;;;    Controller And Feed Forward Terms.            ;;;;
;;;;    Ramp Up And Ramp Down Are Implemented.        ;;;;
;;;; 3) Manul Ope. To Drive The Slider Manaully.      ;;;;
;;;;    Close Loops Are Used To Drive The Slider      ;;;;
;;;;    According The Required Direction.             ;;;;
;;;;;;;;;;;;;;;;;;;;;;;;;;;;;;;;;;;;;;;;;;;;;;;;;;;;;;;;;;;
;;;;;;;;;;;;;;;;;;;;;;;;;;;;;;;;;;;;;;;;;;;;;;;;;;;;;;;;;;;


$TITLE('CONT.A96')

FULL_CONTR          MODULE  MAIN ,STACKSIZE(50)

$INCLUDE(8096.INC)

RSEG AT 0024H
           CSG1:                    DSL      1
           CSG2:                    DSL      1
           CSG3:                    DSL      1
           LONG_WORD:               DSL      1
           C_POINT:                 DSW      1
           CURR_COUNT:              DSW      1
           DEM_PUMP_SPD:            DSW      1
           E_POINT:                 DSW      1
           GGA:                     DSW      1
           GGA1:                    DSW      1
           IN0_11:                  DSW      1
           IN0_12:                  DSW      1
           IN1_11:                  DSW      1
           IN1_12:                  DSW      1
           IN2_11:                  DSW      1
           IN2_12:                  DSW      1
           IB:                      DSW      1
           IR:                      DSW      1
           IR1:                     DSW      1
           IR2:                     DSW      1
           IR3:                     DSW      1
```

```
IR3_E1:                  DSW      1
IR4:                     DSW      1
IR4_E1:                  DSW      1
IR4_R1:                  DSW      1
IR_O1:                   DSW      1
IY:                      DSW      1
IY1:                     DSW      1
IY2:                     DSW      1
IY_O1:                   DSW      1
JDALP:                   DSW      1
JDGAM:                   DSW      1
L_POINT:                 DSW      1
MSSG:                    DSW      1
MW:                      DSW      1
P1_POSN1:                DSW      1
PARA_C:                  DSW      1
PARA_S:                  DSW      1
PER:                     DSW      1
per1:                    dsw      1
POSN:                    DSW      1
POSN_COUNT:              DSW      1
POSN_DIFF:               DSW      1
POSN_E1:                 DSW      1
POSN_C:                  DSW      1
POSN_T:                  DSW      1
P1_POSN:                 DSW      1
R1_POSN1:                DSW      1
R_POINT:                 DSW      1
R1_VEL:                  DSW      1
REQ_SS:                  DSW      1
R1_POSN:                 DSW      1
SPEED:                   DSW      1
STROKE:                  DSW      1
TIME_OLD:                DSW      1
TTT:                     DSW      1
 TTTL   EQU   (TTT)     :BYTE
 TTTH   EQU   (TTT+1)   :BYTE
U1:                      DSW      1
U2:                      DSW      1
U3:                      DSW      1
U1_11:                   DSW      1
U1_12:                   DSW      1
U2_11:                   DSW      1
U2_12:                   DSW      1
U3_11:                   DSW      1
U3_12:                   DSW      1
U11:                     DSW      1
U11_9:                   DSW      1
U11_0:                   DSW      1
U11_5:                   DSW      1
UD1:                     DSW      1
U22:                     DSW      1
U22_9:                   DSW      1
U22_5:                   DSW      1
U22_0:                   DSW      1
VEL1:                    DSW      1
VEL5:                    DSW      1
VEL_C:                   DSW      1
```

```
        VEL_T:                      DSW       1
        VEL_E1:                     DSW       1

        com_sb:                     dsb       1     ;for test
        dir_sb:                     dsb       1
        rec_sb:                     dsb       1

        CLOSE_COUNT:                DSB       1
        DIRECT:                     DSB       1
        DIRECT1:                    DSB       1
        DIRECT2:                    DSB       1
        DIRECT3:                    DSB       1
        JDGAM_NEG:                  DSB       1
        MB:                         DSB       1
        MCOUNT:                     DSB       1
        I_SIGN:                     DSB       1
        P_SIGN:                     DSB       1
        P1_SW_POSN:                 DSB       1
        RECORD:                     DSB       1
        R_SIGN:                     DSB       1
        SW_POSN:                    DSB       1
        PTWD:                       DSB       1
        PTWD2:                      DSB       1
        record1:                    dsb       1
;;;;;;;;;;;;;;;;;;;;;;;;;;;;;;;;;;;;;;;;;;;;;;;;;;;;;;;;;
;;;;;;;;;;;;;;;;;;;;;;;;;;;;;;;;;;;;;;;;;;;;;;;;;;;;;;;;;
CSEG AT 200AH
         DCW          T_SOFT_TIMER1
CSEG AT 2032H
         DCW          T_SERIAL_INT
CSEG AT 2038H
         DCW          T_SOFT_TIMER2

CSEG AT 203AH
         DCW         T_EXT_INT
CSEG AT 203EH
         DCW         T_NMI_SERVE
;;;;;;;;;;;;;;;;;;;;;;;;;;;;;;;;;;;;;;;;;;;;;;;;;;;;;;;;;
;;;;;;;;;;;;;;;;;;;;;;;;;;;;;;;;;;;;;;;;;;;;;;;;;;;;;;;;;
CSEG AT 8000H                               ;8000 -- 2500
     T_SOFT_TIMER1:
              PUSHF
              CALL     SOFT_TIMER1
              POPF
              RET
;;;;;;;;;;;;;;;;;;;;;;;;;;;;;;;;;;;;;;;;;;;;;;;;;;;;;;;;;
;;;;;;;;;;;;;;;;;;;;;;;;;;;;;;;;;;;;;;;;;;;;;;;;;;;;;;;;;
CSEG AT 8050H                               ;8050 -- 2550
     T_SERIAL_INT:
              PUSHF
              PUSH     TTT
              STB      SBUF,TTTL
              stb      tttl,22[c_point]
              CMPB     TTTL,#07CH
              JNE      S_RD
              LDB      SBUF,#0B8H
              BR       S_INT_E
     S_RD:
```

```
                CMPB    TTTL,#0ACH
                JNE     S_ESD
                CLR     MW
                ST      MW,16[C_POINT]
                LDB     SBUF,#0D6H
                ldb     tttl,#050h
                stb     tttl,26[e_point]
                BR      S_INT_E
     S_ESD:
                CMPB    TTTL,#04DH
                JNE     S_INT_E
                CLRB    PTWD
S_INT_E:
                POP     TTT
                POPF
                RET
;;;;;;;;;;;;;;;;;;;;;;;;;;;;;;;;;;;;;;;;;;;;;;;;;;;;;;;;;;;;
;;;;;;;;;;;;;;;;;;;;;;;;;;;;;;;;;;;;;;;;;;;;;;;;;;;;;;;;;;;;
CSEG AT 8100H                                   ;8100 -- 2600
     T_SOFT_TIMER2:
                PUSHF
                PUSH     TTT
                LD       TIMER2,#124H
                ANDB     IOPORT1,#11111110B
                ORB      IOPORT1,#00000001B
                LD       TTT,#600H
                LD       IR1,4[TTT]
                LD       IY1,2[TTT]
                POP      TTT
                POPF
                RET
;;;;;;;;;;;;;;;;;;;;;;;;;;;;;;;;;;;;;;;;;;;;;;;;;;;;;;;;;;;;
;;;;;;;;;;;;;;;;;;;;;;;;;;;;;;;;;;;;;;;;;;;;;;;;;;;;;;;;;;;;
CSEG AT 8150H                                   ;8150 -- 2650
     T_EXT_INT:
                PUSHF
                push    ax
                CLR     MW
                ldb     al,#05ah
                stb     al,26[e_point]
                ST      MW,16[C_POINT]
                st      mw,18[c_point]
                st      mw,20[c_point]
                pop     ax
                POPF
                RET
;;;;;;;;;;;;;;;;;;;;;;;;;;;;;;;;;;;;;;;;;;;;;;;;;;;;;;;;;;;;
;;;;;;;;;;;;;;;;;;;;;;;;;;;;;;;;;;;;;;;;;;;;;;;;;;;;;;;;;;;;
CSEG AT 8200H                                   ;8200 -- 2700
     T_NMI_SERVE:
                PUSHF
                CLRB    PTWD
                CLRB    MCOUNT
                STB     MCOUNT,4[C_POINT]
                STB     MCOUNT,6[C_POINT]
                CLR     MW
                ST      MW,16[C_POINT]
                st      mw,18[c_point]
```

```
        st      mw,20[c_point]
        CLRB    MB
        ldb     sbuf,#0d6h       ;;!for test only
        POPF
        RET

;;;;;;;;;;;;;;;;;;;;;;;;;;;;;;;;;;;;;;;;;;;;;;;;;;;;;;;;;;;;;;
;;;;;;;;;;;;;;;;;;;;;;;  Main Program  ;;;;;;;;;;;;;;;;;;;;;;;
;;;;;;;;;;;;;;;;;;;;;;;;;;;;;;;;;;;;;;;;;;;;;;;;;;;;;;;;;;;;;;
CSEG AT 8300H                               ;8300 -- 2800
BB11:
        LD      SP,#200H
        LDB     IOC1,#00100010B
        LDB     IOC2,#82H
;;;;;;;;;;;;;;;;;;;;;;;;;;;;;;;;;;;;;;;;;;;;;;;;;;;;;;;;;;;;;;
        ORB     IOPORT1,#11111110B
        ANDB    IOPORT1,#00001111B
        LDB     SP_CON,#09H
        LDB     BAUD_RATE,#0cH     ;;! #0ch -- #67
        LDB     BAUD_RATE,#80H     ;;! changed for test
        ANDB    INT_PENDING,#0
        CLRB    IPEND1
        LDB     INT_MASK,#00100100B
        LDB     IMASK1,#00110010B
;;;;;;;;;;;;;;;;;;;;;;;;;;;;;;;;;;;;;;;;;;;;;;;;;;;;;;;;;;;;;;
        CLRB    MB
        CLR     MW
        CLRB    MCOUNT
        CLRB    PTWD
        CLRB    PTWD2
        LD      IR_O1,#687H      ;697h -- 688h
        LD      IY_O1,#6a0H      ;6aah -- 6a0h
        LD      C_POINT,#6000H
        LD      E_POINT,#6050H
        LD      L_POINT,#9500H
        LD      R_POINT,#6100H
INIT1:
        ST      MW,[C_POINT]+
        CMP     C_POINT,#7000H
        JLT     INIT1
        LD      C_POINT,#6000H
        ST      R_POINT,10[C_POINT]

        ldb     wsr,#01h
        LDB     T2CONTROL,#01H
        ldb     wsr,#00h
        LD      TIMER2,#12CH
        LDB     HSO_COMMAND,#39H
        ADD     HSO_TIME,TIMER1,#5DCH
        EI
;;;;;;;;;;;;;;;;;;;;;;;;;;;;;;;;;;;;;;;;;;;;;;;;;;;;;;;;;;;;;;
;;;;;;;;;;;;;;;;;;;;;;;;;;;;;;;;;;;;;;;;;;;;;;;;;;;;;;;;;;;;;;
START:
        LD      TTT,#6FF0H
        LDB     MB,14[TTT]
        CMPB    MB,#00H
        JNE     STMA
        BR      START1
```

```
STMA:
            CMPB    MB,#7CH
            JNE     STBT1
            LDB     MB,#0A8H
            STB     MB,12[TTT]
            STB     MCOUNT,14[TTT]
            BR      START
STBT1:
            CMPB    MB,#5FH
            JNE     STBT2
            STB     MB,12[TTT]
            STB     MCOUNT,14[TTT]
            CLRB    INT_MASK
            CLRB    IMASK1
            CLRB    INT_PENDING
            CLRB    IPEND1
            rst
STBT2:
            CMPB    MB,#4DH
            JNE     STDTUP
            STB     MB,12[TTT]
            STB     MCOUNT,14[TTT]
            CLRB    INT_MASK
            CLRB    IMASK1
            CLRB    INT_PENDING
            CLRB    IPEND1
            BR      INIT_S                  ;WARM
STDTUP:
            CMPB    MB,#9DH
            JE      STDTUP1
            LDB     MB,#0AAH
            STB     MB,12[TTT]
            STB     MCOUNT,14[TTT]
            BR      START
STDTUP1:
            LD      VEL_C,4[TTT]
            LD      VEL_T,6[TTT]
            CMP     VEL_T,#00H
            JLE     STDTUP3
            CMP     VEL_T,#80H
            JGT     STDTUP3
            LD      AX,VEL_T
            JBS     AL,0,STDTUP3
            SUB     VEL_T,#2
            CMP     VEL_C,LMT_1[VEL_T]
            JLT     STDTUP5
            CMP     VEL_C,LMT_2[VEL_T]
            JGT     STDTUP5
            ST      VEL_C,LMT_TABLE[VEL_T]
            clrb    mb
            BR      STDTUP7
STDTUP3:
            LDB     MB,#0cdH                    ;2a -- 0cd
            BR      STDTUP7
STDTUP5:
            LDB     MB,#0cdH                    ;3b -- 0cd
STDTUP7:
            STB     MB,12[TTT]
```

```
            STB     MCOUNT,14[TTT]
            BR      START
START1:
            LDB     MB,4[C_POINT]
            CMPB    MB,#02H
            JE      STARTN
            BR      START2
STARTN:
            LD      MW,16[C_POINT]
            AND     AX,MW,#08000H
            JNE     START10
            LD      MSSG,#0ABCH
            ST      MSSG,[E_POINT]
            BR      START40
START10:
            AND     MW,#7FFFH
            ST      MW,16[C_POINT]
            LD      DEM_PUMP_SPD,18[C_POINT]
            LD      PER,20[C_POINT]
            CMP     DEM_PUMP_SPD,#32H            ;16[L_POINT]
            JGT     START11
            CMP     DEM_PUMP_SPD,#00H
            JGT     START15
START11:
            CLR     DEM_PUMP_SPD
            CLR     PER
            LD      MSSG,#9876H
            ST      MSSG,[E_POINT]
            BR      START40
START15:
            CMP     PER,#64H
            JGT     START16
            CMP     PER,#00H
            JGE     START17
START16:
            CLR     PER
            CLR     DEM_PUMP_SPD
            LD      MSSG,#6789H
            ST      MSSG,[E_POINT]
            BR      START40
START17:
            ld      per1,per
            STB     MB,6[C_POINT]
            CLRB    MB
            LD      SPEED,#01H                  ;;;#03h
            LD      STROKE,2[L_POINT]
            MUL     LONG_WORD,SPEED,STROKE
            DIV     LONG_WORD,#0AH
            LD      REQ_SS,LONG_WORD
            clr     gga1
            clr     gga
            CALL    INIT_OP

            LD      R1_POSN,STROKE
            SHR     R1_POSN,#1
            NEG     R1_POSN
            ADD     R1_POSN,#0BB8H
            CMP     R1_POSN,POSN
```

```
        JGT     NORM_P
        JLT     NORM_N
        CLRB    DIRECT
        ANDB    RECORD,#0F7H
        BR      NORM101S
NORM_P:
        LDB     DIRECT,#01H
        BR      NORM101S
NORM_N:
        LDB     DIRECT,#02H
NORM101S:
        LDB     MCOUNT,#02H
        clrb    dir_sb          ;;! used for test only
        clrb    rec_sb          ;;! used for test only
        BR      NORM1
START2:
        CMPB    MB,#04H
        JE      STARTA
        BR      START3
STARTA:
        LD      MW,16[C_POINT]
        CMP     MW,#0CFCFH
        JE      START20
        LD      MSSG,#0ABCH
        ST      MSSG,[E_POINT]
        BR      START40
START20:
        LDB     MB,#01H
        CALL    INIT_OP
         LD      U22_9,#1D65H
         LD      U11_9,#01H
        LDB     MCOUNT,#14H
        STB     MCOUNT,6[C_POINT]

        BR      AUTO1
START3:
        CMPB    MB,#08H
        JE      STARTM
        BR      START4
STARTM:
        LD      MW,16[C_POINT]
        CMP     MW,#0CFCFH
        JE      START32
START31:
        LD      MSSG,#0ABCH
        ST      MSSG,[E_POINT]
        BR      START40
START32:
        STB     MB,6[C_POINT]
        LDB     DIRECT2,18[C_POINT]
        CMPB    DIRECT2,#02H
        JGT     START31
        STB     DIRECT2,DIRECT
        CALL    INIT_OP
        LDB     MCOUNT,#08H

        BR      MANU1
START4:
```

```
          CMPB    MB,#00H
          JE      START5
          LD      MSSG,#0ABCDH
          ST      MSSG,[E_POINT]
START40:
          CLR     MW
          CLRB    MB
          ST      MW,16[C_POINT]
          STB     MB,4[C_POINT]
START5:
          BR      START
;;;;;;;;;;;;;;;;;;;;;;;;;;;;;;;;;;;;;;;;;;;;;;;;;;;;;;;;;;;;;;;;;;;
;;;;;;;;;;;;;;;;;;;;;;;;;;;;;;;;;;;;;;;;;;;;;;;;;;;;;;;;;;;;;;;;;;;
NORM1:
          LD      MW,16[C_POINT]
          AND     AX,MW,#08000H
          JE      NORM2
          AND     MW,#7FFFH
          ST      MW,16[C_POINT]
          LD      TTT,20[C_POINT]
          CMP     TTT,#64H
          JGT     NORM10
          CMP     TTT,#00H
          JLT     NORM10
          LD      PER1,TTT
          LD      TTT,18[C_POINT]
          CMP     TTT,#32H                    ;16[L_POINT]
          JGT     NORM10
          CMP     TTT,#00H
          JLT     NORM10
          LD      DEM_PUMP_SPD,TTT
          BR      NORM2
     NORM10:
          LD      MSSG,#0B6B6H
          ST      MSSG,20[E_POINT]
     NORM2:
          JBC     RECORD,0,NORM20
          ANDB    RECORD,#11111110B
          CMP     CURR_COUNT,#0000H
          JE      NORM205
     NORM20:
          BR      NORM3
     NORM205:
          ld      per,per1
          LDB     DIRECT2,MB
          CLRB    MB
          CMPB    DIRECT2,#10H
          JGE     NORM215
     NORM21:
          CMP     SPEED,DEM_PUMP_SPD
          JE      NORM219
          JGT     NORM215
          CMPB    DIRECT2,#00H
          JNE     NORM211
          ADD     SPEED,#02H
     NORM211:
          ADD     SPEED,#01H
          CMP     SPEED,DEM_PUMP_SPD
```

```
        JLE     NORM217
        LD      SPEED,DEM_PUMP_SPD
        BR      NORM217
NORM215:
        cmp     speed,#03h
        jgt     norm216
        sub     speed,#01h
        br      norm2160
norm216:
        SUB     SPEED,#03H                  ;warning
norm2160:
        CMP     SPEED,#00H
        JGT     NORM217
        LD      SPEED,#01H
NORM217:
        MUL     LONG_WORD,SPEED,STROKE
        DIV     LONG_WORD,#0AH
        LD      REQ_SS,LONG_WORD
        mul     long_word,speed,speed
        mul     long_word,stroke
        div     long_word,#0627h
        ld      gga,long_word
NORM219:
        CMP     MW,#0000H
        JNE     NORM22
        CLR     DEM_PUMP_SPD
        CMP     SPEED,90[L_POINT]
        JGT     NORM4
        BR      NORMEND
NORM22:
        CMP     MW,#04000H
        JE      NORM4
        DEC     MW
        ST      MW,16[C_POINT]
NORM24:
        BR      NORM4
NORM3:
        JBC     CLOSE_COUNT,0,NORM4
        JBC     RECORD,1,NORM4
        ANDB    RECORD,#11111101B
        CALL    CONT_CHK
        CMP     MSSG,#00H
        JNE     NORMEND
NORM4:
        CMPB    MCOUNT,#00H                   ;;
        JE      NORMEND                       ;;
        BR      NORM1
NORMEND:
        CLRB    MCOUNT
        STB     MCOUNT,4[C_POINT]
        STB     MCOUNT,6[C_POINT]
        CLR     MW
        ST      MW,8[C_POINT]
        ST      MW,16[C_POINT]
        st      mw,18[c_point]
        st      mw,20[c_point]
        CLRB    MB
        BR      START
```

```
;;;;;;;;;;;;;;;;;;;;;;;;;;;;;;;;;;;;;;;;;;;;;;;;;;;;;;;;;;;
;;;;;;;;;;;;;;;;;;;;;;;;;;;;;;;;;;;;;;;;;;;;;;;;;;;;;;;;;;;
AUTO1:
          LD       MW,16[C_POINT]
          CMP      MW,#00H
          JE       AUTOEND1
          CMPB     MCOUNT,#0A0H
          JNE      AUTO2
          BR       AUTOEND
     AUTO2:
          CMPB     MCOUNT,#0C0H
          JNE      AUTO3
          BR       AUTOEND
     AUTO3:
          CMPB     MCOUNT,#84H
          JNE      AUTO1
          CALL     CONT_CHK
          CMP      MSSG,#00H
          JE       AUTO1
          LDB      MCOUNT,#0C0H
          br       autoend
     autoend1:
          clrb     mcount
     AUTOEND:
          STB      MCOUNT,6[C_POINT]
          CLRB     MCOUNT
          STB      MCOUNT,4[C_POINT]
          CLR      MW
          ST       MW,8[C_POINT]
          ST       MW,16[C_POINT]
          st       mw,18[c_point]
          st       mw,20[c_point]
          CLRB     MB
          BR       START
;;;;;;;;;;;;;;;;;;;;;;;;;;;;;;;;;;;;;;;;;;;;;;;;;;;;;;;;;;;
;;;;;;;;;;;;;;;;;;;;;;;;;;;;;;;;;;;;;;;;;;;;;;;;;;;;;;;;;;;
MANU1:
          LD       MW,16[C_POINT]
          CMP      MW,#00H
          JE       MANUEND
          LDB      DIRECT2,18[C_POINT]
          CMPB     DIRECT2,#02H
          JGT      MANU2
          STB      DIRECT2,DIRECT
          BR       MANU3
     MANU2:
          STB      DIRECT2,20[E_POINT]
     MANU3:
          CALL     CONT_CHK
          CMP      MSSG,#00H
          JE       MANU1
     MANUEND:
          CLRB     MCOUNT
          STB      MCOUNT,6[C_POINT]
          STB      MCOUNT,4[C_POINT]
          CLR      MW
          ST       MW,8[C_POINT]
          ST       MW,16[C_POINT]
```

```
        st      mw,18[c_point]
        st      mw,20[c_point]
        st      posn,32[e_point]
        st      p1_posn,34[e_point]
        st      VEL1,36[e_point]
        CLRB    MB
        BR      START
;;;;;;;;;;;;;;;;;;;;;;;;;;;;;;;;;;;;;;;;;;;;;;;;;;;;;;;;;;;;
INIT_OP:
        CLR     JDALP
        CLR     IR3_E1
        CLR     IR4_E1
        CLR     CSG1
        CLR     CSG1+2
        CLR     POSN_COUNT
        CLR     CURR_COUNT
        CLRB    DIRECT
        CLRB    DIRECT1
        CLRB    DIRECT2
        CLRB    DIRECT3
        CLR     POSN_E1
        CLR     CSG3
        CLR     CSG3+2
        CLR     U1
        CLR     U2
        CLR     U3
        CLR     U11
        CLR     U22
        CLR     UD1
        clr     posn_t
        CLR     VEL1
        CLR     VEL5
        clr     r1_vel
        CLRB     I_SIGN
        CLRB     R_SIGN
        CLRB    DIRECT
        clrb    record1
        LDB     CLOSE_COUNT,#1H
        LD      TTT,2[C_POINT]
        ADD     POSN,TTT,#0BB8H
        LD      R1_POSN1,POSN
        LD      P1_POSN1,POSN
        LD      R1_POSN,POSN
        LD      P1_POSN,POSN
        LDB     RECORD,#0FEH
        RET
;;;;;;;;;;;;;;;;;;;;;;;;;;;;;;;;;;;;;;;;;;;;;;;;;;;;;;;;;;;;
    CONT_CHK:
        CLR     MSSG
        SUB     TTT,R1_POSN1,POSN
        AND     BX,TTT,#08000H
        JE      CONT_CHK1
        NEG     TTT
    CONT_CHK1:
        CMP     TTT,8[L_POINT]
        JLE     CONT_CHK2
        LD      MSSG,#1234H
        ST      MSSG,[E_POINT]
```

```
        ST      POSN,2[E_POINT]
        ST      R1_POSN1,4[E_POINT]
        ST      TTT,6[E_POINT]
        BR      CONT_CHK_ED1
    CONT_CHK2:
        SUB     TTT,R1_VEL,VEL1
        AND     BX,TTT,#08000H
        JE      CONT_CHK3
        NEG     TTT
    CONT_CHK3:
        CMP     TTT,10[L_POINT]
        JGT     CONT_CHK4
        CLRB    DIRECT3
        BR      CONT_CHK5
    CONT_CHK4:
        INCB    DIRECT3
        CMPB    DIRECT3,#03H
        JLT     CONT_CHK5
        LD      MSSG,#4321H
        ST      MSSG,[E_POINT]
        ST      VEL1,2[E_POINT]
        ST      R1_VEL,4[E_POINT]
        ST      TTT,6[E_POINT]
        BR      CONT_CHK_ED1
    CONT_CHK5:
        LD      TTT,#1770H
        ADD     TTT,12[L_POINT]
        CMP     TTT,POSN
        JGE     CONT_CHK6
        BR      CONT_CHK7
    CONT_CHK6:
        LD      TTT,POSN
        NEG     TTT
        CMP     TTT,12[L_POINT]
        JGT     CONT_CHK7
        BR      CONT_CHK_END
    CONT_CHK7:
        LD      MSSG,#0123H
        ST      MSSG,[E_POINT]
        ST      POSN,2[E_POINT]
        ST      R1_POSN1,4[E_POINT]
        ST      TTT,6[E_POINT]
    CONT_CHK_ED1:
        LDB     SBUF,#0d6H          ;;! #0d6h -- #09eh
        LDB     PTWD,#01H           ;;! changed for test
    CONT_CHK_END:
        RET
;;;;;;;;;;;;;;;;;;;;;;;;;;;;;;;;;;;;;;;;;;;;;;;;;;;;;;;;;;;;
;;;;;;;;;  Software Interrupt Service Routine  ;;;;;;;;;;
;;;;;;;;;;;;;;;;;;;;;;;;;;;;;;;;;;;;;;;;;;;;;;;;;;;;;;;;;;;;
SOFT_TIMER1:
        PUSHF
        LDB     HSO_COMMAND,#39H
        ADD     HSO_TIME,TIMER1,#5D6H
        LD      TIME_OLD,TIMER1
;;;;;;;;;;;;;;;;;;;;;;;;;;;;;;;;;;;;;;;;;;;;;;;;;;;;;;;;;;;;
        JBS     MCOUNT,2,JAUTO
        JBS     MCOUNT,1,JNORM
```

```
          JBS       MCOUNT,3,JMANU

          JBS       PTWD,2,ST_WD1
          SHLB      PTWD,#01
     ST_WD1:
          BR        EEND
;;;;;;;;;;;;;;;;;;;;;;;;;;;;;;;;;;;;;;;;;;;;;;;;;;;;;;;;;;;;
JAUTO:
          LDB       P1_SW_POSN,SW_POSN
          LDB       SW_POSN,[C_POINT]
          LD        POSN_C,2[C_POINT]
          LD        P1_POSN,POSN
          ADD       POSN,POSN_C,#0BB8H
          LD        R1_VEL,VEL1
          SUB       VEL1,POSN,P1_POSN
          JBS       MCOUNT,4,JAP1
          JBS       MCOUNT,5,JAP2
          JBS       MCOUNT,6,JAP3
          JBS       MCOUNT,7,JAP4
          BR        AUTO_END
JAP1:
          CALL      AP11
          BR        AUTO_END
JAP2:
          CALL      AP22
          BR        AUTO_END
JAP3:
          CALL      AP33
          BR        AUTO_END
JAP4:
          CALL      AP44
AUTO_END:
          BR        EEND
;;;;;;;;;;;;;;;;;;;;;;;;;;;;;;;;;;;;;;;;;;;;;;;;;;;;;;;;;;;;
JNORM:
          CALL      NORM_OPE
          BR        EEND
JMANU:
          CALL      MANU_OPE
EEND:
          JBS       PTWD,2,ST_WD8
          LD        VEL_C,#406H
          JBS       PTWD2,0,ST_WD3
          LDB       PTWD2,#01H
          STB       PTWD2,[VEL_C]
          BR        ST_WD8
     ST_WD3:
          CLRB      PTWD2
          STB       PTWD2,[VEL_C]
     ST_WD8:
          LDB       P_SIGN,8[C_POINT]
          CMPB      P_SIGN,#00H
          JNE       STORE0
          CLRB      R_SIGN
          LD        R_POINT,#6100H
          ST        R_POINT,10[C_POINT]
          BR        STORE3
     STORE0:
```

```
        INCB    R_SIGN
        CMPB    R_SIGN,P_SIGN
        JGE     STORE2
        BR      STORE3
   STORE1:
        LD      R_POINT,#6100H
   STORE2:
        CLRB    R_SIGN
        CMP     R_POINT,#6FEEH
        JGE     STORE1
        ST      posn,[R_POINT]
        add     r_point,#02
        ST      vel5,[R_POINT]
        add     r_point,#02
        ST      IR,[R_POINT]
        add     r_point,#02
        ST      POSN_E1,[R_POINT]
        add     r_point,#02
        st      ir4_r1,[r_point]
        add     r_point,#02
        st      ir4,[R_POINT]
        add     r_point,#02
        ST      U1,[R_POINT]
        add     r_point,#02
        st      R1_VEL,[R_POINT]
        add     r_point,#02
        ST      R_POINT,10[C_POINT]
   STORE3:
        POPF
        RET
;;;;;;;;;;;;;;;;;;;;;;;;;;;;;;;;;;;;;;;;;;;;;;;;;;;;;;;;;;;
NORM_OPE:
        LD      POSN_C,2[C_POINT]
        ADD     POSN,POSN_C,#0BB8H
;;;;;;;;;;;;;;;;;;;;;;;;;;;;;;;;;;;;;;;;;;;;;;;;;;;;;;;;;;;
        jbs     dir_sb,1,neg_sb   ;;! for test only
        cmp     posn,p1_posn
        jlt     zero_sb
        jbs     dir_sb,0,con_sb
        ldb     sbuf,#03ch
        ldb     dir_sb,#01h
        br      con_sb
    zero_sb:
        ldb     sbuf,#03fh
        ldb     dir_sb,#02h
        clrb    rec_sb
        br      con_sb
   neg_sb:
        cmp     posn,#00h
        jne     neg_sb1
        jbs     rec_sb,0,neg_sb1
        ldb     sbuf,#0a3h
        ldb     rec_sb,#01h
   neg_sb1:
        cmp     posn,p1_posn
        jle     con_sb
        ldb     sbuf,#03ch
        ldb     dir_sb,#01h
```

```
        ldb     com_sb,14[c_point]
        cmpb    com_sb,#02h              ;start
        je      neg_sb2
        cmpb    com_sb,#0ffh             ;stop
        jne     neg_sb4
        clrb    com_sb
        stb     com_sb,14[c_point]
        br      neg_sb6
neg_sb2:
        ldb     sbuf,#0c5h
        clrb    com_sb
        stb     com_sb,14[c_point]
        br      con_sb
neg_sb4:
        cmp     dem_pump_spd,#00h         ;stop
        jne     con_sb
neg_sb6:
        ldb     sbuf,#0d6h
;;;;;;;;;;;;;;;;;;;;;;;;;;;;;;;;;;;;;;;;;;;;;;;;;;;;;;;;;;;;
    con_sb:
        JBC      RECORD,3,NORM_OPE1
        JBC      CLOSE_COUNT,0,NMANU2
    NMANU1:
        CALL     CALC_C1
;;;;;;;;;;;;;;;;;;;;;;;;;;;;;;;;;;;;;;;;;;;;;;;;;;;;;;;;;;;;
    NMANU2:
        CALL     CURRENT_CAPT
    NMANU3:
        CALL     CALC_V1
        JBC      CLOSE_COUNT,2,NMANU50
        LDB      CLOSE_COUNT,#1H
        ORB      RECORD,#00000010B
        JBS      DIRECT,0,NMANU4P
        JBS      DIRECT,1,NMANU4N
        INCB     DIRECT1
        CMPB     DIRECT1,#70H
        JLT      NMANU5
        CLRB     DIRECT1
        ANDB     RECORD,#0F7H
        BR       NMANU5
    NMANU4P:
        ADD      R1_POSN1,6[L_POINT]
        CMP      R1_POSN1,R1_POSN
        JLT      NMANU5
        LD       R1_POSN1,R1_POSN
        CLRB     DIRECT
        BR       NMANU5
    NMANU4N:
        SUB      R1_POSN1,6[L_POINT]
        CMP      R1_POSN1,R1_POSN
        JGT      NMANU5
        LD       R1_POSN1,R1_POSN
        CLRB     DIRECT
        BR       NMANU5
    NMANU50:
        SHLB     CLOSE_COUNT,#1H
    NMANU5:
```

```
        BR      END_INT
;;;;;;;;;;;;;;;;;;;;;;;;;;;;;;;;;;;;;;;;;;;;;;;;;;;;;;;;;;
    NORM_OPE1:
        JBS     CLOSE_COUNT,0,INTER_ONE
        BR      NORM_OPE2
    INTER_ONE:
        CALL    CALC_C1
;;;;;;;;;;;;;;;;;;;;;;;;;;;;;;;;;;;;;;;;;;;;;;;;;;;;;;;;;;
    NORM_OPE2:
        CALL     CURRENT_CAPT
        CALL     CALC_V1
        JBS      CLOSE_COUNT,0,END_INT1
        JBS      CLOSE_COUNT,1,INTER_TWO
        LDB      CLOSE_COUNT,#01H
        ORB      RECORD,#02H
        BR       END_INT
    INTER_TWO:
        ORB      RECORD,#01H
        LD       R1_POSN,R1_POSN1
        LD       POSN_COUNT,CURR_COUNT
        CALL     CALC_P1
        LD       R1_POSN1,R1_POSN
        LD       CURR_COUNT,POSN_COUNT
    END_INT1:
        SHLB     CLOSE_COUNT,#1H

    END_INT:
        CALL      CALC_T1
        CALL      CALC_OP1
    NORM_END:
        RET
;;;;;;;;;;;;;;;;;;;;;;;;;;;;;;;;;;;;;;;;;;;;;;;;;;;;;;;;;;
MANU_OPE:
        LD      POSN_C,2[C_POINT]
        ADD     POSN,POSN_C,#0BB8H
        JBC     CLOSE_COUNT,0,IMANU2
    IMANU1:
        CALL    CALC_C1
;;;;;;;;;;;;;;;;;;;;;;;;;;;;;;;;;;;;;;;;;;;;;;;;;;;;;;;;;;
    IMANU2:
        CALL    CURRENT_CAPT
    IMANU3:
        CALL    CALC_V1
        JBC     CLOSE_COUNT,2,IMANU50
        LDB     CLOSE_COUNT,#01H
        ORB     RECORD,#00000010B
        JBS     DIRECT,0,IMANU4P
        JBS     DIRECT,1,IMANU4N
        BR      IMANU5
    IMANU4P:
        ADD     R1_POSN1,#01h        ;6[L_POINT]
        CMP     R1_POSN1,#1770H
        JLT     IMANU5
        LD      R1_POSN1,#1770H
        BR      IMANU5
    IMANU4N:
        SUB     R1_POSN1,#01h         ;6[L_POINT]
        CMP     R1_POSN1,#00H
```

```
        JGT      IMANU5
        CLR      R1_POSN1
        BR       IMANU5
   IMANU50:
        SHLB     CLOSE_COUNT,#1H
   IMANU5:
        CALL       CALC_T1
        CALL       CALC_OP1
        RET
;;;;;;;;;;;;;;;;;;;;;;;;;;;;;;;;;;;;;;;;;;;;;;;;;;;;;;;;;;;
AP11:
        ANDB     AL,SW_POSN,#00010001B
        JE       AP110
        LDB      DIRECT,#01H
        CLRB     U11
        BR       AP11E
   AP110:
        CMP      VEL1,#00H
        JGT      APPOS
        JLT      APNEG
        CLRB     DIRECT
        BR       AP11T
   APPOS:
        LDB      DIRECT,#01H
        BR       AP11T
   APNEG:
        LDB      DIRECT,#02H
   AP11T:
        CMP      U11,#2000H
        JGE      AP11L
        BR       AP115
   AP11L:
        CLR      posn_t
        CMP      VEL1,#00H
        JE       AP111
        CLR      U22
        BR       AP11E2
   AP111:
        INC      U22
   AP112:
        CMP      U22,#64H
        JLT      AP114
        CLR      posn_t
        CLR      U11
        CLR      U22
        JBS      MB,0,AP1131
        JBS      MB,1,AP1132
        BR       APS1
   AP1131:
        LDB      MB,#02H
        BR       AP11E2
   AP1132:
        LDB      MB,#04H
   AP114:
        BR       AP11E2
;;;;;;;;;;;;;;;;;;;;;;;;;;;;;;;;;;;;;;;;;;;;;;;;;;;;;;;;;;;
   APS1:
        JBS      DIRECT1,0,S1RP
```

```
        JBS     DIRECT1,1,S1RN
        JBS     DIRECT2,0,S10YP
        JBS     DIRECT2,1,S10YN
        BR      APS1EF
S1RP:
        JBS     DIRECT2,0,S1Y1
        JBS     DIRECT2,1,S1Y2
        JBS     DIRECT3,0,APS1EF
        JBS     DIRECT3,1,S1B16         ;;6
        BR      APS1EF
S1RN:
        JBS     DIRECT2,0,S1Y3
        JBS     DIRECT2,1,S1Y4
        JBS     DIRECT3,0;S1B13         ;;3
        BR      APS1EF
S10YP:
        JBS     DIRECT3,1,S1B11         ;;1
        BR      APS1EF
S10YN:
        JBS     DIRECT3,0,S1B14         ;;4
        BR      APS1EF
S1Y1:
        JBS     DIRECT3,1,S1B11         ;;1
        BR      APS1EF
S1Y2:
        JBS     DIRECT3,1,S1B16         ;;6
        BR      S1B15                   ;;5 . 5
S1Y3:
        JBS     DIRECT3,0,S1B13         ;;3
        BR      S1B12                   ;;2 . 2
S1Y4:
        JBS     DIRECT3,0,S1B14         ;;4
APS1EF:
        LDB     MCOUNT,#0C0H
        BR      AP11E2
S1B11:
        LDB     DIRECT,#01H
        BR      APS1E
S1B12:
        LDB     DIRECT,#02H
        BR      APS1E
S1B13:
        LDB     DIRECT,#04H
        BR      APS1E
S1B14:
        LDB     DIRECT,#08H
        BR      APS1E
S1B15:
        LDB     DIRECT,#10H
        BR      APS1E
S1B16:
        LDB     DIRECT,#20H
APS1E:
        JBC     SW_POSN,1,AP11E
        JBS     DIRECT,0,APS1E1
        SHRB    DIRECT,#01
        BR      AP11E
APS1E1:
```

```
        LDB     DIRECT,#20H
;;;;;;;;;;;;;;;;;;;;;;;;;;;;;;;;;;;;;;;;;;;;;;;;;;;;;;;;;;;;;
    AP11E:
        CLR     U1
        CLR     U2
        CLR     U3
;;;;;;;;;;;;;;;;;;;;;;;;;;;;;;;;;;;;;;;;;;;;;;;;;;;;;;;;;;;;;
        LD      posn_t,U22_9
        LD      U11_0,posn_t
        SHR     U11_0,#01H
        NEG     U11_0
        JBS     DIRECT,0,S1C11
        JBS     DIRECT,1,S1C12
        JBS     DIRECT,2,S1C13
        JBS     DIRECT,3,S1C14
        JBS     DIRECT,4,S1C15
        JBS     DIRECT,5,S1C16
        LDB     MCOUNT,#0C0H
        BR      AP11E2
    S1C11:
        LD      U1,posn_t
        LD      U2,U11_0
        LD      U3,U2
        LD      R1_POSN,#00H
        BR      APS1PE
    S1C12:
        LD      U3,posn_t
        NEG     U3
        LD      U2,U11_0
        NEG     U2
        LD      U1,U2
        LD      R1_POSN,#0C8H
        BR      APS1PE
    S1C13:
        LD      U2,posn_t
        LD      U1,U11_0
        LD      U3,U1
        LD      R1_POSN,#190H
        BR      APS1PE
    S1C14:
        LD      U1,posn_t
        NEG     U1
        LD      U2,U11_0
        NEG     U2
        LD      U3,U2
        LD      R1_POSN,#258H
        BR      APS1PE
    S1C15:
        LD      U3,posn_t
        LD      U1,U11_0
        LD      U2,U1
        LD      R1_POSN,#320H
        BR      APS1PE
    S1C16:
        LD      U2,posn_t
        NEG     U2
        LD      U1,U11_0
        NEG     U1
```

```
        LD      U3,U1
        LD      R1_POSN,#3E8H
;;;;;;;;;;;;;;;;;;;;;;;;;;;;;;;;;;;;;;;;;;;;;;;;;;;;;;;;;;;
    APS1PE:
        LDB     MCOUNT,#24H
        STB     MCOUNT,6[C_POINT]
        BR      AP11E2
    AP115:
        INC     U11
        CMP     U22,#04H
        JLT     AP116
        CLR     U22
        LD      U11,#7FFFH
        BR      AP11E2
    AP116:
        CMP     posn_t,U22_9
        JGE     AP117
        ADD     posn_t,U11_9
        LD      U11_0,posn_t
        SHR     U11_0,#1
        NEG     U11_0
    AP117:
        CMP     VEL1,#00H
        JNE     AP1170
        CLR     U22
        BR      AP118
    AP1170:
        INC     U22
    AP118:
        JBS     MB,0,AP1181
        JBS     MB,1,AP1182
        LD      U1,U11_0
        LD      U2,U11_0
        LD      U3,posn_t
        LDB     DIRECT3,DIRECT
        BR      AP11E1
    AP1181:
        LD      U1,posn_t
        LD      U2,U11_0
        LD      U3,U11_0
        LDB     DIRECT1,DIRECT
        BR      AP11E1
    AP1182:
        LD      U1,U11_0
        LD      U2,posn_t
        LD      U3,U11_0
        LDB     DIRECT2,DIRECT
    AP11E1:
        CALL    CURRENT_CAPT
        CALL    CALC_T1
        CALL    CALC_OP1
    AP11E2:
        RET
;;;;;;;;;;;;;;;;;;;;;;;;;;;;;;;;;;;;;;;;;;;;;;;;;;;;;;;;;;;
AP22:
        INC     U11
        CMP     U11,#2000H
        JLT     AP225
```

```
        CMP     VEL1,#00
        JNE     AP225
        MUL     LONG_WORD,R1_POSN,#64H
        DIV     LONG_WORD,#0FH
        LD      JDALP,LONG_WORD
        CLR     U11
        CLRB    MB
        CLRB    DIRECT
        LDB     MCOUNT,#44H
        STB     MCOUNT,6[C_POINT]
        ANDB    AL,SW_POSN,#00000011B
        JE      AP225
        LDB     DIRECT,#01H
   AP225:
        CALL      CURRENT_CAPT
        CALL      CALC_T1
        CALL      CALC_OP1
   AP22E:
        RET
;;;;;;;;;;;;;;;;;;;;;;;;;;;;;;;;;;;;;;;;;;;;;;;;;;;;;;;;;;;
AP33:
        ADD     R1_POSN,VEL1
        JBC     DIRECT,0,AP335
        JBC     SW_POSN,3,AP334
        ANDB    DIRECT,#11111110B
        JBS     P1_SW_POSN,3,AP3322
        ORB     DIRECT,#02H
        LD      U11_5,POSN
        LD      AX,VEL1
        LD      BX,R1_VEL
        CMP     AX,#00
        JGE     AP331
        NEG     AX
   AP331:
        CMP     BX,#00
        JGE     AP332
        NEG     BX
   AP332:
        CMP     AX,#04H
        JLT     AP3320
        SUB     R1_POSN,VEL1
   AP3320:
        CMP     BX,#04H
        JLT     AP3322
        SUB     R1_POSN,R1_VEL
   AP3322:
        BR      AP3E1
   AP334:
        cmp     VEL1,#03h
        jgt     ap3341
        cmp     VEL1,#0fffdh
        jlt     ap3341
        DEC     U11
        CMP     U11,#00H
        JGE     AP3341
        ADD     U11,#1F40H
   AP3341:
        BR      AP3E2
```

```
AP335:
        JBC      SW_POSN,1,AP338
        ORB      DIRECT,#00000001B
        JBS      P1_SW_POSN,1,AP338
        LD       U22_5,POSN
        JBC      DIRECT,1,AP338
        SUB      AX,U22_5,U11_5
        SUB      AX,110[L_POINT]
        CMP      AX,#00
        JGE      AP336
        NEG      AX
AP336:
        st       ax,32[e_point]
        st       u11_5,34[e_point]
        st       u22_5,36[e_point]

        CMP      AX,22[L_POINT]
        JGT      AP337
        INCB     MB
        BR       AP3E1
AP337:
        ld       al,#6bh
        stb      al,22[e_point]         ;warning
        CLRB     MB
AP338:
        cmp      VEL1,#0fffdh
        jlt      ap3381
        cmp      VEL1,#03h
        jgt      ap3381
        INC      U11
        CMP      U11,#1F40H
        JLT      AP3381
        SUB      U11,#1F40H
AP3381:
        BR       AP3E2

AP3E1:
        CMPB     MB,#02H
        JLT      AP3E2
        SUB      AX,POSN,R1_POSN
        CMP      AX,#00H
        JGT      AP3E10
        NEG      AX
AP3E10:
        CMP      AX,#258H            ;#4B0H
        JLT      AP3E11
        SUB      AX,#4B0H
        BR       AP3E10
AP3E11:
        CMP      AX,#00H
        JGT      AP3E12
        NEG      AX
AP3E12:
        CMP      AX,#20H           ;94[L_POINT]
        JLE      AP3E15
        LDB      MCOUNT,#0C0H
        st       ax,32[e_point]
        st       r1_posn,34[e_point]
```

```
        st      posn,36[e_point]
        BR      AP3E16
    AP3E15:
        LDB     DIRECT,#01H
        CLRB    DIRECT2
        CLRB    DIRECT3
        LD      R1_POSN1,POSN
        LDB     CLOSE_COUNT,#01H
        LDB     MCOUNT,#0A0H            ;#0a0h -- #84h
    AP3E16:
        STB     MCOUNT,6[C_POINT]
        BR      AP3E3
    AP3E2:
        CALL    CURRENT_CAPT
        CALL    VECTOR2
        CALL    CALC_T1
        CALL    CALC_OP1
    AP3E3:
        RET
;;;;;;;;;;;;;;;;;;;;;;;;;;;;;;;;;;;;;;;;;;;;;;;;;;;;;;;;;;;
AP44:
        LD      POSN_C,2[C_POINT]
        LD      P1_POSN,POSN
        ADD     POSN,POSN_C,#0BB8H
        JBS     CLOSE_COUNT,0,AP441
        BR      AP442
    AP441:
        CALL    CALC_C1
;;;;;;;;;;;;;;;;;;;;;;;;;;;;;;;;;;;;;;;;;;;;;;;;;;;;;;;;;;;
    AP442:
        CALL     CURRENT_CAPT
    AP443:
        CALL     CALC_V1
        JBC      CLOSE_COUNT,2,AP4450
        LDB      CLOSE_COUNT,#1H
        ORB      RECORD,#00000010B
        JBS      DIRECT,0,AP444P
        JBS      DIRECT,1,AP444N
        BR       AP445
    AP444P:
        ADD      R1_POSN1,4[L_POINT]
        CMP      R1_POSN1,#1770H
        JLT      AP445
        LD       R1_POSN1,#1770H
        LDB      DIRECT,#02H
        BR       AP445
    AP444N:
        SUB      R1_POSN1,4[L_POINT]
        CMP      R1_POSN1,#00H
        JGT      AP445
        LDB      MCOUNT,#0A0H
        CLR      R1_POSN1
        BR       AP445
    AP4450:
        SHLB     CLOSE_COUNT,#1H
    AP445:
        CALL      CALC_T1
        CALL      CALC_OP1
```

```
        RET
;;;;;;;;;;;;;;;;;;;;;;;;;;;;;;;;;;;;;;;;;;;;;;;;;;;;;;;;;;
;;;;;;;;;;;;;;;;;;;;;;;;;;;;;;;;;;;;;;;;;;;;;;;;;;;;;;;;;;
CALC_C1:
        CALL    CALC_CSG2
        LD      CSG1,CSG2
        LD      CSG1+2,CSG2+2
        DIV     CSG1,#0AF6H             ;0AF6H - 2E8CH
        LD      IR4_R1,CSG1
        NEG     IR4_R1
;;;;;;;;;;;;;;;;;;;;;;;;;;;;;;;;;;;;;;;;;;;;;;;;;;;;;;
        LD      AX,IR4_R1
        AND     BX,AX,#8000H
        JE      IR4_POS
        NEG     AX
        CMP     AX,#300H                ;44[L_POINT]
        JLE     IR4HH
        LD      IR4_R1,#0300H          ;44[L_POINT]
        NEG     IR4_R1
        BR      IR4LH
    IR4_POS:
        CMP     AX,#300H                ;44[L_POINT]
        JLE     IR4HH
        LD      IR4_R1,#300H           ;44[L_POINT]
    IR4LH:
        CMPB    MB,#70H
        JGE     IR4HH
        INCB    MB
    IR4HH:
        CLR     CSG1
        CLR     CSG1+2
        RET
;;;;;;;;;;;;;;;;;;;;;;;;;;;;;;;;;;;;;;;;;;;;;;;;;;;;;;;;;;
CALC_P1:
        INC      POSN_COUNT
        MUL      LONG_WORD,SPEED,POSN_COUNT
        LD       AX,LONG_WORD
        ld       gga1,gga
        mul      long_word,ax,#2dh
        div      long_word,#4bh
        ld       ax,long_word
    TR_CHK0:
        CMP      AX,#1F40H
        JLT      TR_CHK1
        CLR      AX
        CLR      POSN_COUNT
;;;;;;;;;;;;;;;;;;;;;;;;;;;;;;;;;;;;;;;;;;;;;;;;;;;;;;;;;;
    TR_CHK1:
        SHL      AX,#1
        CMP      AX,#0FA0H
        JGT      TR_CHK2
        LD       POSN_T,TABLE_T[AX]
        LD       POSN_C,TABLE_C[AX]
        LD       VEL_T,AX
        SUB      AX,#0FA0H
        NEG      AX
        LD       VEL_C,TABLE_C[AX]
        BR       CALCTREND
```

```
;;;;;;;;;;;;;;;;;;;;;;;;;;;;;;;;;;;;;;;;;;;;;;;;;;;;;;;;;;;;
    TR_CHK2:
        CMP       AX,#01F40H
        JGT       TR_CHK3
        SUB       AX,#01F40H
        NEG       AX
        LD        POSN_T,TABLE_T[AX]
        LD        POSN_C,TABLE_C[AX]
        NEG       POSN_T
        NEG       POSN_C
        neg       gga1
        LD        VEL_T,AX
        SUB       AX,#0FA0H
        NEG       AX
        LD        VEL_C,TABLE_C[AX]
        BR        CALCTREND
;;;;;;;;;;;;;;;;;;;;;;;;;;;;;;;;;;;;;;;;;;;;;;;;;;;;;;;;;;;;
    TR_CHK3:
        CMP       AX,#2EE0H
        JGT       TR_CHK4
        SUB       AX,#1F40H
        LD        POSN_T,TABLE_T[AX]
        LD        POSN_C,TABLE_C[AX]
        NEG       POSN_T
        NEG       POSN_C
        neg       gga1
        LD        VEL_T,AX
        SUB       AX,#0FA0H
        NEG       AX
        LD        VEL_C,TABLE_C[AX]
        NEG       VEL_T
        NEG       VEL_C
        BR        CALCTREND
;;;;;;;;;;;;;;;;;;;;;;;;;;;;;;;;;;;;;;;;;;;;;;;;;;;;;;;;;;;;
    TR_CHK4:
        SUB       AX,#3E80H
        NEG       AX
        LD        POSN_T,TABLE_T[AX]
        LD        POSN_C,TABLE_C[AX]
        LD        VEL_T,AX
        SUB       AX,#0FA0H
        NEG       AX
        LD        VEL_C,TABLE_C[AX]
        NEG       VEL_T
        NEG       VEL_C
;;;;;;;;;;;;;;;;;;;;;;;;;;;;;;;;;;;;;;;;;;;;;;;;;;;;;;;;;;;;
    CALCTREND:
        SUB       DX,POSN_T,POSN_C
        MUL       LONG_WORD,DX,PER
        LD        DX,LONG_WORD
        LD        CX,LONG_WORD+2
        MUL       LONG_WORD,POSN_C,#64H
        ADD       LONG_WORD,DX
        ADDC      LONG_WORD+2,CX
        DIV       LONG_WORD,#64H
        LD        AX,#0BB8H
        MUL       LONG_WORD,STROKE
        DIV       LONG_WORD,#1770H
```

```
          SUB       R1_POSN,AX,LONG_WORD
;;;;;;;;;;;;;;;;;;;;;;;;;;;;;;;;;;;;;;;;;;;;;;;;;;;;;;;;;;;;;;;;
          MUL       LONG_WORD,VEL_C,#0F57H
          DIV       LONG_WORD,#0EA2H
          MUL       LONG_WORD,REQ_SS
          DIV       LONG_WORD,#1770H
          LD        VEL_C,LONG_WORD
          MUL       LONG_WORD,REQ_SS,VEL_T
          DIV       LONG_WORD,#1770H
          LD        VEL_T,LONG_WORD
          SUB       DX,VEL_T,VEL_C
          MUL       LONG_WORD,DX,PER
          LD        DX,LONG_WORD
          LD        CX,LONG_WORD+2
          MUL       LONG_WORD,VEL_C,#64H
          ADD       LONG_WORD,DX
          ADDC      LONG_WORD+2,CX
          DIV       LONG_WORD,#64H
          LD        R1_VEL,LONG_WORD
          RET
;;;;;;;;;;;;;;;;;;;;;;;;;;;;;;;;;;;;;;;;;;;;;;;;;;;;;;;;;;;;;;;;
;;;;;;;;;;;;;;;;;;;;;;;;;;;;;;;;;;;;;;;;;;;;;;;;;;;;;;;;;;;;;;;;
CALC_CSG2:
          SUB       POSN_E1,R1_POSN1,POSN
          MUL       CSG2,POSN_E1,#6A07h     ;30[L_POINT]
          MUL       LONG_WORD,POSN_E1,#3f0h ;32[L_POINT]
          ADD       CSG3,LONG_WORD
          ADDC      CSG3+2,LONG_WORD+2
          ADD       CSG2,CSG3
          ADDC      CSG2+2,CSG3+2
;;;;;;;;;;;;;;;;;;;;;;;;;;;;;;;;;;;;;;;;;;;;;;;;;;;;;;;;;;;;;;;;
          SUB       VEL5,POSN,P1_POSN1
          MUL       LONG_WORD,VEL5,#7d0H
          DIV       LONG_WORD,#09H
          LD        VEL5,LONG_WORD
          SUB       VEL_E1,R1_VEL,VEL5
          MUL       LONG_WORD,VEL_E1,#054DH ;46[L_POINT]
          ADD       CSG2,LONG_WORD
          ADDC      CSG2+2,LONG_WORD+2
          mul       long_word,gga1,#0c8h
          ADD       CSG2,LONG_WORD
          ADDC      CSG2+2,LONG_WORD+2
          LD        P1_POSN1,POSN
          RET
;;;;;;;;;;;;;;;;;;;;;;;;;;;;;;;;;;;;;;;;;;;;;;;;;;;;;;;;;;;;;;;;
;;;;;;;;;;;;;;;;;;;;;;;;;;;;;;;;;;;;;;;;;;;;;;;;;;;;;;;;;;;;;;;;
CURRENT_CAPT:
          MUL       LONG_WORD,IR1,#15C7H
          DIV       LONG_WORD,#07D0H
          LD        IR,LONG_WORD
          MUL       LONG_WORD,IY1,#1632H
          DIV       LONG_WORD,#07D0H
          LD        IY,LONG_WORD
          SUB       IR,IR_01
          JC        CURR1
          ANDB      I_SIGN,#11111110B
          BR        CURR2
     CURR1:
```

```
        ORB     I_SIGN,#00000001B
    CURR2:
        SUB     IY,IY_01
        JC      CURR3
        ANDB    I_SIGN,#11111011B
        BR      CURR4
    CURR3:
        ORB     I_SIGN,#00000100B
    CURR4:
        ADD     IB,IR,IY
        NEG     IB
        AND     AX,IB,#8000H
        JNE     CURR5
        ORB     I_SIGN,#00010000B
        BR      CURREND
    CURR5:
        ANDB    I_SIGN,#11101111B
    CURREND:
        RET
;;;;;;;;;;;;;;;;;;;;;;;;;;;;;;;;;;;;;;;;;;;;;;;;;;;;;;;;;;;;
;;;;;;;;;;;;;;;;;;;;;;;;;;;;;;;;;;;;;;;;;;;;;;;;;;;;;;;;;;;;
CALC_T1:
        LD      UD1,U1
        CALL    CALC_OP2
        JBC     I_SIGN,0,CALCTM1
        SUB     U1_11,VEL_C,#64H
        SUB     U1_12,VEL_T,#05H
        BR      CALCTM2
    CALCTM1:
        SUB     U1_11,VEL_C,#69H
        ADD     U1_12,VEL_T,#05H
    CALCTM2:
        LD      UD1,U2
        CALL    CALC_OP2
        JBC     I_SIGN,2,CALCTM3
        SUB     U2_11,VEL_C,#64H
        SUB     U2_12,VEL_T,#05H
        BR      CALCTM4
    CALCTM3:
        SUB     U2_11,VEL_C,#69H
        ADD     U2_12,VEL_T,#05H
    CALCTM4:
        LD      UD1,U3
        CALL    CALC_OP2
        JBC     I_SIGN,4,CALCTM5
        SUB     U3_11,VEL_C,#64H
        SUB     U3_12,VEL_T,#05H
        BR      CALCEND
    CALCTM5:
        SUB     U3_11,VEL_C,#69H
        ADD     U3_12,VEL_T,#05H
    CALCEND:
        RET
;;;;;;;;;;;;;;;;;;;;;;;;;;;;;;;;;;;;;;;;;;;;;;;;;;;;;;;;;;;;
;;;;;;;;;;;;;;;;;;;;;;;;;;;;;;;;;;;;;;;;;;;;;;;;;;;;;;;;;;;;
CALC_OP1:
    OCHECK3:
        JBS     IOS0,6,OCHECK3
```

```
        LDB     HSO_COMMAND,#00010000B
        ADD     INO_11,TIME_OLD,U1_11
        ADD     INO_11,#210H
        LD      HSO_TIME,INO_11
        ADD     INO_12,INO_11,U1_12
    OCHECK4:
        JBS     IOSO,6,OCHECK4
        LDB     HSO_COMMAND,#00110000B
        LD      HSO_TIME,INO_12
        ADD     IN1_11,TIME_OLD,U2_11
        ADD     IN1_11,#210H
;;;;;;;;;;;;;;;;;;;;;;;;;;;;;;;;;;;;;;;;;;;;;;;;;;;;;;;;;;;;;;
    OCHECK5:
        JBS     IOSO,6,OCHECK5
        LDB     HSO_COMMAND,#00010001B
        LD      HSO_TIME,IN1_11
        ADD     IN1_12,IN1_11,U2_12
    OCHECK6:
        JBS     IOSO,6,OCHECK6
        LDB     HSO_COMMAND,#00110001B
        LD      HSO_TIME,IN1_12
        ADD     IN2_11,TIME_OLD,U3_11
        ADD     IN2_11,#210H
;;;;;;;;;;;;;;;;;;;;;;;;;;;;;;;;;;;;;;;;;;;;;;;;;;;;;;;;;;;;;;
    OCHECK7:
        JBS     IOSO,6,OCHECK7
        LDB     HSO_COMMAND,#00010010B
        LD      HSO_TIME,IN2_11
        ADD     IN2_12,IN2_11,U3_12
    OCHECK8:
        JBS     IOSO,6,OCHECK8
        LDB     HSO_COMMAND,#00110010B
        LD      HSO_TIME,IN2_12
    RET3:
        RET
;;;;;;;;;;;;;;;;;;;;;;;;;;;;;;;;;;;;;;;;;;;;;;;;;;;;;;;;;;;;;;
;;;;;;;;;;;;;;;;;;;;;;;;;;;;;;;;;;;;;;;;;;;;;;;;;;;;;;;;;;;;;;
CALC_OP2:
        AND     AX,UD1,#8000H
        JE      PRD1
        SUB     UD1,#8206H
        BR      CONTIN
    PRD1:
        ADD     UD1,#7DFAH
    CONTIN:
        LD      LONG_WORD,UD1
        LD      LONG_WORD+2,#0H
        DIVU    LONG_WORD,#2BH
        LD      LONG_WORD+2,#0H
        LD      UD1,LONG_WORD
        LD      AX,#5DCH
        SUB     VEL_T,AX,UD1
        LD      VEL_C,UD1
        SHR     VEL_C,#1H
        RET
;;;;;;;;;;;;;;;;;;;;;;;;;;;;;;;;;;;;;;;;;;;;;;;;;;;;;;;;;;;;;;
;;;;;;;;;;;;;;;;;;;;;;;;;;;;;;;;;;;;;;;;;;;;;;;;;;;;;;;;;;;;;;
CALC_V1:
```

```
        LD          IR2,IR
        SUB         IY2,IY,IB
        MUL         LONG_WORD,IY2,#2D1BH
        DIV         LONG_WORD,#4E20H
        LD          IY2,LONG_WORD
;;;;;;;;;;;;;;;;;;;;;;;;;;;;;;;;;;;;;;;;;;;;;;;;;;;;;;;;;;;
        ld          JDALP,posn
        cmp         JDALP,#0e10h
        jle         c_ang
        sub         JDALP,#0e10h
    c_ang:
        MUL         LONG_WORD,JDALP,#014H
        DIV         LONG_WORD,#03H
        LD          JDALP,LONG_WORD
        LD          JDGAM,JDALP
;;;;;;;;;;;;;;;;;;;;;;;;;;;;;;;;;;;;;;;;;;;;;;;;;;;;;;;;;;;
        SUB         POSN_DIFF,POSN,P1_POSN
        MUL         LONG_WORD,POSN_DIFF,#7D0H
        DIV         LONG_WORD,#03H
        LD          VEL1,LONG_WORD
        LD          P1_POSN,POSN
;;;;;;;;;;;;;;;;;;;;;;;;;;;;;;;;;;;;;;;;;;;;;;;;;;;;;;;;;;;
        CALL        CALC_C5
        MUL         LONG_WORD,IR2,PARA_C
        DIV         LONG_WORD,#0BB8H
        LD          AX,LONG_WORD
        MUL         LONG_WORD,IY2,PARA_S
        DIV         LONG_WORD,#0BB8H
        LD          BX,LONG_WORD
        ADD         IR3,AX,BX
        MUL         LONG_WORD,IY2,PARA_C
        DIV         LONG_WORD,#0BB8H
        LD          AX,LONG_WORD
        MUL         LONG_WORD,IR2,PARA_S
        DIV         LONG_WORD,#0BB8H
        LD          BX,LONG_WORD
        SUB         IR4,BX,AX
;;;;;;;;;;;;;;;;;;;;;;;;;;;;;;;;;;;;;;;;;;;;;;;;;;;;;;;;;;;
        MUL         LONG_WORD,IR3,#01068h ;38[L_POINT]
        DIV         LONG_WORD,#190H
        LD          U11_5,LONG_WORD
        MUL         LONG_WORD,IR3,#069h   ;40[L_POINT]
        DIV         LONG_WORD,#190H
        ADD         IR3_E1,LONG_WORD
        ADD         U11_5,IR3_E1
        SUB         AX,IR4_R1,IR4
        MUL         LONG_WORD,AX,#01068h  ;38[L_POINT]
        DIV         LONG_WORD,#190H
        LD          U22_5,LONG_WORD
        MUL         LONG_WORD,AX,#069h    ;40[L_POINT]
        DIV         LONG_WORD,#190H
        ADD         IR4_E1,LONG_WORD
        ADD         U22_5,IR4_E1
;;;;;;;;;;;;;;;;;;;;;;;;;;;;;;;;;;;;;;;;;;;;;;;;;;;;;;;;;;;
    CALC_STAT:
        MUL         LONG_WORD,VEL1,IR4_R1
        DIV         LONG_WORD,#0FA0H
        LD          LONG_WORD+2,#0H
```

```
        MUL     LONG_WORD,#016H         ;0dh..16h
        DIV     LONG_WORD,#0AH
        LD      U11_0,LONG_WORD
;;;;;;;;;;;;;;;;;;;;;;;;;;;;;;;;;;;;;;;;;;;;;;;;;;;;;;;;;;;
        MUL     LONG_WORD,IR4_R1,#015cH
        DIV     LONG_WORD,#64H          ;adh..15ch
        LD      U22_0,LONG_WORD
        MUL     LONG_WORD,VEL1,#24FH
        DIV     LONG_WORD,#0FA0H
        LD      AX,LONG_WORD
        SUB     U22_0,AX
        SUB     U11,U11_0,U11_5
        ADD     U22,U22_0,U22_5
        LD      U22,U22_0
        CLR     AX
        LD      DX,U11
        LD      BX,U22
        AND     CX,DX,#8000H
        JE      U11_POST
        NEG     DX
        LDB     AL,#1H
    U11_POST:
        CMP     DX,42[L_POINT]
        JLT     U22_TEST
        LD      U11,42[L_POINT]         ;warning
        JBC     AL,0,U22_TEST
        NEG     U11
    U22_TEST:
        AND     CX,BX,#8000H
        JE      U22_POST
        NEG     BX
        LDB     AH,#1H
    U22_POST:
        CMP     BX,44[L_POINT]
        JLT     CHECK_DONE
        LD      U22,44[L_POINT]         ;warning
        JBC     AH,0,CHECK_DONE
        NEG     U22
;;;;;;;;;;;;;;;;;;;;;;;;;;;;;;;;;;;;;;;;;;;;;;;;;;;;;;;;;;;
    CHECK_DONE:
        MUL     LONG_WORD,VEL1,#10H
        DIV     LONG_WORD,#03e8H
        LD      JDGAM,LONG_WORD
        ADD     JDGAM,JDALP
        CALL    CALC_C5
        MUL     LONG_WORD,U11,PARA_C
        DIV     LONG_WORD,#02EEH
        LD      U1,LONG_WORD
        MUL     LONG_WORD,U22,PARA_S
        DIV     LONG_WORD,#02EEH
        LD      AX,LONG_WORD
        ADD     U1,AX
;;;;;;;;;;;;;;;;;;;;;;;;;;;;;;;;;;;;;;;;;;;;;;;;;;;;;;;;;;;
        SUB     JDGAM,#0A6BH
        CALL    CALC_C5
        MUL     LONG_WORD,U11,PARA_C
        DIV     LONG_WORD,#02EEH
        LD      U2,LONG_WORD
```

```
        MUL     LONG_WORD,U22,PARA_S
        DIV     LONG_WORD,#02EEH
        LD      AX,LONG_WORD
        ADD     U2,AX
;;;;;;;;;;;;;;;;;;;;;;;;;;;;;;;;;;;;;;;;;;;;;;;;;;;;;;;;;
        ADD     JDGAM,#14D5H
        CALL    CALC_C5
        MUL     LONG_WORD,U11,PARA_C
        DIV     LONG_WORD,#02EEH
        LD      U3,LONG_WORD
        MUL     LONG_WORD,U22,PARA_S
        DIV     LONG_WORD,#02EEH
        LD      AX,LONG_WORD
        ADD     U3,AX
        RET
;;;;;;;;;;;;;;;;;;;;;;;;;;;;;;;;;;;;;;;;;;;;;;;;;;;;;;;;;
VECTOR2:
        ADD     JDGAM,JDALP,U11
        CALL    CALC_C5
        MUL     LONG_WORD,posn_t,PARA_C
        DIV     LONG_WORD,#0BB8H
        LD      U1,LONG_WORD
;;;;;;;;;;;;;;;;;;;;;;;;;;;;;;;;;;;;;;;;;;;;;;;;;;;;;;;;;
        SUB     JDGAM,#0A6BH
        CALL    CALC_C5
        MUL     LONG_WORD,posn_t,PARA_C
        DIV     LONG_WORD,#0BB8H
        LD      U2,LONG_WORD
;;;;;;;;;;;;;;;;;;;;;;;;;;;;;;;;;;;;;;;;;;;;;;;;;;;;;;;;;
        ADD     JDGAM,#14D5H
        CALL    CALC_C5
        MUL     LONG_WORD,posn_t,PARA_C
        DIV     LONG_WORD,#0BB8H
        LD      U3,LONG_WORD
        RET
;;;;;;;;;;;;;;;;;;;;;;;;;;;;;;;;;;;;;;;;;;;;;;;;;;;;;;;;;
;;;;;;;;;;;;;;;;;;;;;;;;;;;;;;;;;;;;;;;;;;;;;;;;;;;;;;;;;
CALC_C5:
        LDB     JDGAM_NEG,#0
        AND     AX,JDGAM,#8000H
        JE      CHECK_2_P
        LDB     JDGAM_NEG,#1h
        NEG     JDGAM
    CHECK_2_P:
        CMP     JDGAM,#1F40H
        JLT     NEXT_CHECK
        SUB     JDGAM,#1F40H
        BR      CHECK_2_P
;;;;;;;;;;;;;;;;;;;;;;;;;;;;;;;;;;;;;;;;;;;;;;;;;;;;;;;;;
    NEXT_CHECK1:
        CMP     JDGAM,#7D0H
        JGT     NEXT_CHECK2
        LD      AX,JDGAM
        SHL     AX,#1
        LD      PARA_C,TABLE_C[AX]
        SUB     AX,#0FA0H
        NEG     AX
        LD      PARA_S,TABLE_C[AX]
```

```
        BR      TES_CODE
;;;;;;;;;;;;;;;;;;;;;;;;;;;;;;;;;;;;;;;;;;;;;;;;;;;;;;;;;;;;;;;;
    NEXT_CHECK2:
        CMP     JDGAM,#0FA0H
        JGT     NEXT_CHECK3
        SUB     AX,JDGAM,#7D0H
        SHL     AX,#1
        LD      BX,TABLE_C[AX]
        SUB     AX,#0FA0H
        NEG     AX
        LD      CX,TABLE_C[AX]
        LD      PARA_S,BX
        NEG     CX
        LD      PARA_C,CX
        BR      TES_CODE
;;;;;;;;;;;;;;;;;;;;;;;;;;;;;;;;;;;;;;;;;;;;;;;;;;;;;;;;;;;;;;;;
    NEXT_CHECK3:
        CMP     JDGAM,#1770H
        JGT     NEXT_CHECK4
        SUB     AX,JDGAM,#0FA0H
        SHL     AX,#1
        LD      BX,TABLE_C[AX]
        SUB     AX,#0FA0H
        NEG     AX
        LD      CX,TABLE_C[AX]
        NEG     BX
        LD      PARA_C,BX
        NEG     CX
        LD      PARA_S,CX
        BR      TES_CODE
;;;;;;;;;;;;;;;;;;;;;;;;;;;;;;;;;;;;;;;;;;;;;;;;;;;;;;;;;;;;;;;;
    NEXT_CHECK4:
        SUB     AX,JDGAM,#1770H
        SHL     AX,#1
        LD      BX,TABLE_C[AX]
        SUB     AX,#0FA0H
        NEG     AX
        LD      CX,TABLE_C[AX]
        NEG     BX
        LD      PARA_S,BX
        LD      PARA_C,CX
;;;;;;;;;;;;;;;;;;;;;;;;;;;;;;;;;;;;;;;;;;;;;;;;;;;;;;;;;;;;;;;;
    TES_CODE:
        CMPB    JDGAM_NEG,#1H
        JNE     DONE
        NEG     PARA_S
        NEG     JDGAM
    DONE:

        RET
;;;;;;;;;;;;;;;;;;;;;;;;;;;;;;;;;;;;;;;;;;;;;;;;;;;;;;;;;;;;;;;;
;;;;;;;;;;;;;;;;;;;;;;;;;;;;;;;;;;;;;;;;;;;;;;;;;;;;;;;;;;;;;;;;
CSEG    AT    9502H
LMT_TABLE:
DCW 1770H,0001H,0001H,0078H,0FA0H,0050H,1770H,0032H
DCW 02CCH,7DFAH,0006H,0064H,0050H,0014H,4535H,071FH
DCW 2EE0H,4E20H,1068H,0069H,125FH,1718H,0EA6H,0032H
DCW 0000H,0032H,0005H
```

```
GP_TABLE:
DCW 071FH,0718H,0701H,06D3H,292AH
DCW 0000H,0000H,0000H,0000H,0000H,0000H,0000H,0000H
DCW 0000H,0000H,0000H,0000H,0005H,0190H,0020H,2000H
DCW 0028H,7530H,0258H,01F4H,000EH,005CH,0dd6H
;;;;;;;;;;;;;;;;;;;;;;;;;;;;;;;;;;;;;;;;;;;;;;;;;;;;;;;;;;;
LMT_1:
DCW 0E10H,0001H,0001H,0000H,0000H,0000H,0E10H,0000H
DCW 0199H,68FBH,0000H,001EH,0FFB0H,0000H,0000H,0000H
DCW 2EE0H,2EE0H,0834H,0000H,1000H,1700H,0000H,0000H
DCW 0000H,0000H,0000H,0000H,0000H,0000H,0000H,0000H
DCW 0000H,0000H,0000H,0000H,0000H,0000H,0000H,0000H
DCW 0000H,0000H,0000H,0000H,0005H,0190H,0000H,1000H
DCW 0004H,7530H,0258H,01F4H,000EH,005CH,0000H
;;;;;;;;;;;;;;;;;;;;;;;;;;;;;;;;;;;;;;;;;;;;;;;;;;;;;;;;;;;
LMT_2:
DCW 1770H,0003H,0003H,0050H,0FA0H,0028H,1770H,0032H
DCW 02CCH,7DFAH,0014H,00C8H,0050H,0028H,4535H,071FH
DCW 2EE0H,4E20H,1068H,013BH,125FH,1932H,0EA6H,0200H
DCW 0033H,0064H,0005H,071FH,0718H,0701H,06D3H,292AH
DCW 7000H,7000H,7000H,7000H,7000H,7000H,7000H,7000H
DCW 7000H,7000H,7000H,7000H,0028H,07D0H,04B0H,3000H
DCW 0028H,7530H,0258H,01F4H,000EH,005CH,1770H

$INCLUDE(DATA.INC)
;;;;;;;;;;;;;;;;;;;;;;;;;;;;;;;;;;;;;;;;;;;;;;;;;;;;;;;;;;;
END
```

APPENDIX 3:

PAPER provisionally accepted

for Publication in Control Engineering Practise

POSITION CONTROL FOR A SUBSEA PUMP SYSTEM DRIVEN BY A LINEAR MOTOR

T. X. MEI*+ and R. M. GOODALL*

** Loughborough University of Technology, Department of Electronic and Electrical Engineering, Loughborough, Leics. LE11 1TU, U. K.*
+ Linear Motors Ltd., North Road, Loughborough, Leics. LE11 1SR, U. K.

Abstract. This paper presents simulation and control design for a subsea pump system driven by a permanent magnet synchronous linear motor. Linear and non-linear models are established to simulate the electrical, mechanical and fluid characteristics of the overall system. Based on simulation results, a linear but time-variant simplified model with parameter uncertainty is set up to enable design of controllers for the system. The parameter uncertainty is bounded by two extreme load conditions. Three control approaches are studied and compared on the basis of robustness and performance. Full simulations and tests are carried out to prove the design.

Keywords. Control Design, Uncertainty, Fluid dynamics, Simulation, Pump, Permanent Magnet Synchronous Motor.

1. INTRODUCTION

In recent years, more and more permanent magnet synchronous motor drives have been used in high performance applications such as industrial robots and computer numerically controlled machine tools. With advantages of simple mechanical arrangement and direct power delivery, the permanent magnet linear synchronous motors (PLSM) are preferred for some applications (McLean *et al*, 1990; McLean, 1988). The developments in three major areas have made this possible. First of all, vector control theory, PWM techniques and power electronics are well developed so that a.c. motors can be controlled as easily as d.c. motors (Ogasawara *et al*, 1986; Acarnley *et al*, 1987). Secondly, more powerful and cost-effective permanent magnet materials are serving to accelerate these motor development efforts (Lipo, 1988; Bosè, 1986). Finally and most importantly, constant development of control theory and rapid progress of very large scale integrated circuit (VLSI) have enabled design and implementation of different controllers to tackle various problems with high performances and low costs (Pillay *et al*, 1990; Naunin *et al*, 1990).

This paper presents the design of a control system utilising permanent magnet synchronous linear motors for driving a subsea pump for three phase fluids consisting of oil, gas and sea water. The overall pump system consists two single-stage double-acting reciprocating piston pumps, each of which is driven by two parallel connected double sided permanent magnet linear synchronous motors (DPLSM), as shown in Fig. 1.

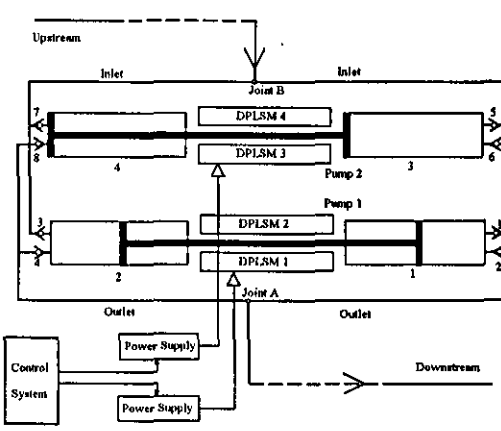

Fig. 1. Diagram of The Pump System.

Two pumps are controlled in conjunction but 90 degrees out of phase. Both have triangular velocity trajectories as shown in Fig. 3, and in this way constant flow rate and pressure can be obtained at the inlet and outlet (joint A and joint B).

This paper concentrates on the control of one pump only, since the two pumps have the same mechanical and electrical configurations and hence the controllers will be the same. The pump is required to handle three phase fluids in unknown and varying ratios. Thus one of the major difficulties in controlling such a pump is the rapid change and non linearity of the load conditions, which results in considerable uncertainty of the system dynamics and associated parameters and the difficulty of identification. In addition, the fluids need to be considered as distributed parameter systems.

This paper is organised as follows. The operation of the entire drive system is described and the system parameters related to the paper are given in section 2. In section 3, a mathematical model is established for computer simulation of the pump system where gas law and a distributed parameter model is set up for fluid dynamics in gas and oil cases respectively. The model includes the mechanics of the moving slider which connects the two pistons of the pump and carries the permanent magnets, and an electrical model is incorporated to simulate the motor. Section 4 describes the derivation of a linear model of the permanent magnet synchronous linear motor through the use of vector control. An inner current loop is introduced to implement the vector control, from which a time-invariant linear second-order model can be used to represent the motor for the control system design analysis. The pump dynamics, including that of the slider and fluids, is simplified to a second-order model which is linear but time-variant. Section 5 presents the design of an outer-loop position control, which is carried out based on a simplified model. Different approaches are studied and compared against system uncertainties in order to obtain the best results in terms of performance, stability and robustness. In section 6, simulations for different load conditions using both the simplified and full models and using the controllers developed in section 5 are carried out to prove the design. Some test results are also presented in section 6.

2. DRIVE SYSTEM AND CONFIGURATION

2.1. Drive System

Figure 2 shows a schematic of the overall drive system. Errors between reference and actual positions are operated upon by the position controller to generate the force reference. Velocity feedback is required for some of the controllers which have been investigated, and this can be derived from the position signal in the control computer. In the vector controller, the force reference is divided by the motor force constant to give the reference d - q axis current. Actual d - q axis currents are calculated from the phase currents and position feedback. The reference and actual currents are used to generate three phase voltages. Voltage control is implemented by the appropriate firing of the Voltage Source Inverter (VSI).

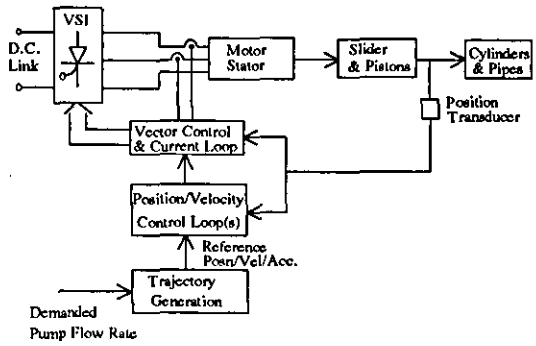

Fig. 2. Schematic of Drive System.

The force produced by the motor drives the slider and pistons to carry out the pumping action. Two cylinders and four non-return valves located outside cylinders work in switching mode. When the slider moves from left to right, valves 2 and 3 open, cylinder 1 pumps fluids out and cylinder 2 sucks in fluids. When the direction of the slider is reversed, valves 1 and 4 open, cylinder 2 pumps out and cylinder 1 sucks in.

2.2. System Parameters

To meet the production requirement, the motor must reach a peak velocity of 4.2 *m/s*. The pump has the maximum stroke length 1.5 *m* and it must be controlled to be better than 5 *mm* at the end of stroke to ensure both mechanical clearance between piston and cylinder and the best possible volumetric efficiency. The profiles for a single piston are shown in Fig. 3.

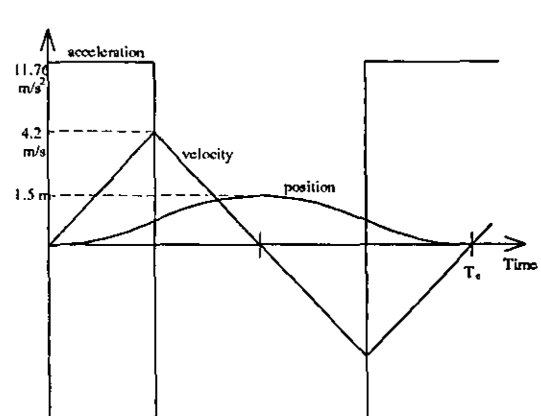

Fig. 3. Reference Profiles for a Single Piston

It can be seen that each DPLSM follows a constant acceleration / deceleration profile over every cycle. The period for a complete cycle is 1.429 *s*. In order to reach the peak velocity in such a time, the required acceleration is 11.76 m/s^2. The particular parameters related to the work in this paper are given as follows:

Diameter of piston	150 *mm*
Diameter of inlet pipe	100 - 150 *mm*
Diameter of outlet pipe	100 - 150 *mm*
Inlet pressure	35 *bar*
Outlet pressure	70 *bar*
Total mass of moving part	1400 *kg*
Viscous friction coefficient	60 - 120 *N s/m*
Pole pitch	150 *mm*
Armature resistance per phase	0.07585 Ω
Self inductance per phase	3.35 *mH*
Mutual inductance per phase	-1.11 *mH*
Assumed equivalent current in the slider	1.0 *A*
Peak mutual inductance between stator coil and equivalent circuit of the magnets	4.983 *H*

3. MATHEMATICAL MODEL OF PUMP

The system modelling can be partitioned into two parts, the electrical motor and the pump. The pump modelling includes both mechanics of the slider and the two pistons and dynamics of the fluids.

3.1. Modelling of Moving Slider

Newton's Law is introduced concerning the total mass of the moving slider and viscous friction.

$$m \cdot \frac{d^2x}{dt^2} + K_v \cdot \frac{dx}{dt} + F_l = F \tag{1}$$

where m is the total mass of the slider with two pistons, K_v is the coefficient of viscous friction of the slider, and F_l is total load force produced by the fluids.

The load force F_l is dominant in this equation since it represents the output of the pumping action. It also represents the largest uncertainty because of the variability of the fluids being pumped. This term could greatly affect the system dynamics; thus it is important to analyse the load characteristics.

3.2. Fluid Dynamics

As mentioned above, the overall pump system is configured such that constant flow rates in transportation pipes are maintained. In addition, the pressures at reservoir and upstream of the outlet pipe are assumed to be constant. In fact these pressures will change slowly as the pumping action continues, but the steady pressures have been used as a design case. Therefore pressures at the joint A and the joint B can also be assumed to be constant, which means that the fluids to be modelled are only that in the pipes between the pump and the joint A, and between the pump and the joint B.

In the modelling, effect of the non-return valves at the junctions between cylinders and pipes must be firstly considered. When the slider moves from one end to the other, say from left to right, there are three different stages in terms of valves' on and off states, regardless of the nature of the fluids.

(i). All valves are closed, pressure in cylinder 1 increases and in cylinder 2 decreases when the slider starts moving to the right. High stiffness appear in both cylinders as the fluids are compressed.

(ii). When the pressure in cylinder 2 is lower than that in the inlet pipe, valve 3 opens. High stiffness still exists in cylinder 1 but the dynamics of the fluid in the inlet pipe and cylinder 2 determine the characteristics to the left of the piston.

(iii). When the slider moves further to the right, the pressure in cylinder 1 will be higher than that in the outlet pipe and valve 2 opens as well. The characteristics of the load are then determined by the fluid dynamics of both inlet and outlet pipes.

When the direction of the movement reverses, the pump repeats the same stages in the opposite direction. It is clear that the system has different characteristics in the different stages; therefore different models have to be used in order to simulate it correctly. Also, the characteristics are greatly dependent upon the actual fluids. Two extreme cases are studied in this paper, where firstly the gas and then the liquids dominate.

It should be emphasised that the pump is designed largely to eliminate leakage across the pistons. The body of the pump is filled with pressurised oil, partly for cooling but also to ensure there is no leakage from the pump cylinders.

Pure Gas. Since dynamic changes are being considered it is appropriate to use adiabatic expansion given by

$$P \cdot v^{\gamma} = const. \tag{2}$$

where $\gamma = C_p / C_v = const.$ is the specific heat ratio, P is the pressure and v is the volume. The effective volume of the cylinder at any time can be decided from the position of the slider since the cross area is constant. Thus eq. 2 becomes:

$$F \cdot L^{\gamma} = const., \tag{3}$$

where F is the load force in one cylinder and L is the length of cylinder, i.e. the effective distance between the piston and non-return valves.

Stage 1: all valves closed. The load force is the sum of two forces developed in the regions on either side of the piston, and is developed as a result of adiabatic expansion or compression of the gas.

$$F_L = K_{11} * (L_1 - x)^{-\gamma} - K_{12} * (L_2 + x)^{-\gamma} \tag{4}$$

where L_1, L_2 are the initial effective lengths of the two cylinders respectively and x is the slider position with respect to its initial position.

Stage 2: suction valve open, discharge valve still closed. Because of the low density of the gas, it can be assumed that pressure in a cylinder is constant when the relevant valve is open. Thus:

$$F_L = K_{11} * (L_1 - x)^{-\gamma} + K_{10} \tag{5}$$

Stage 3: all valves open. The load force is constant due to the basic pump configuration as described in section 2.1.

$$F_L = K_{20} \tag{6}$$

Simulation results are given later which confirm the correctness of various assumptions made (see section 6.4).

Pure Oil. The flow processes are governed by momentum and continuity equations (Wylie and Streeter, 1978). The momentum equation is derived for liquid flow through a cylindrical tube.

$$g \cdot \frac{dH}{dx} + V \cdot \frac{dV}{dx} + \frac{dV}{dt} + \frac{f \cdot V \cdot |V|}{2D} + 2k_c \cdot V = 0 \tag{7}$$

where $H(x,t)$ is called the piezometric head (in m), $V(x,t)$ is the velocity of flow, f is the Darcy-Weibach friction factor due to shear stress, k_c is the friction factor due to roughness of pipe and D is the diameter of pipe.

The continuity equation is developed from the general principle that the mass within a system remains constant with time.

$$V \frac{dH}{dx} + \frac{dH}{dt} - V \cdot \sin\alpha + \frac{a^2}{g} \cdot \frac{dV}{dx} = 0 \tag{8}$$

where $a^2 \approx k/\rho$, k is bulk modulus, μ is viscosity, ρ is density of liquid, α is the pipe angle to horizontal level.

The load force can be derived from:

$$F_l = \rho \cdot g \cdot (H - Z) \cdot A \tag{9}$$

where $Z(x)$ is the elevation of the pipe, and A is the area of the cylinders.

A general solution to the above partial differential equations is not available. However the partial differential equations may be transformed by the method of characteristics into particular total differential equations.

$$\frac{g}{a} \cdot \frac{dH}{dt} + \frac{dV}{dt} - \frac{g}{a} \cdot V \cdot \sin\alpha + \frac{f \cdot V \cdot |V|}{2D} + 2 \cdot k_c \cdot V = 0 \tag{10}$$

$$\frac{dx}{dt} = V + a \tag{11}$$

$$-\frac{g}{a} \cdot \frac{dH}{dt} + \frac{dV}{dt} + \frac{g}{a} \cdot V \cdot \sin\alpha + \frac{f \cdot V \cdot |V|}{2D} + 2 \cdot k_c \cdot V = 0 \tag{12}$$

$$\frac{dx}{dt} = V - a \tag{13}$$

Equations 10 - 13 can be integrated to yield finite difference equations which are conveniently handled numerically in the computer simulation. They are used with different pipe sections for all three stages in the pumping process.

Stage 1: only liquid in two cylinders is involved.

Stage 2: the two cylinders and inlet pipe are simulated.

Stage 3: two cylinders, inlet pipe and outlet pipe are included.

3.3. Mathematical Model of The Motor

The electrical model used for the DPLSM is given in Fig. 4. The relation between three-phase currents and three-phase voltages can be described:

$$\begin{bmatrix} v_R \\ v_Y \\ v_B \end{bmatrix} = \begin{bmatrix} R_s + sL_s & sM_s & sM_s & sM_{fR} \\ sM_s & R_s + sL_s & sM_s & sM_{fY} \\ sM_s & sM_s & R_s + sL_s & sM_{fB} \end{bmatrix} \cdot \begin{bmatrix} i_R \\ i_Y \\ i_B \\ I_f \end{bmatrix} \tag{14}$$

where:

$$M_{fR} = M_{fM} \cdot \cos(\frac{\pi}{P}x)$$
$$M_{fY} = M_{fM} \cdot \cos(\frac{\pi}{P}x - \frac{2\pi}{3})$$
$$M_{fB} = M_{fM} \cdot \cos(\frac{\pi}{P}x + \frac{2\pi}{3}),$$

s is the Laplace operator, P is the pole pitch of the motor stator, I_f is the assumed constant current of the equivalent circuit of the permanent magnets.

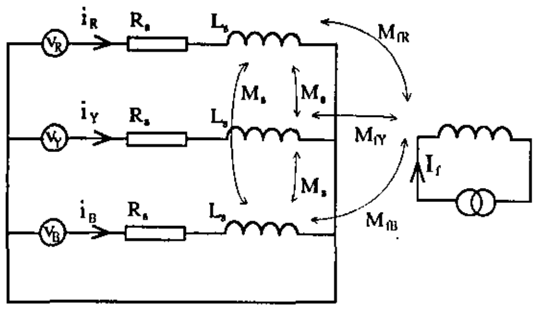

Fig. 4. Electrical Model of the Motor

The force developed in a PLSM is a function of the three phase currents, the self and mutual inductances of the stator and the mutual inductances between slider equivalent circuit and three phases. The equation is given below:

$$F = -I_f M_{fM} \frac{\pi}{P}\left[i_R \sin(\frac{\pi}{P}x) + i_Y \sin(\frac{\pi}{P}x - \frac{2\pi}{3}) + i_B \sin(\frac{\pi}{P}x + \frac{2\pi}{3}) \right] \quad (15)$$

3.4. Simulation Model of The System

The analysis described in the preceding sub-section completes the description of the equations used to simulate the system. Equation 14 is computed to determine the phase currents given the phase voltages produced from power supply and the motor parameters. The force produced by the motor can now be calculated from the phase currents according to Equation 15. The slider position and velocity are given by solving equation 1 where the load force is calculated from equations 4 - 5 for the gas case and 9 - 13 for the oil case. In the gas case, equations 4 - 6 are used for three stages respectively. In the oil case, equations 9 - 13 are used for all stages but with a different configuration of pipes for each stage.

4. SIMPLIFIED MODEL

The characteristics of liquids at any ratio of oil - gas mixture will be between the two extreme cases, which can therefore be used to give bounds for all conditions. However, although the models obtained so far can readily be used for computer simulation, because they are time-variant, non-linear and complex, some simplification is necessary in order to undertake control design. The following paragraphs describe model simplification used for designing the controllers, which have subsequently been assessed by computer simulation using the full model.

The electrical model of the motor can be transformed to the d - q axis equations, given as follows:

$$\begin{bmatrix} R_s + (L_s - M_s)s & \frac{\pi}{P}v(L_s - M_s) \\ -\frac{\pi}{P}v(L_s - M_s) & R_s + (L_s - M_s)s \end{bmatrix} \cdot \begin{bmatrix} i_d \\ i_q \end{bmatrix} = \begin{bmatrix} v_d \\ v_q \end{bmatrix} + \begin{bmatrix} 0 \\ M_{fM}\frac{\pi}{P}vI_f \end{bmatrix} \quad (16)$$

$$F = -\frac{3}{2} \cdot I_f \cdot M_{fM}\frac{\pi}{P} \cdot i_q \quad (17)$$

where i_d, i_q are d - q axis currents, v_d, v_q are d - q axis voltages and v is the velocity of the slider. A PI controller ($K_p = 0.5$ and $K_i = 14.0$) is designed for the current loop. Computer simulation, where different required current inputs with various frequencies and the electrical model of the motor are used, has been carried out to study the characteristics of the control loop. The frequency response of the loop obtained from the simulation is analysed and compared with ideal linear systems. The simulation results show that characteristics of the closed loop can be approximately described by a second-order system. Because this model is derived for the control design, it is given in the format of a transfer function.

$$H_e(s) = \frac{i(s)}{i_{ref}(s)} = \frac{1}{(\tau_{e1} \cdot s + 1)(\tau_{e2} \cdot s + 1)}, \quad (18)$$

where i_{ref} is the reference current input. Typical values of these two electrical time constants are 7.0 *ms* and 0.07 *ms* respectively, meaning that the current loop has a bandwidth of around 20 *Hz*.

When all valves are closed, it can easily be shown that the mass of the fluids in the cylinders can be neglected compared with the mass of the slider. The high stiffness dominates the characteristics, which can be derived from linearisation of the gas law for the gas case, and from the bulk modulus for the liquid case. When the relevant valves are opened, fluids are free to flow and the effect of the stiffness becomes negligible. In the oil case, the computer simulation shows that the characteristics of the liquids are very much determined by the mass of the liquids, viscous friction and a damped oscillatory force. The amplitude and frequency of this oscillation force are mainly decided by the characteristics of the pipes, the initial conditions and actual fluids, and so the effect of the oscillation force can be regarded as a disturbance. In the gas case, a constant load force is used because the mass can be neglected.

Combined with the model for the slider, a second-order system is derived to model the pump.

$$H_m(s) = \frac{x(s)}{i(s)} = \frac{k_{if}}{m_0 \cdot s^2 + k_f \cdot s + k_0} \tag{19}$$

where k_{if} is the conversion constant between the current and the force, m_0 is the sum of the mass of the slider and the effective mass of the fluids, k_f is the overall viscous friction coefficient and k_0 is a stiffness coefficient. A typical uncertainty bound for this application is given as follows:

Stage 1:

$$\begin{aligned} m_0 &= 1400 \\ k_f &= [60, 100] \\ k_0 &= [117.6 \times 10^3, 2.08 \times 10^8] \end{aligned} \tag{20}$$

Stage 2:

$$\begin{aligned} m_0 &= [1400, 2000] \\ k_f &= [60, 500] \\ k_0 &= [117.6 \times 10^3, 2.15 \times 10^7] \end{aligned} \tag{21}$$

Stage 3:

$$\begin{aligned} m_0 &= [1400, 4000] \\ k_f &= [60, 1000] \\ k_0 &= 0 \end{aligned} \tag{22}$$

Multiplying eqs. 18 and 19 together gives the simplified model of the overall system.

$$H(s) = \frac{x(s)}{i_{ref}(s)} = \frac{k_{if}}{(\tau_{e1} \cdot s + 1)(\tau_{e2} \cdot s + 1)} \times \frac{1}{m_0 \cdot s^2 + k_f \cdot s + k_0} \tag{23}$$

where the parameters of the model are bounded by eqs. 20, 21 and 22.

5. POSITION CONTROLLER DESIGN

The pump operation goes through three stages when the slider moves from one end to the other. The timing of every stage depends on the ratio of the oil - gas mixture. The higher the percentage of oil the higher will be the stiffness, meaning the pressure will build up more quickly in the cylinder. The overall cycle time is fixed for a particular flow rate, so if stages 1 and 2 are short, stage 3 will be long. Specifications to design the controller are slightly different at different stages. In stages 1 and 2, especially when high stiffness exists, the time periods of these stages are quite short and therefore stability is more important than performance. However performance characteristics such as transient time, overshoot, steady error, become key issues in stage 3 provided that the closed-loop system is stable.

The controller can be designed using classical frequency domain techniques or modern state-space methods. One of the primary objectives of the study was to establish whether the necessary performance could be achieved for all load cases without using adaptive control. Three types of controllers were studied for the position control, including Optimal Tracking (Anderson and Moore, 1990), Internal Model Control (Morari, 1989) and Cascade Control with and without feedforward terms.

Controller 1 - Optimal Tracking. The diagram of the optimal tracking control is given in Fig. 5. The controller consists of

a PI position compensator	$G_p + G_I / s$
a velocity feedback compensator	G_v
a velocity feed forward term.	G_{ff}

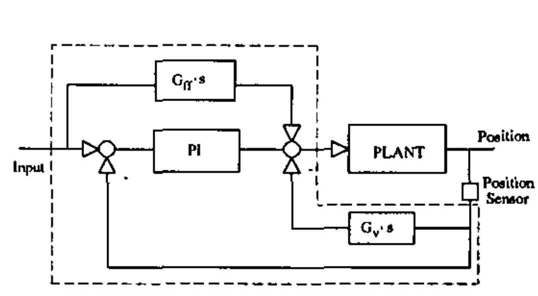

Fig. 5. Optimal Tracking With I term.

The control parameters are functions of the plant parameters and a weighting factor R in the performance index. Integral action is included in the controller to try and eliminate the position error with a high load force. The weighting factor is selected by using simulation. When R is decreased, the gains all increase which should provide better regulation, although there is a limit because in practice at some point the system become unstable. It has been shown that a value of $R = 0.001$ is the best compromise between the stability and control accuracy, which lead $G_p = 1599200$, $G_I = 20781600$, $G_v = 67470$ and $G_{ff} = 44900$.

Controller 2 - Internal Model Control. A block diagram of the internal model control is shown in Fig. 6, in which the same control signal drives both the actual system and an ideal model.

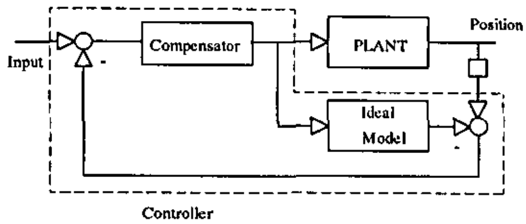

Fig. 6. Internal Model Control

The difference between their outputs is fed back and compared with the reference. The controller is of the form

$$G_{IMC}(s) = \frac{\left(10\lambda^2 s^2 + 5\lambda \cdot s + 1\right)\cdot\left(k_{c1}s^2 + k_{c2}\right)}{\left(\lambda \cdot s + 1\right)^5} \qquad (24)$$

The controller is in fact an inverse of the ideal plant plus a low pass filter, which is constructed in such a way that zero steady-state error is achieved for constant acceleration reference trajectories (Morari, 1989). λ is an on-line tuning parameter and adjusting λ is equivalent to adjusting the speed of the closed loop response. From the computer simulation, it has been shown that the best possible performance is obtained when $\lambda = 0.02$, $k_{c1} = 2000$ and $k_{c2} = 60$. The effect of k_{c2} is not as significant as the other two.

Controller 3 - Cascade Control. As shown in Fig. 7, a cascade controller consists of a position feedback controller with inner velocity control loop.

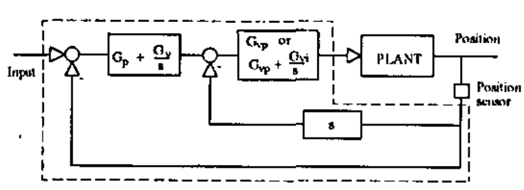

Fig. 7. Cascade Control.

The current loop which forms the innermost control function may be regarded as an impressed current source. Cascade control has many advantages, two of which are simpler design / commissioning, and robustness against model uncertainty because of the high bandwidth inner loops. The design is under the assumption that the bandwidth of the control increases towards the inner loops, which is almost inevitably the case with real systems.

The position loop needs a bandwidth of at least 6 *Hz* in order to obtain desirable tracking performance. A practical limit for the inner current loop has been found to be 20 *Hz*, and so the velocity bandwidth has been chosen to fall somewhere between 6 and 20 *Hz*. To achieve this specification with reasonable phase and magnitude margins, the control gains are selected as follows: $G_p = 20$, $G_i = 165$, $G_{pv} = 150000$ and $G_{vi} = 0$.

To improve the performance, feedforward terms including velocity and acceleration are added in the cascade controller as shown in Fig. 8. $G_{fv} = 1$ is selected to reduce the steady-state error and the selection of G_{fa} is to be discussed in the simulation.

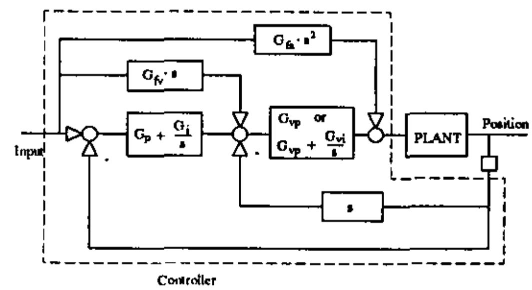

Fig. 8. Cascade Control With Feedforward Terms.

6. SIMULATION AND TEST

6.1. Initial Evaluations

The initial evaluation of the designed control laws is performed by means of a control system analysis and design package, SIMBOL, and using the simplified system model. Firstly the stability of all controllers was checked against the normal margins for the range of parameter variations given by eqs. 20 - 23, and secondly the performance of these controllers was investigated for the uncertainty bounds described in eq. 22.

Position step responses are firstly simulated to give a clear indication of dynamic performance. Fig. 9 gives the responses of three controllers for the low parameter bound.

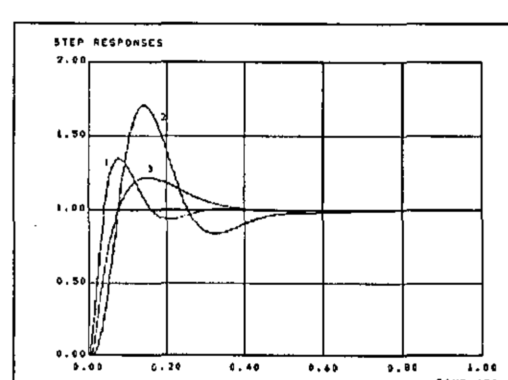

Fig. 9. Step Responses ($m = 1400$ $k_f = 60$)
1) Optimal Tracking , 2) IMC, 3) Cascade Control

Controller 1 gives the shortest transient time and 25% overshoot, controller 3 gives the fastest response and lowest overshoot and controller 2 has both the highest overshoot and the longest transient time.

The responses for the high bound are shown in Fig. 10, where the response of the controller 3 shows an increased overshoot but otherwise little change compared with that in Fig. 9. However controller 1 is very under-damped and controller 2 is unacceptable.

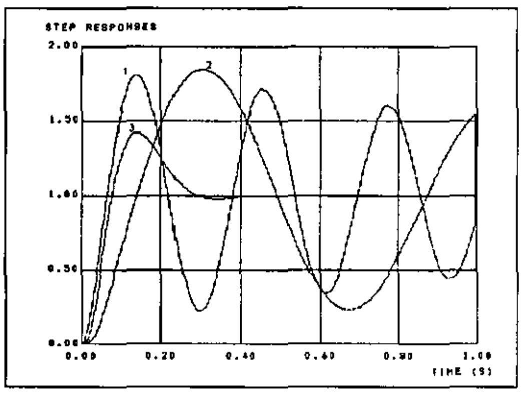

Fig. 10. Step Responses ($m = 4000 \quad k_f = 500$)
1) Optimal Tracking , 2) IMC , 3) Cascade Control

The results obtained so far show that the controller 3 is very robust against the defined parameter variations and has a reasonable response speed. So further studies have been carried out based on the Cascade Controller. Since the actual trajectory required for the system is a quadratic position and triangular velocity as shown in Fig. 3, responses of the system, especially the steady state errors, will be different from those seen with the step responses. This is clearly shown by the simulation results in Fig. 11, where the steady state error is about 70 *mm*.

To improve the control accuracy, two feedforward terms are introduced to the controller as shown in Fig. 8. Since the feedforward terms do not change the poles of the system, stability robustness is not an issue. Both velocity and acceleration feedforward signals are generated from the input trajectory, but one of the important issues when using feedforward is to examine the effect of mismatch in the feedforward terms. The velocity feedforward term is included to compensate for the velocity lag caused by the inner velocity loop. Since this feedback is derived from an incremental encoder its sensitivity will be precise, and so feedforward term derived from the command input will be very effective. However the acceleration feedforward term is dependent upon the mass. This is a physical parameter which cannot be known precisely, and in this case it will be affected by the mixture being pumped. Therefore it becomes particularly important to assess the robustness of the strategy using acceleration feedforward.

Figure 12 gives the simulation results for the cascade control with a velocity feedforward term and Fig. 13 gives that for the controller with velocity and acceleration terms.

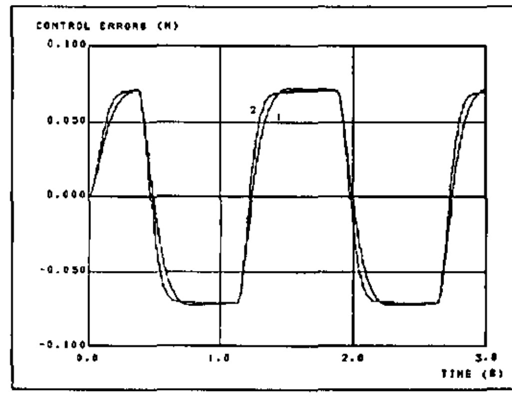

Fig. 11. Control Error of Cascade Control
1) $m = 1400,\ k_f = 60$, 2) $m = 4000,\ k_f = 500$

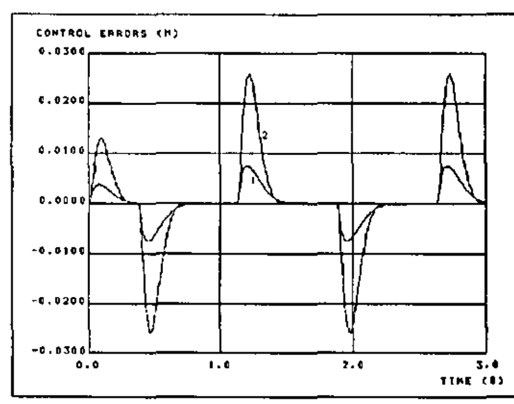

Fig. 12. Control Error of Cascade Control plus G_{fv}
1) $m = 1400,\ k_f = 60$, 2) $m = 4000,\ k_f = 500$

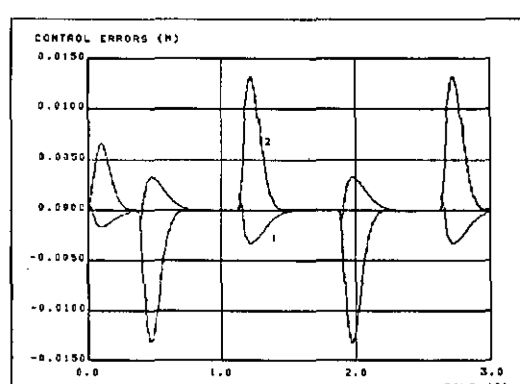

Fig. 13. Control Error of Cascade plus G_{fv}, G_{fa}

In Figs. 12 and 13, the steady state errors are eliminated and transient time in all cases is about 0.3 *s*. Better control accuracy is achieved by adding an acceleration term in addition to the velocity feed forward. In this case a mass of 2000 *kg* is taken to calculate the acceleration feedforward term, this value being around the middle of the range of possible masses.

6.2. Full Simulations

Full simulations using the mathematical models developed in Section 3 and the cascade controller developed above have been implemented on a SUN workstation. Fully digital control is realised in the simulation. The choice of sampling frequencies for those control loops depends upon many factors such as close loop bandwidth of each loop, sampling theory, computing power of the computer used for real-time control, switching frequency of the inverter etc. A sampling period 1.5 *ms* is used for the current loop and 4.5 *ms* for the position and velocity loops in the simulation. A big difference of the full simulation from that using the simplified model is that the full load conditions with high external pressures are applied. These load forces, which were represented by changing the mass and stiffness in the simple model, are the main factors to affect the control performances. In addition, a digital position transducer with resolution of 0.25 *mm* has been included in the simulation.

The required reference trajectory is the same as that shown in Fig. 3. Simulation results of two cases are presented in Figs. 14 to 17, where the cascade controller with the feedforward terms are used.

Figure 14 shows the control error and Fig. 15 gives the generated load force in one of the two cylinders for the pure gas case. Figs. 16 and 17 give results for the 99% oil case, which again shows the control error and the generated load force.

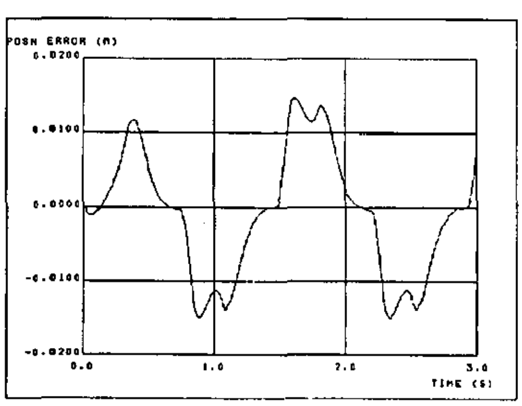

Fig. 14. Full Simulation Result (Pure Gas Case)

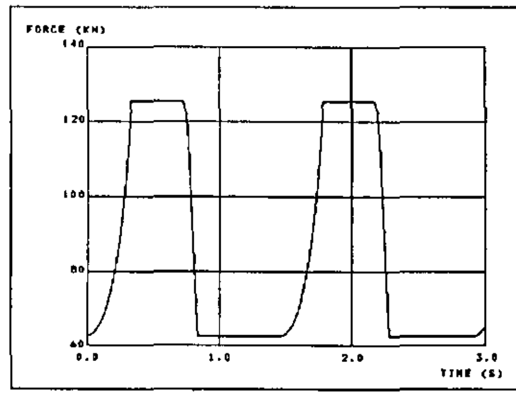

Fig. 15. Full Simulation Result
(Load Force in One Cylinder, Pure Gas Case)

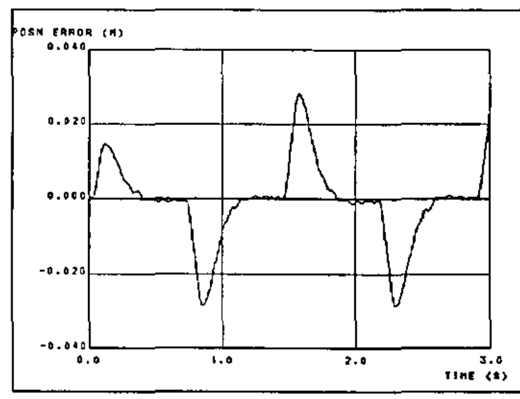

Fig. 16. Full Simulation Result (99 % Oil Case)

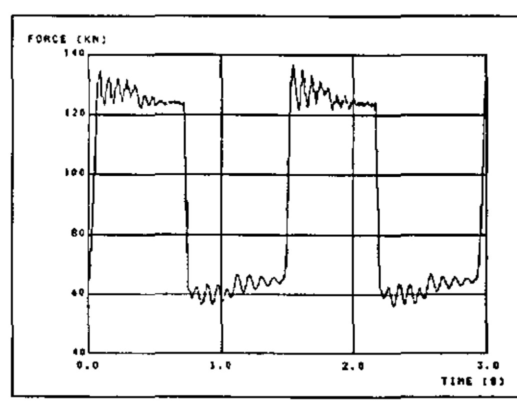

Fig. 17. Full Simulation Result
(Load Force in One Cylinder, 99 % Oil Case)

From Figs 15 and 17, it can be seen that characteristics of the load vary with the nature of the fluids. Gas takes a longer time to built up pressure due to the high compressibility, and the relevant valves open later than in the oil case. Therefore the period of quasi steady state after the valves open is shorter than in the oil case, which requires a faster response of the controller. In contrast, the steady-state time is longer in the oil case but oscillations appear on top of the load force caused by the liquid characteristics, which requires the controller to have high disturbance rejection capability.

The controller deals with the load variation quite well, as shown in Figs 14 and 16. The control errors are increased while the pressures in the cylinders are building up. Once the valves open, the errors start to reduce and reach a steady state value of zero in both cases before the slider arrives the end, although it only takes less than 0.75 *s* for the slider to move from one end to the other. The maximum position error in the oil case is higher than in the gas case, again due to the higher stiffness; also the controller reaches the steady-state situation quicker than it does in the gas case. No overshoots are observed in any of the cases.

6.3. Test of A Scaled Down Motor

As the complete pump system has not been readily available, most of the testing has been is carried out on a scaled down DPLSM. Main parameters of the motor are given as follows:

Total mass of moving part	95 *kg*
Viscous friction coefficient	5–60 *Ns/m*
Pole pitch	150 *mm*
Armature resistance (each side)	1.3 Ω
Self inductance (each side)	32.0 *mH*
Mutual inductance (each side)	-11.0 *mH*
Assumed equivalent current in slider	1.0 *A*
Peak mutual inductance between stator coil and equivalent circuit	1.61 *H*

The parameters of the scaled down motor are different from the full size system, thus the gain of the velocity loop $G_{pv} = 9500$ and the gains of current loop $K_P = 4.0$ and $K_I = 66.67$ were selected in order to achieve the same bandwidths and performances. The gains of the position loop remain unchanged.

Figure 18 gives the test results where the peak velocity is 4.2 *m/s* and the motor is not loaded, the curve 1 is the control error when only velocity feedforward is used in the controller and curve 2 is when both velocity and acceleration feedforward terms are used. As expected, both control errors are small, the transient periods are short and the steady-state errors at the stroke end are much smaller than required. It is also shown that a peak value appears on curve 1 every time the sign of the acceleration is changed and the introduction of the acceleration term reduces the peak error (curve 2).

Figure 19 compares the control errors with and without load. Due to the limited power of the motor, the peak velocity is reduced to 3.0 *m/s* and the load force (1000 *N*) with a similar pattern as Fig. 17 is used. Although this test does not fully represent the case of the actual pump system, it represents a basic response pattern of the controller.

From the result, it can be observed that the pattern of the control errors is very similar to that given in Fig. 16. The error is increased at the beginning of each stroke when the load force is applied on the motor slider. This error is soon compensated by the controller and the transient period is less than 0.35 *s* as required. The steady state error is not affected by the load.

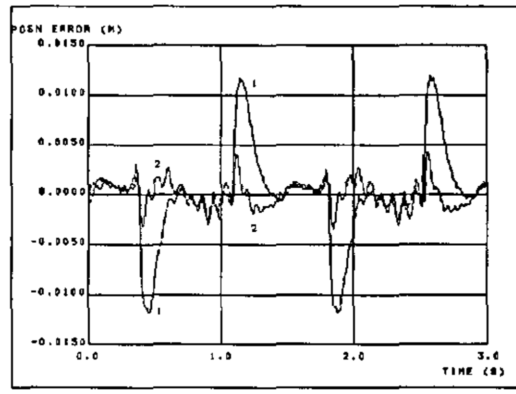

Fig. 18. Test Result (Control Errors)
1) $G_{fa} = 0$ 2) $G_{fa} = 100$

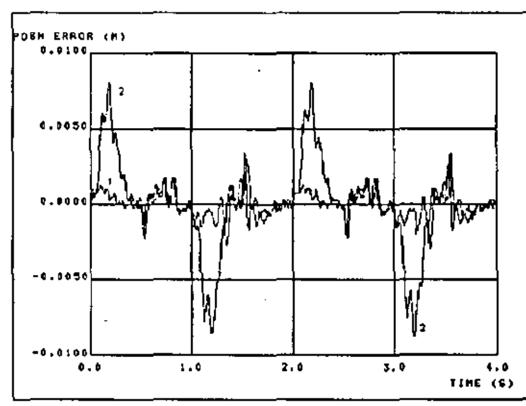

Fig. 19. Test Result (Control Errors)
1) No Load 2) $F_L = 1000\,N$

6.4. Limited Tests on Full Size System

In order to validate the modelling of the pure gas case, limited tests have been carried out on the full size system. Fig. 20 shows a comparison between test and simulation results using the equations above, which are closely agreed with each other.

The results show that the load force is substantially constant when all valves are open, because of its high compressibility and low density.

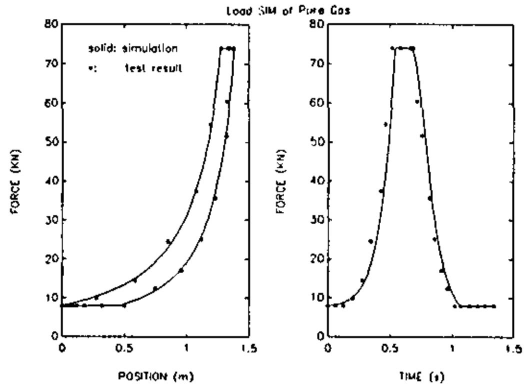

Fig. 20. Load Force of Pure Gas Case

7. CONCLUSION

This paper has presented a design for the position controller of a high performance PLSM pump system. Different approaches were studied using a simplified model with bounded parameter uncertainty. A number of strategies were investigated, but the cascade controller using nested position, velocity and current loops is preferred for the system. The control parameters obtained from the design process using the simplified model were applied to a detailed system simulation which included the cascade controller, the vector controller, the electrical model of the motor and models for fluid dynamics.

Fully digital control has been realised and implemented in the simulation. The results have proved that the final controller has good stability and robustness against uncertainty, and the performances, especially the steady errors, are very much improved by adding velocity and acceleration feedforward terms to the controller. Practical tests have also been carried out on a scaled down motor and a good comparison with simulation results has been shown.

8. REFERENCES

Acarnley, P.P., Finch, J.W. and Atkinson, D.J. (1987). Field Orientation in AC Drives: State Of The Art and Future Prospects. Third International Conference on Electrical Machines and Drives, November, pp 285 - 289.

Anderson, B.D.O. and Moore, J.B. (1990). *Optimal Control - Linear Quadratic Methods.* Prentice-Hall, Inc.

Bose, B.K. (1986). *Power Electronics and AC drives.* Englewood Cliffs, NJ: Prentice-Hall, Inc.

Kreider, J.F. (1985). *Principles of Fluid Mechanics.* Allyn and Bacon, Inc.

Lipo, T.A. (1988). Recent progress in the development of solid-state ac motor drives. IEEE Trans. PE-3, pp. 105 - 107

Lunze, J. (1989). *Robust Multivariable Feedback Control.* Englewood Cliffs, NJ: Prentice-Hall, Inc.

McLean, G.W., Turner, P.J., Creswick, A.R., Chung, W.K.A. and Afshar, A. (1990). Design of a Permanent Linear Synchronous Motor Drive for a Position / Velocity Actuator. International Conference on Electrical Machines. Boston, USA, August, pp. 1136 - 1141.

McLean, G.W. (1988). Review of Recent Progress in Linear Motors. Proc. IEE Vol. 135, pt.B, No.6, Nov. pp. 380 - 416.

Morari, M. (1989). *Robust Process Control.* Englewood Cliffs, NJ: Prentice-Hall, Inc.

Naunin, D., Hetzel, D., Reuss, H.C. and Sechelmann, C.E. (1990). Completely Digital Position Feedback Control for Synchronous Servo drives. IEEE Trans. PE-5, pp. 495 - 502.

Ogasawara, S., Akagi, H. and Nabae, A. (1986). The Generalised Theory of Indirect Vector Control for AC Machines. IEEE Trans. IA-22, pp 117 - 123.

Pillay, P. and Krishnan, R. (1990). Control Characteristics and Speed Controller Design for a High Performance Magnet Synchronous Motor Drive. IEEE Trans. PE-5, pp. 151 - 159.

Wylie, E.B. & Streeter, V.L. (1978). *Fluid Transients.* McGraw-Hill, Inc.